THERMAL HISTORY RECONSTRUCTION IN CHUKCHI SEA WELL BURGER J-001 BASED ON AFTA® AND VR DATA

OCS-Y-2321 #001

GEOTRACK REPORT #1191`

A report prepared for Shell, Houston

Report prepared by: P.F. Green

2016

Geotrack International Pty Ltd ABN 16006 899 209
37 Melville Road, Brunswick West, Victoria 3055 Australia tel: +613 9380 1077 fax: +613 9380 1477

email: mail@geotrack.com.au website: www.geotrack.com.au

THERMAL HISTORY RECONSTRUCTION IN CHUKCHI SEA WELL BURGER J-001 BASED ON AFTA® AND VR DATA

GEOTRACK REPORT #1191

CONTENTS

Continued….

CONTENTS (Continued

TABLES

Continued....

TABLES (Continued)

FIGURES

Continued....

FIGURES (Continued)

THERMAL HISTORY RECONSTRUCTION IN CHUKCHI SEA WELL BURGER J-001 BASED ON AFTA® AND VR DATA

GEOTRACK REPORT #1191

EXECUTIVE SUMMARY

Introduction and Objectives

This report describes a Thermal History Reconstruction study of **Chukchi Sea wells Burger J-001**. The study was commissioned by **Shell, Houston,** and is based on new Apatite Fission Track Analysis (AFTA®) in samples of cuttings from seven depth intervals in the well supplied by Shell. Vitrinite Reflectance (VR) data from the well were also supplied by Shell, and these have been supplemented by new analyses of material from three of the samples provided for AFTA. The AFTA and VR data have been used to *identify*, *characterise* and *quantify* the principle episodes of heating and cooling which have affected the section intersected in the well. This information is then synthesised to provide a thermal history framework for each well, within which the history of hydrocarbon generation and structural development can be understood. In addition, existing AFTA grain mounts for samples from the **Burger-1 well**, originally processed for Geotrack Report GC341 were reprocessed and reinterpreted for this Report. The report was completed in June 2016.

Summary Conclusions

1. Apatite yields from the seven samples provided from the **Burger J-001** well were varied, but by combining data from several of the sample intervals, high quality data were obtained for three depth intervals. High quality AFTA data were also obtained after reprocessing data in one sample from the **Burger-1** well. The resulting thermal history interpretations are regarded as highly reliable within stated uncertainties (95% confidence limits).

2. The quality of the new vitrinite reflectance data in the **Burger J-001** well obtained from Energy Resources Consulting Pty Ltd (ERC) for this report is also generally very high. VR data from both wells supplied by Shell also appear to be high quality but are higher than the ERC VR values and cannot be reconciled with the AFTA data. The preferred Thermal History reconstruction for the **Burger J-001** well is therefore based on constraints provided by the AFTA and ERC VR data.

3. AFTA data in none of the samples analysed from the **Burger J-001** well show any direct evidence that the sampled sedimentary units have ever been hotter than the present-day temperatures at any time after deposition, although they would allow the possibility within certain limits (Table i, Figures i, ii, iii).

4. Both sets of VR data from the well confirm that the section has been hotter in the past. The constraints provided by the AFTA data (Table i) are consistent with the maximum post-depositional paleotemperatures defined from the ERC VR data provided that cooling from those paleotemperatures began **prior to 73 Ma (late Campanian or earlier)**. Given the youngest Cretaceous unit (Nanushuk Formation) preserved in the well is assigned a younger depositional age limit of 99 Ma (Table A.1), the onset of cooling is further defined to **between 99 and 73 Ma (Cenomanian to Late Campanian)**.

5. The paleotemperatures defined from the ERC VR values and the constraints provided by the AFTA data are consistent with a linear paleotemperature profile, sub-parallel to the present-day temperature profile. This suggests that an interpretation of the observed paleotemperatures in terms of heating due to deeper burial and cooling due to exhumation can provide a satisfactory explanation of the AFTA and ERC VR data.

6. In contrast, the VR data supplied by Shell define a separate linear profile characterised by a lower gradient. As above, the paleotemperatures defining this parallel are higher than allowed by the AFTA data in the well and therefore we do not regard this profile as providing reliable definition of the paleo-thermal history of the section intersected in the well.

7. The ranges of paleogeothermal gradients consistent with the **Cenomanian to Late Campanian** paleotemperatures defined from AFTA and ERC VR data in the **Burger J-001** well within 95% confidence limits are summarised in Table ii. The maximum likelihood value of 36.5°C/km is very close to the present-day thermal gradient of 37°C/km for this well, suggesting that an explanation of heating due to deeper burial and cooling due to exhumation is viable.

8. In contrast, the entire range of paleogeothermal gradients allowed by the VR data in the **Burger J-001** well supplied by Shell, from 18.5 to 31.0°C/km, falls below the present-day gradient. Thus, quantitative analysis of paleogeothermal gradients defined from AFTA and the ERC VR data confirms that results from the Burger J-001 are consistent with heating due to deeper burial with no change in basal heat flow, whereas the VR data supplied by Shell would require an increase in heat flow since the Late Cretaceous.

9. Corresponding values of additional burial required to explain the observed **Cenomanian to Late Campanian** paleotemperatures derived from AFTA and ERC VR data in the **Burger J-001** well, for various values of paleogeothermal gradient within the allowed range in each episode are summarised in Table iii. Values derived from analysis of the VR data supplied by Shell are also shown. These are much higher than those defined from the AFTA and ERC VR data due to the lower paleogeothermal gradients required by the Shell data.

10. Figure iv illustrates the preferred thermal history reconstruction for the sedimentary units intersected in the **Burger J-001** well, based on all available data. The corresponding burial history reconstruction is shown in Figure v. Details of additional

section, paleogeothermal gradients and paleo-surface temperatures employed in these reconstructions are listed in the caption to Figure iv.

11. Based on this reconstruction, deeper Cretaceous units intersected in the **Burger J-001** well lie within the Early Mature (Oil) window while shallower units remain immature. Maturity levels in this well reflect the effects of deeper burial prior to exhumation which began in **Cenomanian-Campanian times** and is now represented by the unconformity between the Nanushuk Fm and the overlying Quaternary section.

12. Active maturation from any potential source rocks within deeper Cretaceous units ceased at 80 Ma at the onset of cooling due to exhumation (although any time between 99 and 80 Ma is allowed by the AFTA and VR data from this well)..

13. Reprocessed AFTA data in the single sample from the **Burger-1** well are very similar to the data form the **Burger J-001** well and lead to very similar conclusions in regard to the underlying thermal history. We conclude that in both wells, cooling from the paleotemperatures indicated by VR data must have begun towards the earlier part of the interval represented by the Late Cretaceous-Quaternary unconformity close to sea bed in these wells.

14. Further analyses of samples from the **Burger J-001** well are unlikely to provide improved definition of the paleo-thermal history, but if sand-prone horizons are present within the Jurassic section intersected near TD in the **Burger-1** well, it is possible that further AFTA analyses in samples from those depths would provide improved insights.

15. Given the lack of consistency between the AFTA data presented here and the VR data supplied from Shell, we also recommend that additional VR analyses would be of benefit in resolving some of the remaining inconsistencies.

Table i: Paleotemperature analysis summary: AFTA and VR data from Chukchi Sea wells Burger J-001 and Burger-1 (Geotrack Report #1191)

				Pre-depositional episode 1		Pre-depositional episode 2		post-depositional episode	
Sample number	Mean depth	Strati-graphic age	Present temp-erature[*1]	Maximum paleo-temp-erature[*2]	Onset of cooling[*2]	Max'm paleo-temp.[*2]	Onset of cooling[*2]	Max'm paleo-temp.[*2]	Onset of cooling[*2]
GC1191-	(mkb)	(Ma)	(°C)	(°C)	(Ma)	(°C)	(Ma)	(°C)	(Ma)
Burger J-001									
1191-1 VR	1541	127-123	55					83	
1191-1	1541	127-123	55			>108	144-116	<120 <100 <88	Post-dep'n <100 <75
1191-2&3	1714.5	134-123	61	***Old ages*** >106	337-250	***Young ages*** >107	178 -118	***Young ages*** 75-102 ***Old ages*** 84-93	128-6 187-25
1191-3 VR	1716	134-123	61					88	
1191-4&5	1812	137-134	64	***Old ages*** >118	548-200	***Young ages*** >125	158-107	***Young ages*** <120 <100 <90 ***Old ages*** <120 <90	128-0 73-0 63-0 200-0 102-0
1191-5 VR	1823	137-134	65					99	
Burger-1									
314-23	1713	137-134	46	***Old ages*** >125 93-105	>200 401-133	***Young ages*** >127	254-165	***Young ages*** 80-99 ***Old ages*** *75-105*	106-20 *post-dep'n*
		Combined timing (Ma)[*3]			**337-250**		**254-165 144-118**		**>73**

[*1] Present temperature estimates based on a sea bed temperature of 0°C and a thermal gradient of 37°C/km derived as described in Appendix A.

[*2] Thermal history interpretation of AFTA data is based on an assumed heating rate of 1°C/Myr and a cooling rate of 10°C/Myr (see Section 2). Quoted ranges for paleotemperature and onset of cooling from AFTA correspond to ±95% confidence limits.

[*3] Assuming synchronous cooling in all samples.

Table ii: Paleogeothermal gradient estimates, Chukchi Sea well Burger J-001 (Geotrack Report #1191)

Episode	Present-day thermal gradient[*1] (°C/km)	Maximum Likelihood Estimate[*2] (°C/km)	Lower 95% confidence limit[*2] (°C/km)	Upper 95% confidence limit[*2] (°C/km)
AFTA and ERC VR data	37	36.5	7.5	65.5
VR data supplied by Shell only	37	25	18.5	31.0

[*1] Present-day thermal gradient derived as explained in Appendix A.

[*2] Paleogeothermal gradients estimated from paleotemperatures in each episode derived from AFTA and VR data, using methods described in Section 2.

Table iii: Removed section estimates: Chukchi Sea well Burger J-001 (Geotrack Report #1191)

	Estimates of removed section (metres) [*1]	
	AFTA and ERC VR data	**VR data supplied by Shell only**
Maximum Likelihood Estimate	900	2450
Lower and upper 95% confidence limits	0->10000	1700-3650
Fixed paleo-geothermal gradients		
10°C/km	*Not allowed*	*Not allowed*
20°C/km	2800-3200	3150-3550
25°C/km	1950-2150	2250-2650
30°C/km	1400-1500	1700-1900
37°C/km [*2]	**900-1000**	***Not allowed***
40°C/km	650-750	*Not allowed*
50°C/km	200-300	*Not allowed*
60°C/km	*Not allowed*	*Not allowed*

[*1] Removed section estimated with respect to the unconformity below the section presumed to be of Quaternary age, at a depth of 78.3 m rkb in this well, using an assumed paleo-surface temperature of 0°C.

[*2] Present-day thermal gradient (see Appendix A)

Notes:
Determination of the amount of removed section depends on the assumption that paleogeothermal gradients were linear through both the removed section and the preserved section, in each well. This assumption will not be valid if heating involved non-linear paleogeothermal gradients, which may result either because of vertical contrasts in thermal conductivity through the section, or if heating was not directly related to depth of burial but was due e.g. to hot fluid circulation. In such cases, the estimates quoted here are likely to over-estimate true amounts of removed section.

The quoted values are based on the assumed paleo-surface temperatures listed above. These can easily be converted to apply to other values, by subtracting or adding the difference in depth equivalent to the change in paleo-surface temperature, for the appropriate paleo-gradient. For example, for a paleogeothermal gradient of 30°C/km, a decrease of 10°C in the paleo-surface temperature is equivalent to an increase of 333 metres in the amount of removed section.

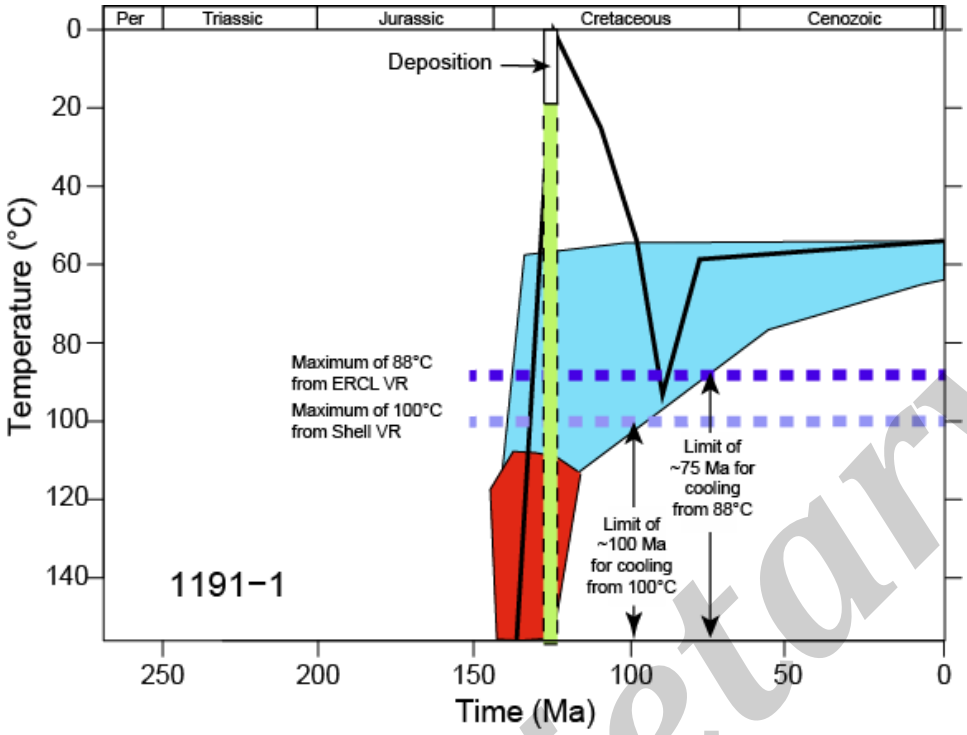

Figure i: Thermal history interpretation summary, Sample GC1191-1, **Chukchi Sea well Burger J-001**

The AFTA data define a single episode of cooling from >108°C in the interval 144 to 116 Ma which is interpreted as occurring prior to deposition in sediment provenance regions. Although the AFTA data in this sample do not require that the sample has been hotter than the present-day temperature at any time after deposition, VR suggest maximum post-depositional paleotemperatures of either 88°C (ERC data) or 100°C (Shell data). The AFTA data are consistent with post-depositional heating to 100°C only if cooling began prior to 100 Ma, while the corresponding younger limit on the onset of cooling from a maximum of 88°C is 75 Ma.

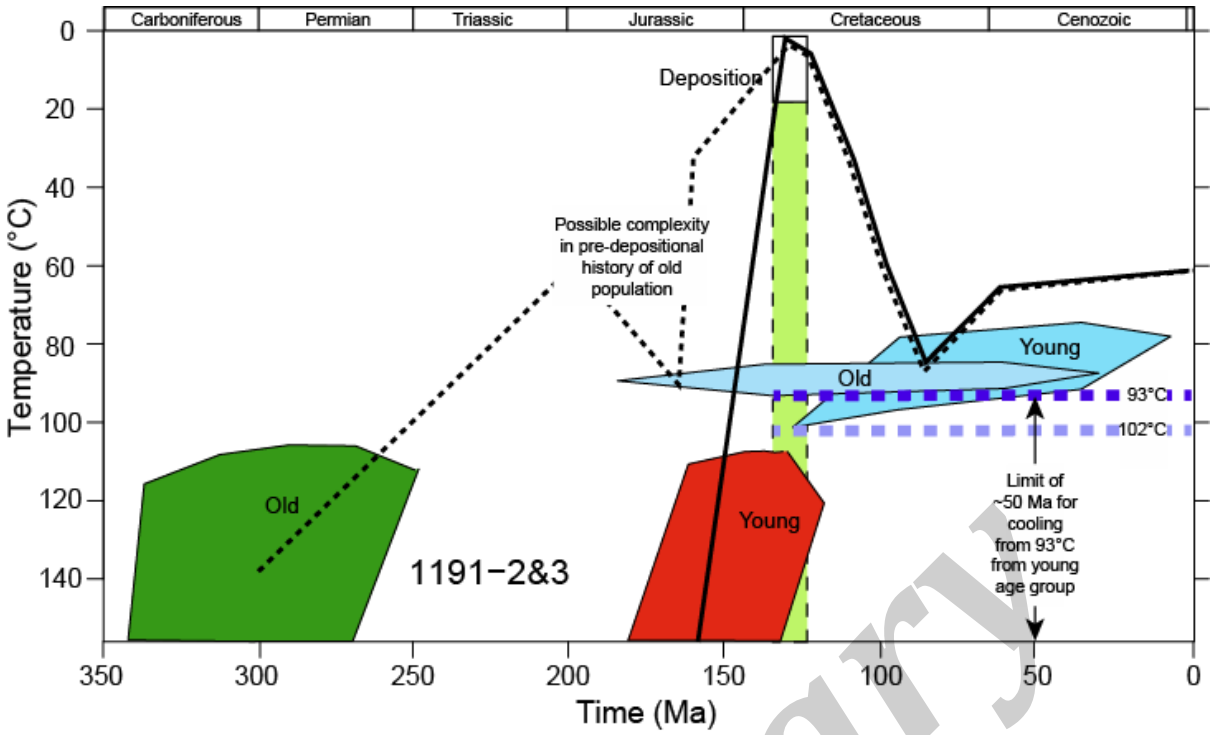

Figure ii: Thermal history interpretation summary, Composite sample GC1191-2&3, **Chukchi Sea well Burger J-001**

The AFTA data in this sample comprise two distinct age populations, one with ages close to the depositional age and one with older ages (see AFTA Data Summary Sheet, Appendix B). Data in each population can be explained by a scenario involving two paleo-thermal episodes, as shown. The onset of cooling in the earlier of two episodes defined from the young population overlaps slightly with the depositional age range at the younger limit but is interpreted as pre-depositional, while the younger episode also overlaps with the depositional age range at the older limit. Thus this episode could also represent a final phase of pre-depositional cooling, or alternatively could represent post-depositional heating and cooling. For the older population, the earlier of the two episodes is clearly pre-depositional, while the onset of cooling in the later episode again overlaps with the depositional age range and therefore this episode could either represent pre- or post-depositional cooling. VR data suggest maximum post-depositional paleotemperatures of either 93°C (ERC data) or 102°C (Shell data). The AFTA data comprising the younger age population are only just consistent with post-depositional heating to 102°C if cooling began within a few Myr after deposition, while the maximum paleotemperature of 93°C is allowed until ~50 Ma (see Figure, next page). In contrast, the age data comprising the older population are only consistent with post-depositional cooling from 93°C at the extreme limit prior to 100 Ma and are not consistent with a maximum paleotemperature of 102°C at any time after deposition. This may be due to additional complexity in the thermal history of the older age population prior to deposition, which cannot be resolved from post-depositional events. On this basis, we regard the constraint from the younger age population, showing that cooling from 93°C must have occurred prior to ~50 Ma, as the most reliable constraint on the thermal history of this sample.

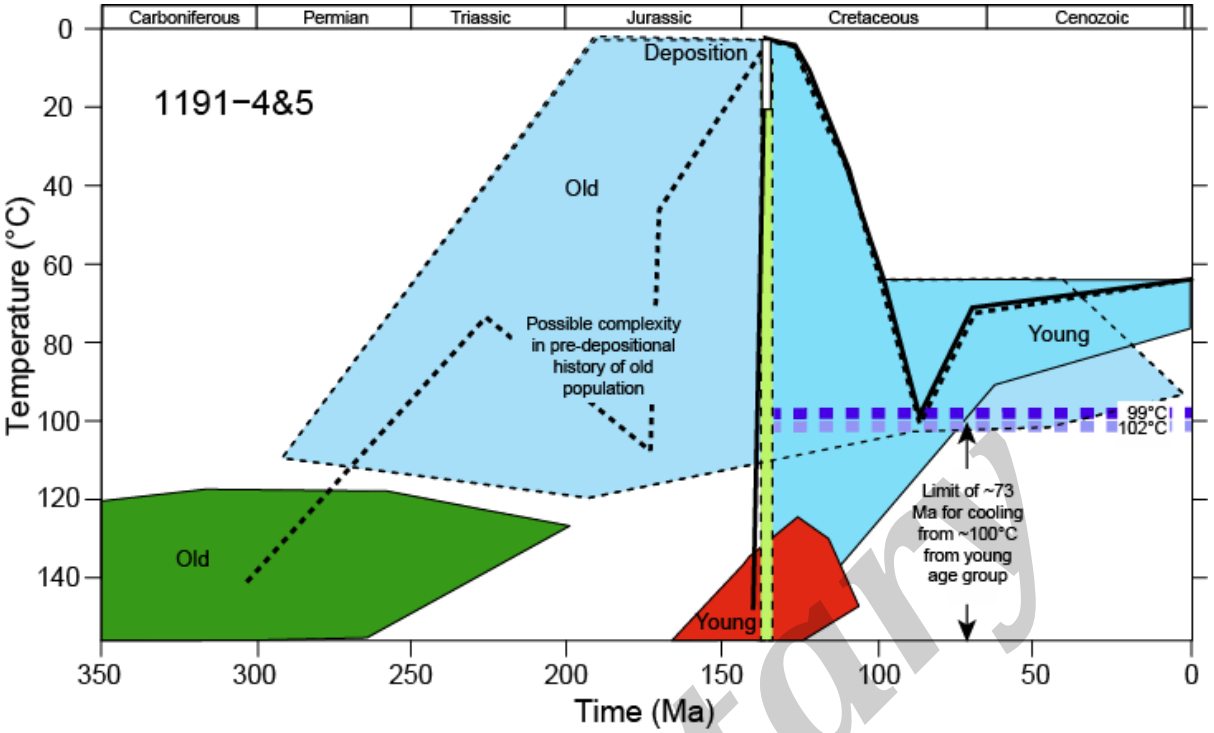

Figure iii: Thermal history interpretation summary, Composite sample GC1191-4&5, **Chukchi Sea well Burger J-001**

The AFTA data in this sample comprise two distinct age populations, a dominant group with ages close to the depositional age and a smaller group with older ages (see AFTA Data Summary Sheet, Appendix B). Data in each population can be explained by a scenario involving a single pre-depositional cooling episode combined with the Default Thermal History, i.e. the data in neither of the populations require that the sample has been hotter in the past, although this possibility is allowed within certain limits, as listed above. The onset of cooling in the single episode definitely required by data from the young population overlaps slightly with the depositional age range at the younger limit but is interpreted as pre-depositional. For the older population, the single cooling episode definitely required by the data is clearly pre-depositional. VR data suggest maximum post-depositional paleotemperatures of either 99°C (ERC data) or 102°C (Shell data). The AFTA data comprising the younger age population are consistent with post-depositional heating to 102°C if cooling began prior to 73 Ma, while the maximum paleotemperature of 99°C is allowed until slightly later. In contrast, data comprising both populations are only consistent with post-depositional cooling from 99°C or more if cooling began prior to 102 Ma. As in sample GC1173-2&3, this is probably due to additional complexity in the thermal history of the older age population prior to deposition, which cannot be resolved from post-depositional events. On this basis, we regard the constraint from the younger age population, showing that cooling from 99°C or more must have occurred prior to ~73 Ma, as the most reliable constraint on the thermal history of this sample.

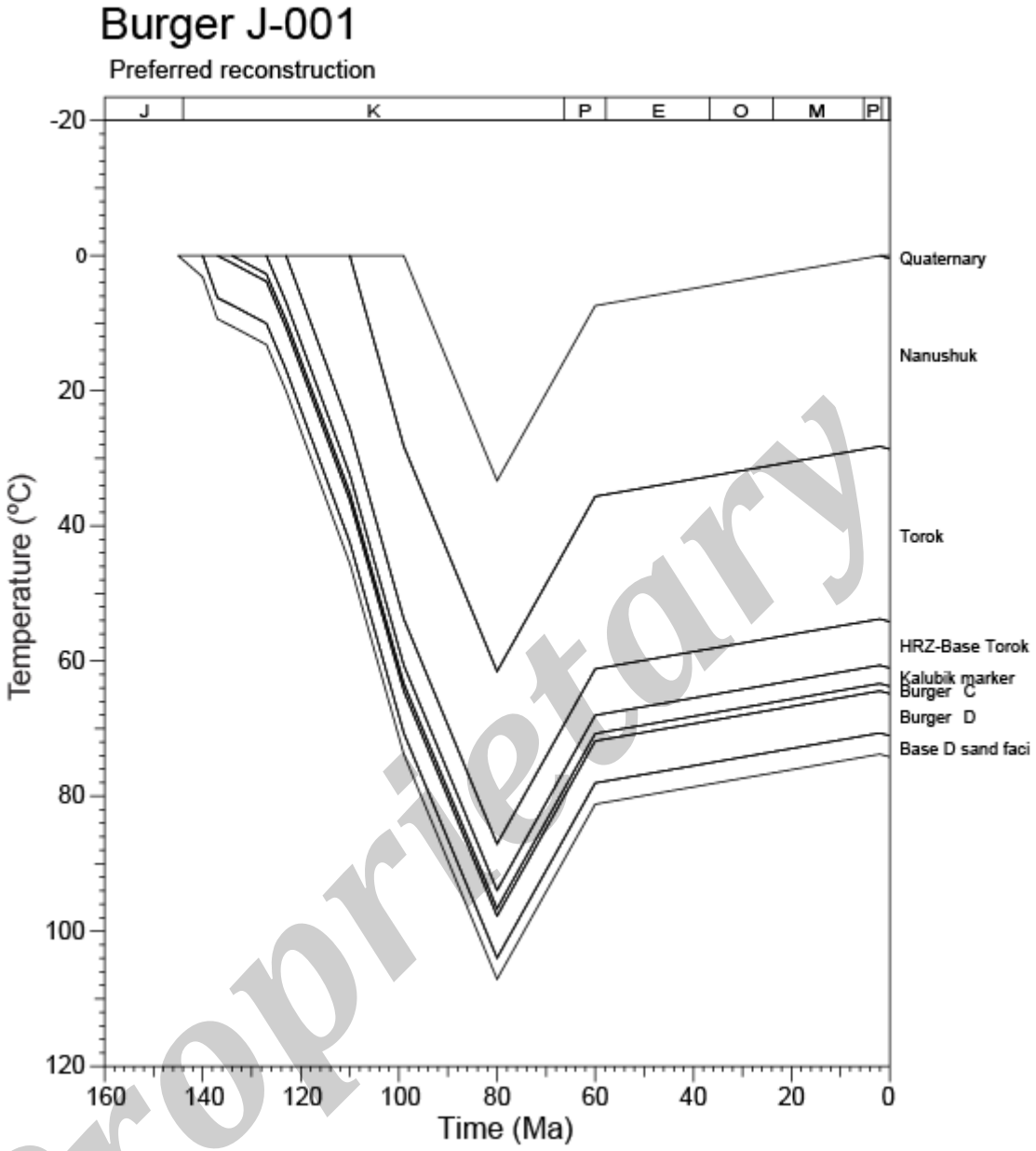

Figure iv: Preferred thermal history reconstruction derived from the interpretation of **AFTA and ERC VR data** in **Chukchi Sea well Burger J-001**.

This reconstruction is based on a constant paleogeothermal gradient of 37°C/km throughout the history, together with a constant surface temperature of 0°C, combined with the burial and uplift history shown in Figure v. Note that a range of alternative combinations of thermal gradient and removed section are equally viable, within the constraints on paleogeothermal gradients and additional burial summarised in Tables ii and iii, but all would result in thermal history reconstruction similar to that shown here, which is well constrained by AFTA and ERC VR data in this well. Note also that the two-stage cooling is not constrained by data and is employed only to ensure cooling rates from the paleo-thermal maximum are close to the value used in the interpretation of the AFTA and VR data.

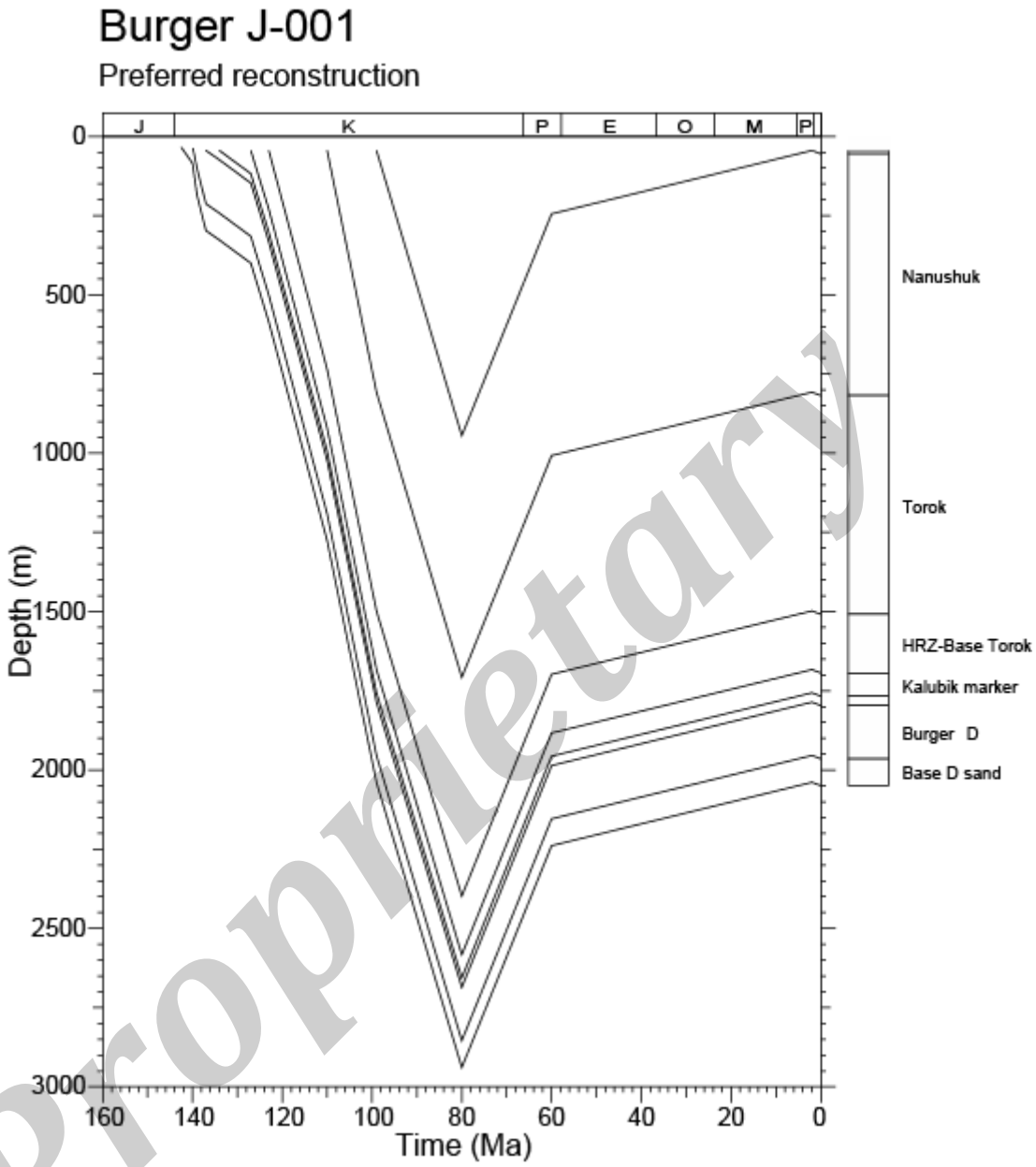

Figure v: Preferred burial and uplift history reconstruction for **Chukchi Sea well Burger J-001**, used in assembling the thermal history reconstruction illustrated in Figure iv.

Full details are provided in the text. It should be emphasised that while the timing of the onset of exhumation is reasonably well defined, based on results from this well, a range of alternative scenarios are possible as regards the amount of additional section deposited and subsequently removed, within the confines of the constraints established in Tables ii and iii. But all viable reconstructions lead to thermal history reconstructions similar to that shown in Figure iv and the resulting maturation history (Figure 5.7) is defined with confidence. Note also that the two-stage nature of cooling from the paleo-thermal and paleo-burial maximum is not constrained by the data, and is included simply to maintain initial cooling rates close to the value used in the thermal history interpretation of AFTA and VR data (see Section 4).

1. Introduction

1.1 Aims and objectives

This report describes a Thermal History Reconstruction study of **Chukchi Sea well Burger J-001** based on AFTA® (apatite fission track analysis) and vitrinite reflectance (VR) data, together with a reinterpretation of existing AFTA data in the nearby **Burger-1 well** from a previous Geotrack Study (Geotrack Report GC314 from 1991). The study was commissioned by **Shell, Houston,** and is based on new Apatite Fission Track Analysis (AFTA®) in samples of cuttings from seven depth intervals in the **Burger J-001** well, provided by Shell. VR data from the **Burger J-001** well were provided by Shell, while new VR analyses of cuttings material from three of the depth intervals provided for AFTA were also undertaken. The VR results have been integrated with the AFTA results to *identify*, *characterise* and *quantify* any episodes of heating and cooling which have affected the section intersected in these wells. This information is then synthesised to provide a regionally consistent thermal history framework, within which the history of hydrocarbon generation and structural development can be understood. Existing AFTA grain mounts for samples from the **Burger-1 well**, originally processed for Geotrack Report GC341 were reprocessed and reinterpreted for this Report. Compositions of all apatite analysed as part of this study were measured by electron microprobe. This Report was completed in June 2016

The primary aim of this study was to provide a thermal history framework in order to constrain the history of hydrocarbon generation and structural development in the region. Specific objectives were to investigate the magnitude and timing of possible paleo-thermal events which may have affected the section intersected in each well, to determine likely mechanisms of heating and cooling, to constrain paleogeothermal gradients and amounts of section removed as a result of uplift and erosion, and to use this information to reconstruct a more complete thermal and burial/uplift history for the sedimentary section in the well.

Details of all AFTA samples are summarised in Table A.1 (Appendix A), together with apatite yields. Details of samples in which VR analyses were obtained, together with analytical results, are presented in Table D.2 (Appendix D). These analyses were undertaken by Paddy Ranasinghe, Principal Organic Petrologist, Energy Resources Consulting Ltd, Wollongong, NSW. Paddy was for many years principal analyst for Keiraville Konsultants, and the techniques employed are the same as

those used for many years by Keiraville Konsultants in previous Geotrack studies. VR data provided by Shell are summarised in Table D.3.

The basic approach adopted for this study involves application of AFTA to determine the magnitude of maximum paleotemperatures in individual samples, and the time at which each sample began to cool from the paleo-thermal maximum. VR data also provide independent estimates of maximum paleotemperatures, the timing of which can be interpreted on the basis of information provided by AFTA. This information is then synthesised to define the timing of any episodes of heating and cooling that have affected the section intersected in the well. The variation of paleotemperature with depth in individual paleo-thermal episodes is used to constrain paleogeothermal gradients, and to characterise the mechanisms of heating and cooling in each episode. Where appropriate, extrapolation of paleogeothermal gradients to assumed paleo-surface temperatures allows estimation of amounts of section removed by uplift and erosion. These results are then integrated into a coherent thermal history framework, which provides a basis for understanding tectonic and maturation histories in the region.

1.2 Report structure

The main conclusions of this report are provided in the Executive Summary. A summary of the thermal history interpretation of AFTA and VR data in individual samples from the **Burger J-001** and **Burger-1** wells is provided in Table i. Table ii summarises constraints on paleogeothermal gradients derived from the AFTA and VR data in the **Burger J-001** well, while Table iii summarises corresponding constraints on amounts of removed section in individual paleo-thermal episodes. Figure i provides schematic illustrations of the thermal history interpretation of AFTA data in individual samples from the **Burger J-001** well, while Figure ii illustrates the variation of paleotemperature with depth in the well defined from AFTA and VR data. Figure iii summarises the preferred thermal history reconstruction for the **Burger J-001** well, based on AFTA and VR data discussed in this report. Reinterpretation of AFTA and VR data from the **Burger-1** well suggests a very similar history for that well.

Introductory aspects of the report are dealt with in Section 1, including comments on data quality. Section 2 briefly explains the principles of interpretation of AFTA (also see Appendix C) and VR data, use of the resulting paleotemperatures to determine paleogeothermal gradients, and how this information can be used (with some

caveats) to estimate amounts of eroded section. In Section 3, AFTA and VR data from the **Burger J-001** well are presented, while Section 4 discusses the thermal history constraints that can be extracted from these data, with Tables and Figures summarising relevant aspects of the results. These constraints are then synthesised to identify and characterise the major paleo-thermal episodes that have affected the section intersected in the wells. Section 5 provides definition of the range of allowed paleogeothermal gradients and corresponding amount of additional section required to explain the observed paleotemperatures. This information is then synthesised to provide reconstructions of the thermal, burial/uplift and hydrocarbon generation histories for the well. Finally the implications regarding regional hydrocarbon prospectivity are briefly discussed. In Sections 6 and 7, reprocessed AFTA data from the **Burger-1 well** (originally analysed in Geotrack Report GC341) are presented, together with VR data provided by Shell. These data are then integarated and compared with the results from the Burger J-001 well. Finally Section 8 provides a discussion of remaining points of uncertainty, together with some suggestions for future work which might resolve these issues.

Supporting information and data are provided in five Appendices (A, B, C, D and E). Details of all AFTA samples are presented in Table A.1 (Appendix A). This Table also contains information on the yields and quality of detrital apatite obtained after mineral separation. Sample preparation and analytical procedures for AFTA are described in Appendix B, followed by the presentation of all AFTA data, including raw track counts, fission track ages and the chlorine contents of dated grains. Appendix C outlines the principles employed in interpreting the AFTA data in terms of thermal history. The VR analyses carried out for this report are described in Appendix D, together with sample details and full details of all results. Appendix D also discusses the principles involved in integrating AFTA and VR data to provide coherent thermal history interpretations. Appendix E contains electron microprobe analyses of apatite compositions for all grains in which fission track ages and/or track lengths were measured for this study.

1.3 Data quality

AFTA data

Apatite yields from the seven samples initially provided for AFTA from the **Burger J-001** well were varied, as summarised in Table A.1 (Appendix A). Excellent yields were obtained in two samples and Fair to Good yields in three samples, while two

samples failed to yield any apatite suitable for analysis. Because many of the samples were collected over a relatively narrow depth range, and because the section over this range varies only slightly in depositional age, AFTA data in samples GC1191-2 and -3 were combined into a single sample, termed GC1191-2&3, and data in samples GC1191-4 and -5 were combined into sample GC1191-4&5. This resulted in three samples providing high quality data, with over 20 single grain ages and between 25 and 63 confined track lengths. In all samples the apatite grains that were recovered were of high quality, and the resulting thermal history constraints are regarded as highly reliable, within the stated uncertainty limits.

The single sample reprocessed from the previous study described in Geotrack Report GC314 represents a similar composite sample of three separate samples initially provided for analysis. With ages determined in 26 grains and 61 confined track lengths these data are also of high quality.

VR data

The quality of the new vitrinite reflectance analyses carried out for this report is very high, with suitable lithologies for organic maturity studies being identified in all samples. Analysis of 25 fields is the usual "target", considered desirable for an analysis of the highest quality, and this was achieved in all three samples analysed from the **Burger J-001** well (Table D.2). The analyses are therefore considered to provide highly reliable indications of maturity levels in the wells. Note that the method by which these analyses are carried out, based on petrographic identification of indigenous vitrinite within polished thick sections (Appendix D), provides additional confidence in the measurements.

No information was provided on analytical techniques employed in determining the VR values provided by Shell. On the basis of the numbers of measurements involved in each determination (Table D.3) these values should also be regarded as reliable. However, comparison of the two VR datasets suggests some systematic differences and AFTA data suggest that the VR values provided by Shell are slightly too high (see Section 3.3 for details).

1.4 Apatite Compositions

The annealing kinetics of fission tracks in apatite are affected by chemical composition, specifically the Cl content, as explained in more detail in Appendix C. For this study, chlorine compositions were determined for all individual apatite

grains analysed for this study (i.e. all grains in which fission track ages were determined and/or lengths were measured). Knowledge of chlorine contents is essential in interpreting AFTA data, and provides both improved accuracy and precision in establishing the time and magnitude of thermal events.

The measured ranges of chlorine contents of dated grains and/or grains used for confined track length measurements are shown in histogram format in the Fission Track Age Data Sheets at the end of Appendix B. Table B.3 (Appendix B) contains single grain fission track age and track length data collected into discrete compositional groups, on the basis of the chlorine contents of the grains from which the data were derived. In addition, plots of single grain age versus weight % chlorine are shown in the Fission Track Age Data Sheets, which also list the chlorine contents of individual age grains.

2. Interpretation strategy

2.1 Thermal history interpretation of AFTA data

Basic principles

Interpretation of AFTA data in this report begins by assessing whether the fission track age and track length data in each sample could have been produced if the sample has never been hotter than its present temperature at any time since deposition. To this end, we consider a "Default Thermal History" for each sample, which forms the basis of interpretation. Default Thermal Histories throughout a well are derived from the stratigraphy of the preserved sedimentary section, combined with constant values for paleogeothermal gradient and paleo-surface temperature which are adopted from present-day values. For outcrop samples, the Default Thermal Histories simply represent long-term residence at the prevailing surface temperature.

Using this history, AFTA parameters are predicted for each sample. If the measured data show a greater degree of fission track annealing (in terms of either fission track age reduction or track length reduction) than expected on the basis of this history, the sample must have been hotter at some time in the past. In this case, the AFTA data are analysed to provide estimates of the magnitude of the maximum paleotemperature in that sample, and the timing of cooling from the thermal maximum. Using proprietary in-house software, for each sample we compare the pattern of AFTA parameters (fission track age and track length distribution and their variation with wt% Cl) predicted from a variety of thermal history scenarios with the measured data in order to define the range of values of maximum paleotemperature and the onset of cooling from the paleotemperature which provide a consistent match to the data within 95% confidence limits. Each sample is initially treated independently. Then by comparing results in all samples we seek to identify the minimum number of regional events that can account for all of the results.

Because of the possible presence of tracks inherited from sediment source terrains, it is possible that track length data might show definite evidence that the sample has been hotter in the past (since deposition) while fission track ages are still greater than predicted from the Default Thermal History (which only refers to tracks formed after deposition). Similarly in samples in which all or most fission tracks were totally annealed in a paleo-thermal episode, and which have subsequently been cooled and then reburied, fission track age data might show clear evidence of exposure to higher

temperatures in the past while track length data may be dominated by the present-day thermal regime and will not directly reveal the paleo-thermal effects. In circumstances such as these, evidence from either track length or fission track age data alone is sufficient to establish that a sample has been hotter in the past.

As AFTA data provide no information on the *approach* to a thermal maximum, they cannot independently constrain the heating rate and a value must therefore be assumed in order to interpret the data. The resulting paleotemperature estimates are therefore conditional on this assumed value. AFTA data do provide some control on the history after cooling from maximum paleotemperatures, through the lengths of tracks formed during this period.

Data from each sample are normally interpreted in terms of one or two episodes of heating and cooling, using assumed heating and cooling rates during each episode. The maximum paleotemperature is assumed to be reached during the earlier episode. The timing of the onset of cooling and the peak paleotemperatures during the two episodes are varied systematically, and by comparing predicted and measured parameters the range of conditions which are compatible with the data can be defined. One additional episode during the cooling history is the limit of resolution from typical AFTA data. Alternatively, if the data can be explained by a single episode of heating and cooling, then a heating rate is assumed and the range of values of maximum paleotemperature and the time of cooling is defined as before. In some cases, resolution of three episodes may be possible.

If AFTA data show a lower degree of fission track annealing (age and/or length reduction) than expected on the basis of the Default Thermal History, this either suggests present temperatures may be overestimated or temperatures have increased very recently. In such cases, the data may allow a more realistic estimate of the present temperature, or an estimate of the time over which temperatures have increased.

AFTA data are predicted using a multi-compositional kinetic model for fission track annealing in apatite developed by Geotrack, described in more detail in Appendix C.

Specific to this report

For all samples analysed for this report, chlorine content has been determined in every apatite grain analysed (i.e., for both fission track age and track length measurement), as explained in more detail in Appendix A. For rigorous thermal

history interpretation the age and length data have been grouped into 0.1 wt% Cl divisions (see Table B.3, Appendix B).

In this report, AFTA data in all samples have been interpreted using heating rates of 1°C/Myr and cooling rates of 10°C/Myr. These values are assumed arbitrarily, and all paleotemperature estimates are conditional on the assumed rates. For the kinetics characterising both AFTA and VR, increasing or decreasing heating rates by an order of magnitude is equivalent to raising or lowering the required maximum paleotemperature by about 10°C.

2.2 Thermal history interpretation of VR data

Basic principles

Interpretation of VR data follows similar principles to those used in interpreting the AFTA data (Section 2.1). If a measured VR value is higher than the value predicted from the Default Thermal History (making due allowance for analytical uncertainty), the sample must have been hotter at some time in the past. In this case, VR data provide an independent estimate of maximum paleotemperature, which can be calculated using an assumed heating rate and timing information provided from AFTA data, if available (assumed, otherwise). Cooling rates do not significantly affect VR data, which are dominated by the maximum paleotemperature provided that cooling occurs immediately after reaching the thermal maximum. If both AFTA and VR data are available from the same sample or well, then an identical heating rate must be used to obtain consistent paleotemperature estimates.

If a measured VR value is lower than expected on the basis of the Default Thermal History, either present temperatures may have been overestimated or temperatures have increased very recently. In such cases, the measured VR value may allow an estimate of the true present-day temperature. Alternatively the measured VR value may underestimate the true maturity for some other reason, e.g., suppression of reflectance in certain organic macerals, misidentification of true "in-situ" vitrinite, presence of caved material etc. Comparison of AFTA and VR data usually allows such factors to be identified, and where applicable they are discussed in the relevant section of text.

Vitrinite reflectance data (specifically $R_o$max values) are predicted using the distributed activation energy model describing the evolution of VR, with temperature

and time developed by Burnham and Sweeney (1989) (see also Sweeney and Burnham, 1990).

Values of VR less than ~0.3% and greater than 4% cannot be assigned to a specific maximum paleotemperature with confidence, and such values are given maximum and minimum limits, respectively, appropriate to the particular heating rate used (see Appendix D). Further discussion of the methodology employed in interpreting VR data are given in Appendix D, which also briefly discusses the benefits of integrating AFTA and VR data.

Specific to this report

For this report, VR data in all samples have been interpreted using heating and cooling rates of 1 and 10°C/Myr (respectively), for consistency with interpretation of the AFTA data, as specified in Section 2.1.

Maximum paleotemperatures determined for the VR samples are attributed to one of the paleo-thermal episodes identified by AFTA on the basis of comparison of the VR-derived maximum paleotemperature with observed paleo-heating of a similar style in adjacent AFTA samples.

2.3 Comparison of paleotemperature estimates from AFTA and VR

Maximum paleotemperatures derived from AFTA and VR ($R_o$max) using the strategies outlined above are usually highly consistent. Estimates of maximum paleotemperature from AFTA (Table i) are often quoted in terms of a range of paleotemperatures, as the data can often be explained by a variety of scenarios. Paleotemperature estimates from VR (Table i) are usually quoted to the nearest degree Celsius, as the value which predicts the exact measured reflectance. This is not meant to imply VR data can be used to estimate paleotemperatures to this degree of precision. VR data from individual samples typically show a scatter equivalent to a range of between ±5 and ±10°C. Estimates from a series of samples are normally used to define a paleotemperature profile in samples from a well, or a regional trend in paleotemperatures from outcrop samples.

2.4 Estimates of paleogeothermal gradients and mechanisms of heating and cooling

Basic principles

A series of paleotemperature estimates from AFTA and/or VR over a range of depths can be used to reconstruct a paleotemperature profile through the preserved section. The slope of this profile defines the paleogeothermal gradient. As explained by Bray et al. (1992) and Green et al. (2002), and as illustrated in Figure 2.1, the shape of the paleotemperature profile and the magnitude of the paleogeothermal gradient provides unique insights into the origin and nature of the heating and cooling episodes expressed in the observed paleotemperatures.

Linear paleotemperature profiles with paleogeothermal gradients close to the present-day geothermal gradient provide strong evidence that heating was caused by greater depth of burial with no significant increase in basal heat flow, implying in turn that cooling was due to uplift and erosion. Paleogeothermal gradients significantly higher than the present-day geothermal gradient suggest that heating was due, at least in part, to increased basal heat flow, while a component of deeper burial may also be important as discussed in the next section. Paleogeothermal gradients significantly lower than the present-day geothermal gradient suggest that a simple conductive model is inappropriate, and more complex mechanisms must be sought for the observed heating. One common cause of low paleogeothermal gradients is transport of hot fluids shallow in the section. However the presence of large thicknesses of sediment with uniform lithology dominated by high thermal conductivities can produce similar paleotemperature profiles and each case has to be considered individually (Figure 2.2).

A paleotemperature profile can only be characterised by a single value of paleogeothermal gradient when the profile is linear. Departures from linearity may occur where strong contrasts in thermal conductivities occur within the section, or where hot fluid movement or intrusive bodies have produced localised heating effects. In such cases a single value of paleogeothermal gradient cannot be calculated, and different values (possibly negative) may apply through different parts of the section. However it is important to recognise that the validity of the paleotemperatures determined from AFTA and/or VR are independent of these considerations, and can still be used to control possible thermal history models.

Estimation of paleogeothermal gradients in this report

Paleogeothermal gradients for this report have been estimated from paleotemperature estimates over a range of depths using methods outlined in Appendix C. These methods provide a best estimate of the gradient ("maximum likelihood value") and upper and lower 95% confidence limits on this estimate (analogous to ±2σ limits). The "goodness of fit" is displayed in the form of a log-likelihood profile, which is expected to show good quadratic behaviour for a dataset which agrees with a linear profile. This analysis depends on the assumption that the paleogeothermal gradient through the preserved section is linear. Visual inspection is usually sufficient to confirm or reject this assumption.

2.5 Determination of removed section

Basic principles

Subject to a number of important assumptions, extrapolation of a linear paleotemperature profile to a paleo-surface temperature allows estimation of the amount of eroded section represented by an unconformity, as illustrated in Figure 2.3 (also see Section C.9, Appendix C).

Specifically, this analysis assumes:

- The paleotemperature profile through the preserved section is linear
- The paleogeothermal gradient through the preserved section can be extrapolated linearly through the missing section.
- The paleo-surface temperature is known.
- The heating rate used to estimate the paleotemperatures defining the paleogeothermal gradient is correct

It is important to realise that any method of determining the amount of eroded section based on thermal methods is subject to these and/or additional assumptions. For example methods based on heat-flow modelling must assume values of thermal conductivities in the eroded section, which can never be known with confidence. Such models also require some initial assumption of the amount of eroded section to allow for the effect of compaction on thermal conductivity. Methods based on geothermal gradients, as used in this study, are unaffected by this consideration, and can therefore provide independent estimates of the amount of eroded section. But

these estimates are always subject to the assumptions set out above, and should be considered with this in mind.

The analysis used to estimate paleogeothermal gradients is easily extended to provide maximum likelihood values of eroded section for an assumed paleo-surface temperature, together with ±95% confidence limits. These parameters are quoted for each well in which the paleotemperature profile suggests that heating may have been due, at least in part, to deeper burial.

Estimates of paleogeothermal gradient and eroded section derived from fitting linear profiles to paleotemperature data as a function of depth are highly correlated, since the profile is constrained to pass through the main body of the data. Thus, higher paleo-gradients within the allowed range correspond to lower amounts of section removed, while lower paleo-gradients correspond to higher amounts of removed section. In plots of paleogeothermal gradient against removed section, paired values of each parameter which are consistent with the paleotemperature data can be defined, thus allowing the range of allowed values at various levels of statistical significance to be contoured. In general, the greater the depth interval over which paleotemperature constraints are available, the tighter the resulting constraints on both the paleogeothermal gradient and the amount of removed section.

However, it is emphasised that reconstructed burial histories produced in this way do not produce unique solutions, and alternative interpretations are always possible. For instance, where the eroded section was dominated by units with high thermal conductivities the paleogeothermal gradient through the missing section may have been much higher than in the preserved section, and extrapolation of a linear gradient will lead to overestimation of the eroded section.

Specific to this report

For the well analysed in this report, estimates of eroded section are conditional on:

- Heating rates of 1°C/Myr and cooling rates of 10°C/Myr in each episode, and
- Paleo-surface temperatures as specified in later Sections

as well as the other assumptions outlined above.

The effects of higher paleo-surface temperatures can be simply allowed for by subtracting the depth increment corresponding to the increase in temperature, for the appropriate value of paleogeothermal gradient. For instance, if the paleogeothermal gradient was 33°C/km and the paleo-surface temperature was *10°C higher* than the

value assumed in this report, the estimated eroded section should be *reduced by 300 metres*. Different heating rates can be allowed for in similar fashion, with an order of magnitude change in heating rate equivalent to a 10°C change in paleotemperature (paleotemperatures increase for higher heating rates, and decrease for lower heating rates). For typical values, the assumed value of heating rate will not affect the shape or slope of the paleotemperature profile significantly.

Multiple exhumation episodes

In the previous discussion, it is important to emphasise that estimates of removed section derived in this way represent the total amount of sediment removed since the onset of cooling (i.e. exhumation) from the maximum (or peak) paleotemperatures from which the estimates were derived. In this sense, these estimates can be thought of as representing "paleo-burial", i.e. the amount by which the preserved section (in which the paleotemperatures were recorded) was more deeply buried, prior to the onset of the exhumation episode.

In the case of a single cooling episode, in which the additional section was fully removed prior to the onset of deposition of sediment which has been preserved to the present day, such estimates of paleo-burial are identical to the amount of removed section in that episode. In such cases, it is clear that the unconformity surface, on which the additional section was deposited, returned to the surface before the re-commencement of deposition. However, where multiple exhumation episodes occur within a relatively long interval for which no sediments are preserved, this is not necessarily true. In this case, there is no evidence to demonstrate whether the unconformity surface at the top of the now preserved section returned entirely to the surface following an initial exhumation episode (i.e. if the entire amount of additional sediment was eroded), or if only part of the additional section was eroded prior to the re-commencement of deposition (after which a later exhumation episode resulted in removal of all the additional section). This situation is summarised in Figure 2.4, in the context of an outcrop sample, although similar principles apply to well samples.

In the notional example shown in Figure 2.4, two cooling episodes are identified by AFTA (grey zones) within a time interval represented by a single unconformity. The sampled unit cooled from its maximum paleotemperature in the Early Tertiary, and subsequently cooled from a lower paleotemperature peak in the Late Tertiary. Since AFTA only records the maximum or peak paleotemperatures in each event, which provide the estimates of paleo-burial for those episodes, no information on the approach to those paleotemperatures is preserved. For this reason, although the

amount of section removed in the Late Tertiary episode, E_2, is well constrained, the amount of additional section deposited in that episode, D_2, is not. Conversely, while the total amount of section removed since the onset of Early Tertiary cooling (i.e. the Early Tertiary paleo-burial), D_1, is well constrained, the amount of section removed by erosion in the earlier exhumation episode (E_1) is not well constrained. Only for the case where the unit returned to the surface (red path) before burial re-commenced, are D_1 and E_1 equal, and E_1 is well constrained. But if sediments laid down in the mid-Tertiary are not preserved to the present-day, then no record of this return to the surface is available, and therefore the absolute magnitude of E_1 is not clear. Similar considerations apply to well samples, except that the present-day depth should be substituted for the surface.

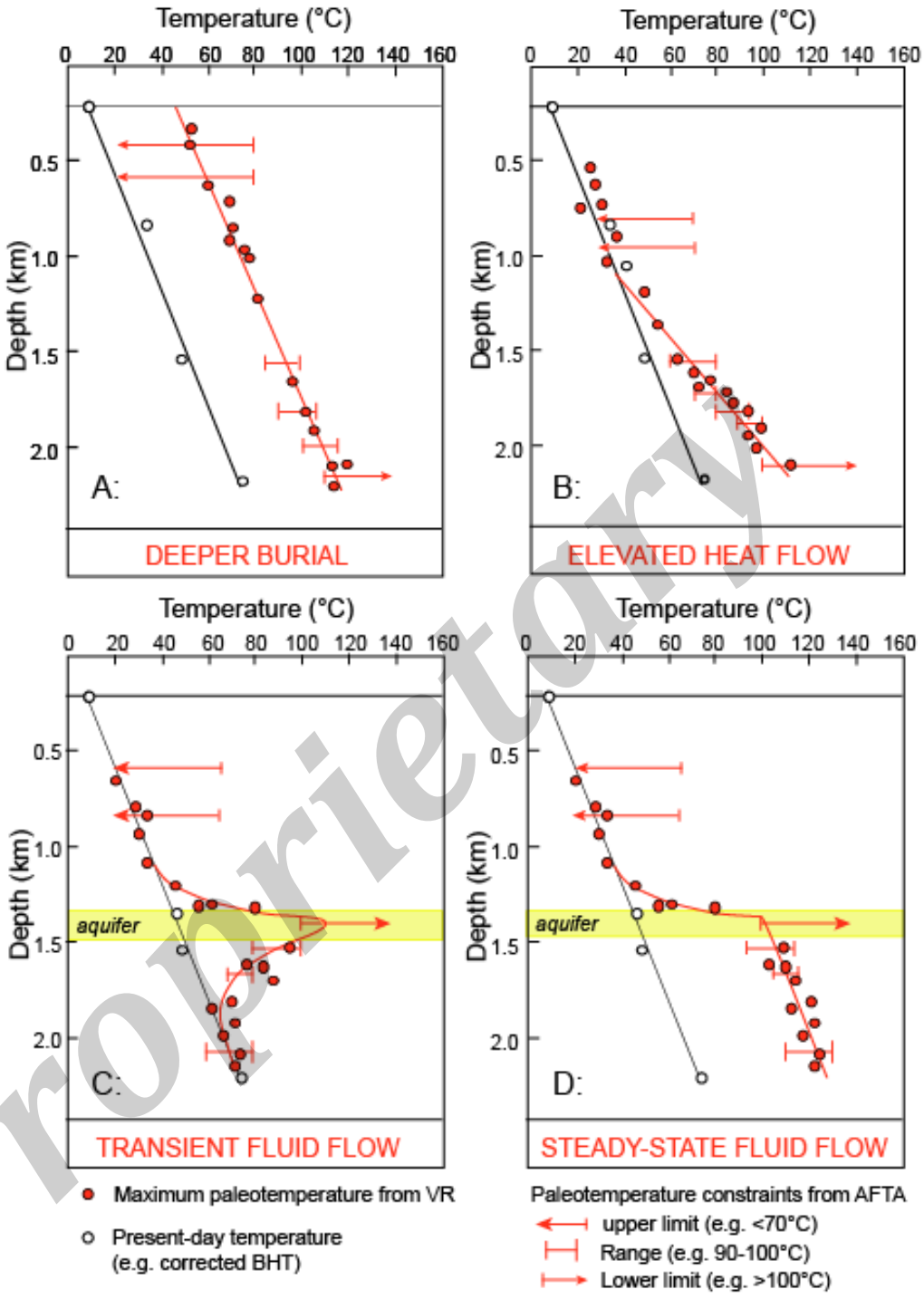

Figure 2.1: The way in which paleotemperatures characterising a particular paleo-thermal episode vary with depth, or the "paleotemperature profile", provides key information on the mechanisms of heating and cooling. Deeper burial followed by exhumation, with little or no change in basal heat flow, typically results in paleotemperatures defining a linear profile sub-parallel to the present-day thermal profile but offset to higher temperatures. Elevated heat flow results in a linear paleotemperature profile with a higher slope compared to the present-day profile. In contrast, transient hot fluid flow through a localised aquifer results in a markedly non-linear profile with a maximum centred on the aquifer, while prolonged fluid flow can result in a linear profile below the aquifer as the deeper section reaches a "steady-state" situation. Combinations of these four simple cases are possible.

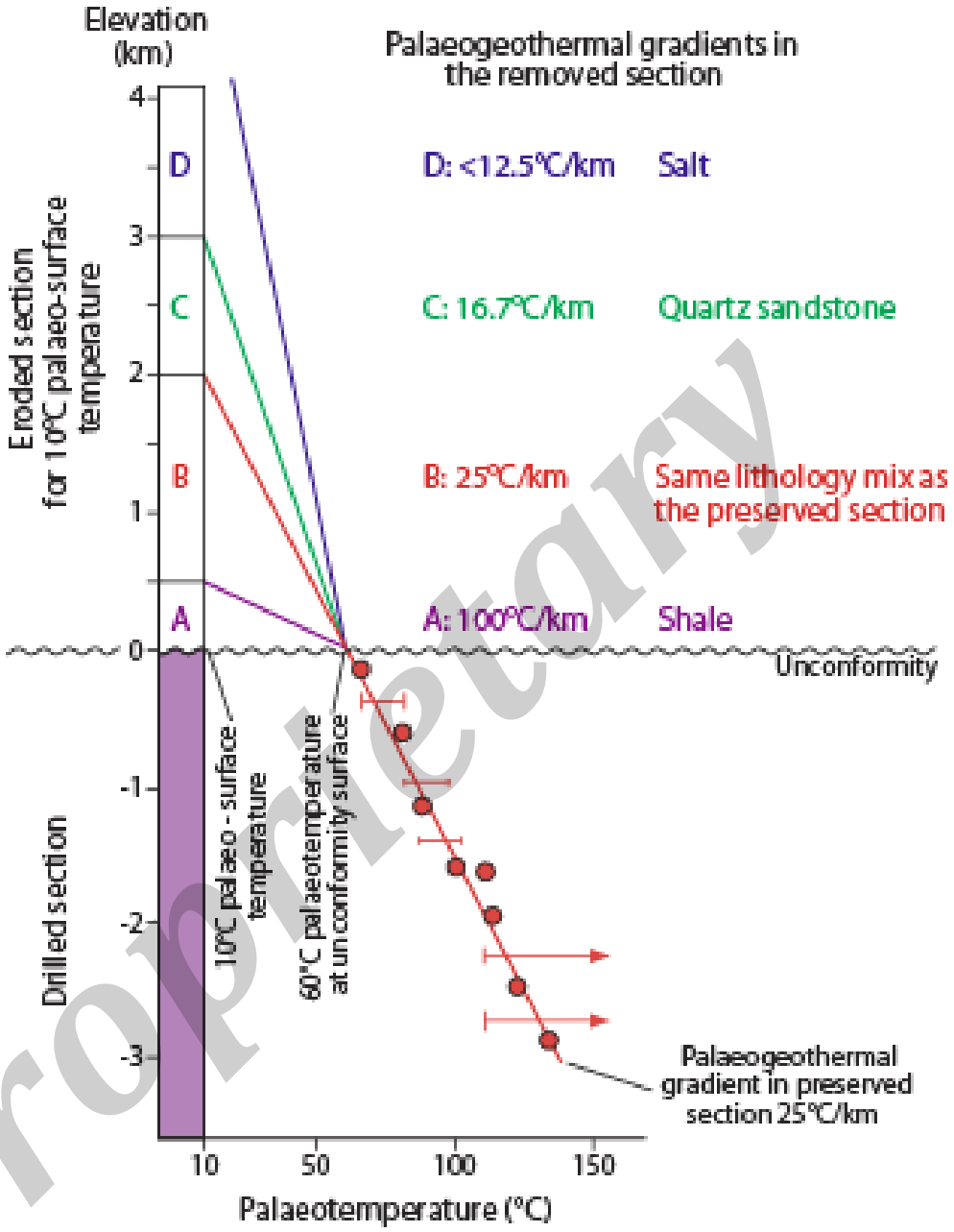

Figure 2.2: This plot illustrates the influence of the thermal conductivity of the removed section on the nature of the palaeotemperature profile through that part of the section. Only where the removed and preserved sections are identical will the thermal gradient be the same throughout the entire section, but in practise the assumption of linearity appears to give reliable results (see text).

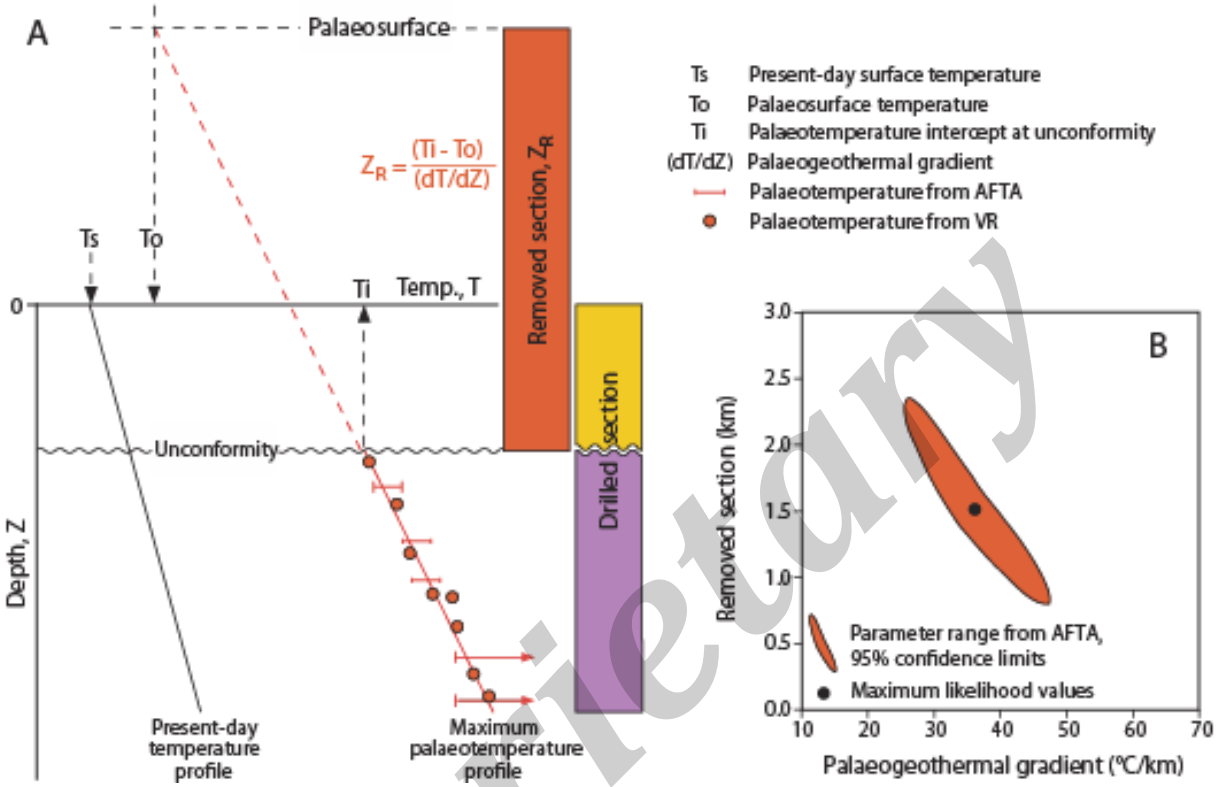

Figure 2.3: Where heating was due to deeper burial, possibly combined with elevated heat flow, amounts of exhumation (or deeper burial) can be estimated by fitting a linear palaeogeothermal gradient to a series of down-hole palaeotemperature constraints and then extrapolating to an assumed palaeo-surface temperature, as shown in A. This approach depends critically on certain assumptions, as discussed in the text. Higher gradients extrapolate to lower values of removed section, while lower gradients correspond to larger amounts of removed section. Statistical analysis allows definition of the range of allowed values of palaeogeothermal gradient and removed section within 95% confidence limits, typically represented by a hyperbolic ellipsoid, as shown in B.

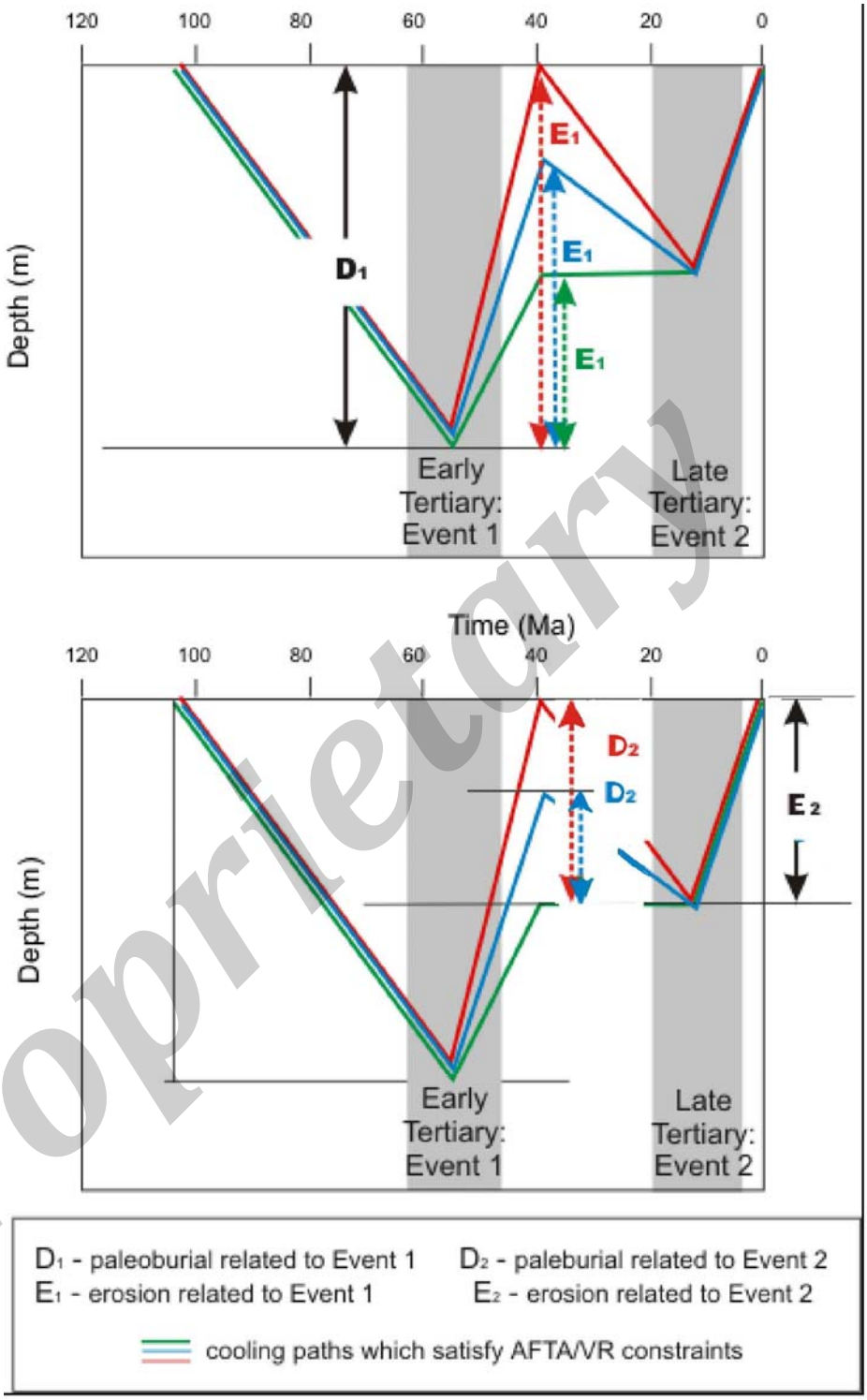

Figure 2.4: Where multiple exhumation episodes occur within an interval represented by a single unconformity, it is not possible to determine the total amount of section removed during the earlier exhumation episode, only the total amount removed between the onset of cooling in that episode and the present day. In this example, E_2 is uniquely defined by the total section removed during the later episode, while D_1 is uniquely defined by the total amount of additional burial required to explain the paleotemperatures in the earlier episode. But E_1 and D_2 are not uniquely defined.

3. AFTA and VR data in samples from Chukchi Sea well Burger J-001

3.1 Geological background

The Burger J-001 well intersected around 10 m of section of unspecified age (assigned a Quaternary age here), unconformably overlying an Early Cretaceous sequence including Nanushuk, Torok, and Burger Formations, reaching TD at 2072.6 m (rkb) in "Burger D Sand facies". The detailed breakdown of this early Cretaceous section is summarised in Table A.1 (conversion to numerical ages is based on Gradstein et al., 2012).

Present temperatures derived at two depths in the well were provided by the client. Together with a sea bed temperature of 0°C, these define a present-day thermal gradient of 37°C/km, which we have used to describe the present-day thermal regime in this well (Table A.3, Appendix A). The AFTA data in each sample are consistent with present-day temperatures calculated in this fashion, although due to the relatively shallow depths of samples analysed from this well, present-day temperatures do not exert any significant influence on the interpretation of the data. Therefore we have adopted the gradient of 37°C/km as the basis of thermal history interpretation of the AFTA and VR data in the **Burger J-001** well.

3.2 Initial assessment of AFTA data

Introduction

For this study, cuttings from seven depth intervals in this well were provided for AFTA. As described in Section 1.3, yields of apatite obtained from the samples were varied, with only one of the seven original samples providing an excellent yield. Because samples GC1191-2, -3, 4 and -5 were all collected within a depth interval of just over 100 metres, data from samples GC1191-2 and -3 were composited in to a single samples referred to as GC1191-2&3, while data from samples GC1191-4 and -5 were similarly composited into sample GC1191-4&5. This process resulted in data for three depth intervals characterised by fission track ages in over 20 single grain ages and a reasonable number of track lengths, capable of providing reliable thermal history constraints.

Fission track ages and mean track lengths in samples analysed from this well are summarised in Table 3.1 and plotted as a function of depth and present temperature

in Figure 3.1, where the fission track age data are contrasted with the variation of stratigraphic age through the section. The variation of fission track age and length vs depth predicted from the Default Thermal History (see Section 2.1) for this well are also shown in Figure 3.1, for selected apatite chlorine contents. Mean values predicted from the Default Thermal History for each sample are also summarised in Table 3.1. These values take explicit account of the distribution of wt% Cl within each sample. The Default Thermal History used in construction of Figures 3.1 and 3.2 is based on the burial history derived from the preserved stratigraphy in the well, illustrated in Figure 3.3, combined with the present-day thermal gradient of 37°C/km derived as explained in Appendix A.

Data for composite samples GC1191-2&3 and GC1191-4&5 are also listed in Table 3.1 and plotted together with data from sample GC1191-1 in Figure 3.2. Discussion of the AFTA data and the resulting thermal history interpretation from this point is focussed on the data in this form.

Visual assessment of the data in Figure 3.2 shows that the measured fission track ages in samples GC1191-1 and GC1191-4&5 are close to the values predicted from the Default Thermal History, as also are the mean track lengths. This indicates that any effects of post-depositional heating to temperatures higher than present-day values are subtle and detailed assessment is required before firm conclusions can be reached. The fission track age of composite sample GC1191-2&3 is older than predicted from the Default Thermal History, and while the mean track length is shorter than expected on this basis this could be due to the presence of shorter tracks inherited from sediment provenance regions. In summary, an initial assessment of the AFTA data from this well shows no clear evidence to suggest that any of these samples has ever been hotter than present-day temperatures at any time since deposition. However, more detailed assessment is required before firm conclusions can be reached. This assessment is presented in Section 4.

3.3 Initial assessment of VR data

Introduction

VR data in samples from nine depth intervals in the well provided by the client are summarised in Table D.3. In addition, new VR analyses were undertaken for this study on material from three of the original AFTA sample intervals. These analyses were performed by Paddy Ranasinghe of Energy Resources Consulting Pty Ltd,

Wollongong, NSW, and results are summarised in Table D.2 (Appendix D), while detailed maceral descriptions and histograms of reflectance measurements in each sample, together with a discussion of the results from this well, are also presented in Appendix D.

Both sets of VR datasets appear to be of high quality. Of the new analyses, 25 measurements (the usual "target" for data of the highest quality) were possible in all three samples. The supplied data are also characterised by between 14 and 36 measurements, although no information on these analyses is available.

Both sets of VR values are plotted against depth in Figure 3.4. A small but systematic difference is evident between the two datasets, with the data provided by the client being consistently around 0.05 to 0.08% higher than the three values determined for this Study. Also shown in Figure 3.4 is the maturity profile predicted from the Default Thermal History - i.e., the thermal history predicted for samples from this well if they are currently at their maximum post-depositional temperatures, as defined in Section 2.1 of this report. The Default Thermal History used in construction of Figure 3.4 is based on the present-day thermal gradient of 37°C/km derived as explained in Appendix A, combined with the burial history derived from the preserved stratigraphy in the wells, illustrated in Figure 3.3.

Evidence that samples have been hotter in the past

All of the measured VR values plot well above the profile predicted from the Default Thermal History in Figure 3.4. This shows clearly that the sampled sedimentary units have been hotter in the past, despite the lack of such evidence in the AFTA data (Section 3.2). Therefore, the elevated paleotemperatures responsible for producing the observed VR levels must have been reached in such a way that the effects on the AFTA data are not immediately apparent.

Magnitude of paleotemperatures from VR

Maximum paleotemperatures derived from the measured VR values in this well, calculated using the strategy outlined in Section 2.2, are summarised in Table 3.2. Values increase with depth from around 66°C in the shallowest samples to 106°C in the deepest sample, over a depth range of ~1.5 km.

In Section 4, the AFTA data are assessed in detail in the light of the maximum paleotemperatures indicated by these VR data.

Table 3.1: Summary of apatite fission track data and Default Thermal History predictions in samples from Chukchi Sea well Burger J-001 (Geotrack Report #1191)

Sample number	Average depth (m)	Present temperature[*1] (°C)	Stratigraphic age (Ma)	Mean track length (µm)	Predicted mean track length[*2] (µm)	Fission track age (Ma)	Predicted fission track age[*2] (Ma)
OCS-Y-2321 Burger J 001							
GC1191-1	1541	55	127-123	12.99±0.16	12.9	111.1±5.4	108
GC1191-2	1705	61	127-123	11.27±0.58	12.5	189.8±33.4	107
GC1191-3	1716	61	134-123	11.70±0.25	12.5	142.7±15.7	108
GC1191-4	1803	64	135-134	13.29±0.51	12.3	128.8±12.1	111
GC1191-5	1823	65	137-134	12.53±0.36	12.4	103.3±14.8	113
GC1191-6	1986	71	145-137	-	-	-	-
GC1191-7	2058	74	145-140	-	-	-	-
Combined data:							
GC1191-2&3	1714.5	61	134-123	11.55±0.26	12.5	154.7±15.0	107
GC1191-4&5	1812	64	137-134	12.74±0.30	12.3	117.2±11.3	112

[*1] See Appendix A for discussion of present temperature data.

[*2] Values predicted from the Default Thermal History (Section 2.1); i.e. assuming that each sample is now at its maximum temperature since deposition. The values refer only to tracks formed after deposition. Samples may contain tracks inherited from sediment provenance areas. Calculations refer to apatites within the measured compositional range for each sample, as discussed in Appendix A. For this reason, predicted ages may not vary smoothly with depth.

Note: all depths quoted are TVD with respect to kb elevation.

Table 3.2: VR data and corresponding maximum paleotemperatures in samples from Chukchi Sea well Burger J-001 (Geotrack Report #1191)

Sample number	Average depth (m)	Present temperature[*1] (°C)	Stratigraphic Age (Ma)	VR values From ERC ($R_o$max)[*2] (%)	VR values provided by Shell[*3] (%)	Maximum paleotemp-erature[*4] (°C)
	498.5	16	110-99		0.40 (31)	66
	644.5	21	110-99		0.46 (22)	78
	992.5	34	123-110		0.46 (19)	78
	1220.5	43	123-110		0.51 (36)	84
	1431	50	123-110		0.57 (25)	94
	1531.5	54	127-110		0.61 (31)	100
GC1191-1	1541	55	127-123	0.53 25		88
	1714.5	61	134-123		0.62 (35)	102
GC1191-3	1716	61	134-123	0.56 25		93
GC1191-5	1823	65	137-134	0.60 25		99
	1921.5	69	137-136		0.68 (15)	113
	2043.5	73	145-140		0.64 (35)	106

[*1] Present temperatures calculated using a present-day thermal gradient of 37°C/km as explained in Appendix A, combined with a sea bed temperature of °C.

[*2] From Table D.2. Numbers in brackets show the numbers of vitrinite fields measured for each sample

[*3] From Table D.3. Numbers in brackets show the numbers of vitrinite fields measured for each sample

[*4] All estimates of maximum paleotemperature were determined using assumed heating and cooling rates of 1°C/Myr and 10°C/Myr, respectively.

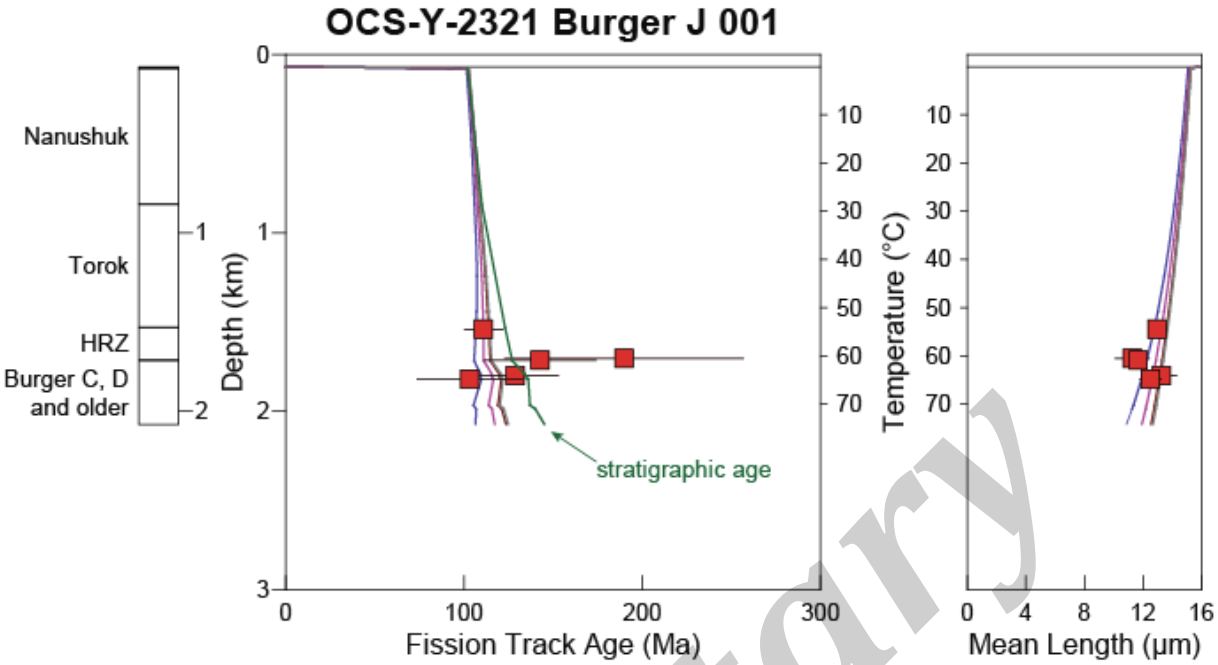

Figure 3.1: AFTA parameters in samples from **Chukchi Sea well Burger J-001**, plotted against sample depth and present temperature.

The variation of stratigraphic age with depth is also shown, as the solid green line in the central panel. Present-day temperatures shown here are based on a sea-bed temperature of 0°C and a present-day **thermal gradient of 37°C/km** for this well provided by the client (see Appendix A). Coloured lines show the pattern of fission track age and mean track length predicted from the Default Thermal History (see Section 2.1) for apatites containing 0.0-0.1, 0.4-0.5, 0.9-1.0 and 1.5-1.6 wt% Cl. The Default Thermal History is based on the thermal structure reported above, combined with the burial history shown in Figure 3.5.

Measured fission track ages and mean track lengths in the five samples analysed from this well are in most cases close to the values predicted from the Default Thermal History, indicating that any paleo-thermal effects are subtle and detailed assessment is required before firm conclusions can be reached.

Prior to detailed assessment of the data in these samples, due to their close proximity, data in samples GC1191-2 and -3 have been combined into a single composite sample GC1191-2&3. Similarly, data in samples GC1191-4 and -5 have been combined into composite sample GC1191-4&5. This provides higher quality data in two samples instead of lower quality data in four samples. The revised dataset is illustrated in similar fashion in Figure 3.2.

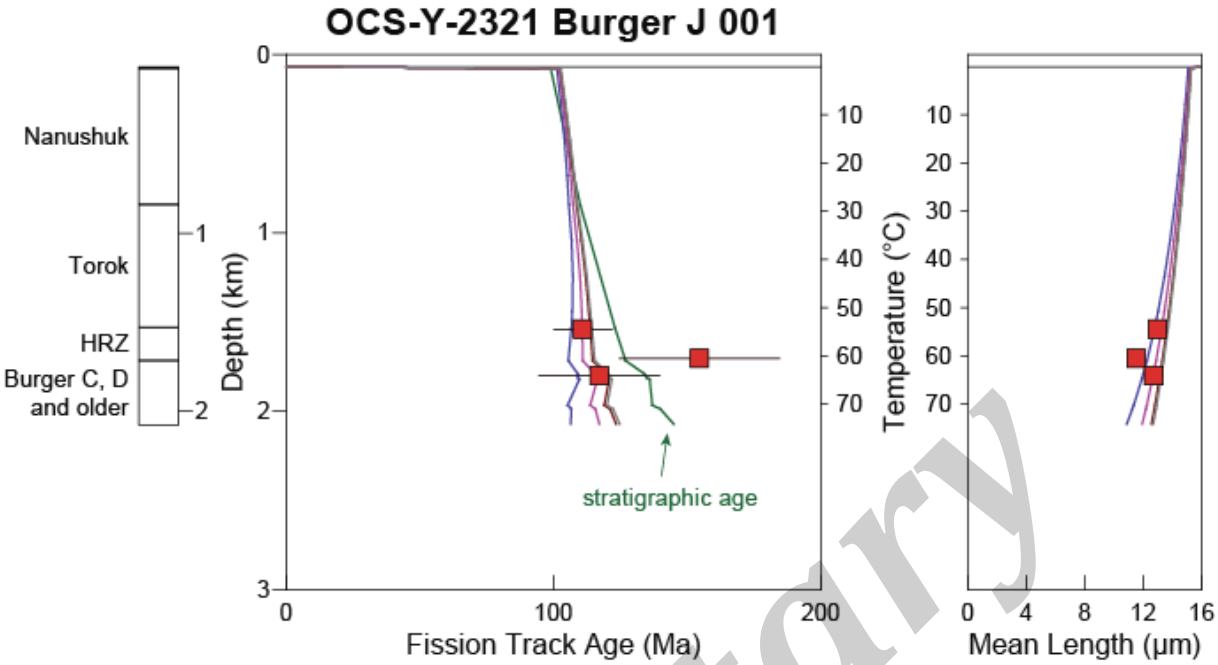

Figure 3.2: Revised AFTA parameters in samples from **Chukchi Sea well Burger J-001** after combining data in two pairs of samples, plotted against sample depth and present temperature.

Details are as in Figure 3.1. Measured fission track ages and mean track lengths in samples GC1191-1 and GC1191-4&5 are close to the values predicted from the Default Thermal History, indicating that any paleo-thermal effects are subtle and detailed assessment is required before firm conclusions can be reached. The fission track age of composite sample GC1191-2&3 is older than predicted from the Default Thermal History, and while the mean track length is shorter than expected on this basis this could be due to the presence of shorter tracks inherited from sediment provenance regions. Thus, as in Figure 3.1, any evidence that these samples have been hotter than present-day temperatures after deposition is extremely subtle, and detailed assessment is required before firm conclusions can be reached.

Detailed assessment of the data is presented in Table 3.2, where thermal history constraints derived from AFTA data in each of the samples are presented and explained.

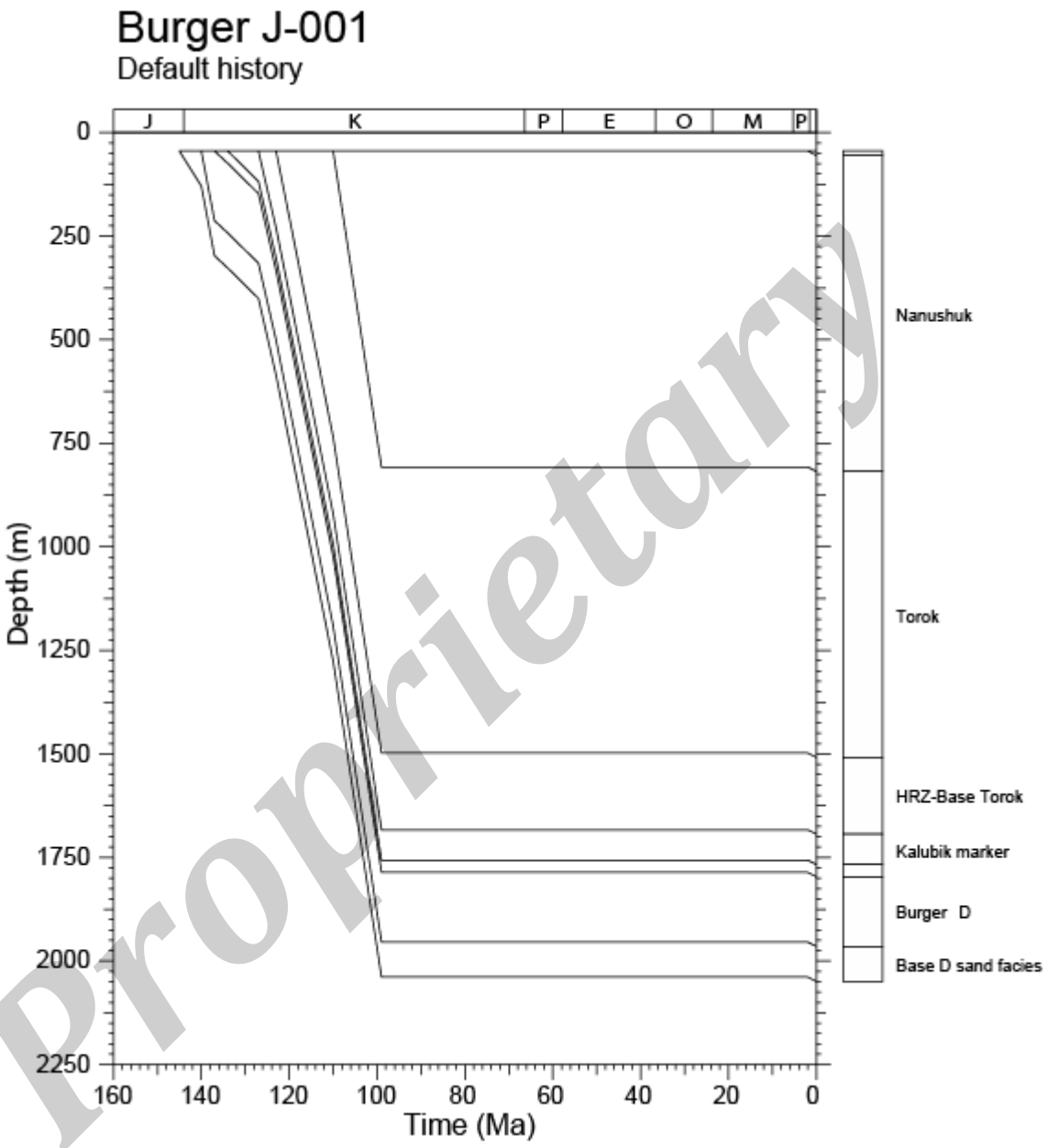

Figure 3.3: Burial history derived from the preserved section in **Chukchi Sea well Burger J-001**.

This history, together with a present-day thermal gradient of 37°C/km (derived as described in Appendix A) and a sea bed temperature of 0°C, has been used to predict the Default Thermal Histories for individual AFTA samples, as employed in the construction of Figures 3.2, and for prediction of the maturity-depth profile in Figure 3.4.

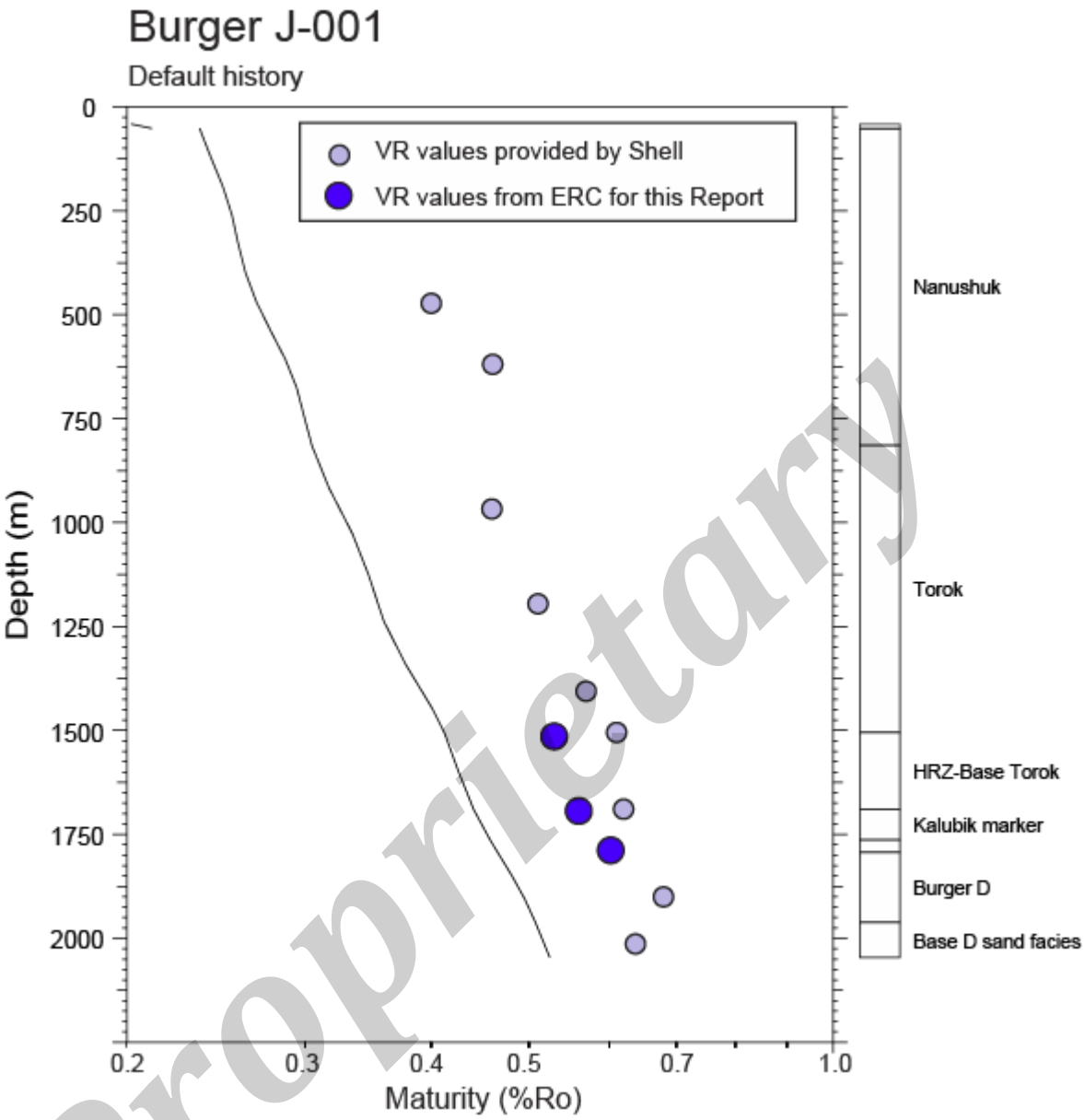

Figure 3.4: Mean vitrinite reflectance (VR) values in **Chukchi Sea well Burger J-001**, plotted against depth (below kb).

Values provided by Shell are listed in Table D.3 (Appendix D) while data from analyses by Energy Resources Consulting (ERC) are listed in Table D.2. The solid black line shows the VR profile predicted by the "Default History", i.e., the profile expected if samples throughout the section are currently at their maximum temperature since deposition (Section 2.1) based on a thermal gradient of 37°C/km, derived as described in Appendix A, together with a sea bed temperature of 0°C. Both sets of measured VR values plot consistently above the predicted profile, showing that the sampled section has been much hotter than present temperatures at some time since deposition. See text for further discussion.

4. Thermal history interpretation of AFTA and VR data in the Burger J-001 well

4.1 Background

Thermal history interpretation of AFTA data in samples analysed for this study is presented in Tables 4.1 to.4.3, and illustrated schematically in Figures 4.1 to 4.3.

For downhole samples, the consistency of the AFTA data with present-day temperatures is assessed. This is typically based on the lengths of the longest tracks in each sample, which are those that have experienced the lowest temperatures and therefore the most recently formed. But at temperatures of around 100°C or more the degree of annealing (i.e. age reduction) of tracks in the more sensitive (i.e. Cl-poor) apatites is also useful.

The data are then assessed in qualitative terms for evidence of whether samples have been hotter after deposition or emplacement (for Phanerozoic sedimentary and igneous rocks, respectively). If samples of Precambrian basement from outcrop have been analysed, they are assessed for evidence of whether they have been hotter in Phanerozoic times.

Quantitative interpretation of the AFTA data is then summarised, in terms of the maximum paleotemperature and the timing of cooling in one or more discrete episodes, as required in order to explain all facets of the data. As explained in Section 2.1 and Appendix C, these thermal history solutions are extracted from the data in each sample using in-house software which compares the AFTA parameters (fission track age and track length distribution and their variation with Cl content) predicted for a range of likely thermal history scenarios with the measured values, defining the range of conditions for which predictions are consistent with the measured data within 95% confidence limits. Similar considerations also allow determination of cooling episodes prior to deposition for sedimentary samples, representing events in sediment provenance regions, where appropriate. Comments are also provided on the consistency between the thermal history constraints derived from the AFTA data and VR values in the same or adjacent samples.

Finally, a schematic illustration of the thermal history solution in each sample is provided. Thermal history constraints are derived within a framework of episodic heating and cooling. It is emphasised that only the coloured polygons represent constraints derived from the AFTA data. The black lines are for guidance only, because the temperature during the interval between each cooling episode is not constrained by the data (except that it did not exceed that in subsequent events). This

type of framework is clearly appropriate for sedimentary rocks, and for basement rocks on which sedimentary remnants are preserved, but we believe that episodic histories are appropriate in most, if not all settings. See Green and Duddy (2012) and Green et al. (2013) for a detailed justification of this approach, together with further details.

Thermal history solutions derived from the AFTA data in each sample are summarised in Table i.

4.2 Extracting thermal history constraints from the AFTA data

Comments on present-day temperatures on the basis of AFTA

Certain aspects of AFTA data are sensitive to the present-day thermal regime (essentially the longest tracks in each sample and the temperatures at which the fission track ages are progressively reduced towards zero). The three AFTA samples analysed from this well are from depths where present-day temperatures are <70°C. In these conditions, AFTA data are not particularly sensitive to present–day temperatures. Nevertheless, as explained in Tables 4.1 to 4.3 the data in the three samples from this well, particularly the longest tracks within the length distribution, are highly consistent with the temperatures calculated using the present-day thermal gradient of 37°C/km derived as explained in Section 3.1 and Appendix A. We therefore proceed to use this gradient as the basis for extracting thermal history constraints from the AFTA and VR data in the well.

Evidence for elevated paleotemperatures from AFTA

As summarised in Tables 4.1 to 4.3, AFTA data in none of the three samples show any direct evidence to suggest that the sampled sedimentary units have ever been hotter than the present-day temperatures at any time after deposition.

But since the VR data provide clear evidence that the section has been hotter in the past, we proceed below to investigate thermal history solutions which can explain both the AFTA and VR data.

Magnitude of paleotemperatures and timing of cooling from AFTA

As summarised in Tables 4.1 to 4.3, AFTA data in each sample define limits on the time that the sample must have cooled from the maximum paleotemperature indicated by VR data at the same depth.

For sample GC1191-1, the AFTA data show that if the sample reached a maximum paleotemperature of 100°C, as indicated by the provided VR value at the corresponding depth, then cooling from that maximum must have begun prior to 100 Ma. Alternatively, if the sample reached a maximum paleotemperature of 88°C, as indicated by the VR value from ERC at the same depth, then cooling from that maximum must have begun prior to 75 Ma.

For composite sample GC1191-2&3, the maximum paleotemperature of 102°C indicated by the provided VR value at the corresponding depth is not consistent with the AFTA data, while cooling from 93°C as defined by the VR value from ERC at the same depth, is allowed if cooling began prior to 50 Ma.

For composite sample GC1191-4&5, the maximum paleotemperatures of 102°C and 99°C indicated by the provided and ERC VR values at this depth are treated together, with the AFTA data showing that cooling from such paleotemperatures is allowed if cooling began prior to 73 Ma.

Integration of the information provided by AFTA and VR data in samples from this well is discussed in Section 4.3.

4.3 Integration of AFTA and VR data

As noted in Section 4.2, AFTA data set limits to the time at which cooling from the maximum paleotemperatures indicated by the VR values must have begun. For samples GC1191-1 and GC1191-4&5, the maximum paleotemperatures defined from both the supplied and ERC VR values are allowed by the AFTA data but for sample GC1191-2&3, only the ERC VR value is allowed while the supplied value is outside the allowed range (Table 4.2, Figure 4.2). Because a consistent interpretation of the ERC VR data and the AFTA data can be achieved we favour the conclusions resulting from this combination of data.

4.4 Definition of dominant paleo-thermal episodes

By combining the limits defined from AFTA data summarised in Section 4.2 we conclude that the Early Cretaceous section in this well began to cool from the maximum paleotemperatures expressed by the VR data **prior to 73 Ma (late Campanian or earlier)**. Given the youngest Cretaceous unit (Nanushuk Formation)

preserved in the well is assigned a younger depositional age limit of 99 Ma (Table A.1), the onset of cooling is further defined to **between 99 and 73 Ma (Cenomanian to Late Campanian)**.

Table 4.1: Thermal history interpretation of AFTA data in sample GC1191-1

Sample type: Cuttings	Well name.	Burger J-001		
Depth (rkb): 1536-1545 m	Present temp:	55°C	Strat. Age:	127-123 Ma
Default history predictions:	Fission track age;	108 Ma	Mean track length;	12.9 µm
Measured values:	Fission track age;	111.1 ± 5.4 Ma	Mean track length;	12.99 ± 0.16 µm

Are AFTA data consistent with present-day temperature?

All aspects of the AFTA data, particularly the longest track lengths within the length distribution, are consistent with the present temperature of 55°C calculated as explained in Appendix A.

Evidence of higher temperatures in the past

from length data?	No: The mean track length is consistent (within analytical uncertainties) with the value predicted from the Default Thermal History.
from fission track age data?	No: The pooled fission track age is consistent (within analytical uncertainties) with the value predicted from the Default Thermal History.
Conclusion:	AFTA data show no direct evidence to suggest that this sample has been hotter than the present-day temperature at any time since deposition, although the possibility would be allowed within certain limits.

Paleo-thermal constraints

Pre-deposition		**post-deposition**	
Maximum paleo-temperature (°C)	Onset Of Cooling (Ma)	Maximum paleo-temperature (°C)	Onset Of Cooling (Ma)
>108	144-116	<120	Post-deposition
		<100	<100
		<88	<75

The AFTA data define a single episode of cooling from >108°C in the interval 144 to 116 Ma which is interpreted as occurring prior to deposition in sediment provenance regions. Although the AFTA data in this sample do not require that the sample has been hotter than the present-day temperature at any time after deposition, VR data (see below) suggest maximum post-depositional paleotemperatures of either 88°C or 100°C. The AFTA data are consistent with post-depositional heating to 100°C only if cooling began prior to 100 Ma, while the corresponding younger limit on the onset of cooling from a maximum of 88°C is 75 Ma (see Figure, below).

High quality AFTA data (29 ages, 63 track lengths) provide an interpretation which is regarded as highly reliable within the stated limits.

Equivalent $R_o$max <0.73%. A measured value of 0.61% from Shell from a similar depth (Table D.3), equivalent to a maximum paleotemperature of 100°C (Table 3.3) is consistent with the AFTA data only if cooling from this paleotemperature began earlier than ~100 Ma. A VR value of 0.53% measured by ERC on material taken from the AFTA sample (Table D.2), equivalent to a maximum paleotemperature of 88°C (Table 3.3) is consistent with the AFTA data only if cooling from this paleotemperature began prior to ~75 Ma

Continued…

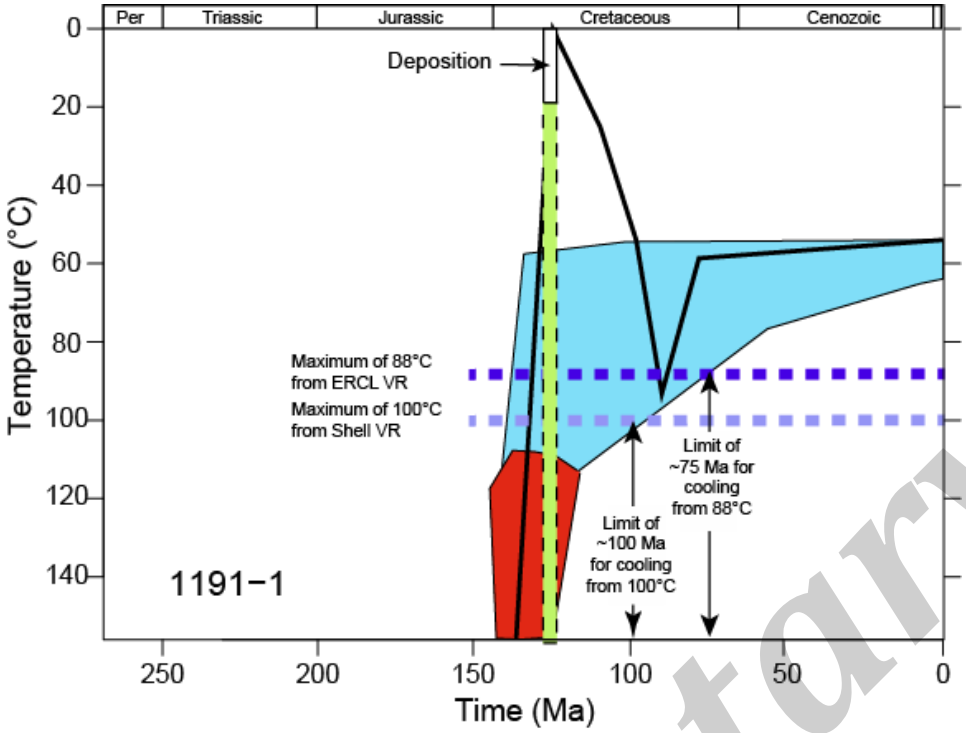

Figure 4.1: Thermal history interpretation summary, Sample GC1191-1

Table 4.2: Thermal history interpretation of AFTA data in sample GC1191-2&3

Sample type: Cuttings	Well name.	Burger J-001		
Depth (rkb): 1704-1725 m	Present temp:	61°C	Strat. Age:	134-123 Ma
Default history predictions:	Fission track age;	107 Ma	Mean track length;	12.5 µm
Measured values:	Fission track age;	154.7 ± 15.0 Ma	Mean track length;	11.55 ± 0.26 µm
Age data structure:				
Young population	Fission track age;	118.7 ± 11.2 Ma	Mean track length;	11.98 ± 0.35 µm
Old population	Fission track age;	224.7 ± 13.2 Ma	Mean track length;	11.59 ± 0.28 µm

Are AFTA data consistent with present-day temperature?

All aspects of the AFTA data, particularly the longest track lengths within the length distribution, are consistent with the present temperature of 61°C calculated as explained in Appendix A.

Evidence of higher temperatures in the past

from length data?	Equivocal: The mean track length is significantly less than predicted from the Default Thermal History. Modelling the AFTA parameters through different thermal history scenarios shows that this could be explained either by the effects of higher temperatures after deposition or by the presence of shorter tracks inherited from sediment provenance regions
from fission track age data?	No: The central fission track age is significantly older than predicted from the Default Thermal History. No single grain age is significantly younger than predicted on this basis.
Conclusion:	AFTA data show no direct evidence to suggest that this sample has been hotter than the present-day temperature at any time since deposition, although the possibility would be allowed within certain limits.

Paleo-thermal constraints

	Pre-deposition		**post-deposition**	
	Maximum paleo-temperature (°C)	Onset Of Cooling (Ma)	Maximum paleo-temperature (°C)	Onset Of Cooling (Ma)
Young population	>107	178-118	75-102	128-6
Old population	>106	337-250	84-93	187-25

The AFTA data in this sample comprise two distinct age populations (see above), one with ages close to the depositional age and one with older ages (see AFTA Data Summary Sheet, Appendix B). Data in each population can be explained by a scenario involving two paleo-thermal episodes, as listed above. The onset of cooling in the earlier of two episodes defined from the young population overlaps slightly with the depositional age range at the younger limit but is interpreted as pre-depositional, while the younger episode also overlaps with the depositional age range at the older limit. Thus this episode could also represent a final phase of pre-depositional cooling, or alternatively could represent post-depositional heating and cooling. For the older population, the earlier of the two episodes is clearly pre-depositional, while the onset of cooling in the later episode again overlaps with the depositional age range and therefore this episode could either represent pre- or post-depositional cooling. VR data (see below) suggest maximum post-depositional paleotemperatures of either 93°C or 102°C (see below). The AFTA data comprising the younger age population are only just consistent with post-depositional heating to 102°C if cooling began within a few Myr after deposition, while the maximum paleotemperature of 93°C is allowed until ~50 Ma (see Figure, next page). In contrast, the age data comprising the older population are only consistent with post-depositional cooling from 93°C at the extreme limit prior to 100 Ma and are not consistent with a maximum paleotemperature of 102°C at any time after deposition. This may be due to additional complexity in the thermal history of the older age population prior to deposition, which cannot be resolved from post-depositional events. On this basis, we regard the constraint from the younger age population, showing that cooling from 93°C must have occurred prior to ~50 Ma, as the most reliable constraint on the thermal history of this sample.

High quality AFTA data (36 ages, 49 track lengths) provide an interpretation which is regarded as highly reliable within the stated limits, although division between two age populations reduces the eventual level of precision.

Equivalent $R_o$max 0.44-0.62% (young ages) or 0.51-0.56% (old ages). A measured value of 0.62% from Shell from a similar depth (Table D.3), equivalent to a maximum paleotemperature of 102°C (Table 3.3) is only just consistent with the extreme higher end of the range allowed by the younger population. A VR value of 0.56% measured by ERC on material taken from the AFTA sample (Table D.2), equivalent to a maximum paleotemperature of 93°C (Table 3.3) is just consistent with the upper limit defined from the AFTA data in the older age population but is consistent with the constraint from the younger population provided that cooling began prior to 50 Ma. *Continued…*

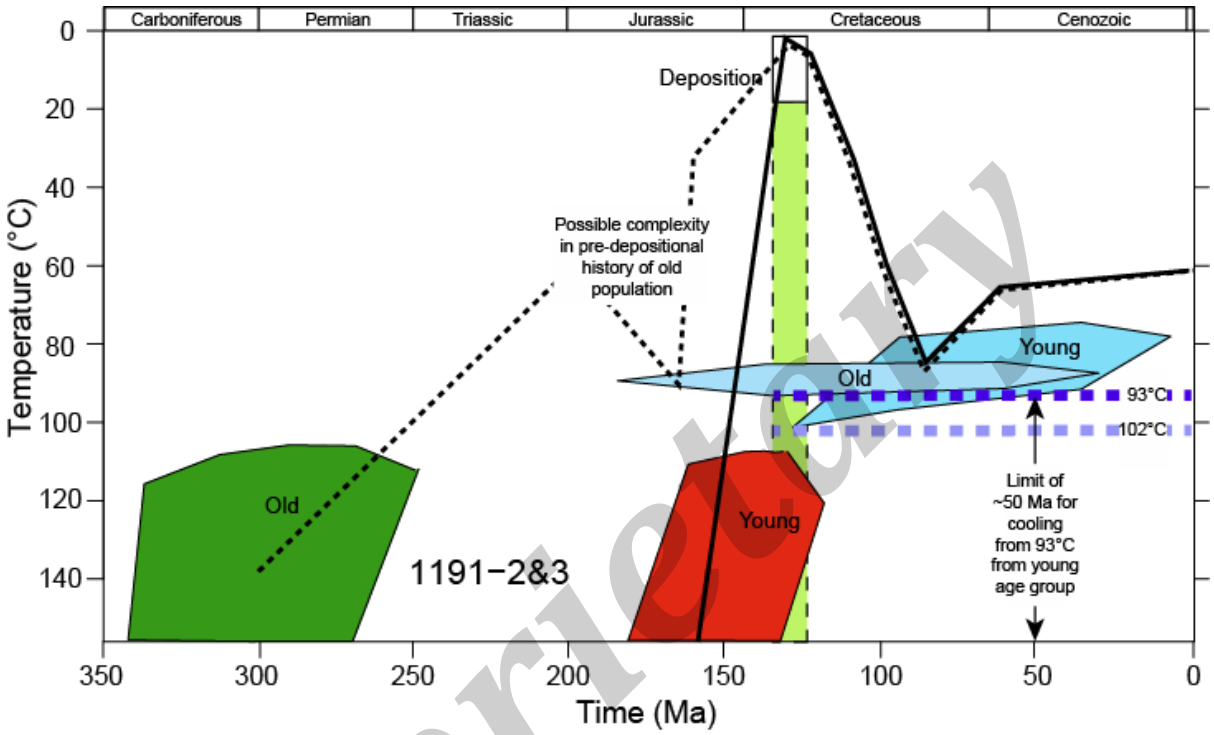

Figure 4.2: Thermal history interpretation summary, Composite sample GC1191-2&3

Table 4.3: Thermal history interpretation of AFTA data in sample GC1191-4&5

Sample type: Cuttings	Well name.	Burger J-001		
Depth (rkb): 1792-1832 m	Present temp:	65°C	Strat. Age:	137-134 Ma
Default history predictions:	Fission track age;	112 Ma	Mean track length;	12.3 µm
Measured values:	Fission track age;	117.2 ± 11.3 Ma	Mean track length;	12.74 ± 0.30 µm
Age data structure:				
Young population	Fission track age;	104.4 ± 7.2 Ma	Mean track length;	12.74 ± 0.29 µm
Old population	Fission track age;	215.8 ± 26.1 Ma	Mean track length;	13.09 ± 0.90 µm

Are AFTA data consistent with present-day temperature?

All aspects of the AFTA data, particularly the longest track lengths within the length distribution, are consistent with the present temperature of 65°C calculated as explained in Appendix A.

Evidence of higher temperatures in the past

from length data?	No: The mean track length is consistent (within analytical uncertainties) with the value predicted from the Default Thermal History.
from fission track age data?	No: The central fission track age is consistent (within analytical uncertainties) with the value predicted from the Default Thermal History. No single grain age is significantly younger than predicted on this basis.
Conclusion:	AFTA data show no direct evidence to suggest that this sample has been hotter than the present-day temperature at any time since deposition, although the possibility would be allowed within certain limits.

Paleo-thermal constraints

	Pre-deposition		**post-deposition**	
	Maximum paleo-temperature (°C)	Onset Of Cooling (Ma)	Maximum paleo-temperature (°C)	Onset Of Cooling (Ma)
Young population	>125	158-107	<120	128-0
			<100	73-0
			<90	63-0
Old population	>118	548-200	<120	200-0
			<90	102-0

The AFTA data in this sample comprise two distinct age populations (see above), a dominant group with ages close to the depositional age and a smaller group with older ages (see AFTA Data Summary Sheet, Appendix B). Data in each population can be explained by a scenario involving a single pre-depositional cooling episode combined with the Default Thermal History, i.e. the data in neither of the populations require that the sample has been hotter in the past, although this possibility is allowed within certain limits, as listed above. The onset of cooling in the single episode definitely required by data from the young population overlaps slightly with the depositional age range at the younger limit but is interpreted as pre-depositional. For the older population, the single cooling episode definitely required by the data is clearly pre-depositional. VR data (see below) suggest maximum post-depositional paleotemperatures of either 99°C or 102°C (see below). The AFTA data comprising the younger age population are consistent with post-depositional heating to 102°C if cooling began prior to 73 Ma, while the maximum paleotemperature of 99°C is allowed until slightly later (see Figure, next page). In contrast, data comprising both populations are only consistent with post-depositional cooling from 99°C or more if cooling began prior to 102 Ma. As in sample GC1173-2&3, this is probably due to additional complexity in the thermal history of the older age population prior to deposition, which cannot be resolved from post-depositional events. On this basis, we regard the constraint from the younger age population, showing that cooling from 99°C or more must have occurred prior to ~73 Ma, as the most reliable constraint on the thermal history of this sample.

Continued…

High quality AFTA data (35 ages, 25 track lengths) provide an interpretation which is regarded as highly reliable within the stated limits, although division between two age populations reduces the eventual level of precision.

Equivalent $R_o$max <0.73% or <0.61% for cooling within the last 73 Myr Measured values of 0.62% from Shell from a slightly shallower depth (Table D.3), and 0.60% measured by ERC on material taken from the AFTA sample (Table D.2), equivalent to maximum paleotemperatures of 102°C and 99°C, respectively (Table 3.3), are consistent with the limits allowed by AFTA in the younger population (considered the most reliable constraint, as discussed above) only if cooling began prior to 73 Ma.

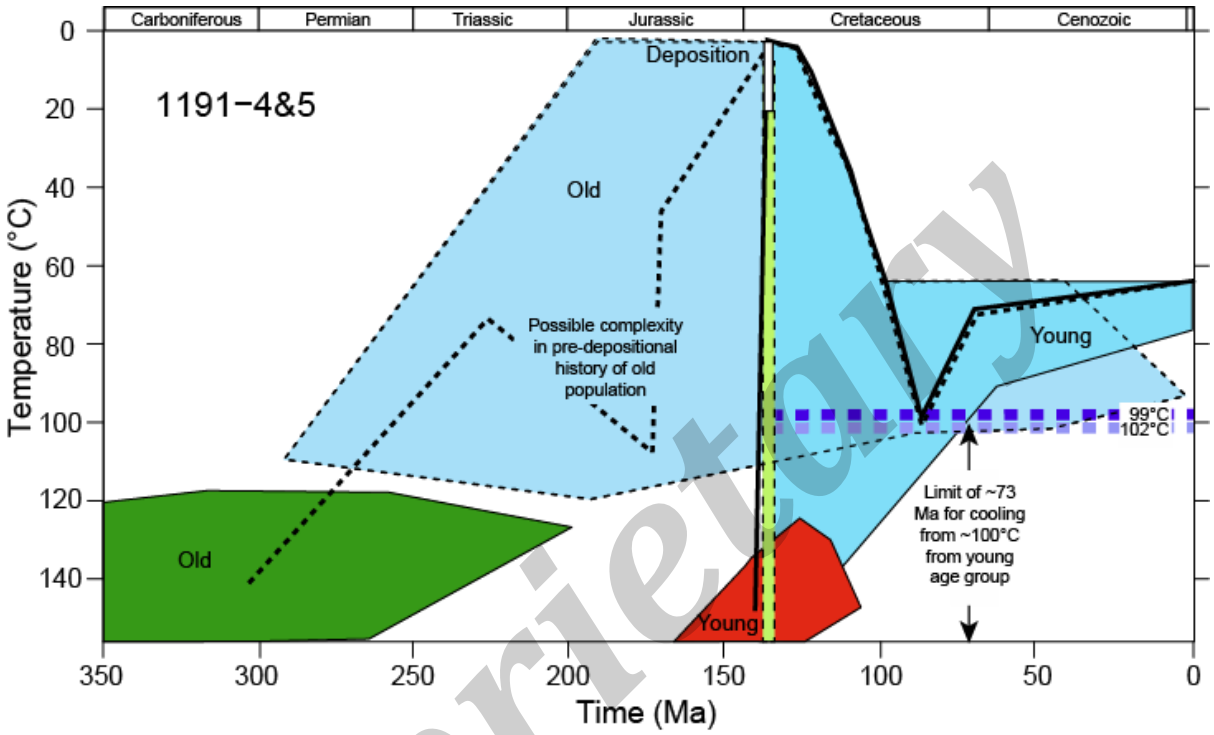

Figure 4.3: Thermal history interpretation summary, Composite sample GC1191-4&5

5. Thermal history reconstruction in Chukchi Sea well Burger J-001

5.1 Paleotemperature profiles and mechanisms of heating and cooling

Paleotemperature constraints from AFTA and VR data (both datasets) in the **Burger J-001** well are plotted against depth (TVD rkb) in Figure 5.1. As discussed in Section 4, the maximum paleotemperatures derived from the ERC VR data are consistent with the constraints provided by the AFTA data provided that cooling began prior to 73 Ma. In contrast, the consistently higher maximum paleotemperatures defined by the VR data supplied by Shell are not consistent with the AFTA data. For this reason, in this section we favour the AFTA and ERC VR data as providing the most reliable definition of paleo-thermal effects in this well.

As shown in Figure 5.2, the paleotemperatures defined from the ERC VR values and the constraints provided by the AFTA data are consistent with a linear paleotemperature profile, sub-parallel to the present-day temperature profile. This suggests that an interpretation of the observed paleotemperatures in terms of heating due to deeper burial and cooling due to exhumation can provide a satisfactory explanation of the AFTA and ERC VR data in this well.

In contrast, the VR data supplied by Shell define a separate linear profile characterised by a lower gradient. As above, the paleotemperatures defining this parallel are higher than allowed by the AFTA data in the well and therefore we do not regard this profile as providing reliable definition of the paleo-thermal history of the section intersected in the well.

While we provide quantitative assessment of both profiles in the following sections, our preferred thermal history reconstruction for the **Burger J-001** well is based on the constraints provided by the AFTA and ERC VR data.

5.2 Paleogeothermal gradients and amounts of missing section

Introduction

Paleogeothermal gradients and amounts of removed section have been determined using the approach explained in Section 2 and Appendix C. Values of "removed section" determined in this manner actually represent the thickness of additional section that was present at the paleo-thermal maximum which has been subsequently

removed by uplift and erosion. In this sense, the terms "additional burial" and "removed section" are synonymous.

As explained in Section 2, values of paleogeothermal gradient and removed section compatible with a given set of paleotemperature constraints are highly correlated, such that higher gradients and lower values of removed section or lower gradients and higher values of removed section are capable of explaining the constraints. The approach adopted here results in definition of the range of correlated values allowed by the data presented as a "hyperbolic ellipsoid". In addition, ranges of paleogeothermal gradients are presented from one-dimensional analyses of each parameter independently, in the form of likelihood profiles. The range of allowed values is defined by the points at which the likelihood falls by 2 from the maximum value.

Estimation of amounts of removed section from paleotemperature data depends critically on various key assumptions (Section 2.5). The principal difficulty lies with definition of the paleogeothermal gradient through the removed section, which cannot be constrained by direct measurement and must therefore always be assumed. In deriving estimates of removed section for each of the paleo-thermal episodes recognised in the well, the paleogeothermal gradient through the removed section is assumed to have been linear and equal to the value through the preserved section. This is equivalent to assuming that the missing section was heterogeneous, and no large thicknesses of uniform lithology are present which might produce non-linear profiles (Figure 2.2). This assumption may also be invalid if the elevated paleotemperatures are caused by processes involving lateral or local introduction of heat, such as by confined fluid flow or igneous intrusions.

Despite the various assumptions involved, it should be stressed that because the amounts of removed section are derived from fits to the paleotemperature data, thermal history reconstructions based on these values will reliably reproduce the main features of the thermal history interpretations of the AFTA and VR data on which they are based (although resulting burial history reconstructions may still be speculative).

Paleogeothermal gradients in the Burger J-001 well

Using the approach outlined in Section 2.4 and methods explained in Appendix C (Section C.9), we have determined the range of paleogeothermal gradients consistent with the **Cenomanian-Campanian (99 to 73 Ma)** paleotemperature constraints from AFTA data and ERC VR data in the **Burger J-001** well, with results listed in Table

5.1. Results are also provided in Table 5.1 for analysis based solely on the VR data provided by Shell. The corresponding likelihood profiles from which these constraints are taken are shown in Figures 5.3A and 5.4A, respectively.

The likelihood profiles in Figure 5.3A and 5.4A both show good quadratic form, characteristic of a well-defined dataset, with well-defined maxima evident in both profiles. Figures 5.3C and 5.4C show the best-fit profiles through the paleotemperature constraints for the respective episodes, plus the profiles corresponding to upper and lower 95% confidence limits (dashed lines).

The range of allowed **Cenomanian-Campanian** paleogeothermal gradients defined from AFTA and the ERC VR data, from 7.5 to 65.5°C/km (Figure 5.3A), is rather broad, due mainly to the narrow depth range over which data are available in the **Burger J-001** well, but the maximum likelihood value of 36.5°C/km is very close to the present-day thermal gradient of 37°C/km for this well derived as explained in Appendix A. In contrast, the entire range of paleogeothermal gradients allowed by the VR data supplied by Shell, from 18.5 to 31.0°C/km, falls below the present-day gradient. Thus, quantitative analysis of paleogeothermal gradients defined from AFTA and the ERC VR data confirms that results from the Burger J-001 are consistent with heating due to deeper burial with no change in basal heat flow, whereas the VR data supplied by Shell would require an increase in heat flow since the Late Cretaceous.

Additional burial / removed section

Principles

Assuming that the paleogeothermal gradient in each episode was linear throughout the entire section at the time of maximum paleotemperatures, extrapolation of the fitted linear profile from the appropriate unconformity to an assumed paleo-surface temperature provides an estimate of the amount by which that unconformity surface was more deeply buried, and hence the amount of section that has since been removed by erosion (Figure 2.2).

Estimation of amounts of removed section (or additional burial) from paleotemperature data in this way depends critically on various key assumptions (Section 2.5). The principal difficulty lies with definition of the paleogeothermal gradient through the removed section, which cannot be constrained by direct measurement and must therefore always be assumed. In deriving estimates of removed section for each of the paleo-thermal episodes recognised in the well, the

paleogeothermal gradient through the removed section is assumed to have been linear and equal to the value through the preserved section. This is equivalent to assuming that the missing section was heterogeneous, and no large thicknesses of uniform lithology are present which might produce non-linear profiles (Figure 2.2). This assumption may also be invalid if the elevated paleotemperatures are caused by processes involving lateral or local introduction of heat, such as by confined fluid flow or igneous intrusions.

Multiple episodes

In considering amounts of section removed in the three episodes, it is important to appreciate the analysis employed (illustrated in Figure 2.2) actually provides determination of the amount of additional section present on the appropriate unconformity at the time when cooling began. Where multiple exhumation events occur within a single unconformity, the analysis defines the amount of additional section present at the onset of each event, but it is not possible to define the total amount of section removed in each episode because of the uncertainty regarding the amount of re-burial between each episode (see Section 2.5 and Figure 2.4). Therefore in considering Figures 5.3 and 5.4, where Removed Section is mentioned, the analysis actually determines the amount of additional burial required to explain the paleotemperatures in each event. The value for any specific event is also equal to the total amount of section removed between the onset of cooling in that event and the present day.

Results from Chukchi Sea well Burger J-001

Amounts of additional section present at the onset of cooling from the **Cenomanian-Campanian** paleo-thermal maximum have been calculated with respect to the unconformity separating the Quaternary section from the underlying Nanushuk Fm at a depth of 78.3 m rkb in this well.

For simplicity, we have employed a paleo-surface temperature equal to the present-day value of 0°C in order to estimate amounts of additional section present at the **Cenomanian-Campanian** paleo-thermal maximum. If alternative values should be preferred, changing the value of paleo-surface temperature is equivalent to a constant offset in the amount of missing section required in order to explain the observed paleotemperatures. The influence of this factor is discussed further below.

Amounts of additional burial required to explain the observed **Cenomanian-Campanian** paleotemperatures defined from AFTA and ERC VR and from the VR

data supplied by Shell are summarised in Table 5.2. Values are quoted corresponding to the maximum likelihood estimate of paleogeothermal gradient and related ±95% confidence limits, derived from the likelihood profiles shown in Figures 5.3B and 5.4B. Figures 5.3D and 5.4D illustrate the extrapolation of the profile fitted to each set of paleotemperature constraints in order to determine removed section. Ranges of additional burial (again corresponding to ±95% confidence limits) are also quoted in Table 5.2 for various specified values of paleogeothermal gradient within the allowed range of values. These are taken from Figures 5.3E and 5.4E, which illustrate the correlation between values of paleogeothermal gradient and removed section allowed by the paleotemperature constraints comprising each dataset within ±95% confidence limits. That is, any set of paired values inside the contoured regions in these plots are compatible with the corresponding paleotemperature constraints for that episode at 95% confidence limits, with higher paleogeothermal gradients requiring correspondingly less removed section, and vice versa. (Note that two-dimensional analyses depicted in Figures 5.3E and 5.4E result in slightly wider ranges of allowed paleogeothermal gradients than the one-dimensional analysis represented in Figures 5.3A and 5.4A due to the more constrained nature of the 2-D analysis).

In developing reconstructions for the **Burger J-001** well in subsequent Sections we have adopted a scenario involving a constant paleogeothermal gradient equal to the present-day value of 37°C/km throughout the entire history, based on the constraints derived from AFTA and the ERC VR data. From Figure 5.3E and Table 5.2 this scenario corresponds to additional burial between 850 and 950 m for the **Cenomanian-Campanian** episode.

Again we stress that a wide range of other combinations of paleogeothermal gradient and additional burial would be compatible with the results from this well, and this preferred scenario represents only one option. Nevertheless, and despite the various assumptions involved in the analyses discussed here, and the resulting uncertainties in values of removed section, it should be stressed that because the amounts of removed section are derived from fits to the paleotemperature data, thermal history reconstructions based on these values (in combination with the appropriate value of paleogeothermal gradient) will reliably reproduce the main features of the thermal history interpretations provided by the AFTA and VR data from which they were derived.

Because the VR data supplied by Shell indicate a lower paleogeothermal gradient compared to the present-day value, and require much larger amounts of removed section, we have not pursued a reconstruction based on these data.

Alternative paleo-surface temperatures

While we have adopted a constant surface temperature equal to the present-day value of 0°C, as outlined above, it is possible that higher or lower values may be more appropriate. Detailed discussion of this issue is beyond the scope of this study. But the magnitude of removed section required to explain the observed paleotemperatures can be easily adjusted to an alternative paleo-surface temperature by subtracting or adding the difference in depth equivalent to the change in paleo-surface temperature, for the appropriate paleo-gradient, as described in Section 2.5. For example, increasing the paleo-surface temperature by 10°C, for a paleogeothermal gradient of 40°C/km, would require a reduction of 250 metres in the amount of removed section needed to explain the observed paleotemperatures.

Other interpretations

In this Section, we have calculated the amount of additional section that must have been deposited and subsequently removed by uplift and erosion in order to explain the observed paleotemperatures, given the constraints on paleogeothermal gradients established from the AFTA and VR data (Figures 5.3E and 5.4E). While an interpretation of heating due to deeper burial seems geologically plausible, other explanations are possible (e.g. long-term heating as a result of hot fluid flow at a shallow level), but the calculations presented here provide a quantitative framework in which the thermal history of the preserved sedimentary sequence can be reconstructed with confidence.

5.3 Thermal and burial/uplift history reconstruction

Introduction

In this Section, we present reconstructed thermal and burial-uplift histories for the **Burger J-001** well, based on the results presented in previous Sections. It should be emphasised that while the preferred reconstruction illustrated here provides a satisfactory explanation of the AFTA and ERC VR data from this well, the reconstruction is not unique, and a range of alternative scenarios could be invoked.

Therefore, in considering these reconstructions, it is important to appreciate those aspects of the histories that are constrained by the data, and those that are not.

Factors that can be confidently defined (within the limits of analytical uncertainty) include:

- Magnitude of heating at the paleo-thermal maximum and the subsequent paleo-thermal peak
- Timing of the onset of cooling in each episode
- Paleogeothermal gradients during each episode (subject to the reliability of the constraints employed)
- Additional burial during each episode for specified values of paleogeothermal gradient, assuming a linear paleotemperature profile (heterogeneous section).

Conversely, aspects which cannot be uniquely defined include:

- Thermal history prior to the paleo-thermal maximum and/or the subsequent paleo-thermal peak
- amounts of re-burial between multiple episodes within a single unconformity
- Detailed style of cooling history from each episode

Any reconstruction that matches the constraints on the magnitude of paleo-thermal effects and the onset of cooling can be considered as reliable, and integration with regional geological trends will be required to further restrict the range of realistic scenarios.

Burger J-001 well

The preferred thermal history reconstruction for well **Burger J-001** is illustrated in Figure 5.5. The corresponding burial-uplift history reconstruction is shown in Figure 5.6.

Key aspects of this reconstruction are:

- Constant sea bed/surface temperature of 0°C.
- Constant paleogeothermal gradient of 37°C/km.
- Deposition of an additional 900 metres of section between 99 and 80 Ma, with subsequent removal of 700 metres between 80 and 60 Ma and the remaining 200 m removed since 60 Ma. Note that this two-stage cooling history is not constrained by the data and is designed to maintain a cooling rate close to that used in deriving thermal history constraints from the AFTA and VR data (10°C/Myr).

The paleo-thermal maximum shown at 80 Ma in Figure 5.5 represents the effects solely of deeper burial. Similarly, cooling is due solely to exhumation (i.e. uplift and erosion).

While many details of this reconstruction remain speculative, as above, the magnitude and timing of the dominant paleo-thermal episode represented in Figure 5.5 is well constrained by the AFTA and VR data from this well, within the stated limits of analytical uncertainty.

Again, we emphasise that while the timing of the paleo-thermal maximum is relatively well defined (within the associated 95% confidence intervals), a range of alternative reconstructions could be designed, some of which would involve larger amounts of exhumation (i.e. uplift and erosion) while others might involve some variation in heat flow with time. Figures 5.5 and 5.6 illustrate one reconstruction which is consistent with the AFTA and ERC VR data in the **Burger J-001** well. A reconstruction based on the VR data supplied by Shell would require a lower paleogeothermal gradient and a much larger amount of additional burial and subsequent erosion.

Viable reconstructions must satisfy the paleotemperature constraints from AFTA and VR in this well, as defined by the contoured regions of paleogeothermal gradient and removed section in either Figure 5.3E or those in Figure 5.4E. All such combinations of paleogeothermal gradient and removed section will result in broadly similar reconstructed thermal histories for the preserved units in this well, although a reconstruction based on the Shell VR data would involve higher temperatures prior to the onset of cooling. But as emphasised previously, the AFTA data are not really compatible with the Shell VR data.

3.8 Implications of thermal history for source rock maturation

Predicted maturity-depth profile

Figure 5.7 shows the maturity-depth profile predicted from the thermal history reconstruction presented in Figure 5.5, together with measured mean VR values (both datasets) from the well (from Figure 3.4). The measured ERC VR values agree well with the predicted profile, which is to be expected since these data have been used to calibrate the reconstruction, while the Shell VR data are consistently higher that the predicted profile.

Based on this reconstruction, deeper Cretaceous units intersected in this well lie within the Early Mature (Oil) window while shallower units remain immature. Maturity levels in this well reflect the effects of deeper burial prior to exhumation which began in **Cenomanian-Campanian times** and is now represented by the unconformity between the Nanushuk Fm and the overlying Quaternary section.

Predicted variation of maturity with time

Figure 5.8 shows the evolution of maturity with time for the **Burger J-001 well** (using the maturation algorithm of Burnham and Sweeney, 1989) derived from the thermal history reconstruction illustrated in Figure 5.5. In this reconstruction, active maturation from any potential source rocks within deeper Cretaceous units ceased at 80 Ma at the onset of cooling due to exhumation (although any time between 99 and 80 Ma is allowed by the AFTA and VR data from this well).

Table 5.1: Paleogeothermal gradient estimates, Chukchi Sea well Burger J-001 (Geotrack Report #1191)

Episode	Present-day thermal gradient[*1] (°C/km)	Maximum Likelihood Estimate[*2] (°C/km)	Lower 95% confidence limit[*2] (°C/km)	Upper 95% confidence limit[*2] (°C/km)
AFTA and ERC VR data	37	36.5	7.5	65.5
VR data supplied by Shell only	37	25	18.5	31.0

[*1] Present-day thermal gradient derived as explained in Appendix A.

[*2] Paleogeothermal gradients estimated from paleotemperatures in each episode derived from AFTA and VR data, using methods described in Section 2.

Table 5.2: Removed section estimates: Chukchi Sea well Burger J-001 (Geotrack Report #1191)

	Estimates of removed section (metres) *1	
	AFTA and ERC VR data	**VR data supplied by Shell only**
Maximum Likelihood Estimate	900	2450
Lower and upper 95% confidence limits	0->10000	1700-3650
Fixed paleo-geothermal gradients		
10°C/km	*Not allowed*	*Not allowed*
20°C/km	2800-3200	3150-3550
25°C/km	1950-2150	2250-2650
30°C/km	1400-1500	1700-1900
37°C/km *2	**900-1000**	***Not allowed***
40°C/km	650-750	*Not allowed*
50°C/km	200-300	*Not allowed*
60°C/km	*Not allowed*	*Not allowed*

*1 Removed section estimated with respect to the unconformity below the section presumed to be of Quaternary age, at a depth of 78.3 m rkb in this well, using an assumed paleo-surface temperature of 0°C.

*2 Present-day thermal gradient (see Appendix A)

Notes:
Determination of the amount of removed section depends on the assumption that paleogeothermal gradients were linear through both the removed section and the preserved section, in each well. This assumption will not be valid if heating involved non-linear paleogeothermal gradients, which may result either because of vertical contrasts in thermal conductivity through the section, or if heating was not directly related to depth of burial but was due e.g. to hot fluid circulation. In such cases, the estimates quoted here are likely to over-estimate true amounts of removed section.

The quoted values are based on the assumed paleo-surface temperatures listed above. These can easily be converted to apply to other values, by subtracting or adding the difference in depth equivalent to the change in paleo-surface temperature, for the appropriate paleo-gradient. For example, for a paleogeothermal gradient of 30°C/km, a decrease of 10°C in the paleo-surface temperature is equivalent to an increase of 333 metres in the amount of removed section.

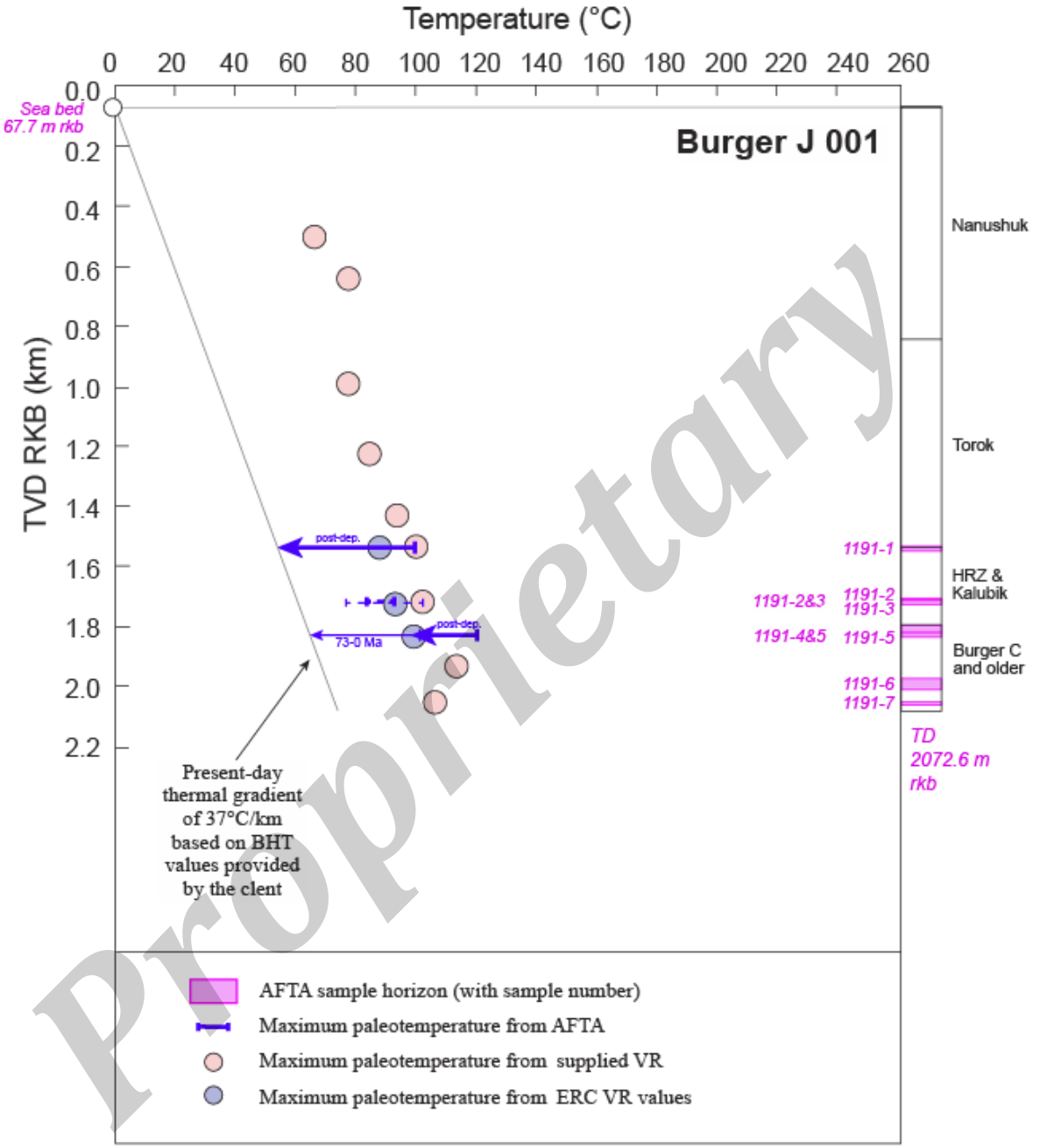

Figure 5.1: Paleotemperature constraints derived from AFTA and VR data in **Chukchi Sea well Burger J-001**, plotted against depth (rkb).

For composite sample GC1191-2&3, the thicker line denotes the constraint from the older age population in this sample while the thinner line denotes the constraint derived from the younger age population. Overall, the constraint from the older age population is narrower and entirely within the range derived from the younger age population, and thus is considered to provide the most reliable constraint for this sample overall. The present-day temperature profile based on a thermal gradient of 37°C/km derived as described in Appendix A), together with a sea bed temperature of 0°C, is also shown. Interpretation of these results is illustrated in Figure 5.2

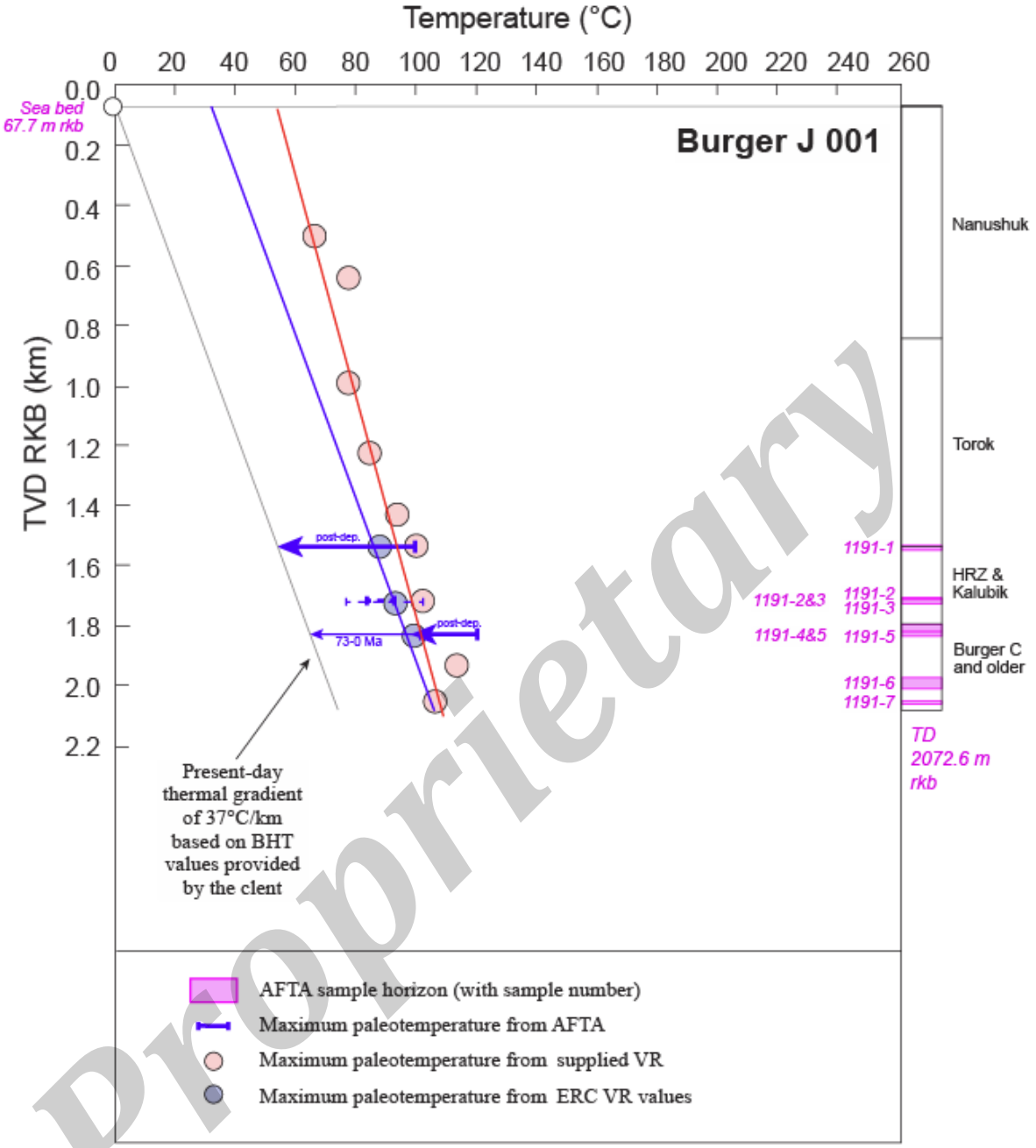

Figure 5.2: Interpretation of paleotemperature constraints derived from AFTA and VR data in **Chukchi Sea well Burger J-001.**

Possible alternative paleotemperature profiles are shown representing different combinations of data in this well. The blue profile is defined by the AFTA data and ERC VR data and is broadly parallel to the present-day temperature profile based on a thermal gradient of 37°C/km, which is also shown. The red profile, drawn though the paleotemperatures defined from the VR values provided by Shell, defines a lower gradient and is not consistent with the AFTA data from sample GC1191-2&3.

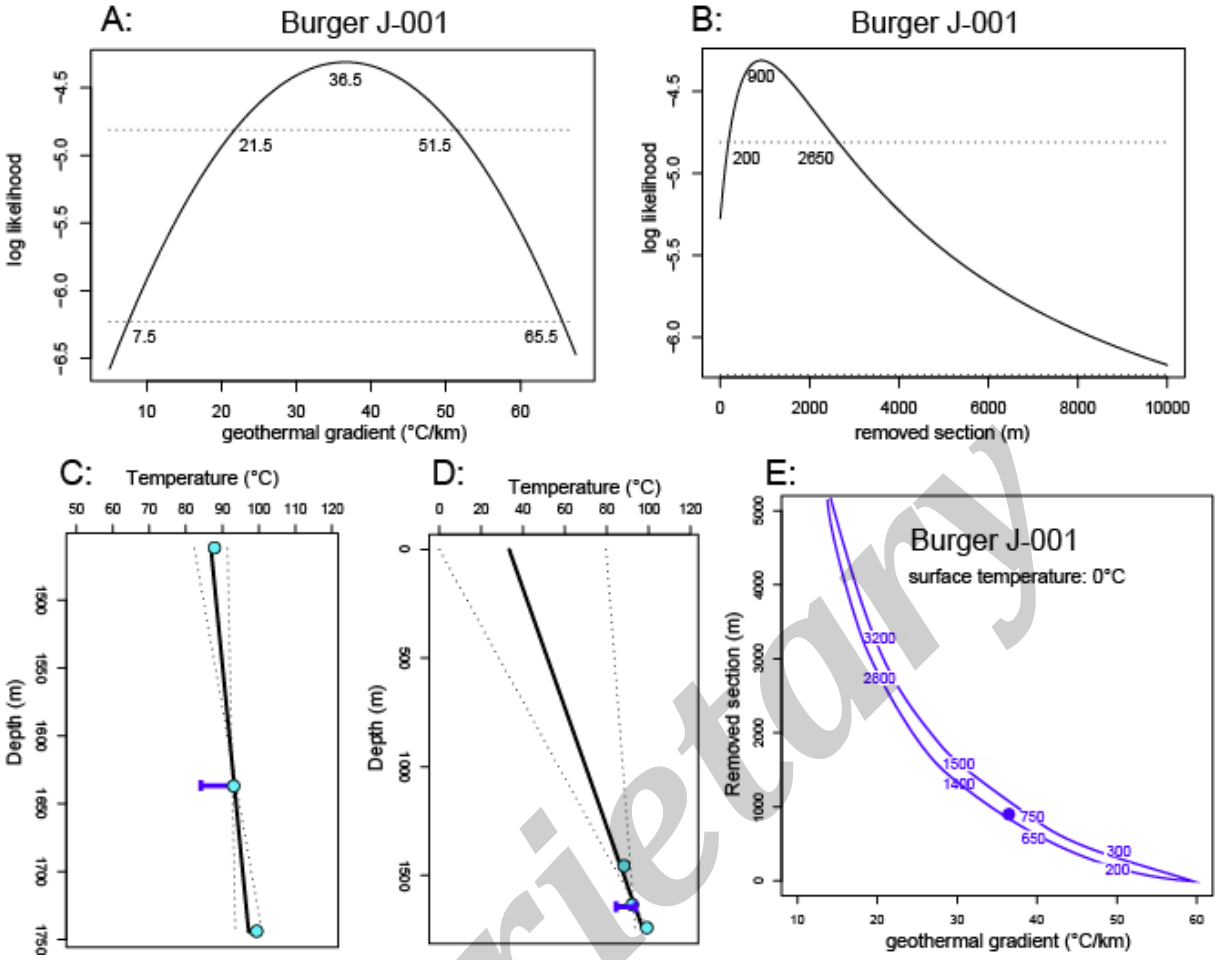

Figure 5.3: **Cenomanan-Campanian (99 to 73 Ma)** paleogeothermal gradients & removed section from **AFTA and ERC VR data** in the **Burger J-001** well**.**

A,B: Maximum likelihood profiles of linear paleogeothermal gradient (A:) and removed section (B:) fitted to **Cenomanan-Campanian (99 to 73 Ma)** paleotemperature constraints from **AFTA and ERC VR data**. The methodology used to construct these profiles is outlined in Appendix C.

C,D: Cenomanan-Campanian (99 to 73 Ma) paleotemperature constraints derived from **AFTA and ERC VR data** are plotted against depth below the unconformity below the presumed Quaternary section at a depth of 78.3 m rkb in this well, also showing the best-fit profile (solid line) and lines (dashed) representing upper and lower 95% confidence limits. In **D:** the fitted gradients are extrapolated to an assumed paleo-surface temperature of 0°C to determine removed section.

E: Crossplot of total section removed against paleogeothermal gradient, showing the ranges of paired values (within the contoured region) compatible with the paleotemperature constraints derived from **Cenomanan-Campanian (99 to 73 Ma)** paleotemperature constraints from **AFTA and ERC VR data** at the 95% confidence level. The values printed within the plot are amounts of removed section corresponding to ±2σ limits at various values of paleogeothermal gradient. For example, for a paleogeothermal gradient of 40°C/km, a thickness of between 650 and 750 metres of additional section is required in order to honour the paleotemperature constraints.

Alternative paleo-surface temperatures can also be accomodated, by subtracting or adding the difference in depth equivalent to the change in paleo-surface temperature, for the appropriate paleo-gradient. For example, for a paleogeothermal gradient of 40°C/km, an increase of 10°C in the paleo-surface temperature is equivalent to a reduction of 250 metres in the amount of removed section.

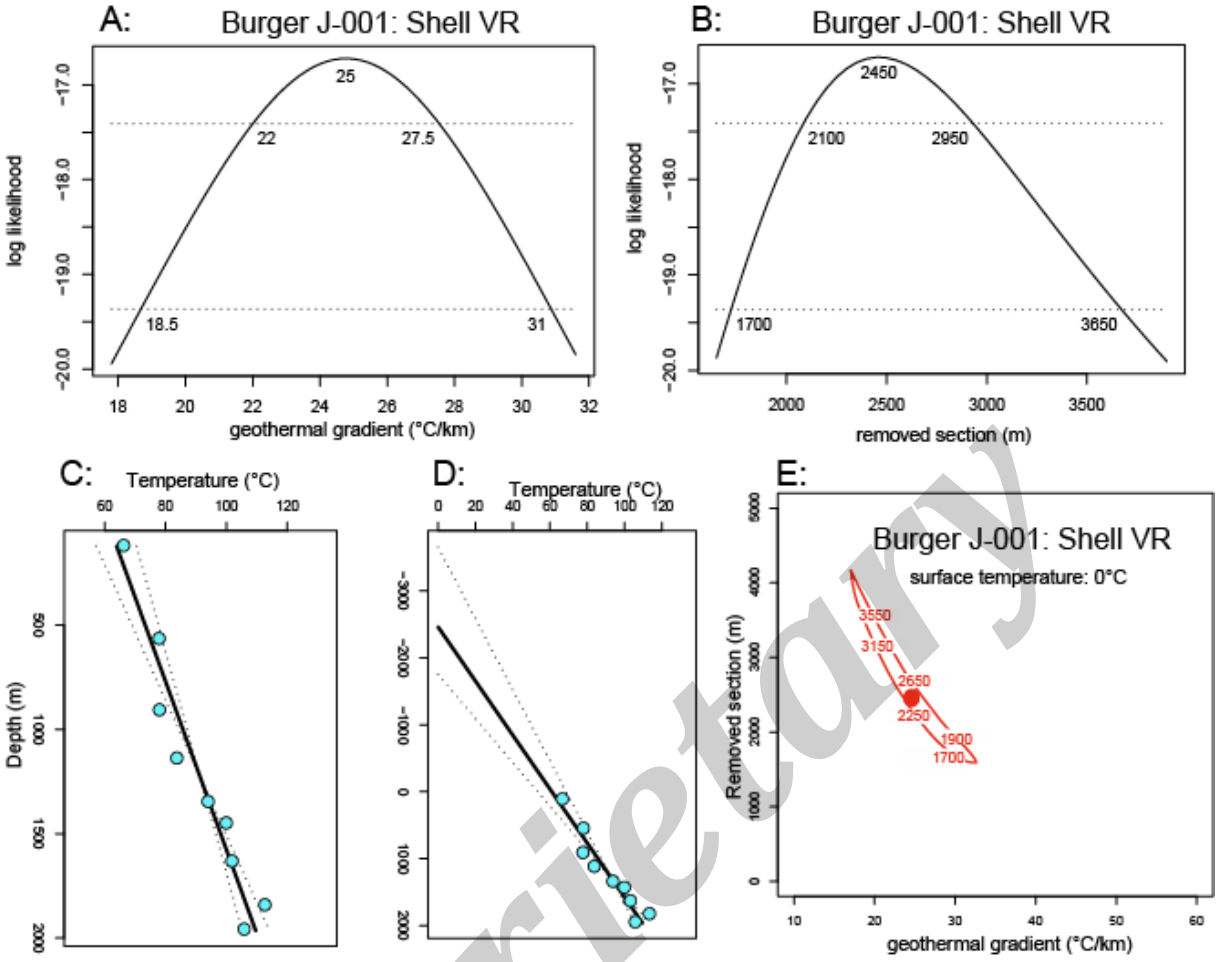

Figure 5.4: **Cenomanan-Campanian (99 to 73 Ma)** paleogeothermal gradients & removed section from **VR data supplied by Shell** in the **Burger J-001** well**.**

A,B: Maximum likelihood profiles of linear paleogeothermal gradient (A:) and removed section (B:) fitted to **Cenomanan-Campanian (99 to 73 Ma)** paleotemperature constraints from **VR data supplied by Shell only**. The methodology used to construct these profiles is outlined in Appendix C.

C,D: Cenomanan-Campanian (99 to 73 Ma) paleotemperature constraints derived from **VR data supplied by Shell only** are plotted against depth below the unconformity below the presumed Quaternary section at a depth of 78.3 m rkb in this well, also showing the best-fit profile (solid line) and lines (dashed) representing upper and lower 95% confidence limits. In **D:** the fitted gradients are extrapolated to an assumed paleo-surface temperature of 0°C to determine removed section.

E: Crossplot of total section removed against paleogeothermal gradient, showing the ranges of paired values (within the contoured region) compatible with the paleotemperature constraints derived from **Cenomanan-Campanian (99 to 73 Ma)** paleotemperature constraints from **VR data supplied by Shell only** at the 95% confidence level. The values printed within the plot are amounts of removed section corresponding to ±2σ limits at various values of paleogeothermal gradient. For example, for a paleogeothermal gradient of 30°C/km, a thickness of between 1700 and 1900 metres of additional section is required in order to honour the paleotemperature constraints.

Alternative paleo-surface temperatures can also be accomodated, by subtracting or adding the difference in depth equivalent to the change in paleo-surface temperature, for the appropriate paleo-gradient. For example, for a paleogeothermal gradient of 30°C/km, an increase of 10°C in the paleo-surface temperature is equivalent to a reduction of 333 metres in the amount of removed section.

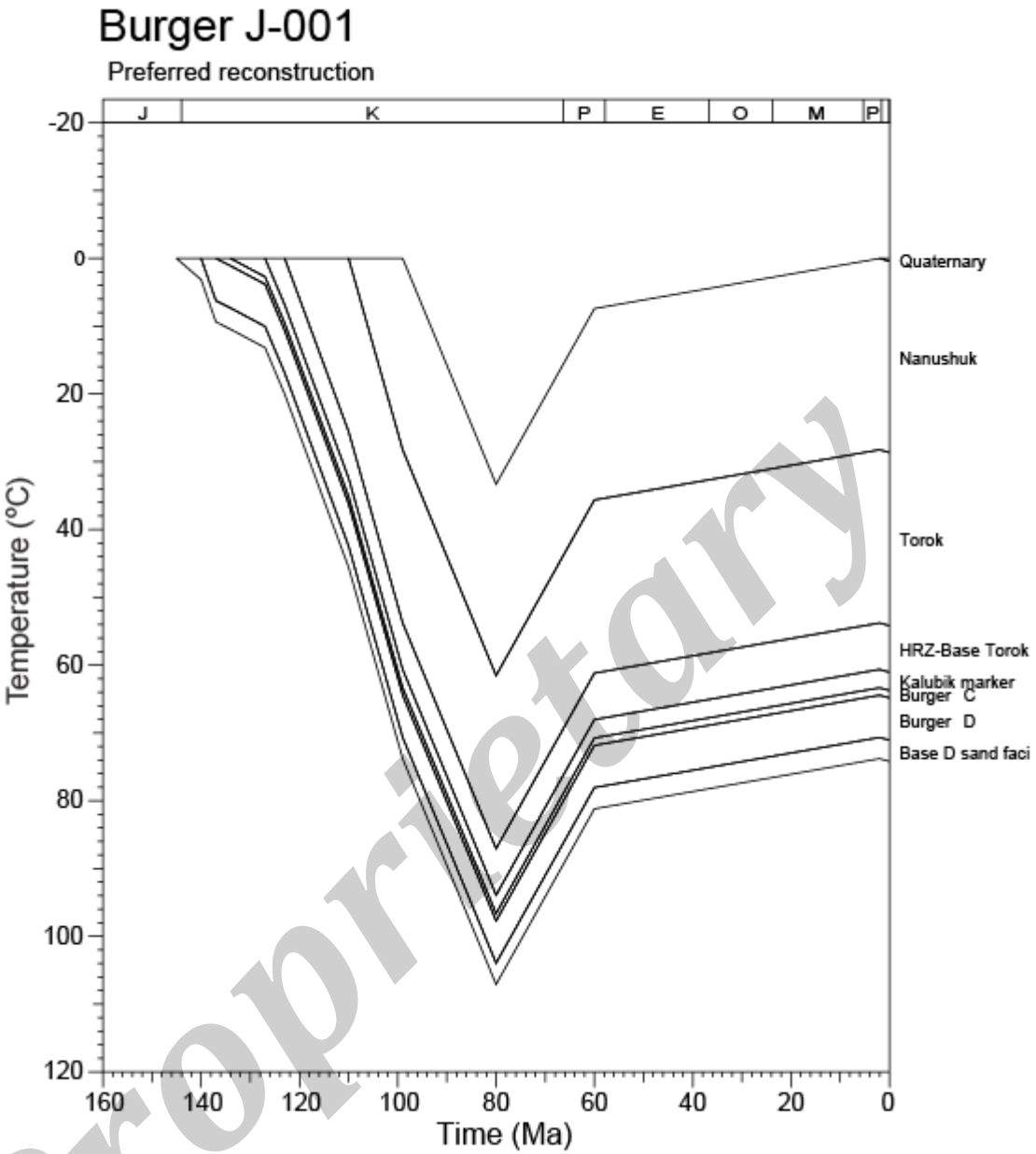

Figure 5.5: Preferred thermal history reconstruction derived from the interpretation of **AFTA and ERC VR data** in **Chukchi Sea well Burger J-001**.

This reconstruction is based on a constant paleogeothermal gradient of 37°C/km throughout the history, together with a constant surface temperature of 0°C, combined with the burial and uplift history shown in Figure 5.6. Note that a range of alternative combinations of thermal gradient and removed section are equally viable, within the constraints on paleogeothermal gradients and additional burial illustrated in Figures 5.3 and 5.4, but all would result in thermal history reconstruction similar to that shown here, which is well constrained by AFTA and ERC VR data in this well. Note also that the two-stage cooling is not constrained by data and is employed only to ensure cooling rates from the paleo-thermal maximum are close to the value used in the interpretation of the AFTA and VR data.

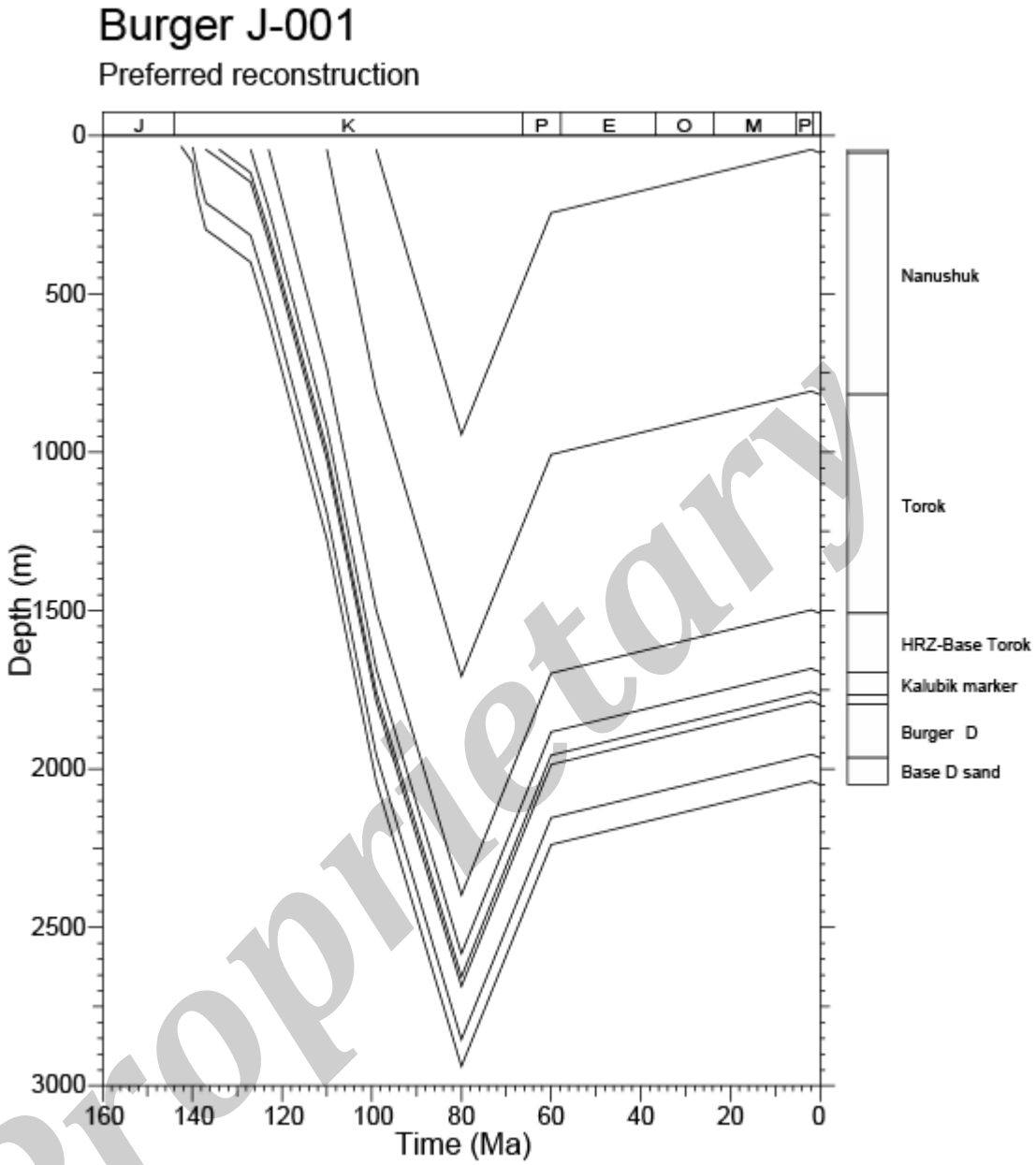

Figure 5.6: Preferred burial and uplift history reconstruction for **Chukchi Sea well Burger J-001**, used in assembling the thermal history reconstruction illustrated in Figure 5.5.

Full details are provided in the text. It should be emphasised that while the timing of the onset of exhumation is reasonably well defined, based on results from this well, a range of alternative scenarios are possible as regards the amount of additional section deposited and subsequently removed, within the confines of the constraints established in Figures 5.3 and 5.4. But all viable reconstructions lead to thermal history reconstructions similar to that shown in Figure 5.5 and the resulting maturation history (Figure 5.7) is defined with confidence. Note also that the two-stage nature of cooling from the paleo-thermal and paleo-burial maximum is not constrained by the data, and is included simply to maintain initial cooling rates close to the value used in the thermal history interpretation of AFTA and VR data presented in Section 4.

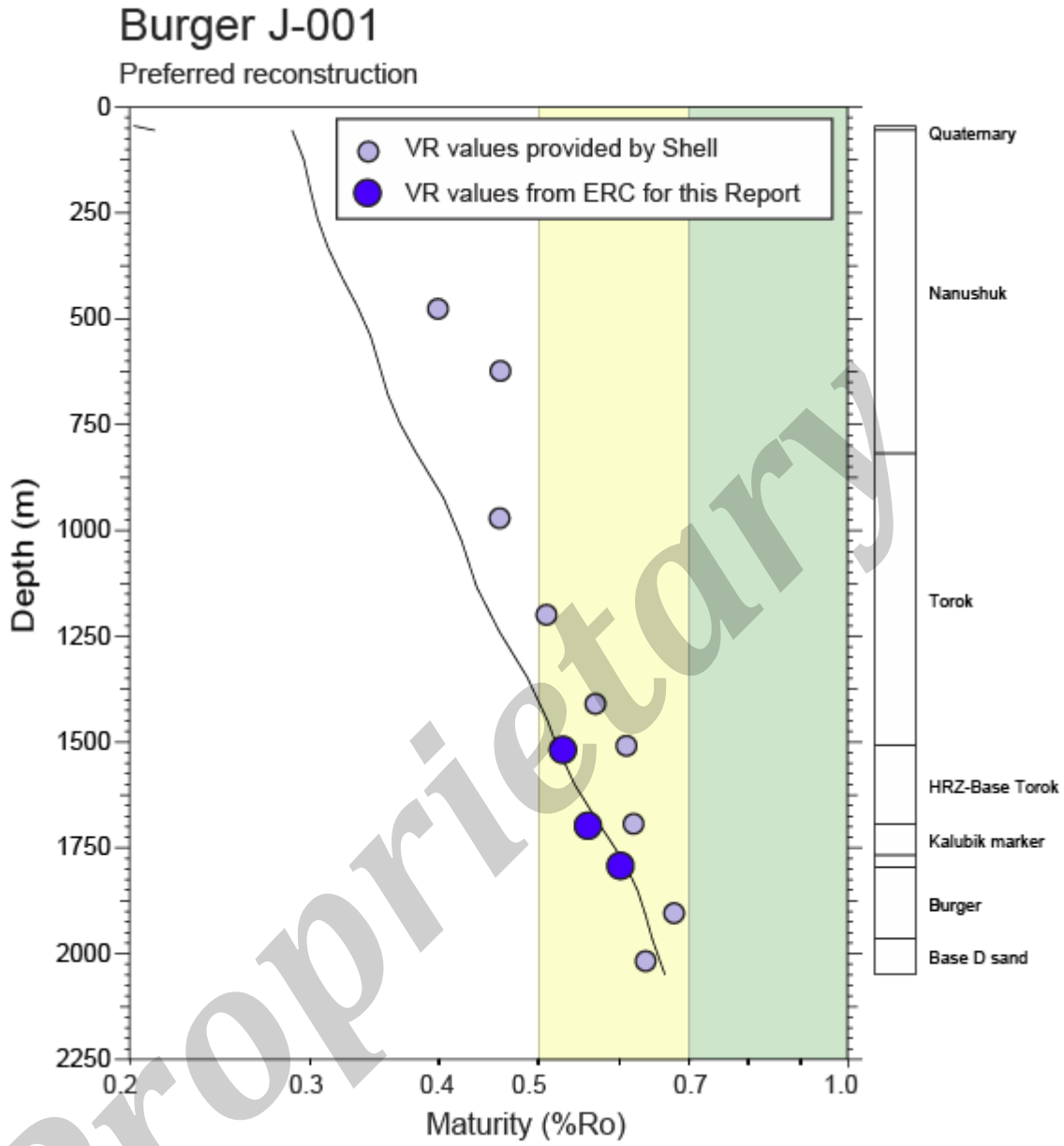

Figure 5.7: Vitrinite reflectance values (Tables D.2 and D.3) in **Chukchi Sea well Burger J-001**, plotted against depth, together with the maturity profile predicted by the preferred Thermal History Reconstruction derived from AFTA and VR data in this well illustrated in Figure 5.5.

Maturity windows corresponding to different stages of source rock maturation are also shown (Yellow - Early Mature (oil), 0.5 – 0.7%Ro: Light Green – Mid Mature (oil), 0.7 – 1.0%Ro). Deeper Cretaceous units intersected in this well lie within the Early Mature (Oil) window while shallower units remain immature. Maturity levels in this well reflect the effects of deeper burial prior to exhumation which began in **Cenomanian-Campanian times** and is now represented by the unconformity between the Nanushuk Fm and the overlying Quaternary section. Note that most of the VR data supplied by Shell are regarded as slightly too high in this reconstruction, which is based on the AFTA data and ERC VR values measured by Energy Research Consulting pty ltd (ERC). However, the deepest of the Shell values is consistent with the trend predicted by the preferred reconstruction.

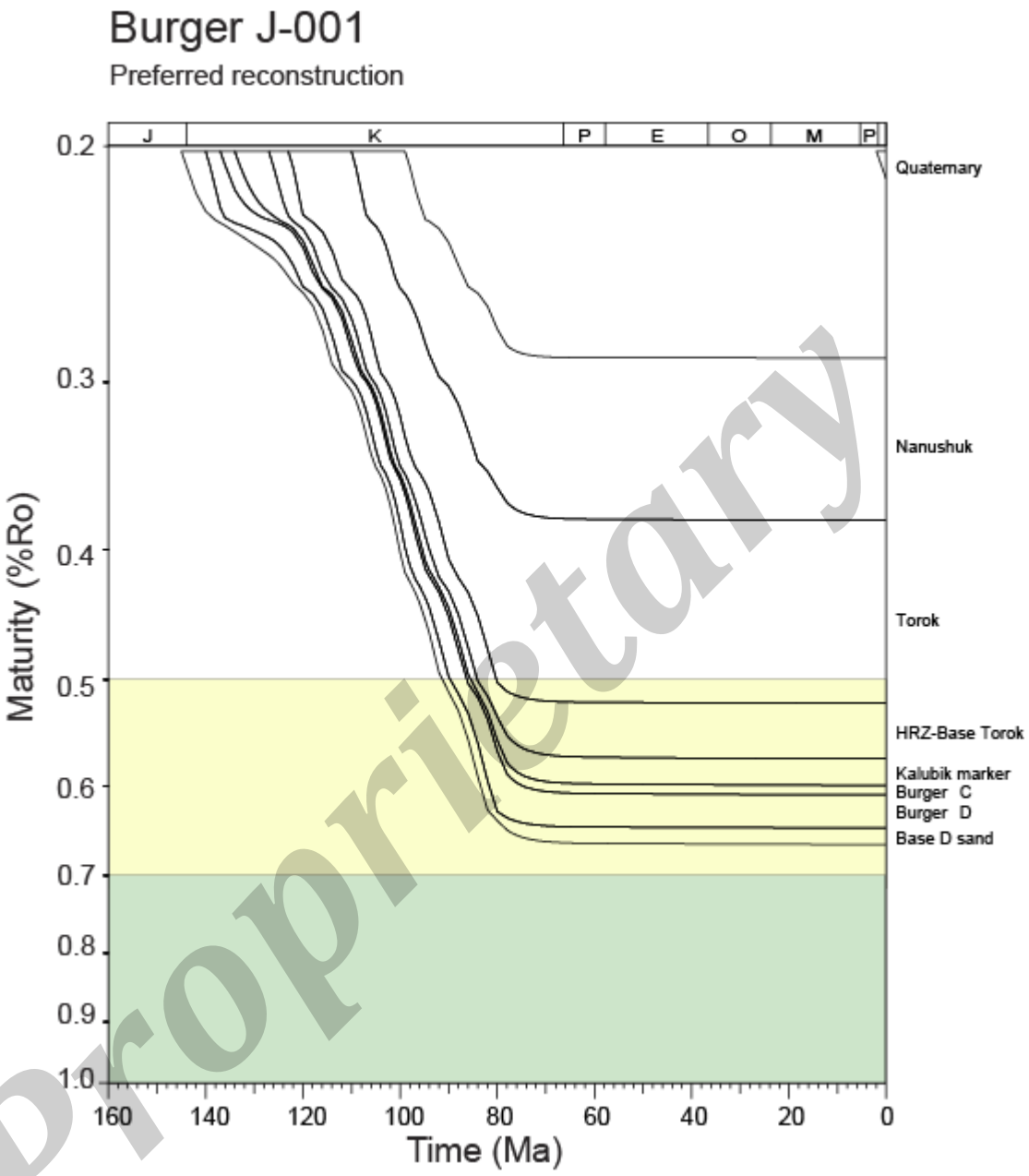

Figure 5.8: Pattern of maturation vs time for the preserved sedimentary section in **Chukchi Sea well Burger J-001,** predicted by the thermal history reconstruction shown in Figure 5.5.

Maturity windows are as in Figure 5.7. In this reconstruction, active maturation from deeper Cretaceous units ceased at 80 Ma at the onset of cooling due to exhumation (although any time between 99 and 73 Ma is allowed by the AFTA data from this well.

6. AFTA and VR data in Chukchi Sea well Burger 1

6.1 Introduction

The Burger 1 well was originally analysed for Geotrack Report GC314, at a time when our interpretive methods were not as advanced as they are today. For this study, sample GC314-23 was reprocessed using modern methods and the data were re-interpreted using the same approach as employed for the samples from the Burger J-001 well as described in Sections 3, 4 and 5. In the previous study, yields of apatite were similar to those in this study, and for that reason, data in three samples collected over a narrow depth interval were consolidated into a single sample, GC314-23.

The Burger 1 well intersected a similar stratigraphic section to that in the Burger J-001 well, with the exception that below the Cretaceous section the well penetrated over 500 m of Jurassic section, in which the well reached TD at 2500 m rkb. The detailed breakdown of the section intersected in the Burger 1 well is summarised in Table A.1 (conversion to numerical ages is based on Gradstein et al., 2012)..

A present-day thermal gradient of 34.1°C/km was provided for this well for the original study, and we have used this value, together with a sea bed temperature of 0°C, to describe the present-day thermal regime in this well (Table A.3, Appendix A). The AFTA data in the single sample analysed from the well are consistent with the present-day temperature calculated in this fashion, although due to the relatively shallow depths of the sample the present-day temperature does not exert any significant influence on the interpretation of the data. Therefore we have adopted the gradient of 34.1°C/km as the basis of thermal history interpretation of the AFTA and VR data in the **Burger 1** well.

6.2 Initial assessment of AFTA data

Introduction

As above, a single AFTA sample was analysed from this well, by combining data from a number of depth intervals within a narrow depth range. The single composite sample, GC314-23, is characterised by fission track ages in 26 single grain ages and 61 confined track lengths, and the data are considered to be highly reliable.

The fission track age and mean track length in this sample are summarised in Table 6.1 and plotted as a function of depth and present temperature in Figure 6.1, where

the fission track age data are contrasted with the variation of stratigraphic age through the section. The variation of fission track age and length vs depth predicted from the Default Thermal History (see Section 2.1) for this well are also shown in Figure 6.1, for selected apatite chlorine contents. Values predicted from the Default Thermal History for the single sample are also summarised in Table 6.1. These values take explicit account of the distribution of wt% Cl within each sample. The Default Thermal History used in construction of Figure 6.1 is based on the burial history derived from the preserved stratigraphy in the wells, illustrated in Figure 6.2, combined with the present-day thermal gradient of 34.1°C/km derived as explained in Appendix A.

Visual assessment of the data in Figure 6.1 shows that the measured fission track age in sample GC314-23 is close to the value predicted from the Default Thermal History, while the mean track length is shorter than predicted from the Default Thermal History. Thus, any effects of post-depositional heating to temperatures higher than present-day values were not sufficient to produce significant age reduction and detailed assessment is required before firm conclusions can be reached. This assessment is presented in Section 7.

6.3 Initial assessment of VR data

Introduction

VR data in samples from the Burger 1 well provided by the client are summarised in Table D.3. No information is available in regard to data quality, but data at depths around 1700 m rkb show considerable scatter suggesting some doubt in regard to precise VR levels at these depths at least.

The VR values are plotted against depth in Figure 6.3. Also shown in Figure 6.3 is the maturity profile predicted from the Default Thermal History - i.e., the thermal history predicted for samples from this well if they are currently at their maximum post-depositional temperatures, as defined in Section 2.1 of this report. The Default Thermal History used in construction of Figure 6.4 is based on the present-day thermal gradient of 34.1°C/km derived as explained in Appendix A, combined with the burial history derived from the preserved stratigraphy in the wells, illustrated in Figure 6.2.

Evidence that samples have been hotter in the past

All of the measured VR values plot well above the profile predicted from the Default Thermal History in Figure 6.3, showing that the sampled sedimentary units have been hotter in the past, although the AFTA data were more equivocal (Section 6.2). Therefore, the elevated paleotemperatures responsible for producing the observed VR levels must have been reached in such a way that the effects on the AFTA data are not immediately apparent – very similar to the situation in the Burger J-001 well (Section 3).

Magnitude of paleotemperatures from VR

Maximum paleotemperatures derived from the measured VR values in this well, calculated using the strategy outlined in Section 2.2, are summarised in Table 6.2. Values increase with depth from around 85°C in the shallowest samples to 139°C in the deepest sample, over a depth range of ~2 km.

In Section 7, the AFTA data are assessed in detail in the light of the maximum paleotemperatures indicated by these VR data.

Table 6.1: Summary of apatite fission track data and Default Thermal History predictions in samples from Chukchi Sea well Burger 1 (Geotrack Report #1191)

Sample number	Average depth (m)	Present temperature[*1] (°C)	Stratigraphic age (Ma)	Mean track length (µm)	Predicted mean track length[*2] (µm)	Fission track age (Ma)	Predicted fission track age[*2] (Ma)
OCS-Y-1413 Burger 1							
GC1191-1	1713	56	137-134	11.29±0.27	12.7	139.4±15.5	116

[*1] See Appendix A for discussion of present temperature data.

[*2] Values predicted from the Default Thermal History (Section 2.1); i.e. assuming that each sample is now at its maximum temperature since deposition. The values refer only to tracks formed after deposition. Samples may contain tracks inherited from sediment provenance areas. Calculations refer to apatites within the measured compositional range for each sample, as discussed in Appendix A. For this reason, predicted ages may not vary smoothly with depth.

Note: all depths quoted are TVD with respect to kb elevation.

Table 6.2: VR data and corresponding maximum paleotemperatures in samples from Chukchi Sea well Burger 1 (Geotrack Report #1191)

Sample number	Average depth (m)	Present temperature[*1] (°C)	Stratigraphic Age (Ma)	VR values provided by Shell[*2] (%)	Maximum paleotemp-erature[*3] (°C)
	467	14	110-99	0.52 (38)	86
	621	19	110-99	0.50 (51)	83
	784	25	110-99	0.53 (55)	88
	934	30	123-110	0.53 (47)	88
	1063	34	123-110	0.58 (49)	96
	1148	37	123-110	0.55 (54)	91
	1255	41	123-110	0.51 (42)	84
	1393	46	123-110	0.53 (52)	88
	1533	50	127-123	0.60 (56)	99
	1596	52	127-123	0.56 (53)	93
	1627	54	127-123	0.57 (58)	94
	1643	54	134-127	0.59 (56)	97
	1654	54	134-127	0.78 (57)	125
	1674	55	134-127	0.86 (50)	132
	1699.5	56	135-134	0.71 (15)	117
	1829	60	137-135	0.63 (42)	104
	1981	66	144-137	0.58 (41)	96
	2134	71	150-148	0.78 (32)	125
	2301	76	150-148	0.83 (40)	129
	2461.5	82	150-148	0.94 (44)	139

[*1] Present temperatures calculated using a present-day thermal gradient of 34.1°C/km as explained in Appendix A, combined with a sea bed temperature of 0°C..

[*2] From Table D.3. Numbers in brackets show the numbers of vitrinite fields measured for each sample

[*3] All estimates of maximum paleotemperature were determined using assumed heating and cooling rates of 1°C/Myr and 10°C/Myr, respectively.

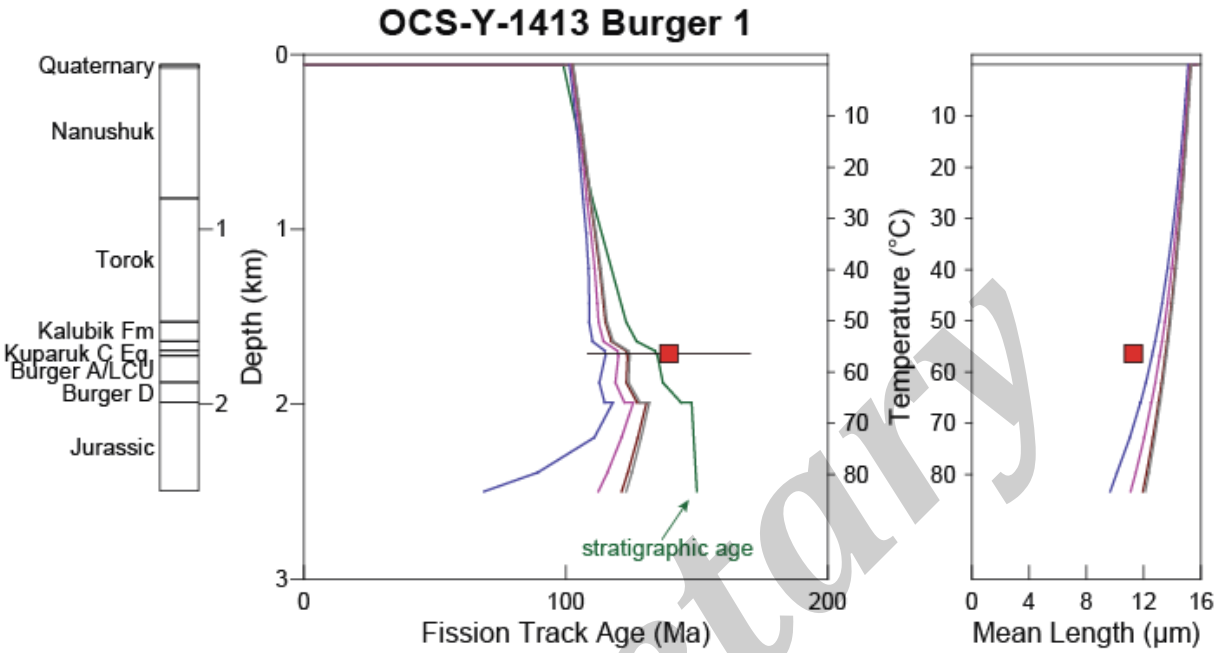

Figure 6.1: AFTA parameters in one sample from **Chukchi Sea well Burger 1**, plotted against sample depth and present temperature.

The variation of stratigraphic age with depth is also shown, as the solid green line in the central panel. Present-day temperatures shown here are based on a sea-bed temperature of 0°C and a present-day **thermal gradient of 34.1°C/km** for this well provided by the client (see Appendix A). Coloured lines show the pattern of fission track age and mean track length predicted from the Default Thermal History (see Section 2.1) for apatites containing 0.0-0.1, 0.4-0.5, 0.9-1.0 and 1.5-1.6 wt% Cl. The Default Thermal History is based on the thermal structure reported above, combined with the burial history shown in Figure 6.2.

The measured fission track age is within analytical uncertainty of the range of values predicted from the Default Thermal History, indicating that any paleo-thermal effects have not been of significant magnitude to produce significant age reduction. The mean track length is less than the range predicted from the Default Thermal History, which could be due to higher temperatures after deposition but could alternatively be explained by the presence of short tracks inherited from sediment source terrains. For this reason detailed assessment is required before firm conclusions can be reached.

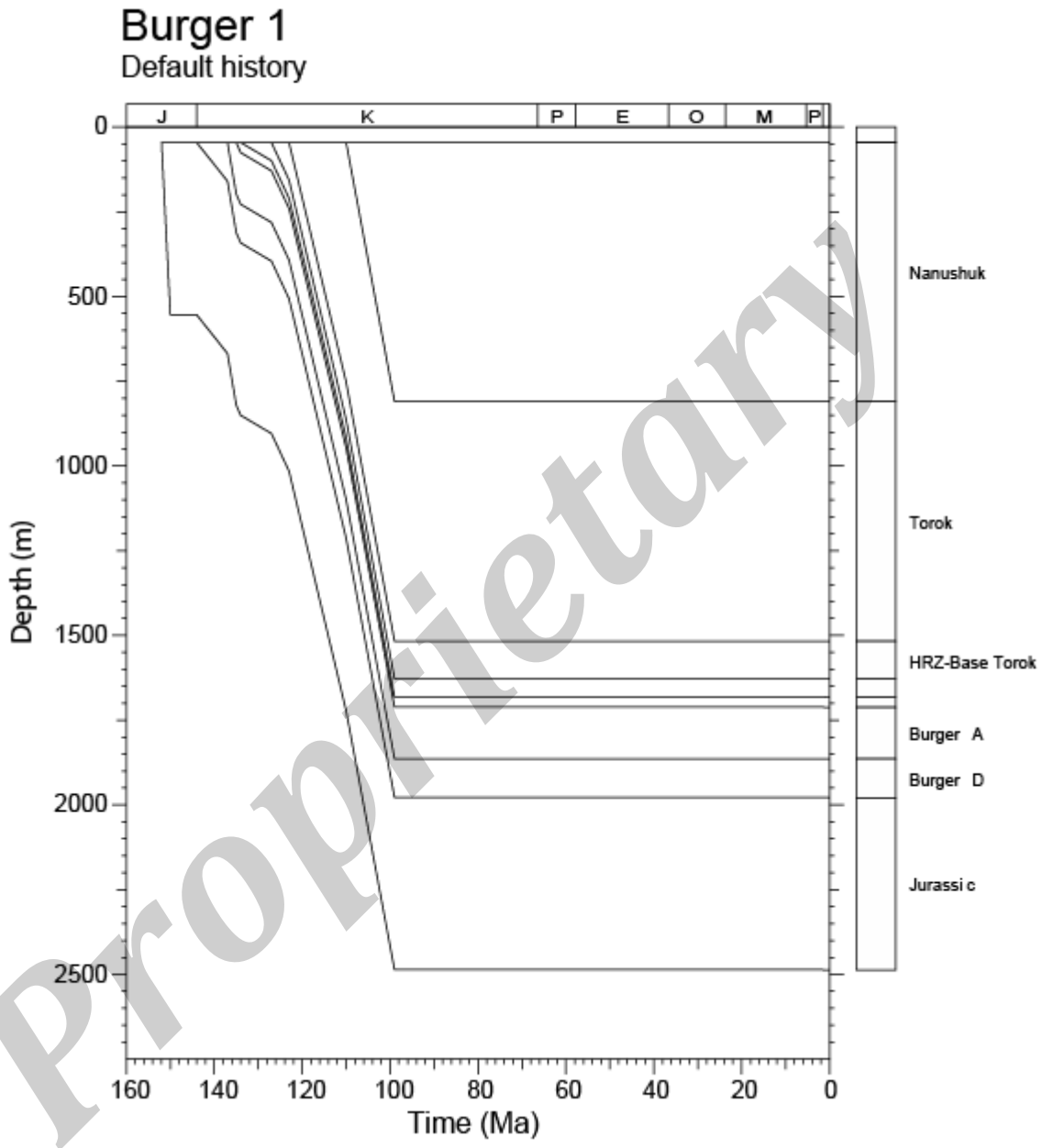

Figure 6.2: Burial history derived from the preserved section in **Chukchi Sea well Burger 1**.

This history, together with a present-day thermal gradient of 34.1°C/km (derived as described in Appendix A) and a sea bed temperature of 0°C, has been used to predict the Default Thermal Histories for individual AFTA samples, as employed in the construction of Figure 6.1, and for prediction of the maturity-depth profile in Figure 6.3.

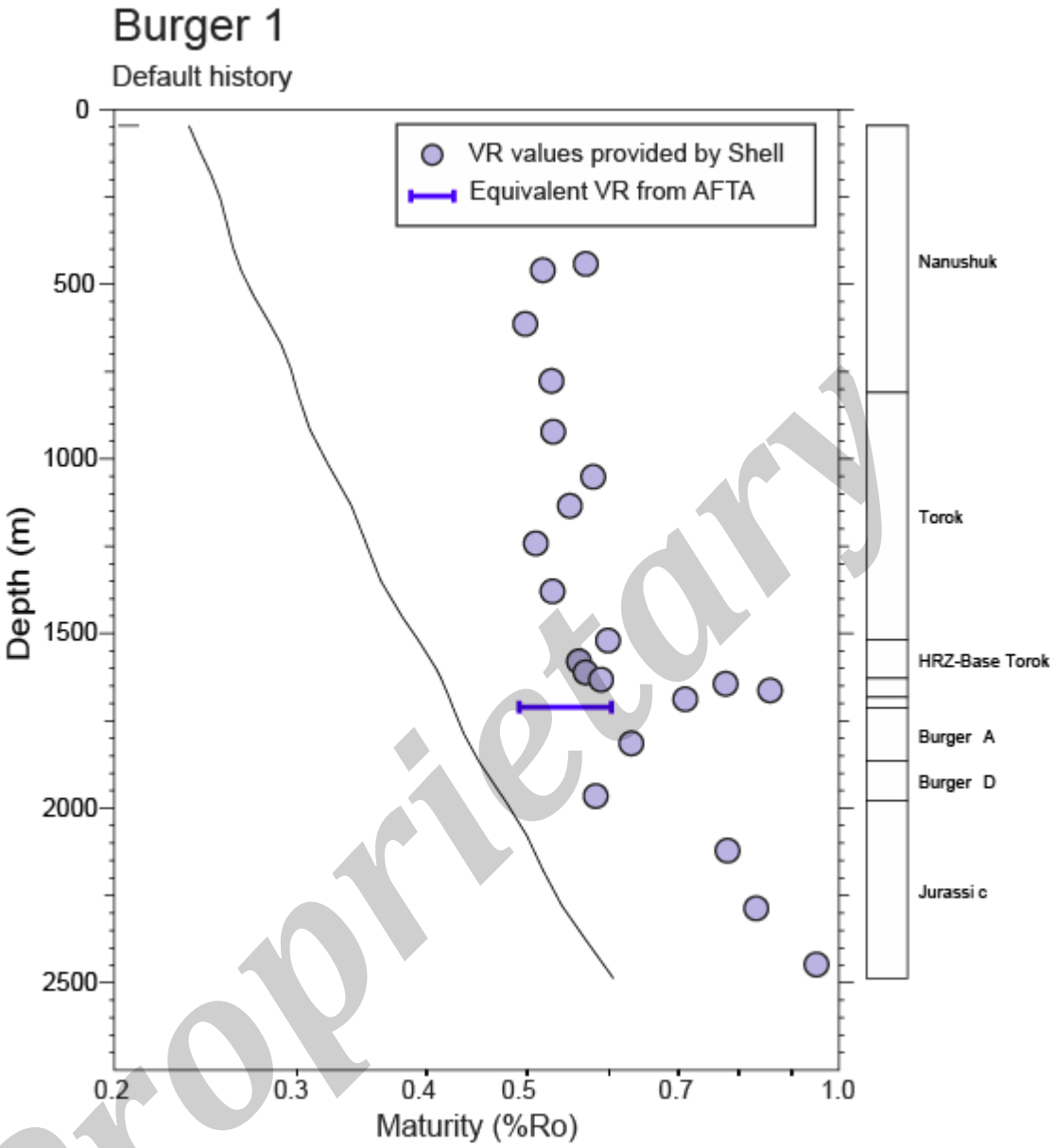

Figure 6.3: Mean vitrinite reflectance (VR) values and equivalent VR level from AFTA data in **Chukchi Sea well Burger 1**, plotted against depth (below kb).

VR values provided by Shell are listed in Table D.3 (Appendix D) while the equivalent VR range derived from AFTA data in sample GC314-23 is explained in Table 6.1. The solid black line shows the VR profile predicted by the "Default History", i.e., the profile expected if samples throughout the section are currently at their maximum temperature since deposition (Section 2.1) based on a thermal gradient of 34.1°C/km, derived as described in Appendix A, together with a sea bed temperature of 0°C. All measured VR values plot above the predicted profile, showing that the sampled section has been much hotter than present temperatures at some time since deposition. See text for further discussion.

7. Thermal history interpretation of AFTA and VR data in the Burger 1 well

7.1 Background

Thermal history interpretation of AFTA data in the single sample analysed from this well is presented in Table 7.1 and illustrated schematically in Figure 7.1.

For downhole samples, the consistency of the AFTA data with present-day temperatures is assessed. This is typically based on the lengths of the longest tracks in each sample, which are those that have experienced the lowest temperatures and therefore the most recently formed. But at temperatures of around 100°C or more the degree of annealing (i.e. age reduction) of tracks in the more sensitive (i.e. Cl-poor) apatites is also useful.

The data are then assessed in qualitative terms for evidence of whether samples have been hotter after deposition or emplacement (for Phanerozoic sedimentary and igneous rocks, respectively). If samples of Precambrian basement from outcrop have been analysed, they are assessed for evidence of whether they have been hotter in Phanerozoic times.

Quantitative interpretation of the AFTA data is then summarised, in terms of the maximum paleotemperature and the timing of cooling in one or more discrete episodes, as required in order to explain all facets of the data. As explained in Section 2.1 and Appendix C, these thermal history solutions are extracted from the data in each sample using in-house software which compares the AFTA parameters (fission track age and track length distribution and their variation with Cl content) predicted for a range of likely thermal history scenarios with the measured values, defining the range of conditions for which predictions are consistent with the measured data within 95% confidence limits. Similar considerations also allow determination of cooling episodes prior to deposition for sedimentary samples, representing events in sediment provenance regions, where appropriate. Comments are also provided on the consistency between the thermal history constraints derived from the AFTA data and VR values in the same or adjacent samples.

Finally, a schematic illustration of the thermal history solution in each sample is provided. Thermal history constraints are derived within a framework of episodic heating and cooling. It is emphasised that only the coloured polygons represent constraints derived from the AFTA data. The black lines are for guidance only, because the temperature during the interval between each cooling episode is not constrained by the data (except that it did not exceed that in subsequent events). This

type of framework is clearly appropriate for sedimentary rocks, and for basement rocks on which sedimentary remnants are preserved, but we believe that episodic histories are appropriate in most, if not all settings. See Green and Duddy (2012) and Green et al. (2013) for a detailed justification of this approach, together with further details.

Thermal history solutions derived from the AFTA data in each sample are summarised in Table i.

7.2 Extracting thermal history constraints from the AFTA data

Comments on present-day temperatures on the basis of AFTA

Certain aspects of AFTA data are sensitive to the present-day thermal regime (essentially the longest tracks in each sample and the temperatures at which the fission track ages are progressively reduced towards zero). The single AFTA sample analysed from this well is from a depth where the present-day temperature is <70°C. In these conditions, AFTA data are not particularly sensitive to present–day temperatures. Nevertheless, as explained in Table 7.1 the data in the sample from this well, particularly the longest tracks within the length distribution, are highly consistent with the temperatures calculated using the present-day thermal gradient of 34.1°C/km derived as explained in Appendix A. We therefore proceed to use this gradient as the basis for extracting thermal history constraints from the AFTA and VR data in the well.

Evidence for elevated paleotemperatures from AFTA

As summarised in Table 7.1, while the fission track age data in sample GC314-23 show no direct evidence that the sample has ever been hotter than the present-day temperatures at any time after deposition, the track length data can only be explained by the effects of higher temperatures after deposition. Note that this is true only for the data in apatite grains comprising the younger age population in this sample. Track length data in grains with older ages are more equivocal, but are consistent with the interpretation of data from the younger age population.

Magnitude of paleotemperatures and timing of cooling from AFTA

As summarised in Table 7.1, AFTA data in grains comprising the younger age population in sample GC314-23 require that the sample began to cool from a maximum paleotemperature between 80 and 99°C at some time between 106 and 20 Ma. Data in the older age population can be explained in terms of cooling from between 75 and 105°C at some time after deposition although this temperature could also have been reached prior to deposition in sediment provenance regions. Based on data from the younger age population, this event can be interpreted as post-depositional,

7.3 Integration of AFTA and VR data

The VR data at similar depths to AFTA sample GC314-23 show some scatter with lowest values between 0.56 and 0.63% suggesting a maximum post-depositional paleotemperatures between 93 and 104°C with a value around 0.59% equivalent to a maximum paleotemperature of 97°C close to the depth of the AFTA sample (Table 6.2, Figure 6.3). As shown in Figure 7.1, the thermal history constraints derived from AFTA data in sample GC314-23 are consistent with this maximum paleotemperatures provided that cooling began prior to ~50 Ma.

The thermal history constraints AFTA data provided by the AFTA data suggest that the higher VR values in Figure 6.3 and too high, while the lower values and the trend that they define appear to be more consistent with the AFTA data (Figure 7.2).

7.4 Comparison with the Burger J-001 well

AFTA data from composite samples GC1191-2&3 and GC1191-4&5 from the **Burger J-001** well are very similar to those in sample GC314-23 from the **Burger 1** well, in showing a population of fission track ages close to the depositional age and a number of older ages.

Thermal history constraints from AFTA data in the two wells are also very similar in showing that cooling from the paleotemperatures indicated by VR data must have begun towards the earlier part of the interval represented by the Late Cretaceous-Quaternary unconformity close to sea bed in these wells.

A third point of similarity between the two wells is the suggestion that many of the VR values supplied by Shell are too high, while lower values within these datasets may be more reliable.

On the basis of this similarity between results from the two wells, we suggest that a common history is appropriate, and that the onset of cooling **between 99 and 73 Ma (Cenomanian-Campanian)** defined for the **Burger J-001** well should also be applied to the **Burger 1** well.

For a constant paleogeothermal gradient of 34.1°C/km in the **Burger 1** well, the range of maximum paleotemperatures between 80 and 99°C defined from AFTA data in sample GC314-23 is equivalent to deeper burial by between 700 and 1250 m of additional section, again very similar to the corresponding estimate for the **Burger J-001** well determined in Section 5.

Table 7.1: Thermal history interpretation of AFTA data in sample GC314-23

Sample type: Cuttings	Well name.	Burger 1		
Depth (rkb): 1698-1728 m	Present temp:	56°C	Strat. Age:	137-134 Ma
Default history predictions:	Fission track age;	116 Ma	Mean track length;	12.8 µm
Measured values:	Fission track age;	138.7 ± 15.0 Ma	Mean track length;	11.29 ± 0.27 µm
Age data structure:				
Young population	Fission track age;	133.7 ± 8.9 Ma	Mean track length;	11.48 ± 0.27µm
Old population	Fission track age;	265.3 ± 34.8 Ma	Mean track length;	10.88 ± 0.50 µm
Anomalously young age		19.3 ± 8.2 Ma		

Are AFTA data consistent with present-day temperature?

All aspects of the AFTA data, particularly the longest track lengths within the length distribution, are consistent with the present temperature of 56°C calculated as explained in Appendix A.

Evidence of higher temperatures in the past

from length data?	Yes: The mean track length of grains comprising the young age population in this sample is significantly less than predicted from the Default Thermal History. Modelling the AFTA parameters through different thermal history scenarios shows that this can be explained only by the effects of higher temperatures after deposition. Track lengths in the older age population are more equivocal, but they do not conflict with the conclusion from the younger population.
from fission track age data?	No: The central fission track age for the entire sample is consistent with the value predicted from the Default Thermal History, as is the pooled age characterising the younger age population (above). One single grain age which is significantly younger than predicted from the Default Thermal History appears to be anomalous and has been excised from the data prior to extraction of thermal history constraints.
Conclusion:	Track length data in grains comprising the younger age population confirm that this sample has been hotter than the present-day temperature after deposition.

Paleo-thermal constraints

	Pre-deposition		**post-deposition**	
	Maximum paleo-temperature (°C)	Onset Of Cooling (Ma)	Maximum paleo-temperature (°C)	Onset Of Cooling (Ma)
Young population	>127	254-165	80-99	106-20
Old population	>125	>300	*75-105*	*Post-deposition*
	93-105	401-133		

The AFTA data in this sample comprise two distinct age populations (see above), one with ages close to the depositional age and one with older ages, together with one anomalously young age which has been excised (see AFTA Data Summary Sheet, Appendix B). The data in grains comprising the younger age population can be explained by a scenario involving two paleo-thermal episodes, as listed above. The onset of cooling in the earlier of two episodes defined from the young population is clearly pre-depositional, while the younger episode is post-depositional, requiring cooling from a maximum paleotemperature between 80 and 99°C which began some time between 106 and 20 Ma. Data in grains comprising the older population define two pre-depositional episodes as shown above, and would allow post-depositional cooling from between 75 and 107°C some time after deposition, but this could alternatively be explained as representing a final stage of pre-depositional cooling (although the interpretation of data from the younger age population suggests that this event is the sa,e post-depositional episode as defined in the younger population). VR data from this well show some scatter with the lowest value suggesting a maximum post-depositional paleotemperature around 97°C (Table 6.2, Figure 6.3). The AFTA data comprising the younger age population are consistent with post-depositional heating to 97°C if cooling began earlier than 69 Ma (see Figure, next page), although allowing a reasonable uncertainty around the VR-derived maximum paleotemperature would allow a wider limit of perhaps prior to 50 Ma for the onset of

cooling. In summary, we conclude that cooling from around 97°C must have occurred prior to ~50 Ma, although the AFTA data allow a wider range, as shown above and in the Figure..

High quality AFTA data (26 ages, 61 track lengths) provide an interpretation which is regarded as highly reliable within the stated limits, although division between two age populations reduces the eventual level of precision.

Equivalent $R_o$max 0.48-0.60% (from young age population). A measured value of 0.59% provided by Shell from a slightly shallower depth (Table D.3), equivalent to a maximum paleotemperature of 97°C (Table 6.3) is consistent with this range and favours an onset of cooling prior to 50 Ma (see Figure). Other values at similar depths show considerable scatter but are all higher than the range allowed from the AFTA data and are regarded as anomalously high.

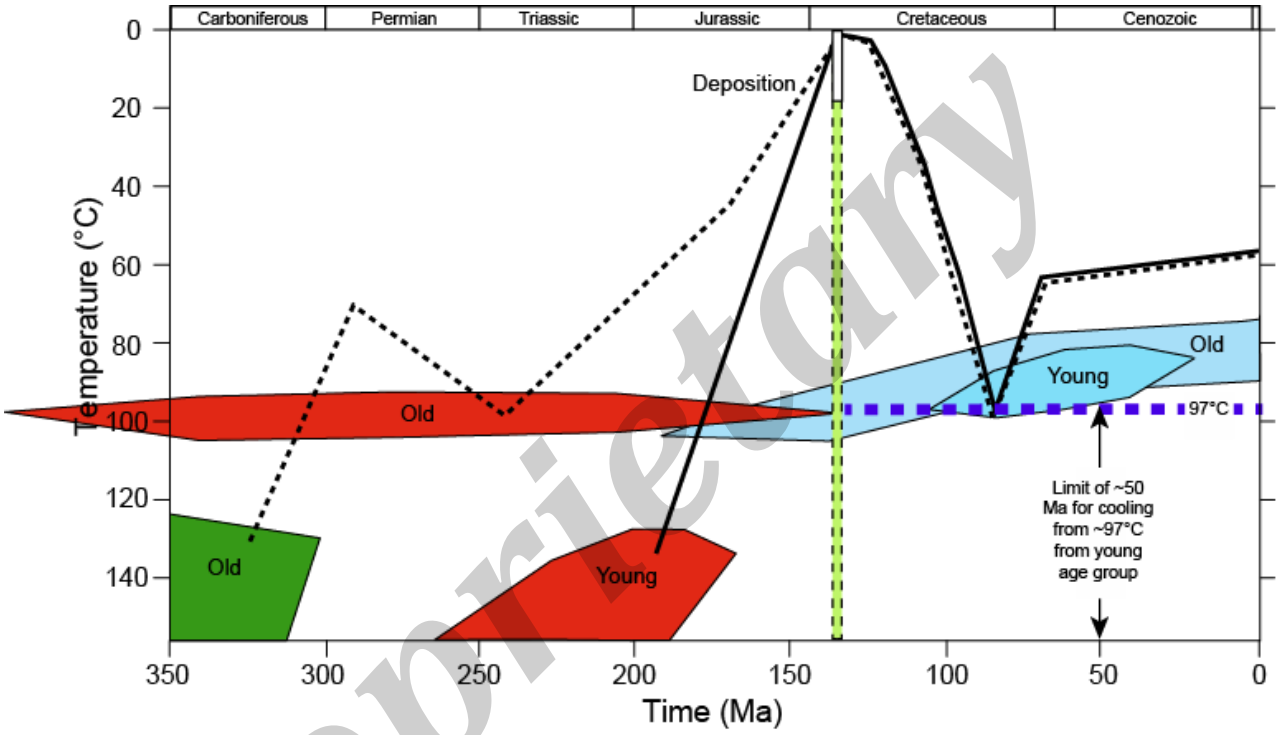

Figure 7.1: Thermal history interpretation summary, Composite sample GC314-23

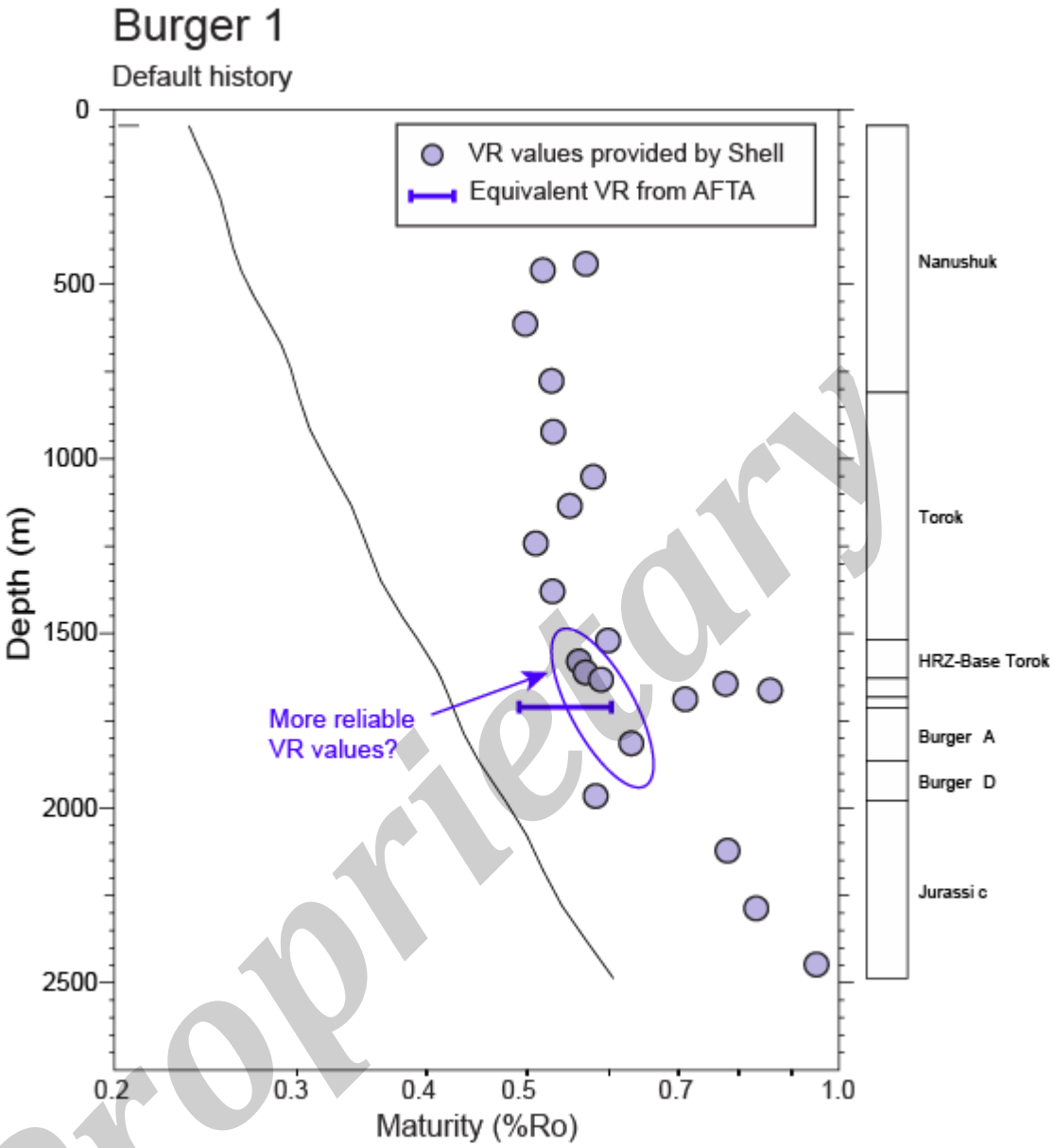

Figure 7.2: Mean vitrinite reflectance (VR) values and equivalent VR level from AFTA data in **Chukchi Sea well Burger 1**, plotted against depth (below kb) as in Figure 6.3, indicating the more reliable VR values at similar depths to the AFTA sample.

8. Recommendations for further work

The timing and magnitude of the major paleo-thermal episode that has affected the sedimentary section intersected in the **Burger J-001** and **Burger-1** wells appear to be well-defined on the basis of the AFTA data presented in this Report. Given that samples analysed from the **Burger J-001** well were close to TD there seems little to be gained from further analyses in that well. However, if sand-prone horizons are present within the Jurassic section intersected near TD in the **Burger-1** well, it is possible that further AFTA analyses in samples from those depths would provide improved insights.

Given the lack of consistency between the AFTA data presented here and the VR data supplied from Shell, we also recommend that additional VR analyses would be of benefit in resolving some of the remaining inconsistencies.

References

Bray, R.J., Green, P.F. and Duddy, I.R., 1992. Thermal History Reconstruction using apatite fission track analysis and vitrinite reflectance: a case study from the UK East Midlands and the Southern North Sea. In: Hardman, R.F.P. (ed.), *Exploration Britain: Into the next decade*. Geological Society Special Publication, **67**, 3-25.

Burnham, A.K. and Sweeney, J.J., 1989. A chemical kinetic model of vitrinite reflectance maturation. *Geochimica et Cosmochimica Acta.*, **53**, 2649-2657.

Gradstein, F.M., Ogg, J.G., Schmidtz, M.D. and Ogg, G.M. 2012. *A geologic time scale 2012*, Cambridge University Press

Sweeney, J.J. and Burnham, A.K., 1990. Evaluation of a simple model of vitrinite reflectance based on chemical kinetics. *AAPG Bulletin*, **74**, 1559-1570.

APPENDIX A

Sample Details, Geological Data and Apatite Compositions

A.1 Sample details

Samples of cuttings from seven depth intervals in **Chukchi Sea well Burger J-001** were submitted for AFTA by **Shell, Houston**. Details of these samples, including sample depths, stratigraphic ages and estimates of present temperature for each sample, are summarised in Table A.1. (Details of present temperature estimation for the well are presented in Section A.3, below). In addition, existing AFTA grain mounts for samples from the **Burger-1 well**, originally processed for Geotrack Report GC341 were reprocessed and reinterpreted for this Report. Yields of apatite obtained from each AFTA sample are listed in Table A.1. These yields are summarised and discussed in Section 1.3, together with discussion of overall AFTA data quality.

The two deepest samples analysed from the **Burger J-001** well each yielded only a very small number of apatite grains suitable for analysis and these samples were not processed further. An excellent apatite yield was obtained from sample GC1191-1 and the resulting data were of sufficient quality to provide a reliable interpretation. However, this was not the case for the four remaining samples. After assessment of apatite yields in these samples (see Section 1.3 and Table A.1), and taking into account the proximity of samples GC1191-2 and -3, as well as samples GC1191-4 and -5 (Table A.1) it was decided, in consultation with the client, that data in samples GC1191-2 and -3 should be combined into a single composite sample GC1193-23 while data in samples GC1191-4 and -5, were combined in composite sample GC1193-45. Thus full AFTA interpretations were obtained for three depth intervals in the **Burger J-001 well.**

Vitrinite reflectance (VR) data from the **Burger J-001 and Burger-1 wells** were also provided by Shell. No additional samples from either well were supplied to Geotrack specifically for VR determinations, although ultimately material from three of the AFTA samples from the **Burger J-001** well was submitted to Paddy Ranasinghe, Principal Organic Petrologist, Energy Resources Consulting Pty Ltd. Paddy was formerly chief analyst at Keiraville Konsultants, Wollongong, New South Wales.

Results of these analyses, together with sample details, are summarised in Table D.2 (Appendix D), while the values provided by Shell are listed in Table D.3.

A.2 Stratigraphic details

Details of the stratigraphic breakdown of the preserved section in both wells were provided by the client. The chronostratic (relative succession) assignment of each sample was converted to a chronometric (numerical) scale using Gradstein et al. (2012), with results summarised in Table A.2. The stratigraphic age of each AFTA sample, derived from this information, is summarised in Table A.1. Similar information for VR samples is summarised in Tables D.2 and D.3.

Any slight errors in the estimated chronometric ages of each sample are not expected to affect the thermal history interpretation of either the AFTA or VR data to any significant degree.

A.3 Present temperatures

In application of any technique involving estimation of paleotemperatures, it is critical to control the present temperature profile, since estimation of maximum paleotemperatures proceeds from assessing how much of the observed effect could be explained by the magnitude of present temperatures.

For this report, formation temperatures at two depths in the **Burger J-001** well were provided by the client. These are plotted against depth in Figure A.1 and together with a sea bed temperature of 0°C they define a thermal gradient of 37°C/km. This value has been adopted for this well, combined with a sea bed temperature of 0°C, as shown in Figure A.1, to represent the present-day thermal regime. For the Burger-1 well, a present-day thermal gradient of 34.1°C/km was taken from information associated with the previous study of this well in Geotrack Report GC314. AFTA data in all samples from both wells are consistent with the present-day temperatures calculated in this way.

A.4 Grain morphologies

The apatite grains in samples analysed for this study are characterised dominantly by euhedral to sub-euhedral morphologies, while some sub-rounded grains are present in each sample. Well-rounded grains are absent in all samples. No clear trends were

evident which could be interpreted in terms of systematic variation in sedimentary provenance between different samples.

A.5 Apatite compositions

The annealing kinetics of fission tracks in apatite are affected by chemical composition, specifically the Cl content, as explained in more detail in Appendix C. In all samples analysed for this report, Cl contents were measured in all apatite grains analysed (i.e. for both fission track age determination and track length measurement), and the measured compositions in individual grains have been employed in interpreting the AFTA data, using methods outlined in Appendix C.

Chlorine contents were measured using a fully automated Jeol JXA-5A electron microprobe equipped with a computer controlled X-Y-Z stage and three computer controlled wavelength dispersive crystal spectrometers, with an accelerating voltage of 15kV and beam current of 25nA. The beam was defocussed to 20 µm diameter to avoid problems associated with apatite decomposition, which occur under a fully focussed 1 - 2 µm beam. The X-Y co-ordinates of dated grains within the grain mount were transferred from the Autoscan Fission Track Stage to a file suitable for direct input into the electron microprobe. The identification of each grain was verified optically prior to analysis. Cl count rates from the analysed grains were converted to wt% Cl by reference to those from a Durango apatite standard (Melbourne University Standard APT151), analysed at regular intervals. This approach implicitly takes into account atomic number absorption and fluorescence matrix effects, which are normally calculated explicitly when analysing for all elements. A value of 0.43 wt% Cl was used for the Durango standard, based on repeated measurements on the same single fragment using pure rock salt (NaCl) as a standard for chlorine. This approach gives essentially identical results to Cl contents determined from full compositional measurements, but has the advantage of reducing analytical time by a factor of ten or more.

Chlorine contents in individual grains are listed in the fission track age summary data sheet for each sample in Appendix B. Table B.3 contains fission track age and length data grouped into 0.1 wt% Cl intervals on the basis of chlorine contents of the grains from which the data are derived. A plot of fission track age against Cl content is also shown in the data sheet for each sample, together with a histogram of Cl contents in all individual apatite grains analysed from each sample (i.e. grains analysed for both age and length measurements).

Lower limits of detection for chlorine content have been calculated for typical analytical conditions (beam current, counting time, etc.) and are listed in Table A.4. Errors in wt% composition are given as a percentage and quoted at 1σ for chlorine determinations. A generalised summary of errors for various wt% chlorine values is presented in Table A.5.

Apatite compositions in this study

In all samples analysed for this study, the histograms of Cl content show a similar pattern, typical of the distribution of Cl contents found in detrital apatites from common quartzo-feldspathic sandstones around the world. The majority of grains have Cl contents between 0 and 0.1 wt%, while a smaller number of grains give values up to ~0.5 wt% (close to the value found in the Durango apatite on which our original kinetic model of fission track behaviour was based, see Appendix C), and occasional grains contain between 0.5 and 1.0 wt% Cl or above.

In each of the samples analysed for this report, the measured distribution of compositions has been employed in interpreting the AFTA data, using methods outlined in Appendix C.

References

Gradstein, F.M., Ogg, J.G., Schmidtz, M.D. and Ogg, G.M. 2012. *A geologic time scale 2012*, Cambridge University Press.

Table A.1: Details of fission track samples and apatite yields - samples from Alaska (Geotrack Report #1191)

Sample number	Depth TVDrKB (m)	Sample type	Stratigraphic Subdivision	Stratigraphic age (Ma)	Present temperature *1 (°C)	Raw weight (g)	Washed weight (g)	Apatite yield *2
OCS-Y-2321 Burger J 001								
GC1191-1	1536-1545 *(5040-5070')*	cuttings	Top HRZ/Base Torok	127-123	55	460	290	excellent
GC1191-2	1704-1707 *(5590-5600')*	cuttings	Top HRZ/Base Torok	127-123	61	470	180	fair
GC1191-3	1707-1725 *(5600-5660')*	cuttings	Kalubik Gamma Ray Marker - Top HRZ/Base Torok	134-123	61	810	260	excellent
GC1191-4	1792-1814 *(5880-5950')*	cuttings	Top Burger C	135-134	64	1220	640	good
GC1191-5	1814-1832 *(5950-6010')*	cuttings	Base A Sand Facies - Top Burger C	137-134	65	1110	460	good
GC1191-6	1969-2003 *(6460-6570')*	cuttings	Base D Sand Facies - Top Burger D	145-137	71	890	350	none
GC1191-7	2053-2063 *(6735-6770')*	cuttings	Base D Sand Facies	145-140	74	730	320	none
OCS-Y-1413 Burger 1								
GC314-23	1698-1728 *(5570-5670')*	cuttings	Burger A/LCU - Kuparuk C Equivalent	137-134	56	10050	1053	excellent

*1 See Appendix A for discussion of present temperature data.

*2 Yield based on quantity of mineral suitable for age determination. Excellent: >20 grains; Good: 15-19 grains; Fair: 10-14 grains; Poor: 5-9 grains; Very Poor: <5 grains.

Table A.2: Summary of stratigraphy - Alaska (Geotrack Report #1191)

	KB elevation (mAMSL)	Water Depth (m)	Stratigraphic Interval	Depth of Top TVD rKB (m)	Age of Top (Ma)
OCS-Y-2321 Burger J 001					
	23.2	44.5	Quaternary	67.7	0
			Unconformity	78.3	1
			Nanushuk	78.3	99
			Torok	841.2	110
			Kalubik Fm	1531.6	123
			Kalubik Gamma Ray Mark	1716.9	127
			Kuparuk C Equivalent	1790.1	134
			Burger A/LCU	1815.1	135
			Base A Sand Facies	1819.7	136
			Burger D	1967.2	137
			Base D Sand Facies	1987.9	140
			TD	2072.6	145
OCS-Y-1413 Burger 1					
	12.8	57.9	Quaternary	57.8	0
			Unconformity	58.5	1
			Nanushuk	58.5	99
			Torok	823	110
			Kalubik Fm	1530.4	123
			Kalubik Gamma Ray Mark	1641.3	127
			Kuparuk C Equivalent	1695	134
			Burger A/LCU	1724.9	135
			Burger D	1877.3	137
			Unconformity	1991.3	144
			Jurassic	1991.3	148
			TD	2500	150

All depths quoted are with respect to KB, except where otherwise stated.

Table A.3: Summary of temperature data - Alaska (Geotrack Report #1191)

KB elevation (mAMSL)	Water Depth (m)	Depth (ft)	BHT (°F)	BHT (°C)	T.S.C (hrs)	Depth (m)	Corrected BHT (°C)	Geothermal gradient (°C/km)
OCS-Y-2321 Burger J 001								
23.2	44.5							37.0
		5922	147.3	64.1	-	1805.0		
		6479	159.5	70.8	-	1974.8		
OCS-Y-1413 Burger 1								
12.8	57.9							34.1
					-			

Quoted BHT values have been corrected by increasing the difference between surface temperature and measured BHT by 20% for measured temperatures <150°F (<66°C) and by 25% for temperatures >150°F (>66°C). A sea-bed temperature of 0°C has been assumed.

All depths quoted are with respect to KB, except where otherwise stated.

*Measurements not used in calculation of geothermal gradient.

Table A.4: Lower Limits of Detection for Apatite Analyses (Geotrack Report #1191)

Element	LLD (95% c.l.)		LLD (99% c.l.)	
	(wt%)	(ppm)	(wt%)	(ppm)
Cl	0.01	126	0.02	182

Table A.5: Per cent errors in chlorine content (Geotrack Report #1191)

Chlorine content (wt%)	Error (%)
0.01	9.3
0.02	8.7
0.05	7.3
0.10	6.1
0.20	4.7
0.50	3.2
1.00	2.3
1.50	1.9
2.00	1.7
2.50	1.5
3.00	1.4

Errors quoted are at 1σ. See Appendix A for more details.

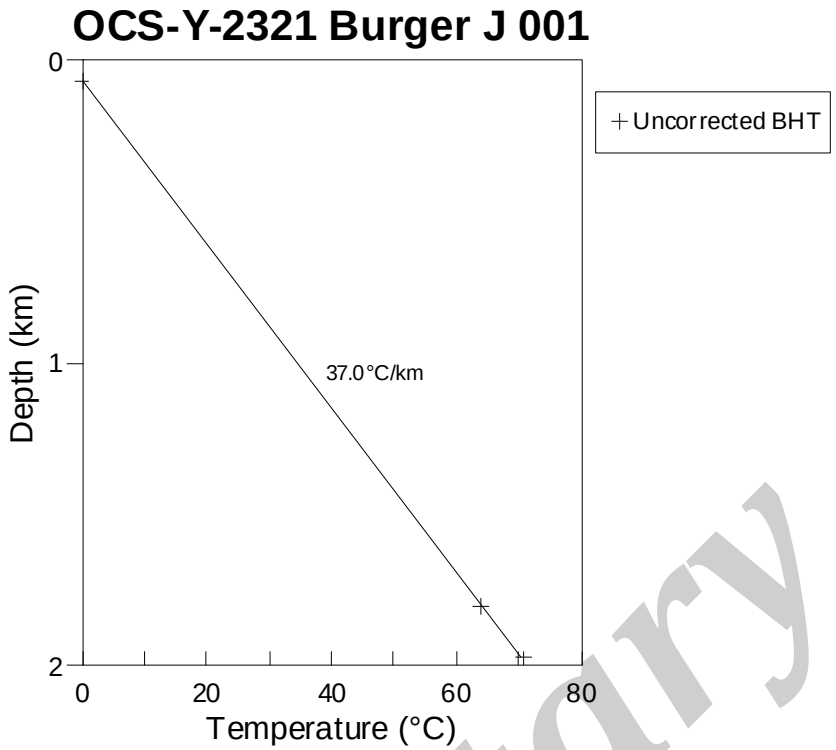

Figure A.1: Present temperature profile calculated for **well OCS-Y-2321 Burger J 001, Alaska.** See Table A.3 and Appendix A for more detail.

APPENDIX B

Sample Preparation, Analytical Details and Data Presentation

B.1 Sample Preparation

Core and outcrop samples are crushed in a jaw crusher and then ground to sand grade in a rotary disc mill. Cuttings samples are washed and dried before grinding to sand grade. The ground material is then washed to remove dust, dried and processed by conventional heavy liquid and magnetic separation techniques to recover heavy minerals. Apatite grains are mounted in epoxy resin on glass slides, polished and etched for 20 sec in 5M HNO_3 at 20°C to reveal the fossil fission tracks.

After etching, all mounts are cut down to 1.5 x 1 cm, and cleaned in detergent, alcohol and distilled water. The mounts are then sealed in intimate contact with low-uranium muscovite detectors within heat-shrink plastic film. Each batch of mounts is stacked between two pieces of uranium standard glass, which has been prepared in similar fashion. The stack is then inserted into an aluminium can for irradiation.

After irradiation, the mica detectors are removed from the grain mounts and standard glasses and etched in hydrofluoric acid to reveal the fission tracks produced by induced fission of ^{235}U in the apatite and standard glass.

B.2 Analytical Details

Fission track ages

Fission track ages are calculated using the standard fission track age equation using the zeta calibration method (equation five of Hurford and Green, 1983), viz:

$$\text{F.T. AGE} = \frac{1}{\lambda_D} \ln \left[1 + \left(\frac{\zeta \lambda_D \rho_s g \rho_D}{\rho_i} \right) \right] \qquad \text{B.1}$$

where:
- λ_D = Total decay constant of ^{238}U (= 1.55125 x 10^{-10})
- ζ = Zeta calibration factor
- ρ_s = Spontaneous track density
- ρ_i = Induced track density
- ρ_D = Track density from uranium standard glass
- g = A geometry factor (= 0.5)

Fission track ages are determined by the external detector method or EDM (Gleadow, 1981). The EDM has the advantage of allowing fission track ages to be determined on single grains. In apatite, tracks are counted in 20 grains from each mount wherever possible. In those samples where the desired number is not present, all available grains are counted, the actual number depending on the availability of suitably etched and oriented grains. Only grains oriented with surfaces parallel to the crystallographic c-axis are analysed. Such grains can be identified on the basis of the etching characteristics, as well as from morphological evidence in euhedral grains. The grain mount is scanned sequentially, and the first 20 suitably oriented grains identified are analysed.

Tracks are counted within an eyepiece graticule divided into 100 grid squares. In each grain, the number of spontaneous tracks (N_s) within a certain number of grid squares (N_a) is recorded. The number of induced tracks (N_i) in the corresponding location within the mica external detector is then counted. Spontaneous and induced track densities (ρ_s and ρ_i, respectively) are calculated by dividing the track counts by the total area counted, given by the product of Na and the area or each grid square (determined by calibration against a ruled stage graticule or diffraction grating). Fission track ages may be calculated by substituting track counts (N_s and N_i) for track densities (ρ_s and ρ_i) in equation B.1, since the areas cancel in the ratio.

Translation between apatite grains in the grain mount and external detector locations corresponding to each grain is carried out using Autoscan™ microcomputer-controlled automatic stages (Smith and Leigh Jones, 1985). This system allows repeated movement between grain and detector, and all grain locations are stored for later reference if required.

Neutron irradiations are carried out in a well-thermalised flux (X-7 facility; Cd ratio for Au ~98) in the Australian Atomic Energy Commission's HIFAR research reactor. Total neutron fluence is monitored by counting tracks in mica external detectors attached to two pieces of Corning Glass Works standard glass CN5 (containing ~11 ppm Uranium) included in the irradiation canister at each end of the sample stack. In determining track densities in external detectors irradiated adjacent to uranium standard glasses, 25 fields are normally counted in each detector. The total track count (N_D) is divided by the total area counted to obtain the track density (ρ_D). The positions of the counted fields are arranged in a 5 X 5 grid covering the whole area of the detector. For typical track densities of between ~5 X 10^5 and 5 X 10^6, this is a convenient arrangement to sample across the detector while gathering sufficient counts to achieve a precision of ~±2% in a reasonable time.

A small flux gradient is often present in the irradiation facility over the length of the sample package. If a detectable gradient is present, the track count in the external detector adjacent to each standard glass is converted to a track density (ρ_D) and a value for each mount in the stack is calculated by linear interpolation. When no detectable gradient is present, the track counts in the two external detectors are pooled to give a single value of ρ_D, which is used to calculate fission track ages for each sample.

A Zeta calibration factor (ζ) has been determined empirically for each observer by analysing a set of carefully chosen age standards with independently known K-Ar ages, following the methods outlined by Hurford and Green (1983) and Green (1985).

All track counting is carried out using Zeiss(R) Axioplan microscopes, with an overall linear magnification of 1068 x using dry objectives.

For further details and background information on practical aspects of fission track age determination, see e.g. Fleischer, Price and Walker (1975), Naeser (1979) and Hurford (1986).

Track length measurements

For track length studies in apatite, the full lengths of "confined" fission tracks are measured. Confined tracks are those which do not intersect the polished surface but have been etched from other tracks or fractures, so that the whole length of the track is etched. Confined track lengths are measured using a digitising tablet connected to a microcomputer, superimposed on the microscope field of view via a projection tube. With this system, calibrated against a stage graticule ruled in 2 µm divisions, individual tracks can be measured to a precision of ± 0.2 µm. Tracks are measured only in prismatic grains, characterised by sharp polishing scratches with well-etched tracks of narrow cone angle in all orientations, because of the anisotropy of annealing of fission tracks in apatite (as discussed by Green et al. 1986). Tracks are also measured following the recommendations of Laslett et al. (1982), the most important of which is that only horizontal tracks should be measured. One hundred tracks are measured whenever possible. In apatite samples with low track density, or in those samples in which only a small number of apatite grains are obtained, fewer confined tracks may be available. In such cases, the whole mount is scanned to measure as many confined tracks as possible.

Integrated fission track age and length measurement

Fission track age determination and length measurement are now made in a single pass of the grain mount, in an integrated approach. The location of each grain in which

tracks are either counted or measured is recorded for future reference. Thus, track length measurements can be tied to age determination in individual grains. As a routine procedure we do not measure the age of every grain in which lengths are determined, as this would be much too time-consuming. Likewise we do not only measure ages in grain in which lengths are measured, as this would bias the age data against low track density grains. Nevertheless, the ability to determine the fission track age of certain grains from which length data originate can be a particularly useful aid to interpretation in some cases. Grain location data are not provided in this report, but are available on request.

B.3 Data Presentation

Fission track age data

Data sheets summarising the apatite fission track age data, including full details of fission track age data for individual apatite grains in each sample, together with the primary counting results and statistical data, are given in the following pages. Individual grain fission track ages are calculated from the ratio of spontaneous to induced fission track counts for each grain using equation B.1, and errors in the single grain ages are calculated using Poissonian statistics, as explained in more detail by Galbraith (1981) and Green (1981). All errors are quoted as $\pm 1\sigma$ throughout this report, unless otherwise stated.

The variability of fission track ages between individual apatite grains within each sample can be assessed using a chi-squared (χ^2) statistic (Galbraith, 1981), the results of which are summarised for each sample in the data sheets. If all the grains counted belong to a single age population, the probability of obtaining the observed χ^2 value, for ν degrees of freedom (where ν = number of crystals -1), is listed in the data sheets as $P(\chi^2)$ or P(chi squared).

A $P(\chi^2)$ value greater than 5% can be taken as evidence that all grains are consistent with a single population of fission track age. In this case, the best estimate of the fission track age of the sample is given by the "pooled age", calculated from the ratio of the total spontaneous and induced track counts in all grains analysed. Errors for the pooled age are calculated using the "conventional" technique outlined by Green (1981), based on the total number of tracks counted for each track density measurement (see also Galbraith, 1981).

A $P(\chi^2)$ value of less than 5% denotes a significant spread of single grain ages, suggesting real differences exist between the fission track ages of individual apatite

grains. A significant spread in grain ages can result either from inheritance of detrital grains from mixed source areas (in sedimentary rocks), or from differential annealing in apatite grains of different composition, within a narrow range of temperature.

Calculation of the pooled age inherently assumes that only a single population of ages is present, and is thus not appropriate to samples containing a significant spread of fission track ages. In such cases Galbraith, has recently devised a means of estimating the modal age of a distribution of single grain fission track ages which is referred to as the "central age". Calculation of the central age assumes that all single grain ages belong to a Normal distribution of ages, with a standard deviation (σ) known as the "age dispersion". An iterative algorithm (Galbraith and Laslett, 1993) is used to provide estimates of the central age with its associated error, and the age dispersion, which are all quoted in the data sheets. Note that this treatment replaces use of the "mean age", which has used been in the past for those samples in which $P(\chi^2)<5\%$. For samples in which $P(\chi^2)>5\%$, the central age and the pooled age should be equal, and the age dispersion should be less than ~10%.

Table B.1 summarises the fission track age data in apatite from each sample analysed.

Construction of radial plots of single grain age data

Single grain age data are best represented in the form of radial plot diagrams (Galbraith, 1988, 1990). As illustrated in Figure B.1, these plots display the variation of individual grain ages in a plot of y against x, where:

$$y = (z_j - z_o) / \sigma_i \qquad x = 1/\sigma_j \qquad \text{B.2}$$

and; z_j = Fission track age of grain j
z_o = A reference age
σ_j = Error in age for grain j

In this plot, all points on a straight line from the origin define a single value of fission track age, and, at any point, the value of x is a measure of the precision of each individual grain age. Therefore, precise individual grain ages fall to the right of the plot (small error, high x), which is useful, for example, in enabling precise, young grains to be identified. The age scale is shown radially around the perimeter of the plot (in Ma). If all grains belong to a single age population, all data should scatter between y = +2 and y = -2, equivalent to scatter within $\pm 2\sigma$. Scatter outside these boundaries shows a significant spread of individual grain ages, as also reflected in the values of $P(\chi^2)$ and age dispersion.

In detail, rather than using the fission track age for each grain as in equation B.2, we use:

$$z_j = \frac{N_{sj}}{N_{ij}} \qquad \sigma_j = \{1/N_{sj} + 1/N_{ij}\} \qquad \text{B.3}$$

as we are interested in displaying the scatter within the data from each sample in comparison with that allowed by the Poissonian uncertainty in track counts, without the additional terms which are involved in determination of the fission track age (ρ_D, ζ, etc).

Zero ages cannot be displayed in such a plot. This can be achieved using a modified plot, (Galbraith, 1990) with:

$$z_j = \text{arc sin}\sqrt{\left\{\frac{N_{sj}+3/8}{N_{sj}+N_{ij}+3/4}\right\}} \qquad \sigma_j = \frac{1}{2}\sqrt{\left\{\frac{1}{N_{sj}+N_{ij}}\right\}} \qquad \text{B.4}$$

Note that the numerical terms in the equation for z_j are standard terms, introduced for statistical reasons. Using this arc-sin transformation, zero ages plot on a diagonal line which slopes from upper left to lower right. Note that this line does not go through the origin. Figure B.2 illustrates this difference between conventional and arc-sin radial plots, and also provides a simple guide to the structure of radial plots.

Use of arc-sin radial plots is particularly useful in assessing the relative importance of zero ages. For instance, grains with $N_s = 0$, $N_i = 1$ are compatible with ages up to ~900 Ma (at the 95% confidence level), whereas grains with $N_s = 0$, $N_i = 50$ are only compatible with ages up to ~14 Ma. The two data would readily be distinguishable on the radial plot as the 0,50 datum would plot well to the right (high x) compared to the 0,1 datum.

In this report the value of z corresponding to the stratigraphic age of each sample (or the midpoint of the range where appropriate) is adopted as the reference value, z_o. This allows rapid assessment of the fission track age of individual grains in relation to the stratigraphic age, which is a key component in the interpretation of AFTA data, as explained in more detail in Appendix C.

Note that the x axis of the radial plot is normally not labelled, as this would obscure the age scale around the plot. In general labelling is not considered necessary, as we are concerned only with relative variation within the data, rather than absolute values of precision.

Radial plots of the single grain age data in apatite from each sample analysed in this report are shown on the fission track age data summary sheets at the end of this Appendix. Use of radial plots to provide thermal history information is explained in Appendix C and Figure C.7.

Track length data

Distributions of confined track lengths in apatite from each sample are shown as simple histograms on the fission track age data summary sheets at the end of this Appendix. For every track length measurement, the length is recorded to the nearest 0.1 μm, but the measurements have been grouped into 1 μm intervals for construction of these histograms. Each distribution has been normalised to 100 tracks for each sample to facilitate comparison. A summary of the length distribution in each sample is presented in Table B.2, which also shows the mean track length in each sample and its associated error, the standard deviation of each distribution and the number of tracks (N) measured in each sample. The angle which each confined track makes with the crystallographic c-axis is also routinely recorded, as is the width of each fracture within which tracks are revealed. These data are not provided in this report, but can be supplied on request.

Breakdown of data into compositional groups

In Table B.3, AFTA data are grouped into compositional intervals of 0.1 wt% Cl width. Parameters for each interval represent the data from all grains with Cl contents within each interval. Also shown are the parameters for each compositional interval predicted from the Default Thermal History (see Section 2.1). These data form the basis of interpretation of the AFTA data, which takes full account of the influence of Cl content on annealing kinetics, as described in Appendix C. Distributions of Cl contents in all apatites analysed from each sample (i.e. for both age and length determinations) are shown on the fission track age data summary sheets at the end of this Appendix.

Plots of fission track age against Cl content for individual apatite grains

Fission track ages of single apatite grains within individual samples are plotted against the Cl content of each grain on the fission track age data summary sheets at the end of this Appendix. These plots are useful in assessing the degree of annealing, as expressed by the fission track age data. For example, if grains with a range of Cl contents from zero to some upper limit all give similar fission track ages which are significantly less than the stratigraphic age, then grains with these compositions must have been totally annealed. Alternatively, if fission track age falls rapidly with decreasing Cl content, the sample displays a high degree of partial annealing.

B.4 A note on terminology

Note that throughout this report, the term "fission track age" is understood to denote the parameter calculated from the fission track age equation, using the observed spontaneous and induced track counts (either pooled for all grains or for individual grains). The resulting number (with units of Ma) should not be taken as possessing any significance in terms of events taking place at the time indicated by the measured fission track age, but should rather be regarded as a measure of the integrated thermal history of the sample, and should be interpreted in that light using the principles outlined in Appendix C. Use of the term "apparent age" is not considered to be useful in this regard, as almost every fission track age should be regarded as an apparent age, in the classic sense, and repeated use becomes cumbersome.

References

Fleischer, R. L., Price, P. B., and Walker, R. M. (1975) Nuclear tracks in solids, University of California Press, Berkeley.

Galbraith, R. F. (1981) On statistical models for fission-track counts. *Mathematical Geology*, 13, 471-488.

Galbraith, R. F. (1988) Graphical display of estimates having differing standard errors. *Technometrics*, 30, 271-281.

Galbraith, R. F. (1990) The radial plot: graphical assessment of spread in ages. *Nuclear Tracks*, 17, 207-214.

Galbraith R.F. & Laslett G.M. (1993) Statistical methods for mixed fission track ages. *Nuclear Tracks* 21, 459-470.

Gleadow, A. J. W. (1981) Fission track dating methods; what are the real alternatives? *Nuclear Tracks*, 5, 3-14.

Green, P. F. (1981) A new look at statistics in fission track dating. *Nuclear Tracks 5*, 77-86.

Green, P. F. (1985) A comparison of zeta calibration baselines in zircon, sphene and apatite. *Chem. Geol. (Isot. Geol. Sect.)*, 58, 1-22.

Green, P. F., Duddy, I. R., Gleadow, A. J. W., Tingate, P. R. and Laslett, G. M. (1986) Thermal annealing of fission tracks in apatite 1. A qualitative description. *Chem. Geol. (Isot. Geosci. Sect.)*, 59, 237-253.

Hurford, A. J. (1986) Application of the fission track dating method to young sediments: Principles, methodology and Examples. *In:* Hurford, A. J., Jäger, E. and Ten Cate, J. A. M. (*eds*), Dating young sediments, CCOP Technical Publication 16, CCOP Technical Secretariat, Bangkok, Thailand.

Hurford, A. J. and Green, P. F. (1982) A user's guide to fission track dating calibration. *Earth. Planet. Sci Lett.* 59, 343-354.

Hurford, A. J. and Green, P. F. (1983) The zeta age calibration of fission track dating. *Isotope Geoscience* 1, 285-317.

Laslett, G. M., Kendall, W. S., Gleadow, A. J. W. and Duddy, I. R. (1982) Bias in measurement of fission track length distributions. *Nuclear Tracks*, 6, 79-85.

Naeser, C. W. (1979) Fission track dating and geologic annealing of fission tracks. *In:* Jäger, E. and Hunziker, J. C. (*eds*), Lectures in Isotope Geology, Springer Verlag, Berlin.

Smith, M. J. and Leigh-Jones, P. (1985) An automated microscope scanning stage for fission-track dating. *Nuclear Tracks*, 10, 395-400.

Table B.1: Apatite fission track analytical results - samples from Alaska (Geotrack Report #1191)

Sample number	Number of grains	ρ_D (N_D) x10^6/cm	ρ_s (Ns) x10^6/cm	ρ_i (Ni) x10^6/cm	Uranium content (ppm)	$P(\chi^2)$ (%)	Age dispersion (%)	Fission track age (Ma)
OCS-Y-2321 Burger J 001								
GC1191-1	29	1.162 (1951)	1.518 (924)	2.996 (1823)	29	12	14	111.1 ± 5.4
GC1191-2	10	1.171 (1951)	2.410 (232)	2.575 (248)	25	<1	39	205.1 ± 19.5 *189.8 ± 33.4**
GC1191-3	26	1.188 (1951)	1.254 (512)	1.735 (709)	17	<1	36	161.2 ± 10.3 *142.7 ± 15.7**
GC1191-4	17	1.214 (1951)	0.826 (195)	1.466 (346)	14	19	25	128.8 ± 12.1
GC1191-5	18	1.231 (1951)	0.620 (186)	1.330 (399)	12	<1	40	108.2 ± 10.0 *103.3 ± 14.8**
GC1191-6			No apatite					
GC1191-7			No apatite					
OCS-Y-1413 Burger 1								
GC314-23	26	1.266 (1965)	1.233 (578)	1.954 (916)	19	<1	41	142.4 ± 8.6 *139.4 ± 15.5**

ρ_s = spontaneous track density; ρ_i = induced track density; ρ_D = track density in glass standard external detector. Brackets show number of tracks counted. ρ_D and ρ_i measured in mica external detectors; ρ_s measured in internal surfaces.
*Central age, used where sample contains a significant spread of single grain ages ($P(\chi^2)$<5%). Errors quoted at 1 σ
Ages calculated using dosimeter glass CN5, with a zeta of 380.4 ± 5.7 (Analyst: C. O'Brien) for samples; GC1191-1 - 5
SRM612, with a zeta of 360.3 ± 6.8 (Analyst: M. Moore) for sample GC314-23

Table B.2: Length distribution summary data - samples from Alaska (Geotrack Report #1191)

Sample number	Mean track length (µm)	Standard deviation (µm)	Number of tracks (N)	Number of tracks in Length Intervals (µm)																			
				1	2	3	4	5	6	7	8	9	10	11	12	13	14	15	16	17	18	19	20
OCS-Y-2321 Burger J 001																							
GC1191-1	12.99 ± 0.16	1.24	63	-	-	-	-	-	-	-	-	-	-	5	9	14	23	11	-	1	-	-	-
GC1191-2	11.27 ± 0.58	2.38	17	-	-	-	-	-	-	-	-	2	6	3	-	1	2	2	-	1	-	-	-
GC1191-3	11.70 ± 0.25	1.43	32	-	-	-	-	-	-	-	-	1	1	9	8	5	6	2	-	-	-	-	-
GC1191-4	13.29 ± 0.51	1.36	7	-	-	-	-	-	-	-	-	-	-	-	2	-	3	2	-	-	-	-	-
GC1191-5	12.53 ± 0.36	1.54	18	-	-	-	-	-	-	-	-	-	-	1	7	5	3	-	1	1	-	-	-
GC1191-6	No apatite	-	-	-	-	-	-	-	-	-	-	-	-	-	-	-	-	-	-	-	-	-	-
GC1191-7	No apatite	-	-	-	-	-	-	-	-	-	-	-	-	-	-	-	-	-	-	-	-	-	-
OCS-Y-1413 Burger 1																							
GC314-23	11.29 ± 0.27	2.15	61	-	-	-	1	-	-	1	1	3	7	14	12	11	6	4	-	1	-	-	-

Track length measurements by: C. O'Brien for samples; GC1191-1 - 5
M. Moore for samples; GC314-23

Table B.3: AFTA Data in Compositional Groups - (Geotrack Report #1191)

Cl Wt %	Default fission track age* (Ma)	Measured fission track age (Ma)	Error in age (Ma)	P (χ^2)	Number of grains	Default fission track length* (µm)	Mean Track length (µm)	Error in length (µm)	Std deviation (µm)	Number of lengths	Number of grains	Number of tracks in length interval (µm) 1	2	3	4	5	6	7	8	9	10	11	12	13	14	15	16	17	18	19	20
OCS-Y-2321 Burger J 001																															
1191-1†	**108**	**111.1**	**5.4**	**11.9**	**29**	**12.9**	**13.0**	**0.2**	**1.2**	**63**	**31**	**0**	**0**	**0**	**0**	**0**	**0**	**0**	**0**	**0**	**0**	**5**	**9**	**14**	**23**	**11**	**0**	**1**	**0**	**0**	**0**
0.0 - 0.1	107	124.9	10.4	24.7	8	12.8	13.4	0.3	1.3	19	8	0	0	0	0	0	0	0	0	0	0	1	1	4	8	4	0	1	0	0	0
0.1 - 0.2	108	106.8	7.6	77.9	13	12.9	12.6	0.2	1.1	31	14	0	0	0	0	0	0	0	0	0	0	3	7	6	12	3	0	0	0	0	0
0.2 - 0.3	109	105.3	18.0	0.3	4	13.0	13.5	0.6	1.4	6	5	0	0	0	0	0	0	0	0	0	0	0	1	2	0	3	0	0	0	0	0
0.3 - 0.4	110	117.1	13.9	83.3	3	13.2	13.0	0.6	1.5	7	4	0	0	0	0	0	0	0	0	0	0	1	0	2	3	1	0	0	0	0	0
0.4 - 0.5	111	178.3	80.3	100.0	1	13.3	0.0	0.0	0.0	0	0	0	0	0	0	0	0	0	0	0	0	0	0	0	0	0	0	0	0	0	0
1191-2†	**107**	**189.8**	**33.4**	**0.3**	**10**	**12.5**	**11.3**	**0.6**	**2.4**	**17**	**3**	**0**	**0**	**0**	**0**	**0**	**0**	**0**	**0**	**2**	**6**	**3**	**0**	**1**	**2**	**2**	**0**	**1**	**0**	**0**	**0**
0.0 - 0.1	106	190.7	64.1	1.8	4	12.3	10.5	0.6	1.9	9	1	0	0	0	0	0	0	0	0	2	3	2	0	0	2	0	0	0	0	0	0
0.1 - 0.2	107	128.3	26.1	23.9	3	12.5	12.5	1.0	2.7	7	1	0	0	0	0	0	0	0	0	0	2	1	0	1	0	2	0	1	0	0	0
0.2 - 0.3	108	233.3	62.4	4.3	2	12.6	9.6	0.0	0.0	1	1	0	0	0	0	0	0	0	0	0	1	0	0	0	0	0	0	0	0	0	0
0.3 - 0.4	-	-	-	-		-	-	-	-	-	-	-	-	-	-	-	-	-	-	-	-	-	-	-	-	-	-	-	-	-	-
0.4 - 0.5	-	-	-	-		-	-	-	-	-	-	-	-	-	-	-	-	-	-	-	-	-	-	-	-	-	-	-	-	-	-
0.5 - 0.6	-	-	-	-		-	-	-	-	-	-	-	-	-	-	-	-	-	-	-	-	-	-	-	-	-	-	-	-	-	-
0.6 - 0.7	113	175.7	118.0	100.0	1	13.1	0.0	0.0	0.0	0	0	0	0	0	0	0	0	0	0	0	0	0	0	0	0	0	0	0	0	0	0
1191-3†	**108**	**142.7**	**15.7**	**0.0**	**26**	**12.6**	**11.7**	**0.3**	**1.4**	**32**	**14**	**0**	**0**	**0**	**0**	**0**	**0**	**0**	**0**	**1**	**1**	**9**	**8**	**5**	**6**	**2**	**0**	**0**	**0**	**0**	**0**
0.0 - 0.1	106	163.3	27.3	4.1	9	12.3	11.4	0.5	1.6	10	4	0	0	0	0	0	0	0	0	1	1	2	2	2	2	0	0	0	0	0	0
0.1 - 0.2	107	87.7	20.8	28.0	2	12.4	11.7	0.6	1.4	6	3	0	0	0	0	0	0	0	0	0	0	2	2	1	0	1	0	0	0	0	0
0.2 - 0.3	108	144.4	28.0	0.0	8	12.6	11.6	0.3	1.2	14	5	0	0	0	0	0	0	0	0	0	0	5	4	2	3	0	0	0	0	0	0
0.3 - 0.4	110	86.3	45.5	25.5	2	12.8	0.0	0.0	0.0	0	0	0	0	0	0	0	0	0	0	0	0	0	0	0	0	0	0	0	0	0	0
0.4 - 0.5	-	-	-	-		-	-	-	-	-	-	-	-	-	-	-	-	-	-	-	-	-	-	-	-	-	-	-	-	-	-
0.5 - 0.6	112	0.0	91.4	0.0	1	13.0	0.0	0.0	0.0	0	0	0	0	0	0	0	0	0	0	0	0	0	0	0	0	0	0	0	0	0	0
0.6 - 0.7	113	161.9	32.0	43.3	4	13.1	14.2	0.3	0.4	2	2	0	0	0	0	0	0	0	0	0	0	0	0	0	1	1	0	0	0	0	0

*Fission Track Age and Mean Track Length predicted from the Default Thermal History (i.e. if the sample has not been hotter in the past)
†Combined data for all compositional groups

Table B.3: Continued - (Geotrack Report #1191)

Cl Wt %	Default fission track age* (Ma)	Measured fission track age (Ma)	Error in age (Ma)	P (χ^2)	Number of grains	Default fission track length* (µm)	Mean Track length (µm)	Error in length (µm)	Std deviation (µm)	Number of lengths	Number of grains	Number of tracks in length interval (µm) 1	2	3	4	5	6	7	8	9	10	11	12	13	14	15	16	17	18	19	20
1191-4†	**111**	**128.8**	**12.1**	**19.1**	**17**	**12.4**	**13.3**	**0.5**	**1.4**	**7**	**5**	**0**	**0**	**0**	**0**	**0**	**0**	**0**	**0**	**0**	**0**	**0**	**2**	**0**	**3**	**2**	**0**	**0**	**0**	**0**	**0**
0.0 - 0.1	109	118.7	17.9	35.8	9	12.0	13.3	0.8	1.6	4	2	0	0	0	0	0	0	0	0	0	0	0	1	0	2	1	0	0	0	0	0
0.1 - 0.2	111	202.1	49.4	18.4	3	12.2	13.4	0.0	0.0	1	1	0	0	0	0	0	0	0	0	0	0	0	0	0	1	0	0	0	0	0	0
0.2 - 0.3	113	104.1	28.2	100.0	1	12.4	0.0	0.0	0.0	0	0	0	0	0	0	0	0	0	0	0	0	0	0	0	0	0	0	0	0	0	0
0.3 - 0.4	114	76.5	62.5	100.0	1	12.5	11.8	0.0	0.0	1	1	0	0	0	0	0	0	0	0	0	0	0	1	0	0	0	0	0	0	0	0
0.4 - 0.5	116	156.1	56.3	100.0	1	12.7	0.0	0.0	0.0	0	0	0	0	0	0	0	0	0	0	0	0	0	0	0	0	0	0	0	0	0	0
0.5 - 0.6	117	249.1	109.1	100.0	1	12.8	0.0	0.0	0.0	0	0	0	0	0	0	0	0	0	0	0	0	0	0	0	0	0	0	0	0	0	0
0.6 - 0.7	-	-	-	-		-	-	-	-	-	-	-	-	-	-	-	-	-	-	-	-	-	-	-	-	-	-	-	-	-	-
0.7 - 0.8	119	0.0	0.0	0.0	0	13.0	14.5	0.0	0.0	1	1	0	0	0	0	0	0	0	0	0	0	0	0	0	0	1	0	0	0	0	0
0.8 - 0.9	-	-	-	-		-	-	-	-	-	-	-	-	-	-	-	-	-	-	-	-	-	-	-	-	-	-	-	-	-	-
0.9 - 1.0	-	-	-	-		-	-	-	-	-	-	-	-	-	-	-	-	-	-	-	-	-	-	-	-	-	-	-	-	-	-
1.0 - 1.1	120	109.9	19.5	100.0	1	13.2	0.0	0.0	0.0	0	0	0	0	0	0	0	0	0	0	0	0	0	0	0	0	0	0	0	0	0	0
1191-5†	**113**	**103.3**	**14.8**	**0.5**	**18**	**12.4**	**12.5**	**0.4**	**1.5**	**18**	**8**	**0**	**0**	**0**	**0**	**0**	**0**	**0**	**0**	**0**	**0**	**1**	**7**	**5**	**3**	**0**	**1**	**1**	**0**	**0**	**0**
0.0 - 0.1	110	90.6	19.7	19.5	6	11.9	11.9	0.8	1.1	2	1	0	0	0	0	0	0	0	0	0	0	0	1	1	0	0	0	0	0	0	0
0.1 - 0.2	112	143.4	36.0	100.0	1	12.1	12.2	0.7	1.3	3	1	0	0	0	0	0	0	0	0	0	0	1	0	1	1	0	0	0	0	0	0
0.2 - 0.3	113	84.8	16.9	41.2	4	12.3	13.7	1.5	2.1	2	2	0	0	0	0	0	0	0	0	0	0	0	0	1	0	0	1	0	0	0	0
0.3 - 0.4	115	83.7	17.4	46.9	4	12.5	12.2	0.4	1.0	6	2	0	0	0	0	0	0	0	0	0	0	0	3	2	1	0	0	0	0	0	0
0.4 - 0.5	117	97.4	21.0	86.1	2	12.6	13.8	0.0	0.0	1	1	0	0	0	0	0	0	0	0	0	0	0	0	0	1	0	0	0	0	0	0
0.5 - 0.6	-	-	-	-		-	-	-	-	-	-	-	-	-	-	-	-	-	-	-	-	-	-	-	-	-	-	-	-	-	-
0.6 - 0.7	-	-	-	-		-	-	-	-	-	-	-	-	-	-	-	-	-	-	-	-	-	-	-	-	-	-	-	-	-	-
0.7 - 0.8	-	-	-	-		-	-	-	-	-	-	-	-	-	-	-	-	-	-	-	-	-	-	-	-	-	-	-	-	-	-
0.8 - 0.9	-	-	-	-		-	-	-	-	-	-	-	-	-	-	-	-	-	-	-	-	-	-	-	-	-	-	-	-	-	-
0.9 - 1.0	121	332.0	92.4	100.0	1	13.1	12.6	1.3	2.6	4	1	0	0	0	0	0	0	0	0	0	0	0	3	0	0	0	0	1	0	0	0

*Fission Track Age and Mean Track Length predicted from the Default Thermal History (i.e. if the sample has not been hotter in the past)
†Combined data for all compositional groups

Table B.3: Continued - (Geotrack Report #1191)

Cl Wt %	Default fission track age* (Ma)	Measured fission track age (Ma)	Error in age (Ma)	P (χ^2)	Number of grains	Default fission track length* (µm)	Mean Track length (µm)	Error in length (µm)	Std deviation (µm)	Number of lengths	Number of grains	Number of tracks in length interval (µm) 1	2	3	4	5	6	7	8	9	10	11	12	13	14	15	16	17	18	19	20
OCS-Y-1413 Burger 1																															
314-23†	**116**	**139.4**	**15.5**	**0.0**	**26**	**12.7**	**11.3**	**0.3**	**2.1**	**60**	**18**	**0**	**0**	**0**	**1**	**0**	**0**	**1**	**1**	**3**	**7**	**14**	**12**	**11**	**6**	**4**	**0**	**1**	**0**	**0**	**0**
0.0 - 0.1	115	130.9	20.5	0.0	15	12.6	11.7	0.5	2.6	22	9	0	0	0	1	0	0	0	0	0	2	3	7	4	2	2	0	1	0	0	0
0.1 - 0.2	116	135.7	15.7	63.0	5	12.7	9.6	0.8	2.1	6	4	0	0	0	0	0	0	1	0	1	1	2	0	1	0	0	0	0	0	0	0
0.2 - 0.3	117	171.0	26.0	14.5	2	12.9	11.2	0.3	1.7	29	2	0	0	0	0	0	0	0	1	2	4	7	4	6	4	1	0	0	0	0	0
0.3 - 0.4	119	251.7	55.2	41.4	2	13.0	12.8	2.0	2.8	2	2	0	0	0	0	0	0	0	0	0	0	1	0	0	0	1	0	0	0	0	0
0.4 - 0.5	-	-	-	-		-	-	-	-	-	-	-	-	-	-	-	-	-	-	-	-	-	-	-	-	-	-	-	-	-	-
0.5 - 0.6	-	-	-	-		-	-	-	-	-	-	-	-	-	-	-	-	-	-	-	-	-	-	-	-	-	-	-	-	-	-
0.6 - 0.7	121	97.0	67.0	100.0	1	13.3	11.4	0.0	0.0	1	1	0	0	0	0	0	0	0	0	0	0	0	1	0	0	0	0	0	0	0	0
0.7 - 0.8	-	-	-	-		-	-	-	-	-	-	-	-	-	-	-	-	-	-	-	-	-	-	-	-	-	-	-	-	-	-
0.8 - 0.9	-	-	-	-		-	-	-	-	-	-	-	-	-	-	-	-	-	-	-	-	-	-	-	-	-	-	-	-	-	-
0.9 - 1.0	-	-	-	-		-	-	-	-	-	-	-	-	-	-	-	-	-	-	-	-	-	-	-	-	-	-	-	-	-	-
1.0 - 1.1	-	-	-	-		-	-	-	-	-	-	-	-	-	-	-	-	-	-	-	-	-	-	-	-	-	-	-	-	-	-
1.1 - 1.2	-	-	-	-		-	-	-	-	-	-	-	-	-	-	-	-	-	-	-	-	-	-	-	-	-	-	-	-	-	-
1.2 - 1.3	-	-	-	-		-	-	-	-	-	-	-	-	-	-	-	-	-	-	-	-	-	-	-	-	-	-	-	-	-	-
1.3 - 1.4	-	-	-	-		-	-	-	-	-	-	-	-	-	-	-	-	-	-	-	-	-	-	-	-	-	-	-	-	-	-
1.4 - 1.5	-	-	-	-		-	-	-	-	-	-	-	-	-	-	-	-	-	-	-	-	-	-	-	-	-	-	-	-	-	-
1.5 - 1.6	124	63.1	18.5	100.0	1	13.6	0.0	0.0	0.0	0	0	0	0	0	0	0	0	0	0	0	0	0	0	0	0	0	0	0	0	0	0

*Fission Track Age and Mean Track Length predicted from the Default Thermal History (i.e. if the sample has not been hotter in the past)
†Combined data for all compositional groups

Estimates	z_i
Standard errors	σ_i
Reference value	z_o
Standardised estimates	$y_i = (z_i - z_o) / \sigma_i$
Precision	$x_i = 1 / \sigma_i$

PLOT y_i against x_i

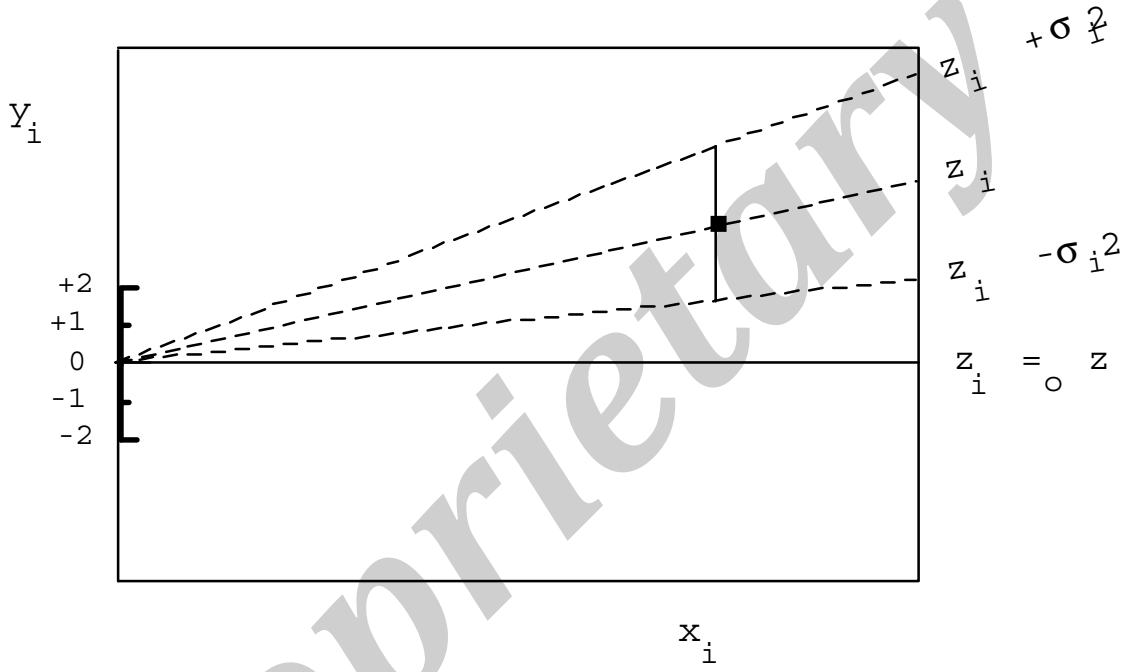

Slope of line from origin through data point $= y_i / x_i$

$= \{(z_i - z_o)/\sigma_i\} / \{1/\sigma_i\}$

$= z_i - z_o$

Key Points:

Radial lines emanating from the origin correspond to fixed values of z

Data points with higher values of x_i have greater precision.

Error bars on all points are the same size in this plot.

Figure B.1 Basic construction of a radial plot. In AFTA, the estimates z_i correspond to the fission track age values for individual apatite grains. Any convenient value of age can be chosen as the reference value corresponding to the horizontal in the radial plot. Radial lines emanating from the origin with positive slopes correspond to fission track ages greater than the reference value. Lines with negative slopes correspond to fission track ages less than the reference value.

Normal radial plot (equations B.2 and B.3)

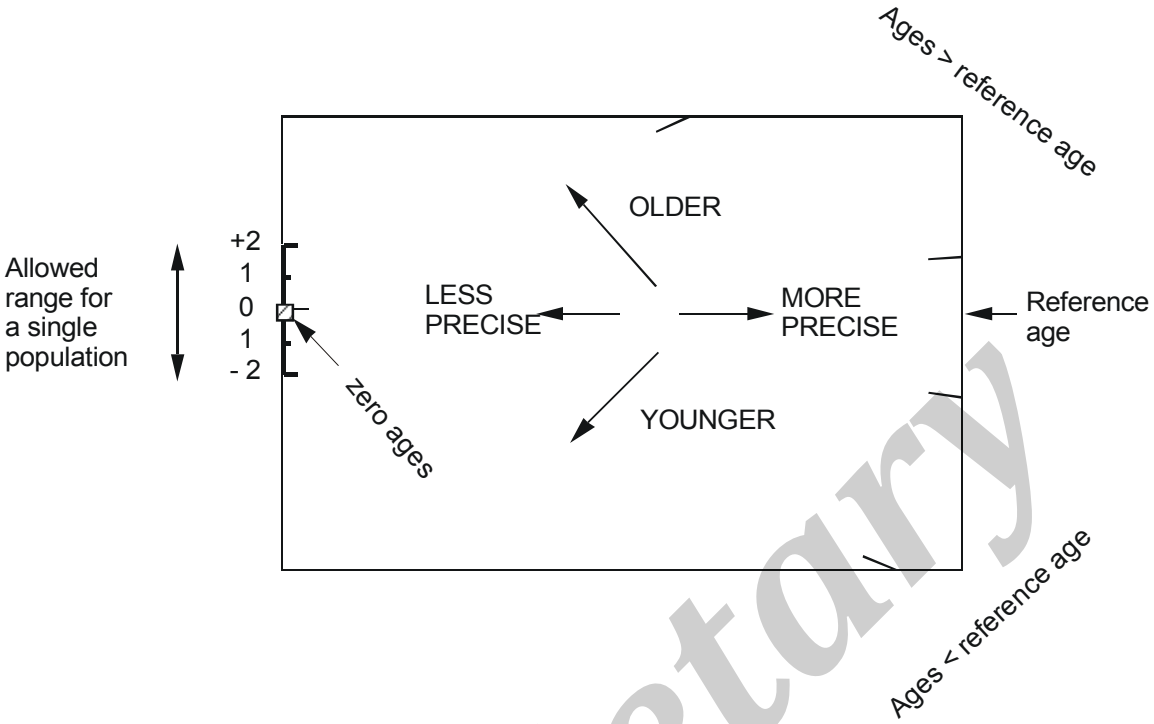

Arc-sin radial plot (equations B.2 and B.4)

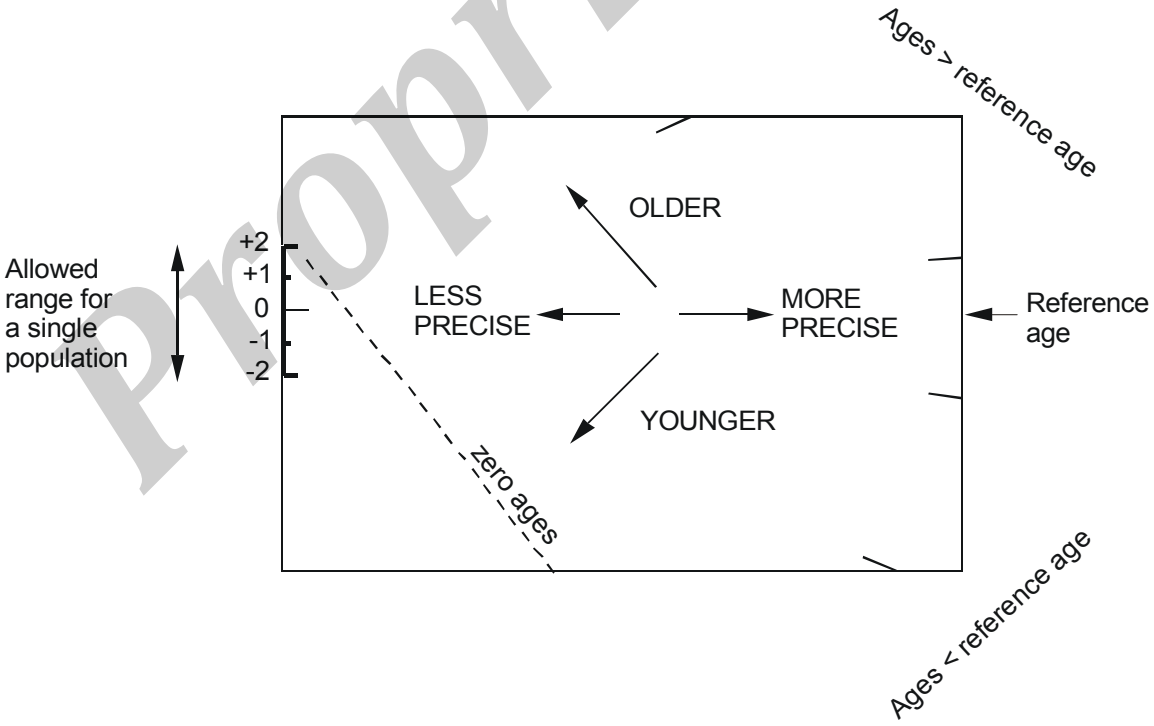

Figure B.2 Simplified structure of Normal and Arc-sin radial plots.

Fission Track Age Data Sheets - Glossary

N_s	=	Number of spontaneous tracks in N_a grid squares
N_i	=	Number of induced tracks in N_a grid squares
N_a	=	Number of grid squares counted in each grain
RATIO	=	N_S/N_i
U (ppm)	=	Uranium content of each grain (= U content of standard glass * ρ_i/ρ_D)
Cl (wt%)	=	Weight percent chlorine content of each grain
ρ_s	=	Spontaneous track density (ρ_s) = N_s/ (N_a*area of basic unit)
ρ_i	=	Induced track density (ρ_i) = N_i/(N_a*area of basic unit)
F.T. AGE	=	Fission track age, calculated using equation B.1
Area of basic unit	=	Area of one grid square
Chi squared	=	χ^2 parameter, used to assess variation of single grain ages within the sample
P(chi squared)	=	Probability of obtaining observed χ^2 value for the relevant number of degrees of freedom, if all grains belong to a single population
Age Dispersion	=	% variation in single grain ages - see discussion in text re "Central age"
N_s/N_i	=	Pooled ratio, total spontaneous tracks divided by total induced tracks for all grains
Mean ratio	=	Mean of (N_s/N_i) for individual grains
Zeta	=	Calibration constant, determined empirically for each observer
ρ_D	=	Track density (ρ_D) from uranium standard glass (interpolated from values at each end of stack)
ND	=	Total number of tracks counted for determining ρ_D
POOLED AGE	=	Fission track age calculated from pooled ratio N_s/N_i. Valid only when P(χ2) > 5%
CENTRAL AGE	=	Alternative to pooled age when P(χ2)< 5%

Key to Figures:

A: Radial plot of single grain ages *(See Figures B.1 and B.2 for details of radial plot construction)*	B: Distribution of Cl contents in apatite grains
C: Single grain age vs weight % Cl for individual apatite grains.	D: Distribution of confined track lengths

GC314-23 Apatite
Counted by: MEM

OCS-Y-1413 Burger 1 5570-5670'

Slide ref	Current grain no	N_s	N_i	N_a	ρ_s	ρ_i	RATIO	U (ppm)	Cl (wt%)	F.T. AGE (Ma)
G168-9	6	34	31	14	3.859E+06	3.519E+06	1.097	34.7	0.04	245.5 ± 61.4
G168-9	8	10	12	21	7.567E+05	9.080E+05	0.833	9.0	0.38	187.4 ± 80.4
G168-9	9	7	19	40	2.781E+05	7.548E+05	0.368	7.4	0.18	83.5 ± 37.0
G168-9	12	4	8	12	5.297E+05	1.059E+06	0.500	10.5	0.02	113.1 ± 69.3
G168-9	15	17	26	16	1.688E+06	2.582E+06	0.654	25.5	0.04	147.5 ± 46.2
G168-9	18	18	15	6	4.767E+06	3.973E+06	1.200	39.2	0.22	268.1 ± 94.1
G168-9	19	13	24	25	8.263E+05	1.526E+06	0.542	15.1	0.06	122.4 ± 42.3
G168-10	11	3	3	16	2.980E+05	2.980E+05	1.000	2.9	0.02	226.2 ± 184.8
G168-10	13	3	4	8	5.959E+05	7.945E+05	0.750	7.8	0.00	170.4 ± 130.3
G168-10	18	81	125	60	2.145E+06	3.311E+06	0.648	32.4	0.02	147.5 ± 21.5
G168-10	19	18	41	12	2.384E+06	5.429E+06	0.439	53.1	0.02	100.3 ± 28.5
G168-11	3	20	28	15	2.119E+06	2.966E+06	0.714	28.7	0.15	163.9 ± 48.2
G168-11	4	25	52	30	1.324E+06	2.754E+06	0.481	26.7	0.00	110.7 ± 27.1
G168-11	5	61	84	40	2.423E+06	3.337E+06	0.726	32.3	0.03	166.6 ± 28.4
G168-11	10	3	7	25	1.907E+05	4.449E+05	0.429	4.3	0.61	98.8 ± 68.3
G168-11	14	35	28	100	5.562E+05	4.449E+05	1.250	4.3	0.37	284.1 ± 72.5
G188-9	4	2	11	24	1.324E+05	7.283E+05	0.182	6.9	0.01	43.3 ± 33.3
G188-9	11	6	10	48	1.986E+05	3.311E+05	0.600	3.1	0.16	141.8 ± 73.4
G188-9	15	93	149	20	7.389E+06	1.184E+07	0.624	111.5	0.11	147.5 ± 19.9
G188-9	19	5	5	30	2.648E+05	2.648E+05	1.000	2.5	0.08	234.7 ± 148.6
G188-9	22	61	89	36	2.693E+06	3.929E+06	0.685	37.0	0.28	161.8 ± 27.3
G188-9	23	32	27	28	1.816E+06	1.532E+06	1.185	14.4	0.09	277.2 ± 72.9
G188-9	24	2	7	30	1.059E+05	3.708E+05	0.286	3.5	0.17	67.9 ± 54.5
G188-9	25	15	54	49	4.864E+05	1.751E+06	0.278	16.5	1.57	66.0 ± 19.4
G188-9	26	6	74	20	4.767E+05	5.880E+06	0.081	55.4	0.03	19.3 ± 8.2
G188-9	27	4	8	20	3.178E+05	6.356E+05	0.500	6.0	0.00	118.4 ± 72.6
		578	916		1.233E+06	1.954E+06		19.3		

Area of basic unit = 6.293E-07 cm^{-2}
χ^2 = 73.185 with 25 degrees of freedom
P(χ^2) = 0.0%
Age Dispersion = 41.406%

Ns / Ni = 0.631 ± 0.034
Mean Ratio = 0.669 ± 0.063

Ages calculated using a zeta of 360.3 ± 6.8 for SRM612 glass
ρ = 1.266E+06cm^{-2} ND = 1965
ρ_D interpolated between top of can; ρ = 1.173E+06cm^{-2} ND = 923
bottom of can; ρ = 1.325E+06cm^{-2} ND = 1042

POOLED AGE = 142.4 ± 8.6 Ma
CENTRAL AGE = 139.4 ± 15.5 Ma

A:

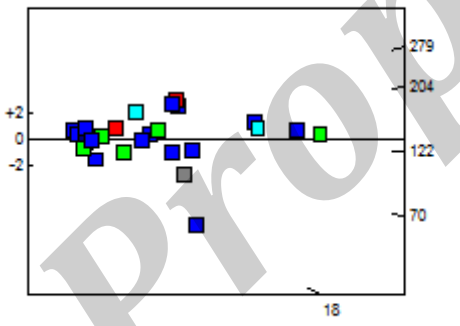

B:

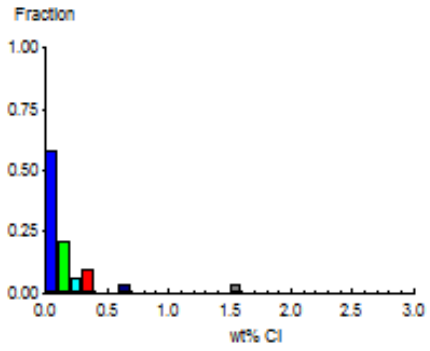

C:

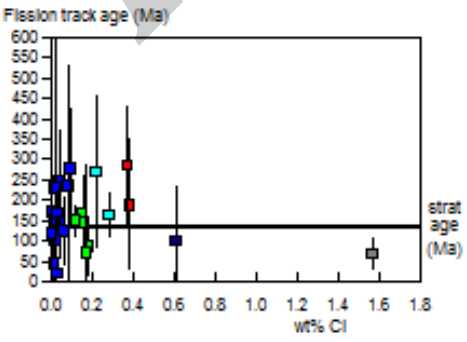

D:

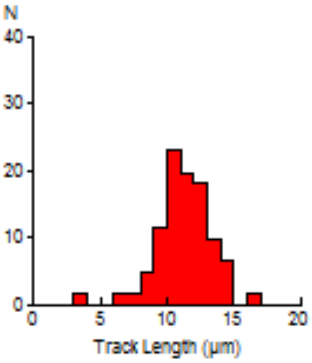

Mean track length 11.29 ± 0.27 µm Std. Dev. 2.15 µm 61 tracks

GC1191-1 Apatite
Counted by: COB

OCS-Y-2321 Burger J 001 5040-5070'

Slide ref	Current grain no	N_s	N_i	N_a	ρ_s	ρ_i	RATIO	U (ppm)	Cl (wt%)	F.T. AGE (Ma)
G1278-1	4	17	44	18	1.501E+06	3.884E+06	0.386	38.1	0.11	84.8 ± 24.3
G1278-1	5	74	107	50	2.352E+06	3.401E+06	0.692	33.4	0.25	151.1 ± 23.2
G1278-1	6	16	28	20	1.271E+06	2.225E+06	0.571	21.8	0.04	125.1 ± 39.3
G1278-1	9	7	10	16	6.952E+05	9.932E+05	0.700	9.7	0.32	152.9 ± 75.5
G1278-1	10	25	64	24	1.655E+06	4.238E+06	0.391	41.6	0.03	85.8 ± 20.4
G1278-1	11	47	111	48	1.556E+06	3.675E+06	0.423	36.1	0.26	92.9 ± 16.4
G1278-1	12	7	13	21	5.297E+05	9.837E+05	0.538	9.7	0.11	117.9 ± 55.4
G1278-1	13	10	12	9	1.766E+06	2.119E+06	0.833	20.8	0.13	181.6 ± 77.9
G1278-1	14	24	43	20	1.907E+06	3.416E+06	0.558	33.5	0.07	122.2 ± 31.3
G1278-1	16	9	11	20	7.151E+05	8.740E+05	0.818	8.6	0.42	178.3 ± 80.3
G1278-1	17	35	69	56	9.932E+05	1.958E+06	0.507	19.2	0.32	111.1 ± 23.3
G1278-1	18	7	21	15	7.416E+05	2.225E+06	0.333	21.8	0.16	73.2 ± 32.0
G1278-1	19	6	10	21	4.540E+05	7.567E+05	0.600	7.4	0.07	131.3 ± 67.9
G1278-1	20	31	30	16	3.079E+06	2.980E+06	1.033	29.2	0.01	224.4 ± 57.8
G1278-1	21	9	12	16	8.939E+05	1.192E+06	0.750	11.7	0.08	163.7 ± 72.3
G1278-1	23	7	10	28	3.973E+05	5.675E+05	0.700	5.6	0.21	152.9 ± 75.5
G1278-1	24	3	4	27	1.766E+05	2.354E+05	0.750	2.3	0.19	163.7 ± 125.1
G1278-1	25	28	74	35	1.271E+06	3.360E+06	0.378	33.0	0.16	83.1 ± 18.6
G1278-1	26	17	28	14	1.930E+06	3.178E+06	0.607	31.2	0.19	132.8 ± 41.0
G1278-1	27	42	83	18	3.708E+06	7.327E+06	0.506	71.9	0.14	110.9 ± 21.2
G1278-1	28	44	93	35	1.998E+06	4.222E+06	0.473	41.4	0.15	103.7 ± 19.2
G1278-1	29	65	145	64	1.614E+06	3.600E+06	0.448	35.3	0.15	98.3 ± 14.9
G1278-1	30	14	17	24	9.270E+05	1.126E+06	0.824	11.0	0.11	179.5 ± 65.0
G1278-1	31	69	208	40	2.741E+06	8.263E+06	0.332	81.1	0.28	72.9 ± 10.3
G1278-1	32	53	100	50	1.684E+06	3.178E+06	0.530	31.2	0.13	116.1 ± 20.0
G1278-1	33	73	136	64	1.813E+06	3.377E+06	0.537	33.1	0.31	117.5 ± 17.4
G1278-1	35	13	29	50	4.132E+05	9.217E+05	0.448	9.0	0.06	98.3 ± 32.9
G1278-1	37	130	229	100	2.066E+06	3.639E+06	0.568	35.7	0.09	124.3 ± 14.1
G1278-1	39	42	82	48	1.390E+06	2.715E+06	0.512	26.6	0.16	112.2 ± 21.5
		924	1823		1.518E+06	2.996E+06		29.4		

Area of basic unit = 6.293E-07 cm^{-2}
χ^2 = 36.988 with 28 degrees of freedom
P(χ^2) = 11.9%
Age Dispersion = 13.561%

Ns / Ni = 0.507 ± 0.020
Mean Ratio = 0.578 ± 0.032

Ages calculated using a zeta of 380.4 ± 5.7 for CN5 glass
ρ = 1.162E+06cm^{-2} ND = 1951
ρ_D interpolated between top of can; ρ = 1.162E+06cm^{-2} ND = 914
bottom of can; ρ = 1.318E+06cm^{-2} ND = 1037

POOLED AGE = 111.1 ± 5.4 Ma
CENTRAL AGE = 112.8 ± 6.5 Ma

A:

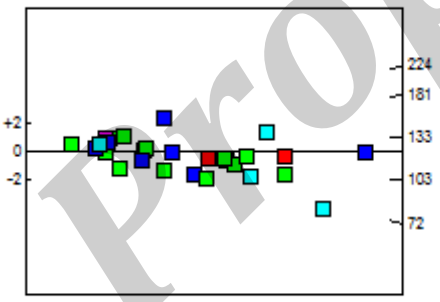

B:

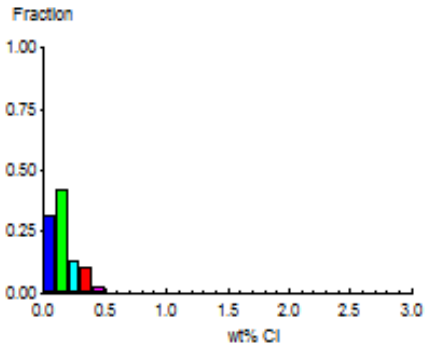

C:

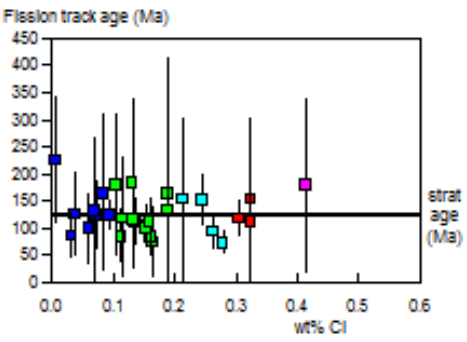

D:

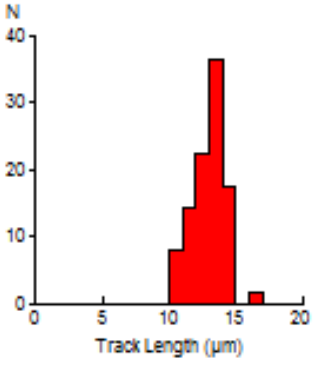

Mean track length 12.99 ± 0.16 µm Std. Dev. 1.24 µm 63 tracks

GC1191-2 Apatite
Counted by: COB

OCS-Y-2321 Burger J 001 5590-5600'

Slide ref	Current grain no	N_s	N_i	N_a	ρ_s	ρ_i	RATIO	U (ppm)	Cl (wt%)	F.T. AGE (Ma)
G1278-2	3	53	66	8	1.053E+07	1.311E+07	0.803	127.7	0.21	176.4 ± 32.9
G1278-2	5	14	14	20	1.112E+06	1.112E+06	1.000	10.8	0.12	218.9 ± 82.9
G1278-2	6	4	5	15	4.238E+05	5.297E+05	0.800	5.2	0.65	175.7 ± 118.0
G1278-2	7	6	9	6	1.589E+06	2.384E+06	0.667	23.2	0.08	146.8 ± 77.4
G1278-2	8	9	5	12	1.192E+06	6.621E+05	1.800	6.4	0.01	388.8 ± 217.1
G1278-3	4	2	4	8	3.973E+05	7.945E+05	0.500	7.7	0.10	111.2 ± 96.3
G1278-3	5	23	49	12	3.046E+06	6.489E+06	0.469	62.7	0.11	104.4 ± 26.5
G1278-3	6	100	76	48	3.311E+06	2.516E+06	1.316	24.3	0.09	288.6 ± 44.6
G1278-3	7	2	11	6	5.297E+05	2.913E+06	0.182	28.2	0.03	40.7 ± 31.3
G1278-3	8	19	10	18	1.677E+06	8.828E+05	1.900	8.5	0.27	412.7 ± 161.6
		232	248		2.410E+06	2.575E+06		25.1		

Area of basic unit = 6.293E-07 cm-²
χ^2 = 25.044 with 9 degrees of freedom
P(χ^2) = 0.3%
Age Dispersion = 38.858%

Ns / Ni = 0.936 ± 0.085
Mean Ratio = 0.947 ± 0.181

Ages calculated using a zeta of 380.4 ± 5.7 for CN5 glass
ρ = 1.171E+06cm-² ND = 1951
ρ_D interpolated between top of can; ρ = 1.162E+06cm-² ND = 914
bottom of can; ρ = 1.318E+06cm-² ND = 1037

POOLED AGE = 205.1 ± 19.5 Ma
CENTRAL AGE = 189.8 ± 33.4 Ma

A:

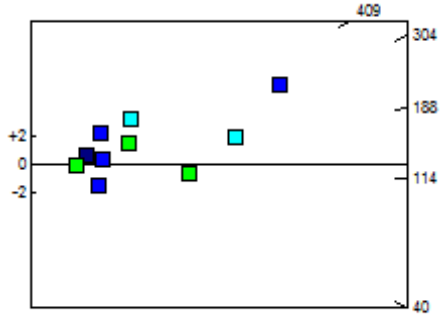

B:

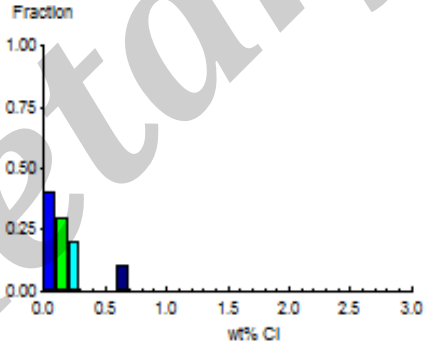

C:

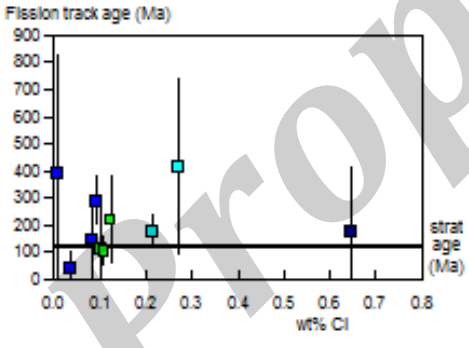

D:

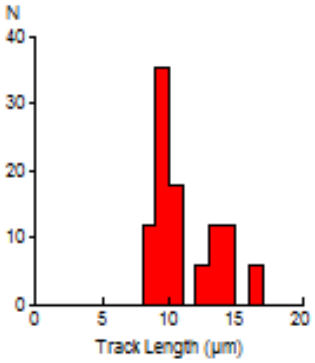

Mean track length 11.27 ± 0.58 µm Std. Dev. 2.38 µm 17 tracks

GC1191-3 Apatite
Counted by: COB

OCS-Y-2321 Burger J 001 5600-5660'

Slide ref	Current grain no	N_s	N_i	N_a	ρ_s	ρ_i	RATIO	U (ppm)	Cl (wt%)	F.T. AGE (Ma)
G1278-4	4	4	4	9	7.063E+05	7.063E+05	1.000	6.8	0.04	222.1 ± 157.2
G1278-4	6	8	8	18	7.063E+05	7.063E+05	1.000	6.8	0.63	222.1 ± 111.2
G1278-4	11	23	28	16	2.284E+06	2.781E+06	0.821	26.7	0.04	183.0 ± 51.7
G1278-4	15	8	10	8	1.589E+06	1.986E+06	0.800	19.1	0.27	178.3 ± 84.7
G1278-5	3	7	8	21	5.297E+05	6.054E+05	0.875	5.8	0.00	196.1 ± 101.7
G1278-5	4	11	10	8	2.185E+06	1.986E+06	1.100	18.9	0.06	245.6 ± 107.5
G1278-5	5	3	4	12	3.973E+05	5.297E+05	0.750	5.0	0.35	168.5 ± 128.8
G1278-5	6	3	5	9	5.297E+05	8.828E+05	0.600	8.4	0.04	135.1 ± 98.8
G1278-5	8	6	23	50	1.907E+05	7.310E+05	0.261	7.0	0.13	59.1 ± 27.1
G1278-5	9	4	7	16	3.973E+05	6.952E+05	0.571	6.6	0.29	128.8 ± 80.8
G1278-5	10	2	2	4	7.945E+05	7.945E+05	1.000	7.6	0.02	223.7 ± 223.8
G1278-5	12	5	7	35	2.270E+05	3.178E+05	0.714	3.0	0.28	160.6 ± 94.1
G1278-5	13	10	31	35	4.540E+05	1.407E+06	0.323	13.4	0.29	73.0 ± 26.6
G1278-5	14	2	9	20	1.589E+05	7.151E+05	0.222	6.8	0.30	50.4 ± 39.4
G1278-5	15	19	41	60	5.032E+05	1.086E+06	0.463	10.3	0.15	104.6 ± 29.2
G1278-5	16	22	62	24	1.457E+06	4.105E+06	0.355	39.1	0.21	80.3 ± 20.0
G1278-5	17	18	24	28	1.022E+06	1.362E+06	0.750	13.0	0.01	168.5 ± 52.7
G1278-5	19	4	6	15	4.238E+05	6.356E+05	0.667	6.1	0.67	150.0 ± 96.9
G1278-5	20	29	85	32	1.440E+06	4.221E+06	0.341	40.2	0.08	77.2 ± 16.7
G1278-5	23	0	5	14	0.000E+00	5.675E+05	0.000	5.4	0.53	0.0 ± 92.1
G1278-6	3	43	44	16	4.271E+06	4.370E+06	0.977	41.3	0.07	220.2 ± 47.6
G1278-6	4	120	105	72	2.648E+06	2.317E+06	1.143	21.9	0.28	256.8 ± 35.0
G1278-6	7	9	21	30	4.767E+05	1.112E+06	0.429	10.5	0.70	97.5 ± 38.9
G1278-6	10	3	8	21	2.270E+05	6.054E+05	0.375	5.7	0.27	85.4 ± 57.9
G1278-6	11	125	132	36	5.518E+06	5.827E+06	0.947	55.1	0.26	213.5 ± 27.3
G1278-6	12	24	27	40	9.534E+05	1.073E+06	0.889	10.1	0.70	200.6 ± 56.5
		512	709		1.254E+06	1.735E+06		16.7		

Area of basic unit = 6.293E-07 cm^{-2}
χ^2 = 65.441 with 25 degrees of freedom
P(χ^2) = 0.0%
Age Dispersion = 36.360%

Ns / Ni = 0.722 ± 0.042
Mean Ratio = 0.673 ± 0.061

Ages calculated using a zeta of 380.4 ± 5.7 for CN5 glass
ρ = 1.188E+06cm^{-2} ND = 1951
ρ_D interpolated between top of can; ρ = 1.162E+06cm^{-2} ND = 914
bottom of can; ρ = 1.318E+06cm^{-2} ND = 1037

POOLED AGE = 161.2 ± 10.3 Ma
CENTRAL AGE = 142.7 ± 15.7 Ma

A:

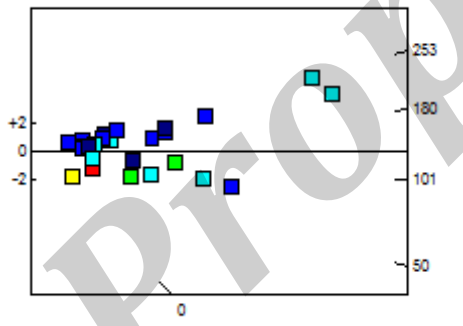

B:

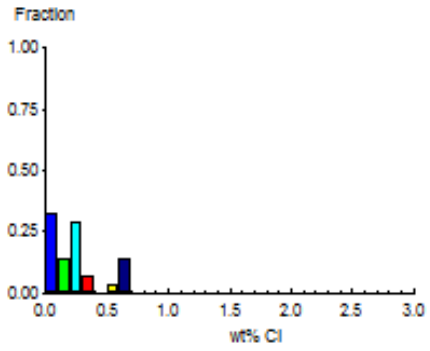

C:

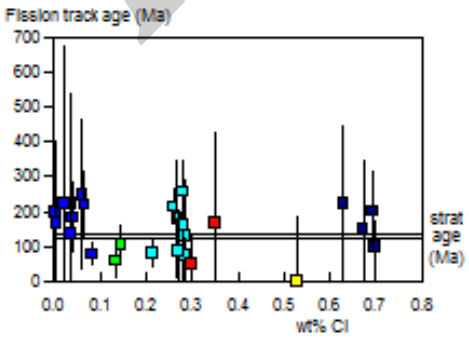

D:

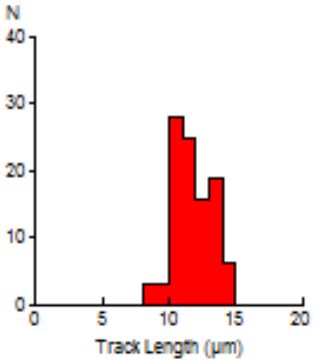

Mean track length 11.70 ± 0.25 µm Std. Dev. 1.43 µm 32 tracks

GC1191-4 Apatite
Counted by: COB

OCS-Y-2321 Burger J 001 5880-5950'

Slide ref	Current grain no	N_s	N_i	N_a	ρ_s	ρ_i	RATIO	U (ppm)	Cl (wt%)	F.T. AGE (Ma)
G1278-7	3	2	7	16	1.986E+05	6.952E+05	0.286	6.5	0.02	65.6 ± 52.7
G1278-7	5	14	15	36	6.180E+05	6.621E+05	0.933	6.2	0.02	212.0 ± 79.0
G1278-7	8	22	31	28	1.249E+06	1.759E+06	0.710	16.5	0.04	161.8 ± 45.3
G1278-7	10	7	14	18	6.180E+05	1.236E+06	0.500	11.6	0.12	114.4 ± 53.1
G1278-8	3	2	6	16	1.986E+05	5.959E+05	0.333	5.6	0.37	77.1 ± 63.0
G1278-8	4	2	3	9	3.531E+05	5.297E+05	0.667	4.9	0.00	153.2 ± 139.9
G1278-8	5	11	10	12	1.457E+06	1.324E+06	1.100	12.3	0.56	250.9 ± 109.8
G1278-8	6	7	18	8	1.390E+06	3.575E+06	0.389	33.3	0.05	89.8 ± 40.1
G1278-8	7	11	39	14	1.249E+06	4.427E+06	0.282	41.3	0.06	65.3 ± 22.4
G1278-8	8	20	44	30	1.059E+06	2.331E+06	0.455	21.7	0.20	104.9 ± 28.4
G1278-8	9	5	7	21	3.783E+05	5.297E+05	0.714	4.9	0.07	164.0 ± 96.1
G1278-8	10	13	19	54	3.826E+05	5.591E+05	0.684	5.2	0.46	157.2 ± 56.7
G1278-8	11	2	6	20	1.589E+05	4.767E+05	0.333	4.4	0.02	77.1 ± 63.0
G1278-8	13	23	18	18	2.030E+06	1.589E+06	1.278	14.8	0.13	290.5 ± 91.8
G1278-8	14	2	4	9	3.531E+05	7.063E+05	0.500	6.6	0.18	115.2 ± 99.9
G1278-8	16	4	7	6	1.059E+06	1.854E+06	0.571	17.3	0.00	131.5 ± 82.5
G1278-8	17	48	100	60	1.271E+06	2.648E+06	0.480	24.7	1.05	110.7 ± 19.7
		195	346		8.263E+05	1.466E+06		13.8		

Area of basic unit = 6.293E-07 cm-²
χ^2 = 20.688 with 16 degrees of freedom
P(χ^2) = 19.1%
Age Dispersion = 24.659%

Ns / Ni = 0.564 ± 0.050
Mean Ratio = 0.604 ± 0.070

Ages calculated using a zeta of 380.4 ± 5.7 for CN5 glass
ρ = 1.214E+06cm-² ND = 1951
ρ_D interpolated between top of can; ρ = 1.162E+06cm-² ND = 914
bottom of can; ρ = 1.318E+06cm-² ND = 1037

POOLED AGE = 128.8 ± 12.1 Ma
CENTRAL AGE = 132.4 ± 15.9 Ma

A:

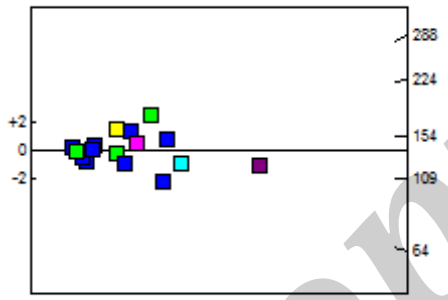

B:

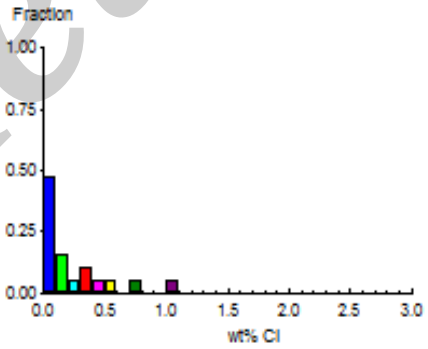

C:

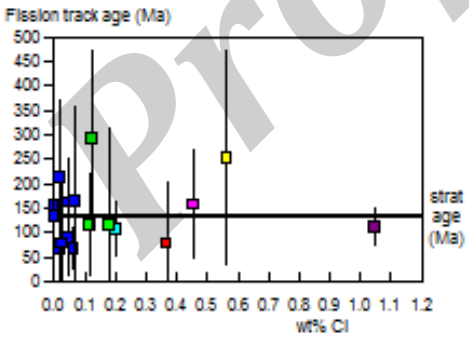

D:

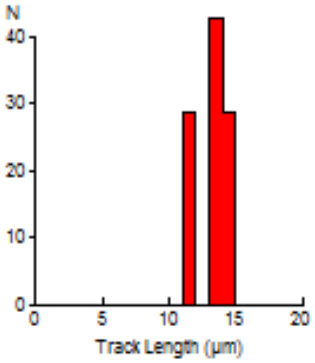

Mean track length 13.29 ± 0.51 µm Std. Dev. 1.36 µm 7 tracks

GC1191-5 Apatite
Counted by: COB

OCS-Y-2321 Burger J 001 5950-6010'

Slide ref	Current grain no	N_s	N_i	N_a	ρ_s	ρ_i	RATIO	U (ppm)	Cl (wt%)	F.T. AGE (Ma)
G1278-9	3	5	8	32	2.483E+05	3.973E+05	0.625	3.7	0.21	144.7 ± 82.6
G1278-9	4	24	59	32	1.192E+06	2.930E+06	0.407	27.1	0.27	94.6 ± 23.0
G1278-9	5	26	42	20	2.066E+06	3.337E+06	0.619	30.9	0.14	143.4 ± 36.0
G1278-9	6	13	45	40	5.164E+05	1.788E+06	0.289	16.5	0.32	67.3 ± 21.3
G1278-9	7	32	22	12	4.238E+06	2.913E+06	1.455	27.0	1.00	332.0 ± 92.4
G1278-9	8	5	22	12	6.621E+05	2.913E+06	0.227	27.0	0.26	53.0 ± 26.3
G1278-9	10	19	44	70	4.313E+05	9.988E+05	0.432	9.2	0.41	100.4 ± 27.7
G1278-9	11	12	39	60	3.178E+05	1.033E+06	0.308	9.6	0.08	71.7 ± 23.7
G1278-9	12	12	30	40	4.767E+05	1.192E+06	0.400	11.0	0.45	93.0 ± 31.9
G1278-10	3	9	11	4	3.575E+06	4.370E+06	0.818	40.2	0.03	190.2 ± 85.6
G1278-10	5	1	5	20	7.945E+04	3.973E+05	0.200	3.7	0.35	47.0 ± 51.5
G1278-10	6	4	13	8	7.945E+05	2.582E+06	0.308	23.7	0.01	72.2 ± 41.3
G1278-10	7	0	2	12	0.000E+00	2.648E+05	0.000	2.4	0.07	0.0 ± 385.5
G1278-10	8	3	11	10	4.767E+05	1.748E+06	0.273	16.1	0.33	64.0 ± 41.7
G1278-10	9	0	5	28	0.000E+00	2.838E+05	0.000	2.6	0.01	0.0 ± 95.3
G1278-10	10	5	7	15	5.297E+05	7.416E+05	0.714	6.8	0.04	166.3 ± 97.5
G1278-10	11	15	28	30	7.945E+05	1.483E+06	0.536	13.6	0.39	125.1 ± 40.2
G1278-10	12	1	7	32	4.966E+04	3.476E+05	0.143	3.2	0.21	33.6 ± 35.9
		186	399		6.196E+05	1.330E+06		12.3		

Area of basic unit = 6.293E-07 cm^{-2}
χ^2 = 35.916 with 17 degrees of freedom
P(χ^2) = 0.5%
Age Dispersion = 40.052%

Ns / Ni = 0.466 ± 0.041
Mean Ratio = 0.432 ± 0.081

Ages calculated using a zeta of 380.4 ± 5.7 for CN5 glass
ρ = 1.231E+06cm^{-2} ND = 1951
ρ_D interpolated between top of can; ρ = 1.162E+06cm^{-2} ND = 914
bottom of can; ρ = 1.318E+06cm^{-2} ND = 1037

POOLED AGE = 108.2 ± 10.0 Ma
CENTRAL AGE = 103.3 ± 14.8 Ma

A:

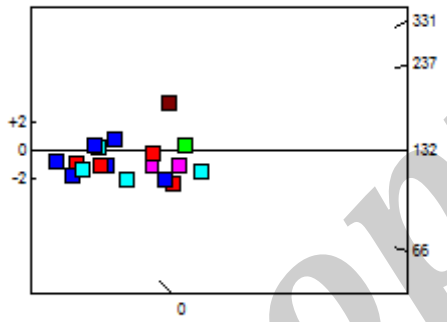

B:

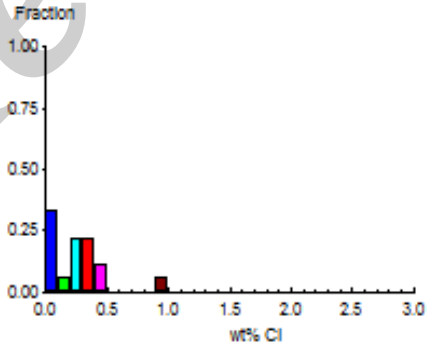

C:

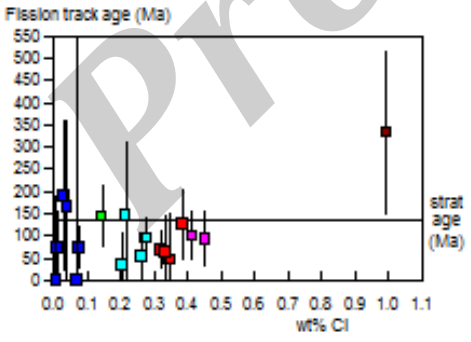

D:

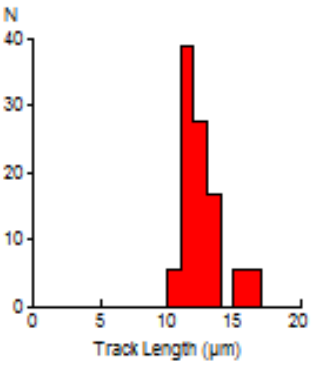

Mean track length 12.53 ± 0.36 µm Std. Dev. 1.54 µm 18 tracks

APPENDIX C

Thermal History interpretation of AFTA data: basic principles and practical application

C.1 Historical background and physical basis

Naturally occurring fission tracks are radiation damage trails produced by the spontaneous fission of ^{238}U atoms, in which a uranium atom splits into two highly energetic fragments, stripped of electrons. Due to electrostatic repulsion between the fragments, they travel rapidly in opposite directions creating a linear zone of intense disruption through the crystal lattice, known as a fission track. Apatite grains typically contain around 10 ppm Uranium (range 1-100 ppm), so over geological time fission tracks accumulate in the crystal lattice. If a collection of apatite grains are mounted and polished, tracks can be revealed where they intersect the polished surface by a simple etching treatment (Fig. C.1). Since spontaneous fission is a form of radioactive decay, in principle the number of tracks in the surface is controlled by uranium content and time, through standard decay laws, so by counting the number of tracks and measuring the uranium content, a "fission track age" can be measured which, in the absence of other factors, should indicate the time over which tracks have accumulated. Reviews of the basics of fission track dating are provided by e.g. Fleischer et al. (1975), Wagner and Van den Haute (1992) and Galbraith (2006).

Fig. C.1: Spontaneous fission tracks in a detrital apatite grain ~ 0.25 mm in length. Fission tracks were revealed by etching in 5M HNO3 for 20 seconds at 20°C. The majority of linear features in the image are fission tracks. They are randomly orientated in 3 dimensions and the number of tracks revealed in the surface is controlled by the uranium content of the grain, the time over which tracks have accumulated, and the distribution of track lengths, which in turn is a function of the thermal history

Early insights into the thermal sensitivity of fission tracks in apatite

Early applications of fission track dating to accessory apatites from crystalline basement rocks revealed that the technique was extremely thermally sensitive, suggesting that fission track ages could be reset at relatively low temperatures around 100°C over geological timescales (e.g. Wagner and Reimer, 1972). This was supported by early laboratory annealing studies (Wagner, 1968; Naeser and Faul, 1969), and subsequently confirmed by direct measurement of fission track ages in sub-surface samples (Naeser and Forbes, 1976). Integration of fission track ages with confined track length measurements (Fig. C.2), first reported by Bhandari et al. (1971), led to deeper understanding of the method. Early measurements showed that even in volcanic rocks which have experienced only very low temperatures after initial post-eruption cooling, mean confined track lengths (around 14 to 15 μm) were shorter than induced tracks (~16 μm) in the same apatites. Green (1980) showed that this can be understood in terms of thermal annealing of these tracks at low temperatures (<50°C) over geological timescales, highlighting the sensitivity of the technique.

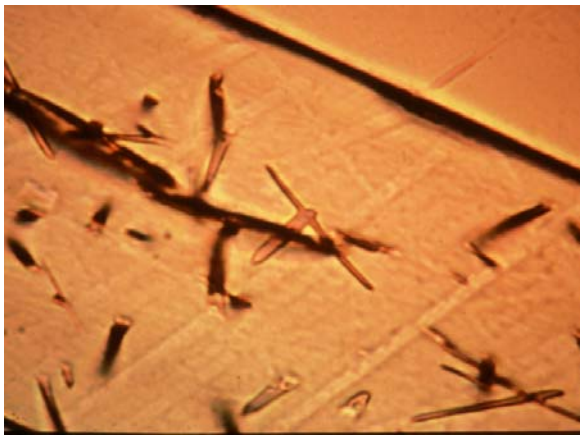

Fig. C.2: Confined fission track lengths in apatite. In order to determine the distribution of track lengths, measurements are made of the full length of horizontal tracks which are totally enclosed within the body of the crystal, which have been etched via fractures or other tracks which intersect the surface of the grain. Note that difference in width of the tracks is due to a difference in etch rate with crystallographic orientation, with a higher etch rate parallel to the C-axis

Results from boreholes in the Otway Basin of SE Australia (Gleadow and Duddy, 1981) provided the first quantitative insights into the thermal stability of tracks in geological conditions, revealing the progressive reduction in fission track age with depth

and temperature, and showing that this was complemented by a corresponding decrease in track length (Fig. C.3). Compilation of confined track length data in a large number of apatite samples showed that the form of the track length distribution was a sensitive indicator of the style of thermal history (Gleadow et al. 1986). Laboratory studies (Green et al. 1985, 1986; Green 1988), together with detailed mathematical analysis (Laslett et al. 1982; Galbraith and Laslett 1988, 1990), established that the reduction in track length (which is, in turn, a manifestation of the reduction in the degree of damage within the track region) causes the reduction in fission track age, by reducing the proportion of tracks that can intersect a polished grain surface. This realization underpins all subsequent studies involving quantitative prediction of apatite fission track (AFT) parameters and extraction of thermal history information from such data. .

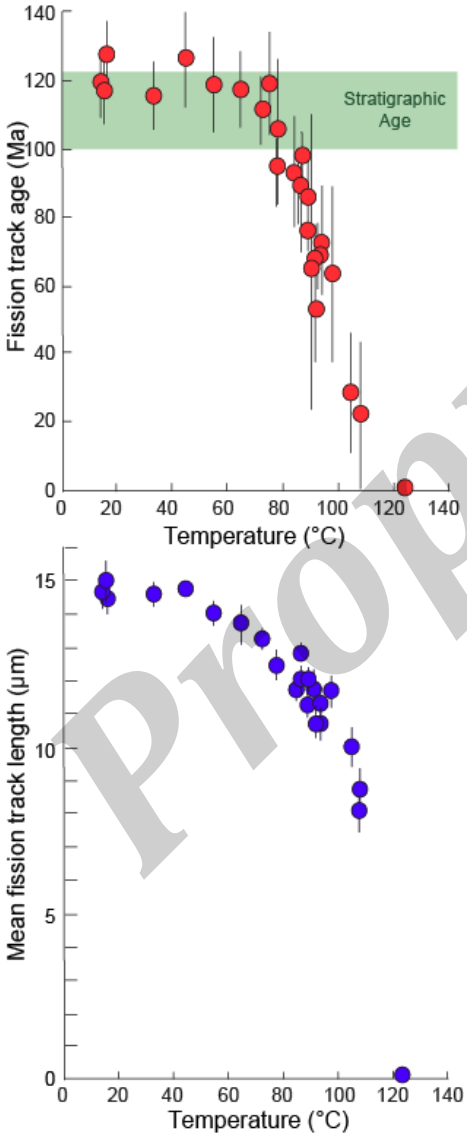

Fig. C.3: Variation of measured fission track age and mean track length with present-day temperature in samples from Otway Basin (Australia) exploration wells which are at maximum temperatures at the present-day. With increasing maximum temperature there is a progressive reduction in fission track age to zero at ~125°C which is the result of the progressive reduction in mean confined track length. These observations provide a direct expression of the thermal stability of fission tracks in geological conditions (after Gleadow and Duddy, 1981).

The Laslett et al. (1987) model

Early laboratory annealing studies, based on measurement of track density as an indicator of the degree of annealing, in accessory apatites of varying character, led to a wide variety of kinetic models of conflicting styles (as reviewed by Green et al. 1986; Green et al. 1988). Based on the recognition of the key role of track length in the annealing process, coupled with the fact that track lengths can be measured with greater precision than track densities, Green et al. (1986) carried out a series of detailed annealing experiments on a well-characterised apatite of uniform composition (Durango apatite, Young et al, 1969), in which mean track length was used to indicate the degree of annealing. This study demonstrated that as a result of heating, the mean track length is progressively reduced and the tracks effectively "shrink" from each end, until in the final stages individual tracks may break up into several segments. This behaviour can be understood in terms of a progressive reduction in the degree of radiation damage within the track region, as displaced atoms return to their original lattice sites by thermally activated diffusion, until in the final stages, discrete zones of etchability are separated by regions which are fully "healed". Laslett et al. (1987) subsequently showed that the variation of mean track length with temperature and time was well described by a "fanning Arrhenius plot" model, in which contours of equal track length reduction form straight lines in a plot of time against inverse absolute temperature, with the slope of these lines (reflecting an "activation energy") increasing as the degree of annealing increases (Fig. C.4).

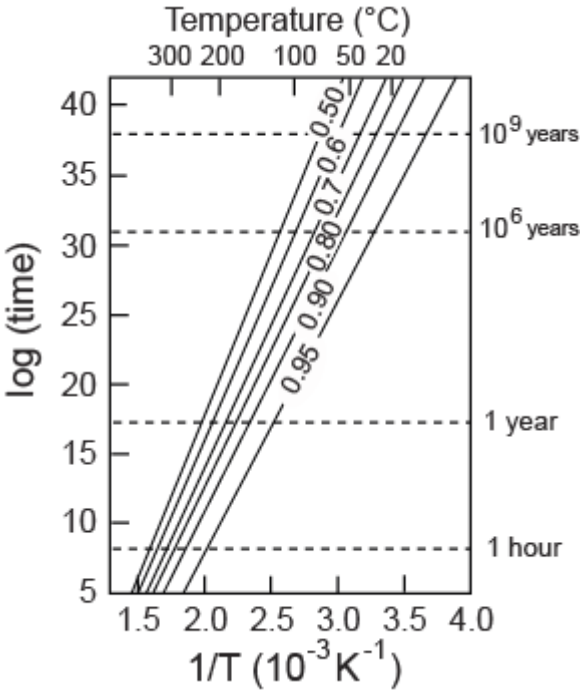

Fig. C.4: Fanning Arrhenius plot" adopted by Laslett et al. (1987) to describe the variation of mean track length with temperature and time for Durango apatite. In this plot, contours of equal track length reduction form straight lines in a plot of log(time) against inverse absolute temperature (contoured values are the ratio of predicted length to initial length, L/L_o).

Variable temperature behaviour

The improved definition of the kinetics of fission track annealing provided by using mean confined track length as the fundamental parameter (Laslett et al. 1987), combined with a detailed understanding of the way in which reduction in track length is manifested in the fission track age (Green, 1988), provided the basis for making realistic predictions of apatite fission track parameters in geological situations. A key step in this process is the transition from isothermal annealing models to variable temperature behaviour as encountered in geological settings. Duddy et al. (1988) provided a way forward by adopting the principle of 'equivalent time" (originally postulated by Goswami et al., 1984), by which the rate of annealing of a track at any given time depends only on the length to which the track has already been reduced, and the prevailing temperature, and not on the history of how the track reached that length. The validity of this assumption is by no means straightforward, and Duddy et al. (1988) provided experimental verification through a series of variable temperature annealing experiments, laying the basis for the successful extension of isothermal annealing models to variable temperature geological histories.

Quantitative modelling of AFTA parameters

Green et al. (1989) built on the advances described above to develop methods for quantitatively modelling the response of fission tracks in apatite to various styles of thermal history. The basis of the approach is the recognition that track length reduction is the controlling process in determining the AFTA parameters that result from any particular history. New fission tracks are continually generated as time passes, such that different tracks sample different proportions of the whole history. If a specified thermal history is broken down into discrete intervals, the pattern of track length reduction with time for populations of tracks formed at different times through the history can be calculated by applying the principle of equivalent time (above) to the thermal history appropriate to each population, resulting in a predicted mean length for each population of tracks at the present day (Fig. C.5).

Fission tracks show an inherent spread in track length, reflecting the range of energies and masses of the fission fragments produced by spontaneous fission. This spread, measured by the standard deviation of the length distribution, increases as the mean length is reduced, largely as a result of an increasing anisotropy of the annealing process (Green et al., 1986). So to calculate the final distribution of track lengths predicted for a sample at the present day, the component distributions of track length resulting from populations of tracks produced at different times throughout the history must be summed, employing the appropriate spread of lengths for each population. The component populations must also be added in the appropriate proportions, allowing for the biases involved in revelation of tracks of different length (Laslett et al., 1982). By summing components of fission track age appropriate to the length of each time interval, moderated by the effect of length reduction on the reduction of age (Green, 1988), the final fission track age for the sample can also be predicted.

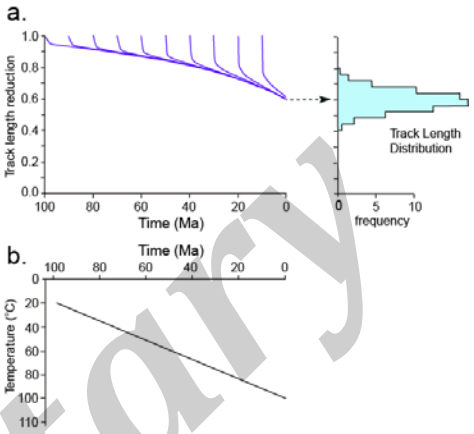

Fig. 5: a). Predicted pattern of track length reduction with time (left) and final track length distribution (right) for populations of tracks formed at different times through the notional thermal history shown in b.), involving progressive heating from 20 to 100°C over 100 Myr. The final track length distribution is calculated by applying the principle of equivalent time to each population of tracks using the Fanning Arrhenius model of Laslett et al. (1987), and summing the track lengths distributions for all populations of tracks in the appropriate length-biassed proportions (Laslett et al., 1982). After Green et al. (1989).

Influence of apatite composition on annealing rates

Studies of apatite fission track parameters in subsurface samples from the Otway Basin (Gleadow and Duddy, 1981; Green et al., 1985, 1986) showed that chlorine content exerts a systematic influence on annealing rates (Fig. C.6). This has subsequently been confirmed in laboratory studies by Carlson et al. (1999) and Barbarand et al. (2003a). In both these studies, the authors tend to downplay the influence of chlorine in favour of other factors. But results from both studies clearly illustrate the first-order control exerted by chlorine (Fig. C.7), while also suggesting that other possibly more exotic factors may exert second-order control in some cases. The importance of differential annealing within individual samples related to wt% Cl has now been demonstrated in a number of geological studies (e.g. Argent et al., 2002; Crowhurst et al., 2002; Green et al., 2002; Green, 2005).

A number of studies have suggested that etch pit diameters can be used as an indicator of differential annealing rates between various apatite species (Burtner et al. 1994; Ketcham et al. 1999; Barbarand et al. 2003a). However, Green et al. (2005) demonstrated that annealing rates in the Barbarand et al. (2003a) dataset show a much stronger correlation with wt% Cl than to etch pit size (Fig. C.8).

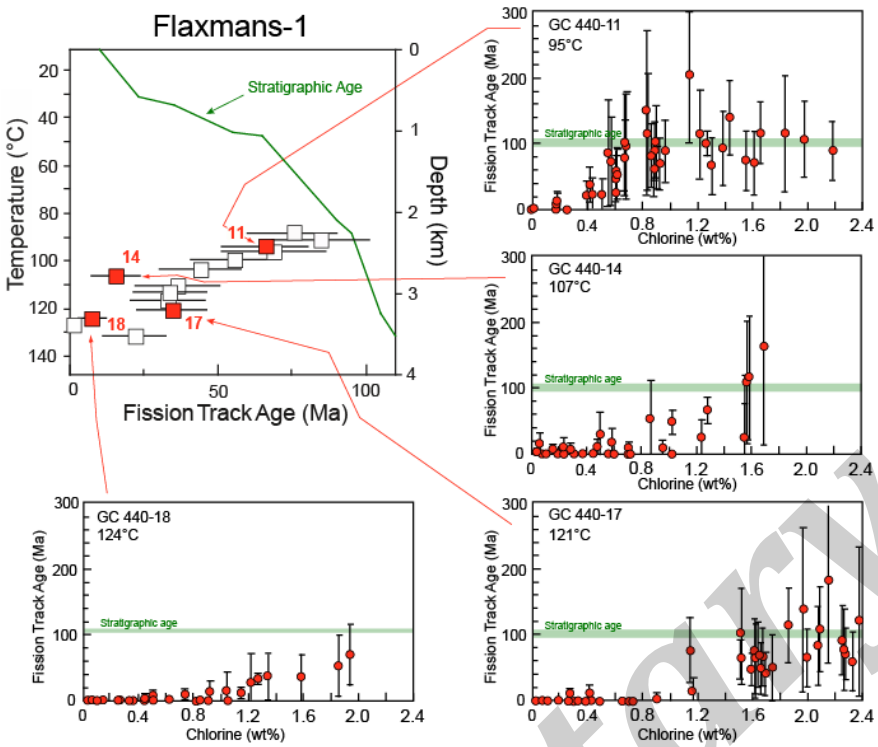

Fig. C.6: Variation of central fission track age with depth for samples from the Flaxmans-1 well, Otway Basin, SE Australia, together with the variation of fission track age with chlorine content for individual apatite grains from four selected samples. In each of these samples the most sensitive (i.e. low wt% chorine) grains are totally annealed (i.e. zero FT age) while grains with more retentive (higher Cl) grains giving ages up to the depositional age and above. With increasing present-day down-hole temperature (the maximum post-depositional temperature in these samples), the transition to total annealing shifts to progressively higher Cl contents, demonstrating the systematic influence of chlorine content on annealing (Gleadow and Duddy, 1981; Green et al., 1985, 1986). Note that while most of the central fission track ages define a generally smooth decrease with increasing temperature, the age for sample GC440-14 is off trend. This is due to the absence of grains with chlorine >1.6 wt% Cl compared to adjacent samples, which are dominated by more retentive grains and therefore give higher central ages. This major effect of chlorine on apatite fission track age must be taken into account in order to extract meaningful geological constraints from apatite fission track data.

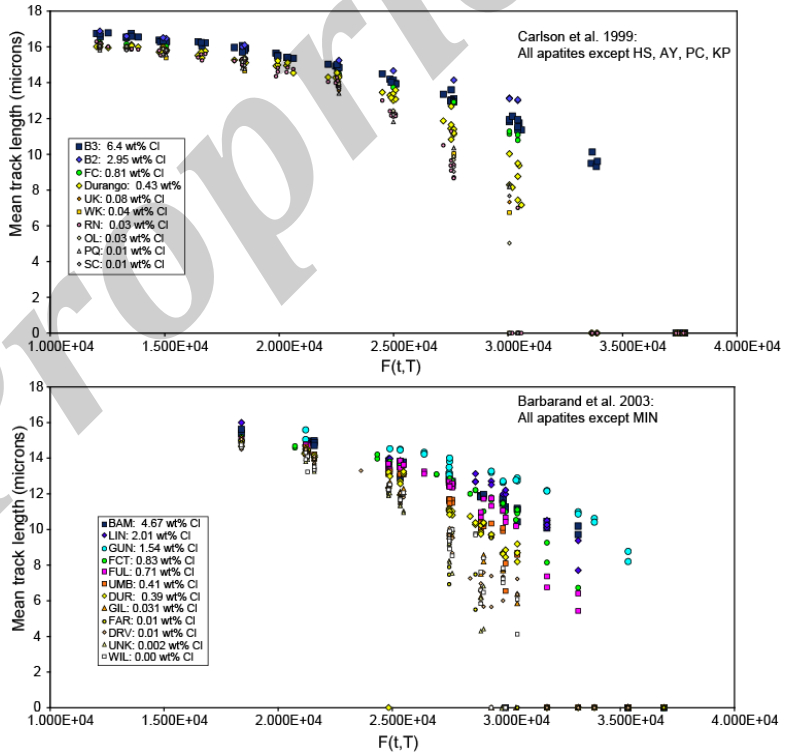

Fig. C.7: Mean track lengths from laboratory annealing experiments reported by Carlson et al. (1999) and Barbarand et al. (2003a), plotted against a unifying function of temperature and time, which reduces all data to a common scale. This function is of the form $F(t,T) = [\log t - \log t_o]/[(1/T)-(1/T_o)]$, where $\log t_o = -10$ and $1/T_o = 0.001$. Apatites of different Cl content are coded to illustrate this variation, with high Cl contents (>1 wt% Cl) shown in blue colours and large symbols, apatites low in Cl (<0.1 wt % Cl) shown in pale colours and small symbols, and intermediate compositions shown in yellow, red and green colours. The Durango apatite (yellow diamonds) and Fish Canyon Tuff apatite (green circles) are common to both datasets. These results clearly illustrate the first order control on annealing rates exerted by Cl content, with apatites high in chlorine giving longer lengths for any given heat treatment than those low in Cl. While the first order control from chlorine is clear, other elements produce additional variation, and several apatites have been omitted from these plots as they are not consistent with the main body of data.

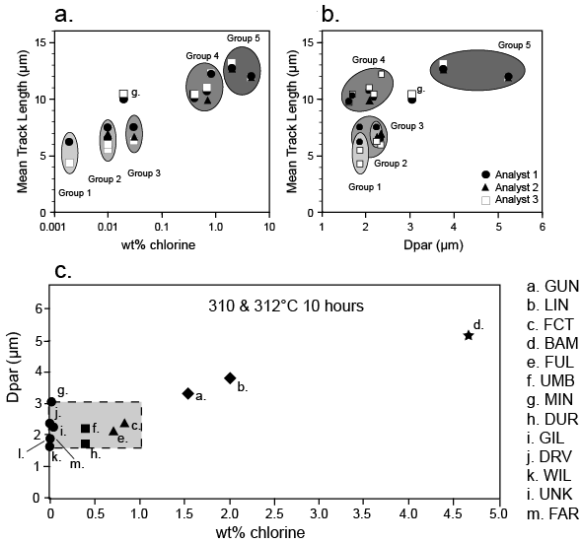

Fig. C.8: Comparison of the variation in mean track length with chlorine content (a.) and with the width of track openings parallel to the c-axis (Dpar) (b.) from the laboratory annealing experiments of Barbarand et al. (2003a). Track size shows only a poor correlation with mean fission track length, whereas chlorine contents hows a very strong correlation, illustrating that Dpar is only a poor proxy for fission track annealing rates. Similar behaviour is seen in results from other annealing conditions reported by Barbarand et al. (2003a) data set, as discussed in detail by Green et al (2005a). The track-size parameter Dpar shows only a poor correlation with chlorine contents between 0.and 1 wt% (c.), and it should therefore be expected that Dpar would provide only a limited indication of differential annealing sensitivities between different apatite species.

Evidence for systematic differences in annealing rates in natural geological samples due to any element other than Cl has yet to be demonstrated. In practical application of AFTA, variation in fission track age and track length with wt% Cl allows identification of any anomalous grains that might represent unusual annealing properties (e.g. Crowhurst et al. 2002). This approach also allows detection of contaminant grains, which can be important in working with ditch cuttings in sub-surface samples, where "caving" of material from shallower levels can be recognised in this way (Japsen et al., 2005; Green et al., 2011). Such anomalous grains can be eliminated from the dataset prior to extraction of thermal history solutions.

In geological conditions, differential annealing effects within individual samples are maximised in rocks which have been heated into the critical temperature range (typically 90-120°C) where the most sensitive (i.e. low Cl) apatites are totally annealed while more resistant apatites (high Cl) are unaffected (Fig. C.6). In such cases, the systematic dispersion in fission track age, correlating with wt% Cl, provides added precision to a thermal history solution (Crowhurst et al., 2002) (Fig. C.9).

Numerous examples exist in the literature of apparently anomalous observations that can probably be simply explained in terms of differences in wt% Cl. One example is the apparent difference in resistance to erosion attributed to adjacent Gneissic and Charnockitic terrains in India reported by Gunnel (2000), which is more likely to be due to a difference in annealing rates in apatites from the two rock types (with Charnockitic apatites likely to be richer in Cl, and hence giving older ages). In such cases, measurement of Cl contents in the analysed grains can easily resolve such effects.

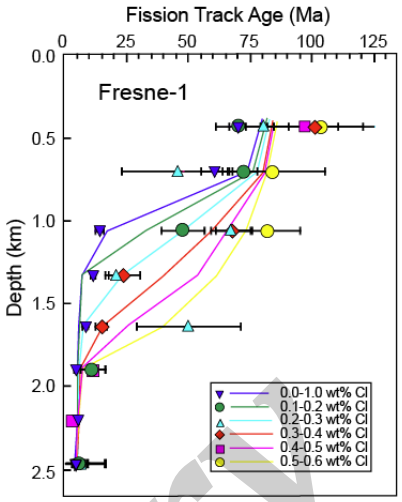

Fig. C.9: Variation of fission track age with depth for apatites of different chlorine content in samples from the Fresne-1 well, Taranaki Basin, New Zealand (after Crowhurst et al., 2002). Apatites with lower chlorine content achieve a given degree of annealing (as expressed by the reduction in fission track age) at shallower levels, corresponding to lower maximum paleotemperatures, compared to apatites with higher chlorine. In particular, note the progressive shift in the transition from partial to total annealing (defined by the inflection in the age-depth trend), with apatites containing 0.5-0.6 wt% Cl becoming totally annealed almost 1 km deeper than samples containing between 0.0 and 0.1 wt% Cl. Curves show the variation of fission track age for each compositional group predicted from the final reconstructed history for the Fresne-1 well, as reported in Crowhurst et al. (2002).

Later kinetic models

Subsequent to publication of the Laslett et al. (1987) kinetic model of fission track annealing, various refinements or alternative forms of the basic fanning Arrhenius plot model have been published. Carlson (1990) suggested a model based on the laboratory annealing data from Green et al. (1986) and other (then unpublished) data, and claimed that because this model was "based on explicit physical mechanisms, extrapolations of annealing rates to the lower temperatures and longer timescales required for the interpretation of natural fission track length distributions can be made with greater confidence than is the case for purely empirical relationships fitted to the experimental annealing data". However, as explained by Green et al. (1993), all aspects of Carlson's model are in fact purely empirical, and this model is inherently no more reliable than any other model. In addition, as reported by Crowley (1993), detailed inspection shows that Carlson's model does not fit the laboratory data set at all well.

Crowley et al. (1991) published new annealing data in three apatites of different composition, including the Durango apatite for which the Laslett et al, (1987) model was derived, and fitted kinetic models which are similar to the Laslett et al., (1987) model, except for the use of a non-zero inverse temperature intercept ($1/T_o$). It should be noted that Laslett et al. (1987) considered such models but showed that the best estimate of $1/T_o$ in their analysis was not significantly different from zero, and because the assumption of $1/T_o = 0$ simplifies the mathematical description, they preferred the simpler model.

Despite an apparently superior experimental design compared to the Green et al. (1986) study, the kinetic models offered by Crowley et al. (1991), as well as that of Carlson (1990) give predictions in geological conditions that are not consistent with observations (as reviewed in more detail later), and these models have not achieved widespread use. Crowley et al (1991) investigated Arrhenius plot models in which contours of equal annealing are curved, although linear models were favoured. Crowley et al. (1991) also fitted a revised model to the annealing data for Durango apatite published by Green et al. (1986). Predictions of the revised model are not very much different to those from the Laslett et al. (1987) model (below) and this model has also not found widespread use.

Subsequently, Laslett and Galbraith (1996) showed that rather than using the reduced track length L/L_o (where L_o is the mean length of unannealed tracks) as the controlling parameter, improved models could be achieved by fitting to the measured mean track lengths, L, instead of L/L_o, while L_o becomes simply an additional empirical parameter to be estimated. This is of particular importance because Donelick et al. (1990) showed that tracks produced by thermal neutron irradiation begin to anneal (shorten) over very short timescales (minute to hours) even at room temperature. For this reason, mean lengths of unannealed induced confined tracks which are measured weeks to months after irradiation have already undergone some degree of length reduction, and therefore have no fundamental significance.

In our own work, we use a series of Fanning Arrhenius Plot models of the form advocated by Laslett and Galbraith (1996) with finite $1/T_o$ intercept and fitted to measured track lengths, employing coefficients which vary smoothly with wt% Cl, such that the overall annealing rate decreases as wt% Cl increases. This model is based on a combination of laboratory annealing data and geological constraints, using data from a series of exploration wells in which the thermal histories can be reconstructed with confidence. This avoids uncertainties associated with extrapolation of models from laboratory to geological timescales (discussed below). Effectively the relative behaviour of different apatite species in laboratory conditions (similar to that shown in Fig. C.7) is mapped on to the variation within the geological dataset, as there is insufficient overlap over the full range of apatite compositions in the geological data to provide a satisfactory basis for model fitting based on these data alone.

In similar fashion, Ketcham et al. (1999) fitted a number of models to laboratory annealing data (Fig. C.7) in a variety of apatite species reported by Carlson et al. (1999), and showed how these could be combined into a multi-kinetic model which predicts parameters in samples where a range of kinetic species are present. While their laboratory data favour linear fanning Arrhenius plot models, Ketcham et al. (1999) found that the predictions of curvilinear models provide a closer match to their chosen geological constraints than the linear models.

Precision and accuracy of model predictions in geological conditions

Application of any empirically-constructed kinetic model based on laboratory data to derive meaningful constraints from measured data in geological conditions depends critically on the accuracy and precision involved in the extrapolation of the model over many orders of magnitude in time, and validation of such models is an important step in reliable practical application.

Green et al. (1989) quantitatively assessed the precision associated with extrapolation of the Laslett et al. (1987) model from laboratory to geological timescales, suggesting typical uncertainties of ~0.5 µm for mean lengths around 10 µm or less, and ~0.3 µm for mean lengths longer than 10 µm. These figures are equivalent to an overall uncertainty in estimates of maximum paleotemperature derived using this approach of around ±5°C (95% c.l.).

Accuracy in this context means the degree to which model predictions reproduce the behaviour of the natural system. This was also assessed in detail by Green et al. (1989), who showed that predictions based on the Laslett et al. (1987) model agree well with observed AFTA parameters in samples from temperatures less than about 70°C from a series of reference wells in the Otway Basin of south-east Australia (Fig. C.10). A systematic mismatch above 70°C (Fig. C.10) can be explained by the difference between the composition of the Durango apatite used in the Laslett et al. (1987) model and the apatites in samples from the Otway Basin, which contain a much broader range of Cl contents (see Fig. C.6 which shows chlorine data in samples from the same data set). As also shown in Fig. C.10, other mono-compositional models provide predictions which differ widely from those of the Laslett et al. (1987) model, and are clearly not as accurate in geological conditions. Corrigan (1993) reached somewhat different conclusions from a similar analysis based on data from the US Gulf Coast, but the most important factor is that different laboratory models give different predictions in geological conditions. Any mismatch between predicted and observed geological behaviour inevitably implies that use of such models to extract thermal history information will inevitably result in unreliable results.

In comparing model predictions with measured data from geological samples, it is vital to ensure that the models used are appropriate to the apatite compositions present in the sample. Fig. C.10 also shows predictions from our own multi-compositional model, together with those from the model of Ketcham et al. (1999). Both these approaches take explicit account of the distribution of wt% Cl in the

sample and the systematic change in annealing properties with increasing Cl content, and both provide a close match to the measured data, with the main difference being a greater dispersion of data in apatites from different Cl contents using the Ketcham et al. (1999) model. Both approaches are also calibrated by a combination of laboratory and geological annealing constraints, so the improved match for the multi-compositional models in Fig. C.10 should perhaps not be too surprising. But the improved accuracy of these models compared to the mono-compositional models reflects the inherent limitations of models based on laboratory data alone, and illustrates the benefits of incorporating geological constraints into model calibration.

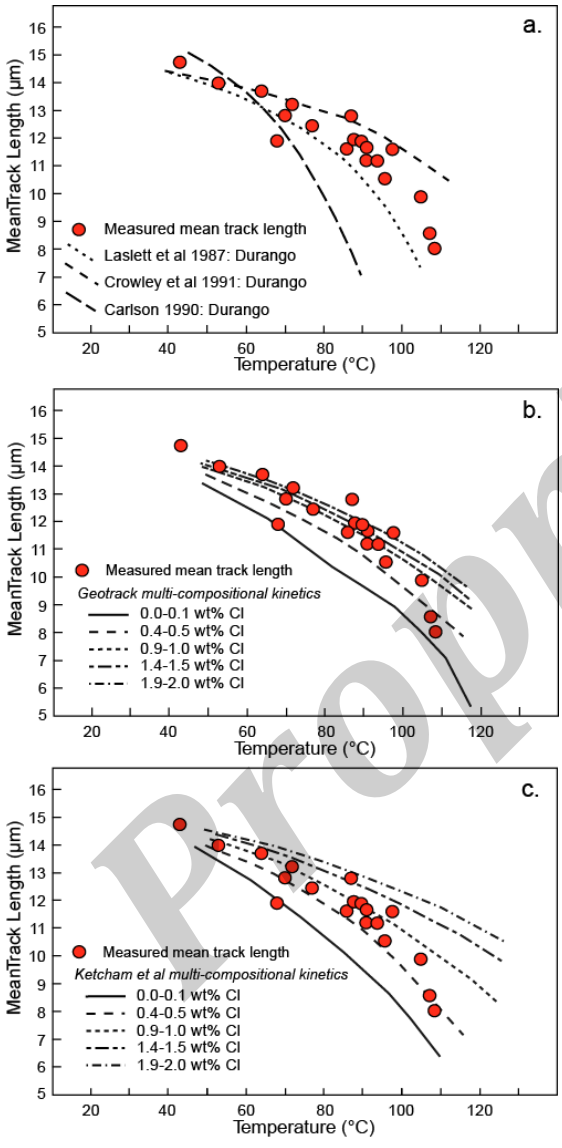

Fig. C.10: Measured mean track lengths in samples from a series of reference wells in the Otway Basin of southeast Australia, compared with values predicted from various annealing models. In a., three mono-compositional annealing models, all based on laboratory annealing in Durango apatite, show various degrees of mismatch to the measured data, emphasising the need for geological calibration in order to make reliable predictions. The Laslett et al. (1987) model provides a reasonable match to the data, while those of Crowley et al (1991) and Carlson (1990) depart significantly from the measured values. In contrast, predictions from Geotrack's multi-compositional model (b.) show a good match to the measured values (which should not be surprising, as data similar to these were employed in construction of the model). Predictions from the model of Ketcham et al (1999), using chlorine as the kinetic parameter (c.) also show a reasonable fit to the data, but show a greater dispersion over the range from 0.0 to 2.0 wt% Cl compared to the Geotrack model.

Accuracy of model predictions at low temperatures

Application of the Laslett et al. (1987) kinetic model to extract thermal history information from AFT data in outcrop samples (using approaches discussed in a later Section) has in many cases resulted in histories involving Late Cenozoic cooling from temperatures around 60°C. This is widely considered to represent an artefact, reflecting the inaccuracy of the model at low temperatures (e.g. Hendriks and Andriessen, 2002; Stephenson et al. 2006).

Vrolijk et al. (1992) studied low temperature annealing in detail, using data in apatites from samples of core from Ocean Drilling Program sites in the Western Pacific, which they suggested can confidently be shown to have never experienced temperatures in excess of 25°C at any time after deposition. In their key sample, MB-7, Vrolijk et al. (1992) reported a mean track length of 14.6±0.1 µm, which is considerably shorter than the value of ~15.3 µm predicted from the Laslett et al. (1987) model for the reconstructed thermal history of these samples. Thus, they concluded that the Laslett et al. (1987) overestimated the observed track length, suggesting that the model is over-retentive at low temperatures. Predicted values using a number of other models were also longer than the observed mean track length.

However, the comparison of predicted and measured values in the Vrolijk et al. (1992) study is compromised by several issues. For example, the Laslett et al. (1987) model strictly relates only to data generated in exactly the same manner as the data from which the model was originally derived (Green et al., 1986). Inter-laboratory differences, and even within-laboratory differences between different analysts, can easily account for differences in mean track length of the order of 0.5 µm (Barbarand et al., 2003a,b). In addition, the confined track length measurements reported by Vrolijk et al. (1992) were produced using collimated ^{252}Cf fission fragment tracks as hosts for "Tracks-IN-Track" (TINTS). As Barbarand et al. (2003b) reported that measurements on TINTS tend to produce rather shorter mean lengths compared to measurements of "Track-IN-CLEavageS" (TINCLES), some of the reported difference between measured and predicted mean length reported by Vrolijk et al. (1992) could have arisen from this source.

But perhaps the most important factor that could explain at least some of the reported difference is apatite composition. Vrolijk et al. (1992) report a mean Cl content of 0.13 wt% for the MB-7 apatite, as compared with 0.43 wt% in Durango apatite on which the Laslett et al. (1987) model is based. On the basis of evidence discussed earlier, the MB-7 apatite should thus be more easily annealed, and therefore should give a shorter mean track length, than predicted from the Laslett et al. (1987) model, exactly as observed. In fact, since most common apatites tend to contain less than 0.1 wt% Cl, it

should be expected that the apatites analysed in most published studies might be more sensitive than Durango apatite. Thus, it is possible that much of the so-called anomalous Late Cenozoic cooling reported in many studies could be due to such compositional effects, rather than any innate deficiencies in the model (Green, 2004).

In addition to the factors discussed above, it seems far from clear that the thermal histories employed by Vrolijk et al. (1992) are as well controlled as they suggest, and changing the maximum temperature of a sample by as little as 10°C could have a major impact on the expected mean track length.

Spiegel et al. (2007) developed and extended the concept of analysing samples from ODP cores, making explicit allowance for compositional influences on annealing. They compared measured mean track lengths in shallowly buried volcanic apatites with values predicted from reconstructed thermal histories based on the Laslett et al. (1987) model and the Ketcham et al. (1999) model, finding that each model successfully predicted some values and performed less well with others, with differences related to apatite composition. In Fig. C.11, we compare the measured mean track lengths with the predicted values from these two models and also with values predicted using the Geotrack multi-compositional model. For the Geotrack and Ketcham et al. (1999) models, kinetics appropriate to the Cl content of each sample have been used. We note that in three of the samples reported by Spiegel et al. (2007) (samples 43-10, 47-3 and 47-7) the measured mean track lengths appear to be anomalously low compared to those in adjacent samples with similar compositions. This is most likely due to the presence of shorter track lengths from grains derived from older sources, which is supported by the larger than usual standard deviations reported for these three samples compared to the rest of the dataset (Spiegel et al. 2007, Table 4). Results from these three samples have therefore been omitted from Fig. C.11.

Values predicted using the three models give rather different results in Fig. C.11. Values predicted using the Geotrack model are up to ~0.25 µm less than the measured values at the highest and lowest mean Cl contents, although the agreement is excellent for compositions between 0.2 and 0.8 wt% Cl. Values predicted using the Ketcham et al. (1999) model are more consistently around 0.5 µm less than measured values over the entire compositional range. In contrast, values predicted using the Laslett et al. (1987) model for apatites containing 0.0-0.2 wt% Cl are around 0.5 µm longer than the measured values (as expected from the above discussion), and this difference first increases and then decreases with increasing wt% Cl, such that for Cl contents around 0.8 wt% Cl the agreement is excellent. While mean track lengths for apatites of similar composition to Durango apatite (~0.4 wt% Cl) are shorter than predicted, the general level of agreement of values predicted from the Laslett et al. (1987) model in Fig. C.11 should be regarded as impressive, since this model is based purely on extrapolation of laboratory data, with no geological control, yet the agreement is almost as good as for models which directly incorporate geological constraints. It should be clear from Fig. C.11 that any failure of this model at low temperatures is relatively minor, and in particular, the prediction from this model of significant length reduction even at temperatures as low as 10°C over geological timescales closely reproduces the natural system behaviour, as discussed further below. We should also note that the comparisons by Spiegel et al. (2007) are subject to the same issues with respect to possible analytical differences as discussed in relation to the Vrolijk et al. (1992) study, above.

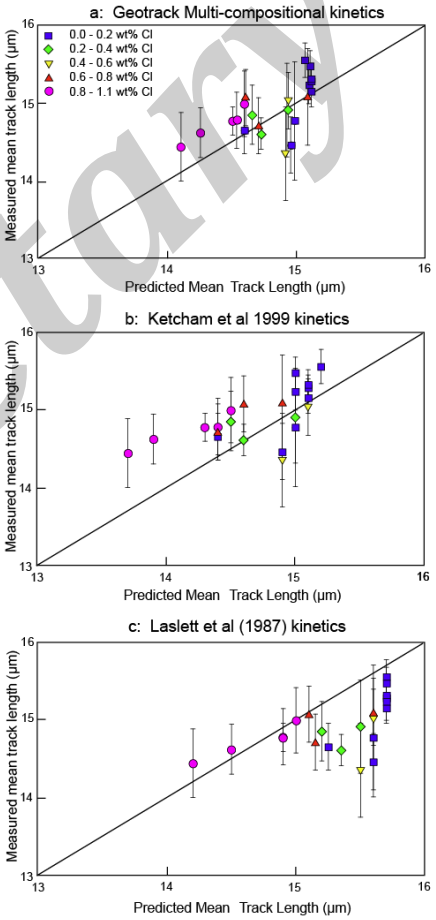

Fig. C.11: Measured mean track lengths in a series of samples designed to provide constraints on low temperature annealing behaviour in geological conditions (from Spiegel et al., 2007), plotted against the values predicted from various annealing models. Apatite compositions are shown, and kinetics appropriate to each composition have been used for the two multi-compositional models in a. and b.. Values predicted using the Geotrack model (a.) show generally excellent agreement overall, while being up to ~0.25 µm less than the measured values at the highest and lowest mean Cl contents. Values predicted using the Ketcham et al. (1999) model (b.) are more consistently around 0.5 µm less than measured values over the entire compositional range, while values predicted using the Laslett et al. (1987) model (c.) are around 0.5 µm longer than the measured values for apatites containing 0.0-0.2 wt% Cl, with the disparity increasing to slightly over 0.5 µm for compositions similar to Durango apatite (~0.4 wt% Cl) and ten decreasing at higher Cl contents, such that around 0.8 wt% Cl the agreement is excellent. While it is clear that multi-compositional models provide better matches to the low temperature constraints, the general level of agreement of values predicted from the Laslett et al. (1987) model should be regarded as impressive, since this model is based purely on extrapolation of laboratory data, with no geological control, yet the agreement is almost as good as for models which directly incorporate geological constraints. This disproves the common misconception that the Laslett et al. (1987) model is too sensitive at low temperatures, as discussed in the text.

C.2 Extracting thermal history information from AFTA data

Basic system response

Understanding the thermal history response of fission tracks in detrital apatites to heating and cooling is fundamental to appreciating how the technique can be applied in practice. The basic system response within a typical sedimentary basin framework, based on principles outlined in Fig. C.5, is illustrated in Fig. C.12. The nature of this response is common to all forms of kinetic models discussed earlier, and is a fundamental property of the AFT system.

.

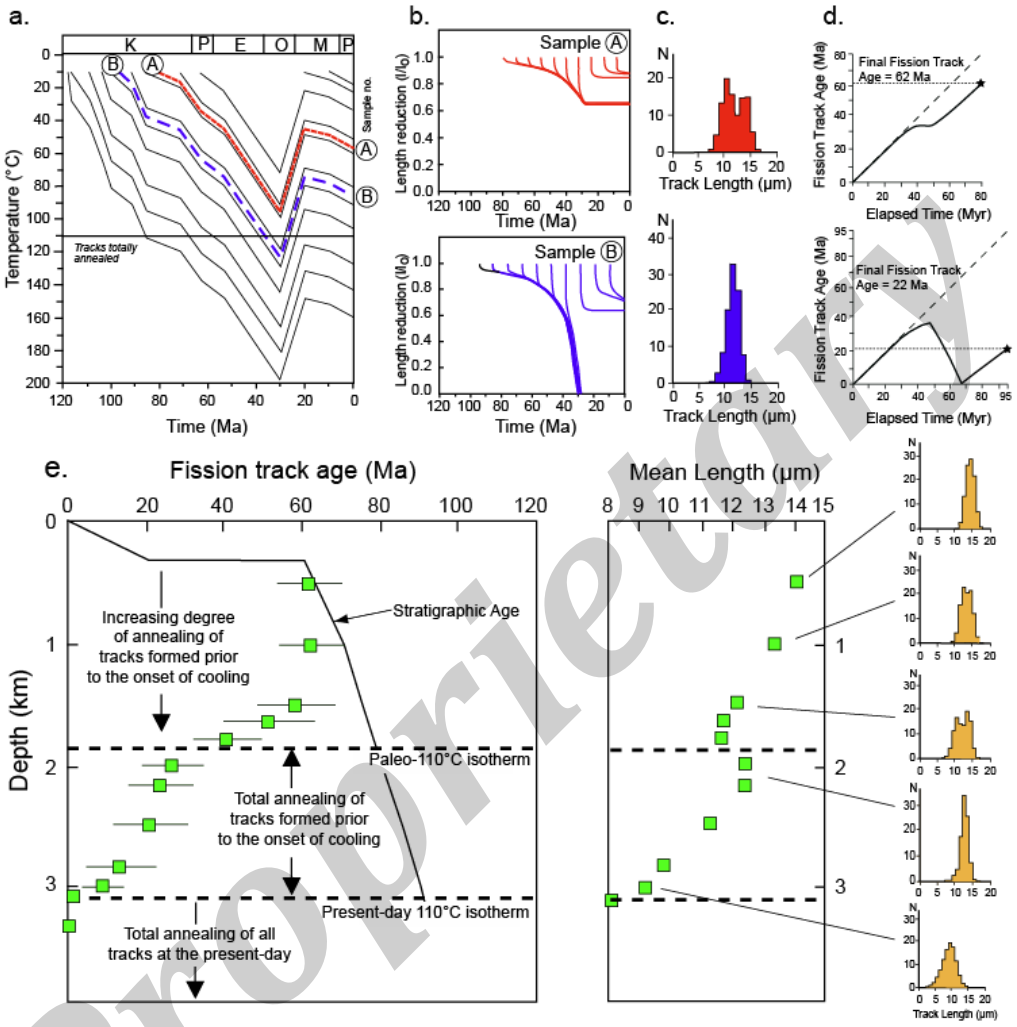

Fig. C.12: Thermal history response of fission tracks in apatite under geological conditions. While this is based on a mono-compositional apatite of Durango composition using the Laslett et al. (1987) model, the nature of this response is common to all forms of kinetic models, and is a fundamental property of the AFT system governed by a fanning Arrhenius plot. **a.** Notional thermal history for a sedimentary sequence that underwent progressive burial through the Cretaceous to middle Cenozoic, followed by cooling due to uplift and erosion commencing at 30 Ma and completed by 20 Ma, with minor reburial from 20 Ma to the present-day. The thermal histories of two samples A. and B. are shown. **b.** Track length shortening trajectories for tracks produced at different times in Samples A and B. As temperature increases, the length of all tracks is progressively reduced, and because temperature dominates over time in the kinetics of annealing, at any time during this phase of the history all but the most recently formed tracks at any given time have the same mean length (although each population of tracks has a finite spread in length). At the point when the maximum temperature is reached and the history changes from heating to cooling, all tracks formed up to that point in time are effectively "frozen" at the length to which they have been reduced. They do not undergo further shortening because annealing rates are much slower at the reduced temperatures now prevailing, and they do not get longer because the annealing process is irreversible. Those tracks formed after the onset of cooling remain longer because of the lower annealing rates at the prevailing lower temperatures. Sample B reached a maximum temperature sufficient to reduce the length of all tracks produced up to that time to zero. At the present day, this sample contains only one track population, formed after the sample cooled to temperatures at which tracks could be retained (~110°C for typical apatite compositions). **c.** Track length distributions for sample A and B resulting from the thermal histories shown in **a.** For sample A, two populations of tracks are present in this sample at the present-day; a shorter population representing tracks formed up until the onset of cooling from the paleo-thermal maximum, and a longer population formed after the onset of cooling. For sample B, the measured track length distribution will reflect the thermal history in the post-cooling period only. **d.** Evolution of fission track age with time resulting from the thermal histories shown in **a.** For sample A, the final measured fission track age will represent the summed contributions from the shorter population of tracks which will contribute a reduced component to the fission track age compared to the time interval over which tracks have been retained, while the contribution to the fission track age of the longer population will be much closer to the time elapsed since the onset of cooling. For sample B, the final fission track age will be determined by the time when the sample began to retain tracks, but moderated by the degree of length reduction of tracks formed during the cooling history. **e.** Predicted variation of fission track parameters with depth for a well section which has undergone a thermal history of the style shown in **a.** Fission track age declines rapidly with increasing depth through the shallower section, as the mean length of the shorter population of tracks (formed up to the onset of cooling) is progressively shortened and the proportion of these tracks that can reach the polished grain surface and be revealed decreases. Similarly, the mean track length reduces due to the decreasing mean length of the shorter population. But as the depth (and temperature of ~110°C) corresponding to total annealing of all tracks formed prior to the onset of cooling is approached, the mean track length begins to increase again, as the shorter population of tracks becomes increasingly difficult to reveal and therefore contributes less to the overall mean for the sample which is increasingly dominated by the longer population of tracks formed after cooling. As the transition from partial to total annealing of tracks formed prior to cooling is crossed at the paleo-isotherm of ~110°C, the mean track length increases abruptly as the sample is now dominated only by longer tracks formed after the onset of cooling. And the fission track age reduction shows a characteristic "break in slope", below which only a single component of tracks is present, with parameters controlled by the history after the onset of cooling. With further increase in depth, both the fission track age and mean track length show progressive reduction to zero at a the present-day ~110°C, although in detail this temperature is controlled by apatite composition and the timescale of heating/burial.

For Sample A in Fig. C.12a, as temperature increases (representing increased burial depth in this example) the length of all tracks is progressively reduced, and because temperature dominates over time in the kinetics of annealing, at any time during this phase of the history all but the most recently formed tracks at any given time have the same mean length (Fig. C.12b) (but remember that each population of tracks has a finite spread in length). At the point when the maximum temperature is reached and the history changes from heating to cooling, all tracks formed up to that point in time are effectively "frozen" at the length to which they have been reduced. They do not undergo further shortening because annealing rates are much slower at the reduced temperatures now prevailing, and they do not get longer because the annealing process is irreversible. Those tracks formed after the onset of cooling remain longer because of the much lower annealing rates at the prevailing lower temperatures.

At the end of the history (i.e. the present day), two populations of tracks are present in Sample A; a shorter population representing tracks formed up until the onset of cooling from the paleo-thermal maximum, and a longer population formed after the onset of cooling, resulting in a bimodal track length distribution (Fig. C.12c). The shorter population of tracks will contribute a reduced component to the fission track age, compared to the time interval over which tracks have been retained, while the contribution to the fission track age of the longer population will be much closer to the time elapsed since the onset of cooling. The final measured fission track age will represent the summed contributions of both components (Fig. C.12d).

Sample B in Fig. C.12a reached a maximum temperature sufficient to reduce the length of all tracks produced up to that time to zero (Fig. C.12b) (i.e. all the radiation damage has been repaired and no etchable tracks remain). At the present day, this sample contains only one track population (Fig. C.12c), formed after the sample cooled to temperatures at which tracks could be retained (~110°C for typical apatite compositions). The track length distribution in this sample will reflect the thermal history in the post-cooling period, while the fission track age will be determined by the time when the sample began to retain tracks, but moderated by the degree of length reduction of tracks formed during the cooling history (Fig. C.12d).

Extending these basic principles through the vertical section results in the variation of fission track age and mean track length with depth shown in Fig. C.12e, which is characteristic of a section which has cooled from higher temperatures. Fission track age declines rapidly with increasing depth through the shallower section, as the mean length of the shorter population of tracks (formed up to the onset of cooling) is progressively shortened and the proportion of these tracks that can reach the polished grain surface to be revealed decreases. Similarly, the mean track length reduces due to the decreasing mean length of the shorter population. But as the depth (and temperature) corresponding to total annealing of all tracks formed prior to the onset of cooling is approached, the mean track length begins to increase again, as the shorter population of tracks becomes increasingly difficult to reveal and therefore contributes less to the overall mean for the sample, which is increasingly dominated by the longer population of tracks formed after cooling. As the transition from partial to total annealing of tracks formed prior to cooling is crossed, the mean track length increases abruptly as the sample is now dominated only by longer tracks formed after the onset of cooling. And the fission track age reduction shows a characteristic "break in slope", below which only a single component of tracks is present, with parameters controlled by the history after the onset of cooling. With further increase in depth, both the fission track age and mean track length show progressive reduction to zero at a temperature controlled by apatite composition and the timescale of heating/burial, similar to the simple situations illustrated in Fig. C.3.

What information is contained in fission track age and length data?

Fig. C.12 illustrates how samples at different depths through a vertical section contain different types of information regarding the underlying thermal history. In samples shallower than the transition from partial to total annealing, which we will refer to as the "paleo-110°C isotherm" (although we stress that in detail this temperature will depend on apatite composition and timescale of heating), the length of the shorter component of the track length distribution is determined by the maximum temperature to which each sample was heated. And the proportion of short to long tracks at any given horizon is determined by the ratio of the time prior to cooling and the time after cooling (moderated by the geometric biases in revealing tracks of different length as described by Laslett et al. 1982). The fission track age is determined by a combination of these factors, and has no fundamental significance in its own right (i.e. the fission track age does not denote a time at which some specific event occurred). In contrast, samples from below the paleo-110°C isotherm contain only tracks formed after cooling, and therefore only provide a minimum estimate of the maximum temperature. But the fission track age in such samples is controlled by the time at which the samples cooled through the paleo-110°C isotherm, again moderated by the track length reduction as a result of the history after the onset of cooling.

To summarise, for the style of history illustrated in Fig. C.12, which is typical of exhumed sedimentary basins, AFTA can provide the following information:

In samples shallower than the paleo-110°C isotherm:

- maximum paleotemperature from the mean length of the shorter component
- onset of cooling from the proportion of short to long tracks
- additional refinement of the above from the degree of fission track age reduction

In samples deeper than the paleo-110°C isotherm:

- minimum estimate of the maximum paleotemperature
- onset of cooling from the combination of fission track age and track lengths

Thus, we obtain different types of thermal history information from different facets of the data at different positions within the section in Fig. C.12. The practical consequence of this is that in order to obtain the maximum amount of information from AFTA it is necessary to analyse a sequence of samples spanning a range of vertical horizons. As a corollary of this, the amount of information that can be obtained from a single sample may be limited.

What information is NOT contained in AFTA data?

Also implicit in Fig. C.12 is the fact that there is a definite limit to the amount of information that can be obtained from AFTA data in such situations. In any sample from a depth shallower than the paleo-110°C isotherm, when the paleo-thermal maximum is reached track populations formed at different times through the history are reduced to more or less the same mean track length (but note that a finite spread in length will be present because of the inherent distribution of track lengths). For this reason, all information on the prior history of such samples has been lost (except for the total duration over which tracks have been retained, and this can be very difficult to reconstruct, as discussed below. Fig. C.13 illustrates how successive heating episodes overprint the effects of earlier episodes, leaving only evidence of the maximum temperature episode and the subsequent history after cooling from the paleo-thermal maximum. Thus **AFTA data are sensitive only to the magnitude of the maximum temperature and the timing of the onset of cooling (in relation to the overall time over which tracks have been retained), and preserve no information on the prior history (except that temperatures must have been lower than at the paleo-thermal maximum).**

Similar considerations apply to scenarios involving continuous cooling histories, as shown in Fig. C.14, which illustrates the insensitivity of such histories to the detailed variation of temperature with time. Perhaps most importantly, the final AFTA parameters are particularly insensitive to the earliest history, which provides such a minor degree of information to the fission track age and track length distribution that huge differences in time produce insignificant changes in the expected parameters which are beyond practical resolution. Thus, in monotonic cooling histories, the data are insensitive to the early history and specifically to the time at which the sample began to retain tracks.

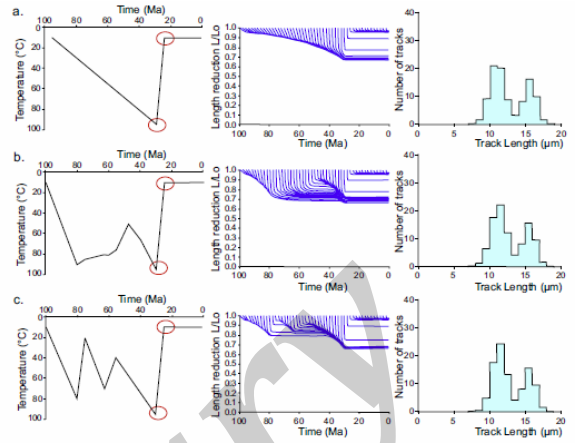

Fig. C 13: Shortening trajectories (centre) for tracks produced at different times through three thermal history scenarios (left) representing increasing levels of complexity from a. through c. The resulting track length distributions are also shown (right). Despite the obvious differences in the thermal histories, the resulting track length distributions are effectively identical because the time and magnitude of maximum temperatures and the rate of cooling from maximum paleotemperatures are the same for each history (circled points on the thermal histories). This outcome reflects the fundamental kinetics of the AFT system such that the data are sensitive only to the magnitude of the maximum temperature and the timing of the onset of cooling (in relation to the overall time over which tracks have been retained), and preserve no information on the prior history (except that temperatures must have been lower than at the paleo-thermal maximum). Thus, successive heating episodes overprint the effects of earlier episodes, leaving only evidence of the maximum temperature episode and the subsequent history after cooling from the paleo-thermal maximum.. by the evolution of track lengths with time for history. It is therefore not possible to discriminate between these three scenarios from apatite fission track data.

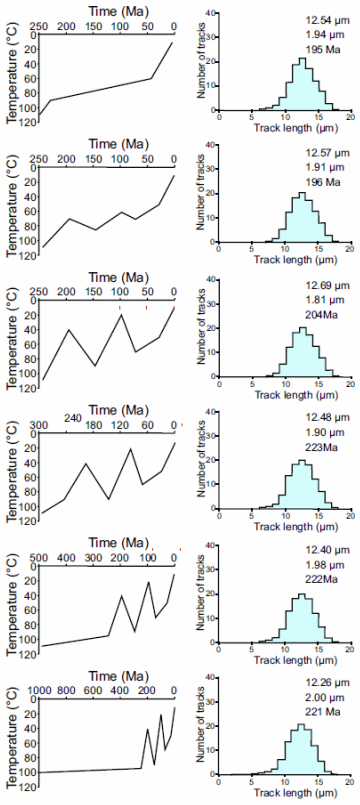

Fig. C.14: Predicted track length distributions (also listing the predicted mean track length, standard deviation of the length distribution and apatite fission track age) for a series of cooling histories of increasing complexity. The fission track parameters resulting from these histories are indistinguishable, despite the time of cooling below 110°C varying from 250 Ma to 1000 Ma, and for histories

ranging from progressive cooling to various more complex heating and cooling histories. The final AFTA parameters are particularly insensitive to the earliest history, which provides such a minor degree of information to the fission track age and track length distribution that huge differences in time produce insignificant changes in the expected parameters which are beyond practical resolution. Predictions based on a mono-compositional apatite of Durango composition using the Laslett et al. (1987) model.

Note that Figs. C.12, C.13 and C.14 are constructed for mono-compositional apatites, but the principles involved are equally applicable to apatites containing a range of annealing properties (due to differing Cl contents). As illustrated in Fig. C.9, AFTA data from the Fresne-1 well in the Taranaki Basin of New Zealand (Crowhurst et al. 2002) provides a multi-compositional counterpart involving real data for comparison with the notional mono-compositional data in Fig. C.10.

Practical implementation

Because of the high degree of redundancy in the data (i.e. many histories result in the same measured age and length parameters, Figs. C.13, C.14), extraction of explicit thermal history solutions directly from apatite fission track data is not possible. Instead, the problem is approached by forward modelling the parameters expected from a range of specified thermal histories and defining the range of conditions that provide predictions that are consistent with the measured data.

Our approach is designed primarily for application to sedimentary basins, and takes account of the fact that sedimentary horizons are deposited at the surface and then buried/heated to some maximum depth/temperature, after which they may be exhumed and cooled. By modelling expected AFTA parameters resulting from a range of possible thermal histories, we can define the range of values of maximum paleotemperature and the onset of cooling giving predictions which match the measured data within 95% confidence limits, using likelihood theory similar to that described by Gallagher (1995). The basic principles involved are illustrated in Fig. C.15 for a mono-compositional apatite, while Fig. C.16 illustrates the extension of these principles to multi-compositional data.

It is important to stress that no attempt is made to define the whole thermal history, because the post-depositional history prior to the onset of cooling is overprinted by the paleo-thermal maximum (Fig. C.12). For this reason we focus on determining those aspects of the thermal history that directly control the measured AFTA parameters, viz. the maximum paleotemperature and the time at which cooling from the paleo-thermal maximum began. Additional episodes of heating and cooling following the onset of cooling from the paleo-thermal maximum can often be resolved, as discussed in more detail in Section C.3.

The episodic heating and cooling approach is designed specifically for application to sedimentary basins, but we also believe that it is relevant to many (if not all) basement terrains, and such an approach is essential in basement regions where sedimentary outliers occur, revealing earlier cycles of exhumation, burial and re-exhumation (e.g. Green and Duddy, 2006; 2007).

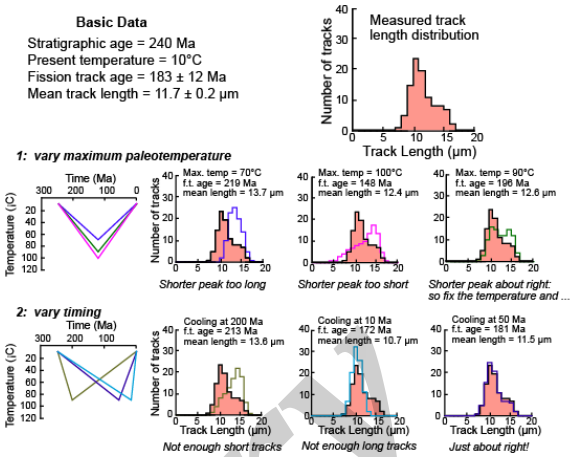

Fig. C.15: Principles of AFT interpretation illustrated for a mono-compositional apatite, showing how a thermal history solution can be extracted from measured AFTA parameters (fission track age, mean track length and track length distribution). For samples of sedimentary rock it is necessary to know the stratigraphic age and present temperature of the sample. In principle, the surface temperature at the time of deposition is also required, but because the maximum temperature is the major control on track length (e.g. Figs. C.12 to C.14), the influence of the depositional temperature is minimised once the sediment is heated above ~50°C. By predicting the AFTA parameters for various thermal history scenarios we can define the best-fit thermal history. As a first step, we assume that cooling from the maximum paleotemperature occurred at the midpoint of the history (120 Ma in this case). By varying the maximum temperature and comparing measured and predicted parameters, we find a good match with the shorter population of tracks in the measured track length distribution at a maximum paleotemperature of 90°C. But the predicted track length distribution contains too many long tracks. A good match between the predicted and measured track length distributions, as well as the fission track age, is achieved with cooling commencing at 50 Ma. while keeping the maximum temperature constant at 90°C. Note that no attempt is made to define the whole thermal history, because the history prior to the onset of cooling is overprinted by the thermal maximum. Note also that by itself, the measured fission track age of 183 ± 12 Ma provides no information on the time of cooling, which only comes from kinetic modelling of the details of the track length distribution together with the fission track age. Predictions based on a mono-compositional apatite of Durango composition using the Laslett et al. (1987) model.

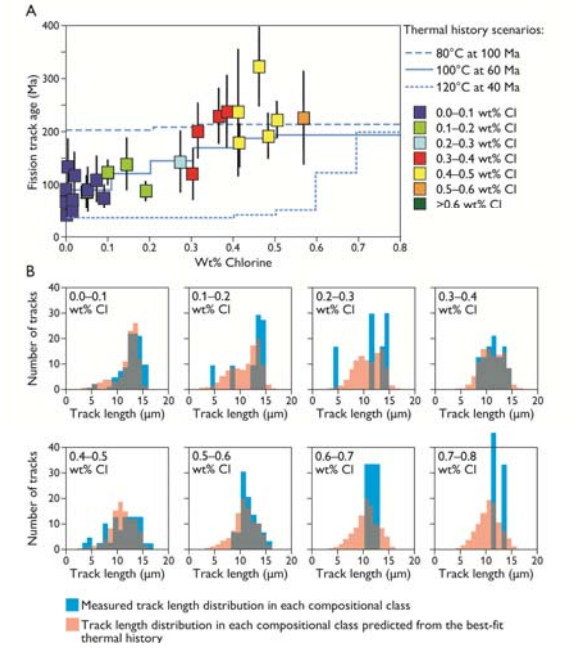

Fig. C.16: AFT interpretation methodology for a multi-compositional apatite. The same basic information and interpretation strategy as described in Fig. C.15 is used for samples which contain apatite of different compositions, but supplemented by the wt% chlorine of each apatite grain (measured by electron microprobe) in which a fission track age or track length is measured. Fission track ages and track lengths are grouped according to the chlorine content into 0.1 wt% Cl intervals and a multi-compositional annealing model is used which takes specific account of the influence of wt% Cl on annealing rates. The

matching procedure is the same as for a single composition, but now involves the simultaneous matching of fission track age and the details of the track length distribution in all compositional groups present in the sample. In the example, 8 groups are present containing between 0 and 0.8 wt% Cl, and the best-fit match to the data is achieved for cooling from a maximum temperature of 100°C beginning at 60 Ma (real data in a Permian sandstone outcrop sample from NE England).

A multi-compositional annealing model is used which takes specific account of the influence of wt% Cl on annealing rates. This model consists of a series of parallel kinetic equations, each taking the form of a linear fanning Arrhenius plot with non-zero intercept (Laslett et al., 1987; Crowley et al, 1991; Ketcham et al., 1999), with coefficients which vary systematically with wt% Cl. In many respects the Geotrack multi-compositional annealing model is similar to that of Ketcham et al. (1999), and gives similar predictions (cf Fig. C.10).

Wherever possible, AFTA data are integrated with data from other paleo-thermal indicators such as vitrinite reflectance, and/or indicators of burial such as sonic velocity (discussed later). Such data provide an independent check on the interpretation of the AFTA data, and ensure that the resulting thermal histories and the information derived from them are not affected by artefacts of any individual technique.

One of the advantages of this approach is that determination of maximum paleotemperatures from AFTA data in a series of samples over a range of depths or elevations allows definition of the variation of paleotemperatures with depth, which in turn provides unique insights into the underlying mechanisms of heating and cooling, as described in a later section.

Summary comments.-

In all approaches which involve extracting quantitative thermal history constraints from apatite fission track data, it should be appreciated that the resulting thermal history solution will only ever be an approximation to the true underlying history. Whether monotonic cooling histories or episodic heating and cooling is employed, for any but the simplest of histories, factors such as the natural spread in the track length distribution, which increases as tracks are progressively shortened (Green et al., 1986), plus the high level of redundancy in the data resulting from the basic nature of the system response, as discussed earlier, impose fundamental limits to the detail that can be resolved.

These factors must be borne in mind in considering information derived from AFT data in individual samples. We suggest that failure to fully appreciate the limitations of the method lies behind many perceived problems with published AFT studies (e.g. Gunnel, 2000), and in many cases too much is expected from the technique. We suggest that it is when attention is focussed on the unique information that can be obtained that the power of the technique becomes apparent.

C.3 Practical issues in interpreting and understanding AFTA data

The meaning of a fission track age

Fission track ages from crustal sections are often discussed in terms of a zonation of ages (e.g. Naeser et al., 1989) with ages being unaffected at shallow depths (“Zone of No Annealing”, <70°C), while at depths greater than ~3 - 4 km (temperatures in excess of ~125°C), no tracks are retained (“Total Annealing Zone”). Between these two extremes, fission track ages are progressively reduced to zero through a “Partial Annealing Zone” or “PAZ”. While this zonation provided a simple conceptual basis for early studies based on ages alone, the combination of borehole data (Gleadow and Duddy, 1981) and laboratory experiments (Green, 1988) showed that fission track age and length reduction proceed even at temperatures below 70°C, albeit more slowly than at higher temperatures. This can be seen most easily in confined track length data due to the higher precision of these measurements compared to fission track ages (Fig. C.3).

For this reason, a measured fission track age only rarely indicates the time over which tracks have been retained in an apatite grain. In the same way, a fission track age rarely reflects a “cooling age”, and we recommend that this term should not be used in any circumstances. In slowly cooled terrains, radiometric ages are often referenced to a “closure temperature”, below which the daughter product (in our case, a fission track) is effectively retained. However, given the lack of stability of fission tracks in apatite even at low temperatures, this concept is of dubious validity for fission track ages in apatite, and it is not possible to literally relate a fission track age to a specific point on a cooling path. Instead, **an apatite fission track age should be regarded as an integrated measure of the balance between the production of tracks by spontaneous fission and the reduction in track density due to the reduction in track length which results from the thermal history.**

Only in samples which have cooled extremely rapidly to temperatures less than 50°C and subsequently remained at such temperatures will the fission track age be close to the time over which the sample has been cool enough to retain tracks. Experience has shown that such situations are rare. More commonly, the fission track age and length data must be assessed in tandem, using the quantitative modelling approach described earlier in order to extract information on the timing (and magnitude) of cooling events from the data.

Long term residence in the Partial Annealing Zone vs heating and cooling

It is a common fallacy that the presence of an exhumed partial annealing zone, as identified for

example by a break in slope in the variation of fission track age with depth (cf. Figs. C.3, C.9) represents a prolonged period of residence in the Partial Annealing Zone prior to exhumation. Consideration of Fig. C.12 shows that this is not necessary, as this type of data is easily produced by heating (e.g. by burial) of the sequence to temperatures characterising the PAZ followed immediately by rapid subsequent cooling/exhumation. This misunderstanding arises, in part, because of the common adoption of monotonic cooling histories for explaining apatite fission track data, which is discussed in more detail below.

"Boomerang plots"

Green (1986) showed that in a sequence of rocks from the NW of England that have undergone a single dominant episode of heating and subsequent cooling, with individual samples reaching different maximum temperatures prior to the onset of cooling, the relationship between mean confined track length and fission track age showed a systematic variation defining a "boomerang-shaped" trend (Fig. C.17). Samples that have undergone only minor thermal disturbance have old ages with relatively long mean track lengths, while samples in which all fission tracks were totally annealed prior to the onset of cooling give much younger fission track ages ("reset ages"), also characterised by long (~14 μm) mean lengths. Between these two extremes, as the fission track age decreases (representing increasing maximum paleotemperatures prior to the onset of cooling) the mean track length decreases as the partially annealed tracks are progressively shortened. This continues until the final stages of age reduction, when the partially annealed tracks become so short that their contribution to the mean length is diminished and the mean length increase with further reduction in fission track age, trending upwards towards the long mean length characterising the reset ages. The variation in Fig. C.17 is analogous to that illustrated in Fig. C.10, except that samples from different depths/temperatures return to the surface at low temperature after the onset of cooling, and thus each sample contains a similar population of long tracks, in addition to the shorter population which has been annealed to differing degrees in different samples reflecting different maximum paleotemperatures prior to the onset of cooling.

Returning to the question of the meaning of a fission track age, from above, Fig. C.17 illustrates the way in which partially reset fission track ages reflect the degree of shortening of those tracks formed prior to the onset of cooling. Only those samples in which all tracks were totally annealed give fission track ages around 60 Ma, but ALL samples underwent cooling at this time. The measured fission track age in any other sample provides no direct indication of the timing of any event in its own right.

Gallagher and Brown (1997) emphasised the usefulness of this type of plot in considering the implications of regional AFT datasets, albeit in the context of monotonic cooling. But in many regions, age vs. length data show a very different type of trend to the simple pattern reported by Green (1986). For example, results from Norway (Rohrman et al. 1995) show an almost opposite relationship to the classic "boomerang" trend, while data from Africa and Brazil (Gallagher and Brown. 1999a, 1999b) show wide dispersion with only a slight tendency towards longest lengths associated with the youngest ages. Compared to the simple situation in NW England where a single dominant heating/cooling episode has produced a well-defined trend, non-boomerang style relationships imply a much more complex history, most likely involving a series of paleo-thermal episodes, each of which may vary in magnitude across the region. Therefore, such plots should be interpreted with care, and should always be considered together with the systematic change in the form of the track length distribution through the plot, which was central to the original description by Green (1986).

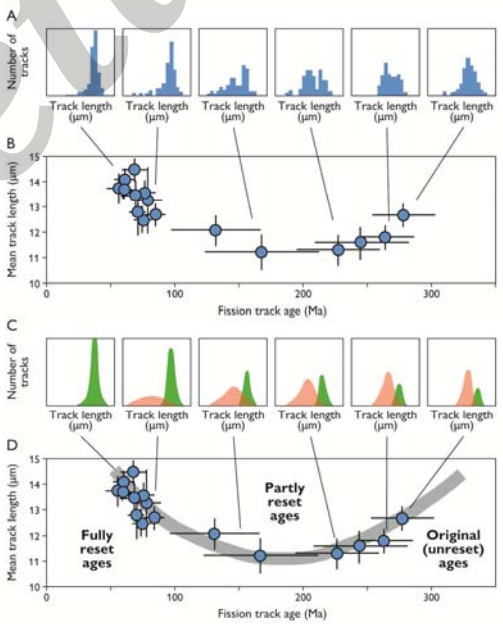

Fig. C.17: Boomerang plot: relationship between mean track length and fission track age for a suite of outcrop samples which have undergone cooling from different maximum paleotemperature at the same time (Green (1986). Samples that have experienced low maximum temperatures have old ages with relatively long mean track lengths, while samples in which all fission tracks were totally annealed prior to the onset of cooling give much younger fission track ages ("reset ages"), also characterised by long (~14 μm) mean lengths. Between these two extremes, as the fission track age decreases (representing increasing maximum paleotemperatures prior to the onset of cooling) the mean track length decreases as the partially annealed tracks are progressively shortened. This continues until the final stages of age reduction, when the partially annealed tracks become so short that their contribution to the mean length is diminished and the mean length increase with further reduction in fission track age, trending upwards towards the long mean length characterising the reset ages. This dataset can be considered analogous to the situation illustrated in Fig. C.12, but with all samples cooling to low (near surface) temperatures, such that each contains a population of long tracks formed after cooling.

Monotonic cooling vs episodic heating and cooling

While clearly not applicable to sedimentary basins, many thermochronological studies are carried out

within a framework involving monotonic cooling from above ~110°C to surface temperatures. Such approaches are routinely applied to basement terrains but even in such regions the presence of the merest veneer of sedimentary cover means that the underlying basement was at the surface when that cover was deposited. Failure to understand this issue can result in quite erroneous interpretations (e.g. Persano et al., 2006; Brown, 2007; Gibson, 2007; Green and Duddy, 2007). While episodic heating and cooling is clearly more realistic in sedimentary basins, as witnessed by the common occurrence of unconformities in sedimentary sequences, we suggest that such histories may also be quite reasonable for many basement terrains. This is clearly appropriate where sedimentary outliers are present, but we see no reason why it should not also be true in areas devoid of present-day cover, which could simply indicate that the former cover has been totally stripped.

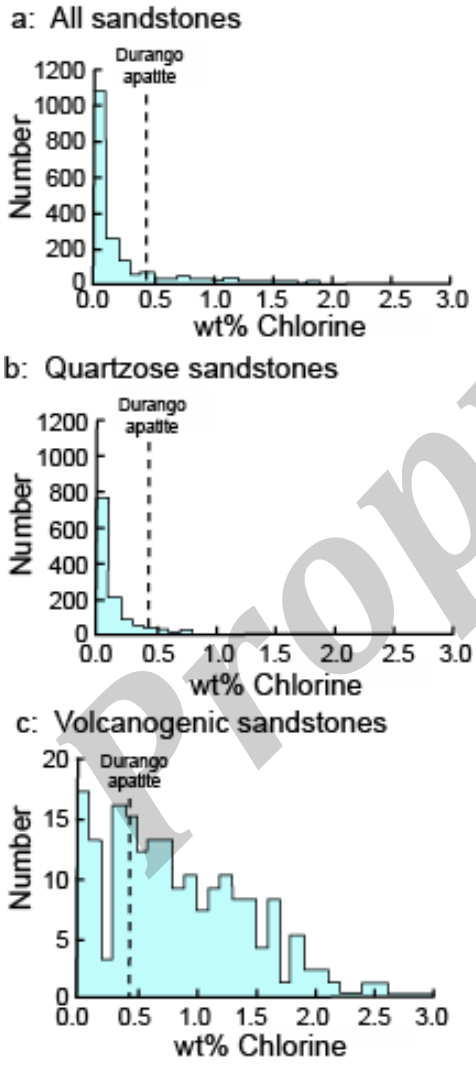

Fig. C.18: Typical distributions of wt% Cl in apatites from different sources. **a:** Histogram of Cl contents (wt%) in over 1750 apatite grains from over 100 samples of various sedimentary and igneous rocks. Most samples give Cl contents below ~0.5 wt %, while those apatites giving higher Cl contents are characteristic of volcanogenic sandstones and basic igneous sources. **b.** Histogram of Cl contents (wt%) in 1168 apatite grains from 61 samples which can loosely be characterised as "normal quartzo-feldspathic sandstone". The distribution is similar to that in the upper figure, except for a lower number of grains with Cl contents greater than ~1%. **c.** Histogram of Cl contents (wt%) in 188 apatite grains from 15 samples of volcanogenic sandstone. The distribution is much flatter than the other two, with a much higher proportion of Cl-rich grains.

The impact of composition on thermal history interpretation of AFTA data

Natural apatites essentially have the composition $Ca_5(PO_4)_3(F,OH,Cl)$. Most common detrital and accessory apatites are predominantly fluor-apatites, but come contain appreciable amounts of chlorine (Fig. C.18). In most quartzo-feldspathic sandstones, the majority of grains contain between 0 and 0.1 wt% Cl, while a smaller number of grains give values up to ~0.5 wt% Cl and occasional grains contain up to 1 wt% Cl and above (Fig. C.18a). In contrast, volcanogenic sandstones typically contain apatites showing a much broader spread of Cl contents up to 2 or even 3 wt% and beyond (Fig. C.18b). Cl contents in granitic basement samples and silicic high-level intrusives are typically much more dominated by compositions close to end-member Fluorapatite (Fig. C.18c) while apatites from Gabbroic and other basic intrusive rock types may contain appreciable amounts of Cl, although many exceptions occur to these general rules.

As discussed earlier, the amount of chlorine in the apatite lattice exerts a subtle control on fission track annealing rates, which is typically most pronounced in the temperature range 90 to 120°C (Figs. C.9, C.10). In samples heated to such temperatures, individual apatite grains may show a significant spread in the degree of annealing (i.e. length reduction and fission track age reduction). Such within-sample variation can be very useful in identifying samples exposed to paleotemperatures in this range.

Ignoring the effects of compositional variation can lead to major errors in interpretation, particularly if analytical procedures are not designed to take such effects into account. To illustrate the potential problems that can arise, Fig. C.19a shows a dataset in which grains were selected in a continuous transect across the grain mount, with a thermal history solution extracted by making due allowance for the variation of fission track age and length with wt% Cl. Fig. C.19b illustrates the result of a biassed analysis in which fission track ages were measured only in high wt% Cl grains which contain high track densities and which could represent a favourable "target" for counting, while track lengths have been measured in the more common (and more sensitive) apatites containing lower amounts of chlorine. In this case, the thermal history solution extracted from the biassed data results in a wildly inaccurate interpretation (Fig. C.19b).

Some workers prefer to use the size of etch pits as a kinetic parameter for resolving differences in annealing within samples (Burtner et al. 1994). But as discussed earlier, etch pit dimensions provide only a very poor indicator of annealing sensitivity (Fig. C.8), and due to the relatively small range of etch pit sizes for most common apatites this approach lacks the resolution that is possible using chlorine content.

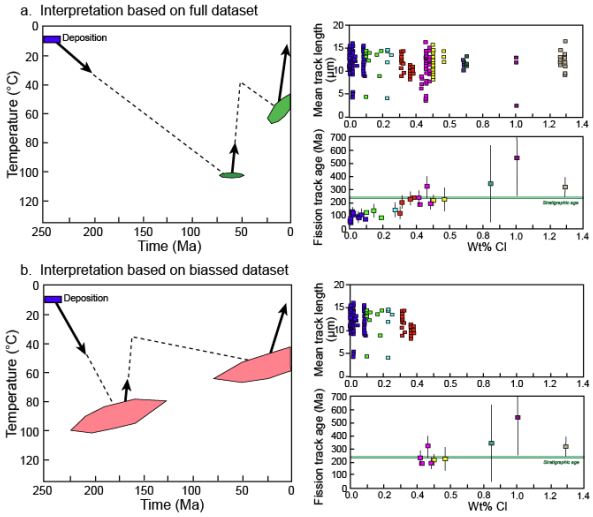

Fig. C.19: Thermal history solutions extracted from AFTA data from the same Triassic outcrop sample. In **a.**, complete allowance made for the variation of fission track age and track length with apatite chlorine content. In **b.**, the solution is based on track length data from only the most abundant (low wt% Cl) grains while fission track ages are measured only in the higher wt% Cl grains. Such a situation could easily arise if ages are only measured in grains containing high track densities, without making due allowance for the influence of wt% Cl. The solution in this case is very different from the correct solution (a.), illustrating the problems that can arise if compositional effects are not correctly taken into account.

In addition, use of etch pit sizes is extremely demanding of etching procedures, which must be reproducible to the standards employed in the original calibration experiments (Carslon et al. 1999). And in borehole studies involving conditions where fission tracks in some apatites are totally annealed, measurement of etch-pit sizes in these grains is clearly not possible.

Therefore, to ensure accurate thermal history interpretations from AFTA it is an essential step in data collection that grains should be analysed without reference to track density, Cl content should be measured in every grain for which either fission track age or track length measurements are made, and the data should be assessed in terms of their variation with wt% Cl, as illustrated in Fig. C.16.

Influence of tracks inherited from sediment source terrains

An apatite in which the fission track age is older than the depositional age of the host sedimentary rock clearly retains tracks that were formed in the sediment provenance terrain, prior to deposition. The effect of such tracks is often posed as a potential problem for AFTA. However, this rarely poses practical problems, and can sometimes prove advantageous.

The contribution to the measured fission track age and the length distribution made by these "inherited tracks" will be characteristic of the thermal history of the sediment provenance terrains. The influence of such tracks on the ability to extract information on the post-depositional thermal history of a sedimentary rock from AFTA data will depend essentially on the relative duration and severity of heating during the pre-depositional and post-depositional history. For example, in apatites derived from an ancient basement terrain and deposited in Neogene sedimentary rocks, in which only a small proportion of tracks may have formed after deposition of the host sediment, AFTA data will be dominated by tracks formed prior to deposition. In samples of this nature which have been heated to only moderate temperatures after deposition (say <60°C), it may not be possible to resolve the effects of this heating from the influence of the pre-depositional history. But as the severity of post-depositional annealing increases (i.e. with increasing maximum post-depositional temperature), the effects of the pre-depositional history are progressively "overprinted", and the AFTA parameters become dominated by the post-depositional history.

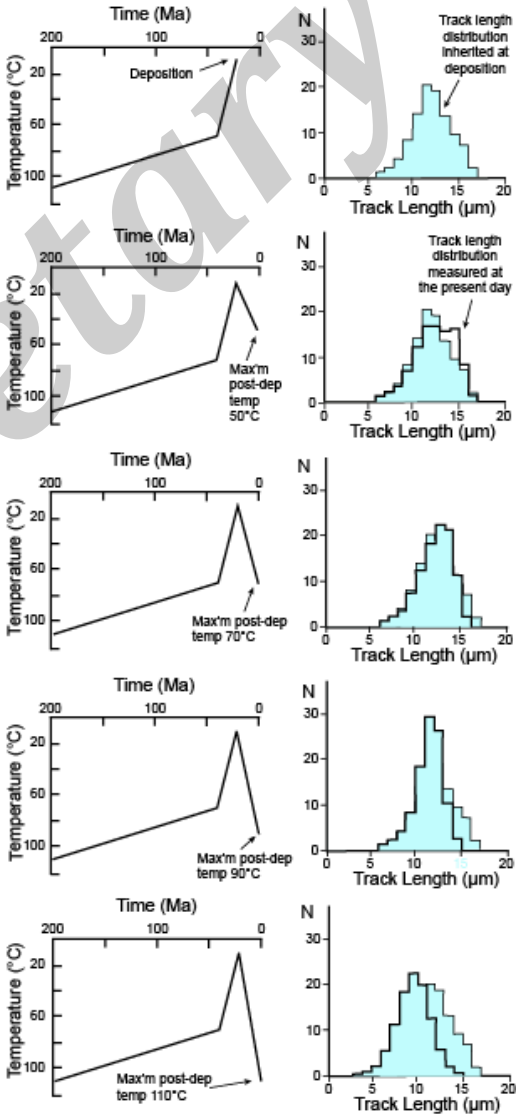

Fig. C.20: Progressive overprinting of inherited tracks by post-depositional heating. For samples containing a mixture of tracks formed pre- and post-deposition, only the shortest tracks retain a provenance signature. In the Figure, as the post-depositional temperature increases, the pre-depositional track length distribution (in outline) is progressively overprinted from longer lengths to shorter lengths, as the latter have experienced higher pre-depositional temperatures, and require even higher post-depositional temperatures to be further shortened. Once the effects of post-depositional annealing begin to dominate over the pre-depositional history at temperatures above about 90°C in the example, the resulting AFTA data can provide reliable constraints on the post-depositional history.

Fig. C.20 illustrates how in samples containing a mixture of tracks formed pre- and post-deposition, only the shortest tracks retain a provenance signature. The pre-depositional track length distribution is progressively overprinted from longer lengths to shorter lengths, as the latter have experienced higher pre-depositional temperatures, and require even higher post-depositional temperatures to be further shortened. This is a direct consequence of the principle of "equivalent time", discussed earlier. Once the effects of post-depositional annealing begin to dominate over the pre-depositional history, the resulting AFTA data can provide reliable constraints on the post-depositional history. As heating becomes sufficiently severe, the fission track age will be reduced to a value less than the depositional age, and the age data will also become dominated by the effects of the post-depositional history.

In general, inherited tracks pose practical problems in extracting information on the post-depositional thermal history only for samples in which the majority of tracks were formed prior to deposition, perhaps in a Neogene sediment in which apatites were derived from a stable Paleozoic shield with fission track ages of ~400 Myr or more, or in samples that have experienced only very minor post-depositional heating (say <50°C). In such cases, often the only information on the post-depositional thermal history that can be obtained from AFTA might be that the sample has not been heated above say 90°C at any time after deposition.

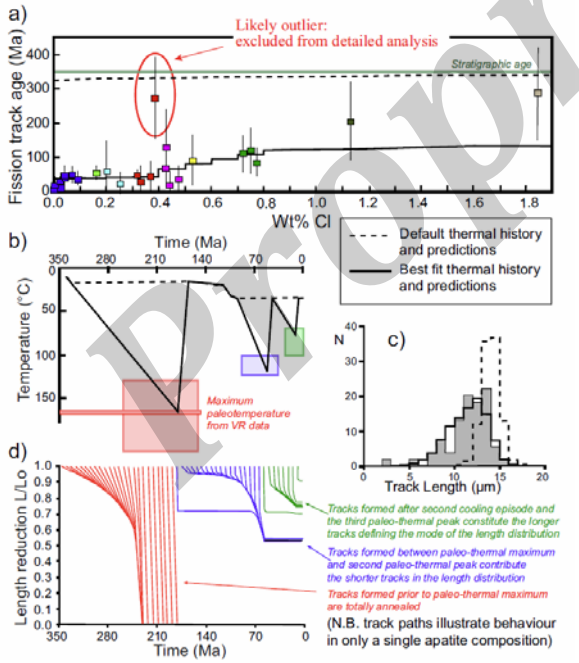

Fig. C.21: Resolution of multiple episodes from AFTA data in a single sample is possible where the events are sufficiently separated in temperature ands time. In this example, based on AFTA data (**a.**) in combination with vitrinite reflectance results in a sample from the Dodo Canyon K-03 well in the Mackenzie valley, North West Territories, Canada, three thermal episodes are resolved (**b.**). Predicted track shortening trajectories for the three-episode history (**c.**) shows how all tracks are erased in the earliest episode (prior to 180 Ma), a population of shorter tracks are produced at the paleo-thermal peak in the second episode and a longer population of tracks (which constitutes the main mode of the distribution) is produced in the final episode. These tracks are still shorter than expected at surface temperatures, which allows resolution of this final episode (as illustrated by comparing the measured track length distribution in d. with the distribution predicted by the default thermal history).

Resolving multiple paleo-thermal episodes in individual samples

In samples which have undergone two episodes of heating and cooling, AFTA data can often provide constraints on both episodes, provided that the magnitude and timing of the paleo-thermal maximum and subsequent peak are sufficiently separated (Fig. C.21). In rare cases (e.g. Green et al. 2001a; Turner et al. 2008), three discrete episodes can be resolved in data from a single sample. This is most likely when the earliest event involves a maximum paleotemperature sufficient to totally anneal all tracks (typically >110°C), followed by a subsequent peak around 90 to 100°C which reduces tracks to a mean length around 10 microns, and then cooling to low temperature is followed by re-heating to around 70°C sufficient to reduce lengths of tracks formed after the second event to around 12-13 microns. In such circumstances, integration of AFTA data with results from other techniques (particularly vitrinite reflectance) can provide corroborative evidence of the earliest, maximum temperature, episode, as discussed in the next section.

C.4 Integration with other methods

Introduction

Significant advantages can be obtained by combining AFTA data with results from other methods. One reason for this is the inherent redundancy in the AFTA method, in the sense that a large number of thermal histories can result in very similar AFTA parameters, due to the dominance of maximum paleotemperatures in the kinetics of annealing (Figs. C.13, C.14). In addition, the natural spread in the length distribution imposes limits on the recognition of low temperature events, and can cause problems in resolving complex histories involving multiple episodes. Integration with independent techniques not only provides corroboration of conclusions derived from AFTA, but can also refine the range of thermal history solutions defined from AFTA alone and provide a coherent thermal history framework. Here we discuss some of the techniques that have been used in tandem with AFTA and discuss the benefits that can be obtained.

Geological data

In order to ensure that the information obtained from AFTA is meaningful, it is essential that interpretation is carried out within the context of the known geological setting. AFTA data in isolation can often be explained by such a wide range of histories that unless the depositional age of a sample is specified (in as much detail as possible), together with the present-day temperature, no meaningful thermal history information can be obtained. By specifying the time at which the apatite was at the surface, and the present temperature, these fundamental constraints on two points of the temperature-time

history provide a framework within which the post-depositional history of the host sedimentary rock can be defined.

To provide the required geological context we define a "Default Thermal History", which is that part of the history which can be defined on the basis of the available geological evidence (or alternatively - the history that would be appropriate if no paleo-thermal events have affected the sample). This can be particularly important for samples from sedimentary sections containing a number of unconformities separating thin units of different ages, as the presence of the overlying section shows that the deeper units were close to the surface when the shallower units were deposited.

Vitrinite reflectance

Vitrinite reflectance (VR), based on the increase in reflectivity of the organic maceral vitrinite (a key constituent of coal) with temperature, is the standard measure of organic maturity for hydrocarbon exploration (e.g. Tissot and Welte, 1984). The kinetics of this process are well understood (Burnham and Sweeney, 1989), and are very similar to those of fission track annealing in apatite (Duddy et al, 1994, 1998), with VR values of 0.65% to 0.7% corresponding to total annealing of fission tracks in typical apatites (Duddy et al. 1994). These factors make VR an ideal complement to AFTA data applied to sedimentary sequences, as demonstrated in a wide range of studies (e.g. Duddy, 1997; Green et al. 2004; Japsen et al. 2005, 2007a; Turner et al. 2008).

In particular, VR provides independent determination of maximum post-depositional paleotemperatures, which can provide support for those indicated by AFTA. This is important, because data from either technique alone might be viewed with suspicion, but when two independent techniques provide consistent paleotemperatures the conclusions can be regarded as reliable. A classic example is provided by studies of wells on the East Midlands Shelf in the Southern North Sea of the UK, where early VR data were disregarded as indicating amounts of eroded section which were "not consistent with the known geological evolution" (Cope 1986). Subsequent application of AFTA to wells from this region (Green, 1989) confirmed the heating suggested by the VR data, showing that the section in these wells had indeed been more deeply buried and then exhumed.

Integration of VR data from fine grained units with AFTA data from sandstones also allows determination of paleotemperatures over a wider range of depths than possible from AFTA alone. The combination of both techniques can provide much tighter control on paleogeothermal gradients and amounts of removed section than would be possible from either technique on its own. In addition, integration of VR with AFTA data can be of great assistance in confirming earlier events soon after deposition, which may not be confidently defined from AFTA alone (e.g. Green et al. 2004).

Despite the importance of VR data to the oil exploration industry and its widespread routine application, in recent years it has become apparent that VR data generated by different analysts are not equivalent (see discussion in Green et al. 2002). We find a high degree of consistency between thermal history interpretations from AFTA and VR data generated using an approach involving measurement of maximum reflectance under oil ($R_o$max) in polished thick sections (Cook, 1982). In this approach, which is recommended by the International Commission on Organic and Coal Petrography (www.iccop.org), identification of the indigenous vitrinite population is made on textural grounds. This allows independent assessment of the possible presence of reworked vitrinite populations from petrographic evidence, as well as allowing identification of caved material in sub-surface samples. Alternation between reflectance and fluorescence modes allows checking for associated fluorescing liptinite, bitumen impregnation, or the presence, intensity, and source of oil-cut which may affect the reading. An alternative approach, often encountered in hydrocarbon industry reports, involves measurements of random reflectance ($R_o$rand) in strewn slides of organic concentrates, with the indigenous vitrinite population often identified only after the analysis is complete by inspection of histograms of measurements and separation into perceived sub-populations. In our experience, this approach can lead to serious errors in determining maturity levels (usually resulting in underestimation). Integration of AFTA with VR data allows such cases to be readily identified.

A key factor in interpreting VR data is the possible suppression of reflectance levels, as often observed for example in H-rich source-rock horizons (e.g. Wilkins et al., 1992). Suppression can often be recognised by local departures from an overall trend, but where few data are available this is less straightforward. This can be particularly problematical where VR data (and other organic maturity indicators) are only measured in source rock horizons. Again, integration with AFTA allows detection of anomalous vitrinite reflectance values.

Data from a range of additional organic-based methods for assessing maturity levels, such as biomarker reactions (e.g. MacKenzie and McKenzie, 1983), Spore Colour Index (Fisher et al. 1980) or Rock Eval Tmax (Tissot and Welte, 1978), can be converted to equivalent VR values which can also be integrated with AFTA data. While biomarker reactions show promise as quantitative thermal indicators, expense and difficulties with elucidating the true kinetic descriptions have so far limited their usefulness, while SCI values are less commonly available and Rock Eval Tmax values are subject to variability as a result of variation in organic facies.

While these methods and others have some practical limitations all may be used, where available, to complement VR and AFTA data.

Fluid inclusions

Fluid inclusions are micron-sized vacuoles of liquid or gas which have been trapped within crystal imperfections during mineral growth. Univariant phase transitions observed during heating and freezing of fluid inclusions in the laboratory can yield valuable information concerning the composition and density of the fluids trapped within the inclusions and the temperature and pressure conditions at which the mineral precipitated. Taking advantage of the independent constraint on maximum paleotemperature provided from fluid inclusions, AFTA has been used to estimate the duration of heating related to diagenesis (Duddy et al., 1998; O'Brien et al., 1996; Parnell et al. 2005) and impact events (Parnell et al. 2007). Integration of AFTA data with information from fluid inclusions has also defined the timing of episodes of hot fluid circulation (Parnell et al. 1999) and has clarified issues related to the timing of hydrocarbon generation (Mark et al. 2008) in the UK West of Shetland region.

Sonic velocities

The progressive compaction of sediments with increasing burial has been widely used as the basis for estimating former burial depths in exhumed basins (e.g. Marie, 1975; Bulat and Stoker, 1987; Hillis, 1995; Japsen, 2000). Comparison of compaction proxies such as sonic velocity in an exhumed formation with a reference curve defining the expected variation with depth in sequences at maximum burial depth provides an indication of the amount of net exhumation. Selection of appropriate reference curves has been problematical in some areas, leading to erroneous conclusions regarding the extent and magnitude of exhumation (Cope, 1986; Green et al. 2001b). More rigourous definition of the necessary reference curves in recent years (Japsen et al. 2007b) allows more reliable estimation of former burial depths, and integration of such data with constraints from AFTA and VR data has provided highly consistent reconstructions of eroded section in Denmark (Japsen et al. 2007a) and Cardigan Bay, Western UK (Holford et al., 2005).

Since these compaction-based methods are controlled primarily by maximum burial depths, in situations where they provide consistent indications of former burial depths with those derived from paleo-thermal methods such as AFTA and VR, the results can be regarded with confidence. In addition, while results from AFTA and VR can often be explained by a range of paleogeothermal gradients and amounts of removed section, additional constraints from compaction-based methods can significantly reduce the range of viable solutions, as illustrated for example by results from the Hans-1 well, Offshore Denmark (Japsen et al. 2007a).

Zircon fission track analysis (ZFTA)

Zircon is another common uranium-bearing detrital mineral amenable to fission track analysis. From both laboratory annealing studies and geological evidence (Hurford, 1986; Tagami et al, 1996), fission tracks in zircon are known to be more resistant to annealing than fission tracks in apatite. Investigation of zircon data in samples with different levels of vitrinite reflectance suggests that no significant fission track age reduction occurs in zircon at VR levels below ~4% (Geotrack unpublished results). VR values in excess of 5% (equivalent to maximum paleotemperatures in excess of 300°C) are required in order to produce any significant age reduction. Some evidence suggests that the rock needs to reach the stage of Greenschist facies metamorphism in order to produce observable effects in zircon. Therefore in most sedimentary basin settings, ZFTA can provide little or no information on post-depositional heating, except where intrusions are present or in cases of extremely high heat flow (e.g. Logan and Duddy, 1998). However, the relative stability of tracks in zircon makes ZFTA a useful tool for investigating sediment provenance. ZFTA data can also provide useful constraints on depositional ages (e.g. Morais Neto et al., 2008), since in the absence of post-depositional resetting, a zircon fission track age must represent cooling of sediment source regions, thereby providing an upper limit on the depositional age.

C.5 Application of AFTA to Thermal History Reconstruction in sedimentary basins

AFTA data in individual samples can provide constraints on the paleo-thermal maximum as well as one or possibly two subsequent paleo-thermal peaks. But the amount of information that can be obtained from a single sample is limited, and the real strength of the technique emerges from application to sequences of samples over a range of depths in boreholes, or over a range of elevations in an outcrop section. In such cases, integrated AFTA and VR analyses can provide a well-defined thermal history framework, involving quantitative definition of the timing and magnitude of major paleo-thermal events as well as determination of paleogeothermal gradients, allowing unique insights into mechanisms of heating and cooling. This information allows reconstruction of the thermal and burial/uplift histories of the sedimentary section, as explained below.

Default Thermal Histories

As discussed earlier, AFTA and VR data must be investigated within a context in order to provide

meaningful information on the magnitude of possible paleo-thermal effects (i.e events in which a rock sample was hotter in the past than it is today, due to either deeper burial, elevated basal heat flow, local igneous intrusion or hot fluid movements). In sedimentary sections, this context is provided by a Default Thermal History, which represents the history that can be constructed in the absence of any paleo-thermal effects. For sub-surface samples, this is calculated by combining the burial history derived from the preserved sedimentary section with the present-day geothermal gradient and surface temperature. Because both AFTA and VR data are dominated by the maximum temperatures experienced, this provides a basic point of reference for the expected degree of fission track annealing and the organic maturity. If measured AFTA and/or VR data are consistent with the values predicted from the Default Thermal History, then the sample is presently at or close to its maximum post-depositional temperature, and the data retain little or no information on any palaeo-thermal effects (because the data are dominated by maximum temperature, as explained earlier). But if AFTA data show a greater degree of fission track annealing or VR data show higher maturity than expected on the basis of the Default Thermal History, then the sampled horizon must have been hotter in the past. In this case, AFTA allows determination of the time at which cooling began, and both AFTA and VR can define the magnitude of the maximum palaeotemperature reached by individual samples.

A key factor in defining Default Thermal Histories for sub-surface samples is definition of the present-day thermal regime. Information on present-day temperatures in hydrocarbon exploration wells usually comes in the form of bottom-hole temperatures (BHTs) from logging runs, or in less common circumstances from Drill Stem Tests (DSTs) which sample formation fluids directly. A key problem in using such information to reconstruct present-day temperatures is the disturbance to the thermal field imposed by drilling of a well due to the introduction of drilling fluids which produce significant cooling. BHT values, which are normally recorded within a short time after drilling must be "corrected" to estimate the true formation temperature. Conversely, DST temperatures are generally thought to more closely reflect true ambient temperatures and can be used directly.

The most common BHT correction method is the "Horner correction", based on an exponential increase towards the true temperature with time, but this requires repeated temperature measurements from multiple logging runs, as well as the time between runs. This information is not always available, so a number of simpler methods have been suggested. In our own work, we use a simple method based on observations of borehole temperatures over timescales of years (Andrews-Speed et al, 1984). In this approach, quoted BHT values are corrected by increasing the difference between the surface or sea-bed temperature and the uncorrected BHT by 20% for uncorrected temperatures below 150°F (66°C), and by 25% above 150°F. In wells where multiple temperature measurements are available at a given depth, the earliest recorded BHT value was used. If no circulation times are available, the lowest temperature value at each depth is used. Whilst simplistic, this procedure has the advantage of allowing a common approach in all cases, and results in present-day temperatures which are consistent with the kinetic descriptions of AFTA and VR employed to extract information on paleo-thermal histories. Thus, a self-consistent framework is achieved, which is essential in any approach to this subject.

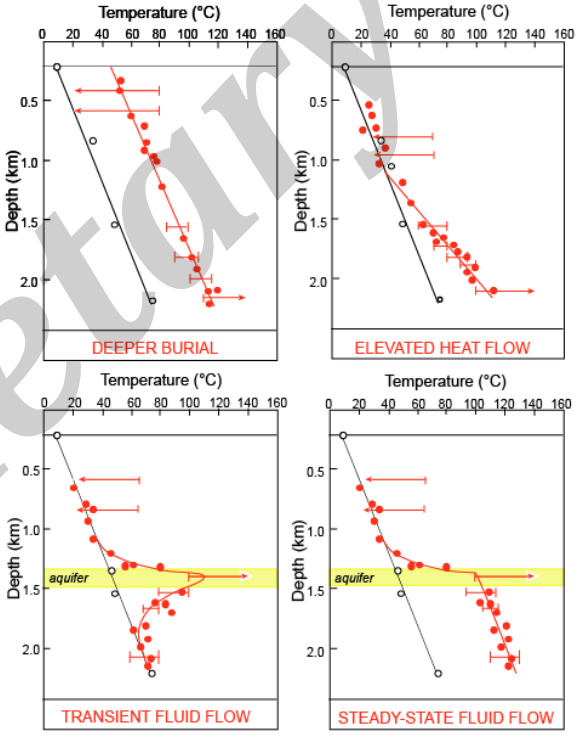

Fig. C.22: The way in which paleotemperatures characterising a particular paleo-thermal episode vary through a vertical sequence of rocks (the "paleotemperature profile") provides key information on the mechanisms of heating and cooling. Deeper burial followed by exhumation, with no change in basal heat flow, will result in paleotemperatures defining a linear profile parallel to the present-day thermal profile but offset to higher temperatures. Elevated heat flow results in a linear paleotemperature profile with a higher slope compared to the present-day profile. In contrast, transient hot fluid flow through a localised aquifer results in a markedly non-linear profile with a maximum centred on the aquifer, while prolonged fluid flow can result in a linear profile below the aquifer as the deeper section reaches a "steady-state" situation. Combinations of these four simple cases are possible.

Paleotemperature profiles

The variation of paleotemperatures with depth, or the "paleotemperature profile", provides key information on likely mechanisms of heating and cooling (Bray et al., 1992; Duddy et al., 1994; Green et al., 2002) (Fig. C.22). Provided that heterogeneities in lithology through the section are sufficient to smooth out any potential large-scale variations in thermal conductivity, heating due solely to deeper burial should produce a more or less linear paleotemperature profile with a similar gradient to the present temperature profile. In contrast, heating

due primarily to increased basal heat flow (perhaps also with some component of deeper burial) should produce a more or less linear paleotemperature profile with a higher gradient than the present temperature profile. Non-linear profiles may be produced by contact heating around intrusive bodies, or in the absence of intrusions are diagnostic of lateral introduction of heat, most likely due to passage of hot fluids within confined aquifer horizons.

Estimating additional burial (removed section)

Where heating can be attributed to some degree of deeper burial, possibly combined with elevated heat flow, fitting a linear profile to paleotemperatures as a function of depth allows the palaeogeothermal gradient at the paleo-thermal maximum to be determined and extrapolation of the palaeogeothermal gradient from the depth of the appropriate unconformity to an assumed palaeo-surface temperature (Fig. C.23) provides an estimate of the amount of additional section that was once present and was removed during cooling (see Bray et al., 1992; Duddy et al., 1994; Green et al., 2002, 2004). The inverse correlation between these two parameters results in a hyperbolic ellipsoid region of allowed values as shown in Fig. C.23. If a preferred value of paleogeothermal gradient is available (e.g. if the present-day gradient if heat flow has not changed through time) or if amounts of additional burial can be independently constrained (e.g. from sonic velocity data), then the complementary parameter can be defined with greater confidence from such plots.

It should be stressed that estimating amounts of removed section by extrapolating a linear paleotemperature profile assumes that the additional section had the same average thermal conductivity as the preserved section. If independent evidence suggests that this assumption is not appropriate, then a more detailed analysis using suitable thermal conductivities is required in order to provide a more accurate solution. But we submit that this approach is inherently more reliable than extrapolation of VR profiles to values of 0.2% to estimate amounts of removed section, since the underlying principles are more explicit, and problems such as those highlighted by Dow (1977) and Katz et al (1988) are more easily avoided.

This method also requires use of a preferred value for the paleo-surface temperature, which can be obtained from paleo-climate studies (e.g. Zachos et al. 2001). The influence of this factor can be assessed by dividing the change in temperature by the appropriate paleogeothermal gradient. For instance, for a paleogeothermal gradient of 30°C/km, a 10°C increase in paleo-surface temperature is equivalent to a reduction of 333 metres of removed section. Thus, subtle changes in surface temperature may be equivalent to major changes in amounts of removed section. This, combined with discussion of possible non-linear paleotemperature profiles above, emphasises that estimation of removed section in this way is not a precise method, and the results can only ever be regarded as providing a general indication of the true amount.

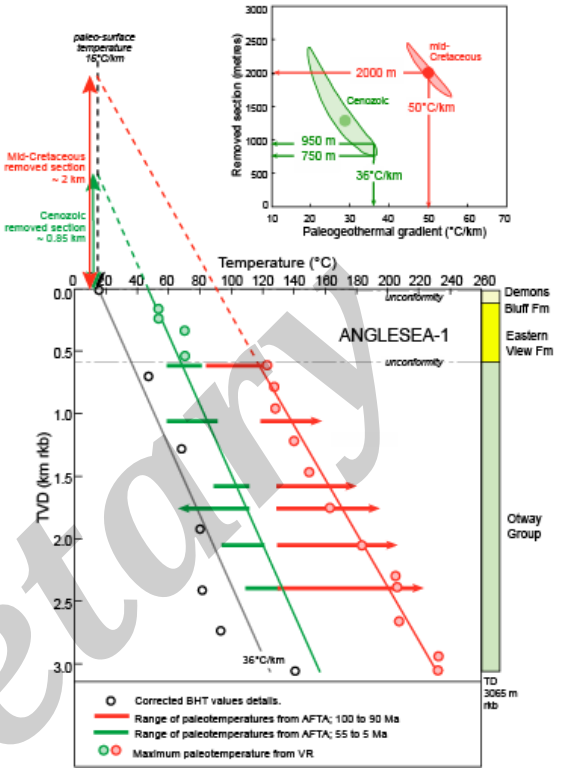

Fig. C.23: Extrapolation of paleotemperature profiles to estimate eroded section in the Anglesea-1 well, Otway Basin (after Green et al., 2004). AFTA and VR results define linear paleotemperature profiles for two thermal episodes: Mid-Cretaceous (cooling beginning between 100 and 90 Ma) associated with the unconformity between the Otway Group and the Eastern View Formation and Tertiary (cooling beginning between 55 and 5 Ma) associated with the unconformity at the top of the Demons Bluff Formation at the ground surface. Fitting of linear profiles using maximum likelihood methods defines the range of paleogeothermal gradients consistent with the observed paleotemperatures. Linear extrapolation of these paleo-gradients to an appropriate paleo-surface temperature (in this case 15°C) defines the magnitude of additional section required to explain the paleotemperatures in each episode (subsequently removed by erosion). A cross-plot of allowed values paleogeothermal gradient and removed section shows the allowed ranges (±95% confidence limits) for the Mid-Cretaceous and Tertiary thermal episodes. The paleogeothermal gradient for the mid-Cretaceous episode was between 45 and 55°C/km, significantly higher than the present-day gradient of 36°C/km, and was associated with 2000 ± 300 m of additional burial. The results allow a wider range of paleogeothermal gradient for the Tertiary episode (~20 to 37°C/km), encompassing the present-day gradient of 36°C/km, for which 750-950 m of additional burial is required to explain the Tertiary paleotemperature constraints. Note that this analysis assumes that the thermal conductivity of the eroded sequences was the same as that of the preserved sequences.

Thermal History Reconstruction

By integrating the information on the timing and magnitude of the main paleo-thermal events that have affected the sedimentary section with information provided by the preserved section (i.e. the Default Thermal History), a more complete thermal and burial/uplift history can be reconstructed (e.g. Green et al., 2004).

It should be evident from the above discussion that rigorous control on paleogeothermal gradients and therefore on amounts of additional burial is usually possible only at limited times in the history (i.e. the main paleo-thermal maxima and possibly one or two subsequent paleo-thermal peaks). It is not possible to

define the complete burial or thermal history, and instead we focus on defining the key paleo-thermal events in as much detail as possible. In doing so, it is important to realise that processes other than burial may play key roles in controlling the thermal history. Elevated basal heat flow may produce a paleo-thermal maximum which does not correlate with the time of maximum burial and may in fact occur within a period of continuing burial, while heating as a result of hot fluid movement can occur at any time (Duddy et al., 1994; 1998). In addition, variation in surface temperature may cause significant cooling of a sedimentary section during progressive burial, as illustrated by Japsen et al. (2007a) in the Eastern North Sea during the Cenozoic.

Precision and accuracy in thermal history reconstruction

In discussing precision and accuracy in thermal history reconstruction it is important to distinguish between the degree to which thermal history constraints can be defined, on the one hand, and how this translates to uncertainty in the corresponding burial history. Green et al. (2002) discussed these issues at some length, and only the basic points are reproduced here. Precision in this context describes the narrowness of the 95% confidence intervals on maximum paleotemperatures, corresponding amounts of additional burial and the onset of cooling, while accuracy deals with how close to the true values the estimates might be.

Accuracy of the thermal history constraints derived from AFTA is determined by how well the kinetic model used to define those constraints describes the natural system. As discussed earlier and as illustrated in Figs. C.7 and C.11, multi-compositional models provide reasonably accurate predictions when compared to data from geologically well-controlled situations. Obtaining consistent indications of maximum paleotemperatures from multiple techniques provides an additional check on accuracy. The precision of paleotemperatures determined from AFTA depends critically on the paleotemperature itself. Below around 60°C, mean track length varies only slowly with temperature, and it is often only possible to place an upper limit on the maximum paleotemperature. At higher temperatures, track length changes more rapidly with increasing temperature and the fission track age reduction becomes increasingly pronounced (Fig. C.2), and maximum paleotemperatures in this range becomes more precise, such that maximum paleotemperatures around 100°C can be defined within an overall uncertainty (95% confidence limits) of ~5°C. In other words, it is possible to define that a sample reached a paleotemperature between 100 and 105°C. But as the paleotemperature increases further, and tracks become totally annealed, the only constraint that is possible is a minimum estimate of the maximum paleotemperature.

Translating paleotemperatures defined from AFTA to estimates of former burial depth is much less precise, and also potentially a lot less accurate. Precise estimation requires control on paleogeothermal gradient that can only be obtained by paleotemperature constraints over a range of depth, ideally from both AFTA and VR data. Even with high quality datasets with consistent constraints from AFTA and VR over a depth interval of ~3 km, a 95% confidence interval of around 10°C/km around a best-fit paleogeothermal gradient of ~50°C/km is the best that can be achieved (i.e 50±5°C/km). This translates to a confidence interval of around 600 m or more for best-fit values of removed section around 2 km (i.e. 2.0±0.3 km). So even for the most tightly-constrained datasets, estimating amounts of removed section in this way is not a precise method, and for less-well defined datasets, uncertainties can be much higher. This is exacerbated by considering the accuracy of predicting amounts of removed section by extrapolation of paleotemperature profiles, since assumptions regarding such factors as the paleo-surface temperature and the linearity of the profile through the removed section play a key role in the process (see Green et al., 2002 for a thorough review of these factors).

In terms of the timing information that can be obtained from AFTA, the numbers of fission tracks that can be counted for the fission track age determination and the numbers of track lengths that can be measured play a major role in determining precision. In any given sample, these are determined by the apatite abundance, the quality of the grains and the thermal history of the sample. In a best-case scenario, the onset of cooling from paleotemperatures sufficiently high to totally anneal all tracks may be defined with an uncertainty of around ±5% (e.g. 200±10 Ma). So this technique does not provide the sort of high precision analyses that can be obtained from mass spectrometer-based techniques. But AFTA does provide information that cannot be obtained from any other approach, and since the systematics of the method are extremely well understood, the information is highly reliable, provided that appropriate procedures are employed at every step of the process. But as we have tried to highlight in the foregoing discussion, failure to correctly implement any step of the process can result in highly misleading information.

Sample requirements for AFTA and sampling strategies

Apatite is a common accessory phase in many crystalline rocks, and being among the most resistant of detrital minerals (Morton, 1984) forms a common detrital constituent of most sandstones and other coarse sedimentary rocks, which can readily be extracted using standard heavy mineral separation methods. AFTA® can be applied either to outcrop samples or to ditch cuttings or core for sub-surface samples, and in both situations similar considerations

apply regarding sampling. In sedimentary sequences, medium grained sandstones are the most suitable lithologies for analysis, although coarse grits to or coarse silts can be used. It is advisable to collect around 1 kg of material from the most mineralogically immature units available. In general, experience shows that 80 to 90% of sandstone samples collected on this basis contain sufficient apatite for analysis.

Note that since a high quality analysis can be derived from as few as 20 grains of apatite, the overall abundance of apatite required is very low. Inspection of thin sections or even heavy mineral separates may not reveal apatite in samples which contain sufficient for analysis, so the ultimate test is to refine the apatite fraction as far as possible and then to prepare, polish and etch a grain mount. Since apatite is the only mineral that can be etched by dilute nitric acid, the etched apatite grains can easily be identified within a mass of other grains (multi-mineral composites, carbonates, sulphides) with similar density. The presence of these additional grains on the grain mount has no effect on the resulting analysis.

In downhole studies, samples of cuttings can be composited over a depth interval representing a range in downhole temperature of up to ~5°C, corresponding to a depth range of about 150m for a typical geothermal gradient of 30°C/km. Sample should not be composited across an unconformity or major stratigraphic boundary. Where core samples are available, an integral solid piece of core, since the sample will be crushed anyway. Offcuts, rubble or scraps remaining from previous sampling can all be used, and again compositing over a range of depths is possible.

The most appropriate sampling strategy depends to some extent on the problems to be addressed, but in general, in order to obtain as much information as possible on key aspects of the paleo-thermal history such as paleogeothermal gradients, removed section etc, a vertical sequence of samples is required, spanning as wide a range of depths as possible from near surface to a depth where present downhole temperatures exceed about 110°C (corresponding to around 3 to 3.5 km for a typical geothermal gradient of 30°C/km), where tracks are totally annealed in the present day thermal regime. Integration with VR data is recommended as routine practice, for reasons discussed earlier. VR samples should be distributed more or less evenly through a well section, including the temperature realm above 110°C, and integrating information from this depth range with AFTA data provides a more complete reconstruction that would otherwise be available.

References

Andrews-Speed, C.P., Oxburgh, E.R., and Cooper, B.A., 1984. Temperatures and depth-dependent heat flow in Western North Sea: AAPG Bulletin, v. 11, p. 1764 - 1784.

Argent, J.D., Stewart, S.A., Green, P.F. and Underhill, J.R., 2002, Heterogeneous exhumation in the Inner Moray Firth, UK North Sea: constraints from new AFTA® and seismic data: Journal of the Geological Society of London, v. 159, p. 715-729.

Barbarand, J., Carter, A., Wood, I. and Hurford, A.J., 2003a, Compositional and structural control of fission track annealing in apatite: Chemical Geology, v. 198, p. 107-137.

Barbarand, J., Hurford, A.J. and Carter, A., 2003b, Variation in apatite fission-track length measurement: implications for thermal history modelling: Chemical Geology, v. 198, p. 77-106.

Bhandari, N., Bhat, S.G., Lal, D., Rajagopalan, G., Tamhane, A.S. and Venkatavaradan, V.S., 1971, Fission fragment tracks in apatite: recordable track lengths: Earth and Planetary Science Letters, v.13, p. 191-199.

Bray, R.J., Green, P.F. and Duddy, I.R., 1992. Thermal History Reconstruction using apatite fission track analysis and vitrinite reflectance: a case study from the UK East Midlands and the Southern North Sea: *in* Hardman, R.F.P., ed., Exploration Britain: Into the next decade, Geological Society Special Publication, v. 67, p. 3-25.

Brown, M.C., 2007, Discussion on 'Apatite (U – Th)/He age constraints on the Mesozoic and Cenozoic evolution of the Bathurst Region, New South Wales: evidence for antiquity of the continental drainage divide along a passive margin': Australian Journal of Earth Science, v. 54, p. 1011–1012.

Bulat, J. and Stoker, S.J., 1987, Uplift determination from interval velocity studies, UK, southern North Sea: *in* J. Brooks & K.W. Glennie, eds., Petroleum Geology of North West Europe, Graham & Trotman, pp. 293–305.

Burnham, A.K. and & Sweeney, J.J., 1989, A chemical kinetic model of vitrinite reflectance maturation: Geochimica et Cosmochimica Acta, v. 53, p. 2649-2657.

Burtner, R.L., Nigrini, A. and Donelick, R.A., 1994, Thermochronology of lower Cretaceous source rocks in the Idaho-Wyoming thrust belt: AAPG Bulletin, v. 78, p. 1613-1636.

Carlson, W.D., 1990, Mechanisms and kinetics of apatite fission-track annealing: American Mineralogist, v. 75, p. 1120 – 1139.

Carlson, W.D., Donelick, R.A. & Ketcham, R.A., 1999, Variability of apatite fission-track annealing kinetics: I. Experimental results. American Mineralogist, v. 84, p. 1213-1223.

Cook, A., ed. 1982, The origin and petrology of organic matter in coals, oil shales and petroleum source rocks: The University of Wollongong, Wollongong, N.S.W., 106 pp.

Cope, M. J., 1986, An interpretation of vitrinite reflectance data from the Southern North Sea Basin: *in* Brooks, J. Goff, J.C. & Van Hoorn, B.. eds) Habitat of Palaeozoic gas in northwest Europe: Geological Society, London, Special Publications, v. 23, p. 85-98.

Corrigan, J.D., 1993, Apatite fission-track analysis of Oligocene strata in South Texas, U.S.A.: Testing annealing models: Chemical Geology, v. 10, p. 227-249.

Crowley, K.D., Cameron, M. and Schaeffer, R.L., 1991, Experimental studies of annealing of etched fission tracks in fluorapatite: Geochimica et Cosmochimica Acta, v. 55, p. 1449-1465.

Crowley, K.D. 1993, Mechanisms and kinetics of apatite fission-track annealing – Discussion: American Mineralogist, **v.** 78, p. 210 – 212.

Crowhurst. P.V., Green, P.F. & Kamp, P.J.J., 2002, Appraisal of (U-Th)/He apatite thermochronology as a thermal history tool for hydrocarbon exploration: an example from the Taranaki Basin, New Zealand: AAPG Bulletin, v. 86, p. 1801-1819.

Donelick, R.A., Roden, M.K., Mooers, J.D., Carpenter, B.S. and Miller, D.S., 1990, Etchable length reduction of induced fission tracks in apatite at room temperature (~23C): crystallographic orientation effects and "initial" mean lengths: Nuclear Tracks and Radiation Measurements, v. 17, p. 261-265.

Dow, W. 1977. Kerogen studies and geological interpretations. Journal of Geochemical Exploration, v. 7, p. 79-99.

Duddy, I.R., 1997, Focussing exploration in the Otway Basin: understanding timing of source rock maturation, APPEA Journal, v. 37, p. 178-191.

Duddy, I.R., Green, P.F. & Laslett G.M., 1988, Thermal annealing of fission tracks in apatite 3. Variable temperature behaviour: Chemical Geology (Isotope Geoscience Section), **v.** 73, p. 25-38.

Duddy, I.R., Green, P.F., Bray, R.J. and Hegarty, K.A., 1994, Recognition of the Thermal Effects of Fluid Flow in Sedimentary Basins: *in* Parnell, J. ed., 1994, Geofluids: Origin, Migration and Evolution of Fluids in Sedimentary Basins, Geological Society, London, Special Publications, v. 78, p. 325-345.

Duddy, I.R., Green, P.F., Hegarty, K.A, Bray, R.J. and O'Brien, G.W., 1998, Dating and duration of hot fluid flow events determined using AFTA® and vitrinite reflectance-based thermal history reconstruction: *in* Parnell, J., ed., 1998, Dating and duration of hot fluid flow and fluid-rock interaction. Geological Society, London, Special Publications, v. 144, p. 41-51.

Fisher, M.J., Barnard, P.C. and Cooper, B.S. 1980. Organic maturation and hydrocarbon generation in the Mesozoic sediments of the Sverdrup Basin, Arctic Canada. IV Int. Palynol. Conf. Lucknow (1976-77). v.2, p. 581-588.

Fleischer, R.L., Price, P.B. and Walker, R.M., 1975, Nuclear tracks in solids. University of California Press, Berkeley.

Galbraith, R.F., 2006, Statistics for fission track analysis. Chapman and Hall/CRC.

Galbraith, R.F. and Laslett, G.M., 1988, Some calculations relevant to the thermal annealing of fission tracks in apatite: Proceedings of the Royal Society, London. v. A419, p. 305-321.

Galbraith, R.F. and Laslett, G.M., 1990, Apatite fission track analysis: geological thermal history analysis based on a three-dimensional random process of linear radiation damage: Philosophical Transcripts of the Royal Society of London, v. 332, p. 419-438.

Gallagher, K., 1995, Evolving temperature histories from apatite fission-track data: Earth and Planetary Science Letters, v. 136, p. 421-435.

Gallagher, K. and Brown, R., 1997 The onshore record of passive margin evolution: Journal of the Geological Society, London, v. 154, p.451-457.

Gallagher, K. and Brown, R., 1999a, Denudation and uplift at passive margins: the record on the Atlantic Margin of Southern Africa: Philosophical Transactions of the Royal Society of London, v. 357, p. 835–859.

Gallagher, K and Brown, R., 1999b, The Mesozoic denudation history of the Atlantic margins of southern Africa and southeast Brazil and the relationship to offshore sedimentation: *in* Cameron, N.R., Bate, R.H. and Clure, V.S., eds., The oil and gas habitats of the South Atlantic, Geological Society Special Publications, v. 153, p. 41-53.

Gibson, D.L., 2007, Discussion on 'Apatite (U – Th)/He age constraints on the Mesozoic and Cenozoic evolution of the Bathurst Region, New South Wales: evidence for antiquity of the continental drainage divide along a passive margin': Australian Journal of Earth Science, v. 54, p. 1012–1015.

Gleadow, A.J.W. and Duddy, I.R., 1981, Fission track analysis: a new tool for the evaluation of thermal histories and hydrocarbon potential: APEA Journal, v. 23, p. 93-102.

Gleadow, A.J.W., Duddy, I.R., Green, P.F. and Lovering, J.F., 1986, Confined fission track lengths in apatite – a diagnostic tool for thermal history analysis: Contributions to Mineralogy and Petrology, v. 94, p. 405-415.

Goswami, J.N., Jha, R. and Lal, D., 1984, Quantitative treatment of annealing of charged particle tracks in common rock minerals: Earth and Planetary Science Letters, v. 71, p. 120-128.

Green, P.F., 1980, On the cause of the shortening of spontaneous fission tracks in certain minerals: Nuclear Tracks, v. 4, p. 91-100.

Green, P.F., 1986, On the thermo-tectonic evolution of Northern England: evidence from fission track analysis: Geological Magazine, v. 123, p. 493-506.

Green, P.F.,1988, The relationship between track shortening and fission track age reduction in apatite: combined influences of inherent instability, annealing anisotropy, length bias and system calibration: Earth and Planetary Science Letters, v. 89, p. 335 – 352.

Green, P.F., 1989, Thermal and tectonic history of the East Midlands shelf (onshore UK) and surrounding regions assessed by apatite fission track analysis: Journal of the Geological Society of London, v. 146, p. 755-773.

Green P., 2004, The importance of validating annealing models: 10th International Conference on Fission Track Dating and Thermochronology, Amsterdam, The Netherlands (abstract), p.53.

Green, P.F., 2005, Post-Carboniferous burial and exhumation histories of Carboniferous rocks of the Southern North Sea and adjacent Onshore UK. *In:* Collinson, J.D., Evans, D.J., Holliday, D.W. and Jones, N.S. (eds), Carboniferous hydrocarbon geology: the Southern North Sea and surrounding Onshore areas. *Occasional Publications, Yorkshire Geological Society*, v. 7, p. 25-34.

Green, P.F. and Duddy, I.R., 2006, Interpretation of apatite (U-Th)/He ages and fission track ages from cratons: Earth and Planetary Science Letters, v. 244, p. 541-547.

Green, P.F and, Duddy, I.R., 2007, Discussion on 'Apatite (U – Th)/He age constraints on the Mesozoic and Cenozoic evolution of the Bathurst Region, New South Wales: evidence for antiquity of the continental drainage divide along a passive margin': Australian Journal of Earth Science, v. 54, p. 1009-1011.

Green, P.F., Duddy, I.R., Gleadow, A.J.W., Tingate, P.R. and Laslett, G.M., 1985, Fission-track annealing in apatite: track length measurements and the form of the Arrhenius plot: Nuclear Tracks, v. 10, p. 323-328.

Green, P.F., Duddy, I.R., Gleadow, A.J.W., Tingate, P.R. and Laslett, G.M., 1986, Thermal annealing of fission tracks in apatite 1. A qualitative description: Chemical Geology (Isotope Geoscience Section), v. 59, p. 237-253.

Green, P.F., Duddy, I.R. and Laslett, G.M., 1988. Can fission track annealing be described by first-order kinetics? Earth and Planetary Science Letters, v. 87, p. 216 – 228.

Green, P.F., Duddy, I.R., Laslett, G.M., Hegarty, K.A., Gleadow, A.J.W. and Lovering, J.F., 1989. Thermal annealing of fission tracks in apatite 4. Quantitative modelling techniques and extension to geological timescales: Chemical Geology (Isotope Geoscience Section), v. 79, p. 155-182.

Green, P.F., Laslett, G.M. and Duddy, I.R., 1993, Mechanisms and kinetics of fission-track annealing, American Mineralogist, v. 78, p. 441 – 445.

Green, P.F., Duddy, I.R., Bray, R.J., Duncan, W.I. and Corcoran, D.V., 2001a, The influence of thermal history on hydrocarbon prospectivity in the Central Irish Sea Basin: *in* Shannon, P.M., Haughton, P.D.W. and Corcoran, D.V., eds., The Petroleum Exploration of Ireland's Offshore Basins, Geological Society, London, Special Publications, v. 188, p. 171-188.

Green, P.F., Thompson, K. and Hudson, J.D., 2001b, Recognising tectonic events in undeformed regions: contrasting results from the Midland Platform and East Midlands Shelf, Central England: Journal of the Geological Society, London, v. 158, p. 59-73.

Green, P.F., I.R. Duddy, and K.A. Hegarty, 2002, Quantifying exhumation from apatite fission-track analysis and vitrinite reflectance data: precision, accuracy and latest results from the Atlantic margin of NW Europe: *in* Doré, A.G., Cartwright, J., Stoker, M.S., Turner, J.P. and White, N., Exhumation of the North Atlantic Margin: Timing, mechanisms and Implications for Petroleum Exploration, Geological Society Special Publication, v. 196, p. 331-354.

Green P.F., Crowhurst P.V., Duddy I.R., 2004, Integration of AFTA and (U-Th)/He thermochronology to enhance the resolution and precision of thermal history reconstruction in the Anglesea-1 well, Otway Basin, SE Australia: *in* Eastern Australian Basins Symposium II, Boult, P.J., Johns, D.R., Lang, S.C., eds., Petroleum Exploration Society of Australia, Special Publication, p. 117–131.

Green, P.F., Duddy, I.R. and Hegarty, K.A., 2005, Comment on "Compositional and structural control of fission track annealing in apatite" by J. Barbarand, A. Carter, I. Wood and A.J. Hurford, Chemical Geology, 198 (2003) 107-137: Chemical Geology, v. 214, p. 351-358.

Green, P.F., Japsen, P.J., Chalmers, J.A. & Bonow, J.M. 2011: Erosion surfaces and missing section in West Greenland. Journal of the Geological Society (London) **168**, 817-829.

Gunnell, Y., 2000, Apatite fission-track thermochronology: an overview of its potential and limitations in geomorphology: Basin Research, v. 12, p. 115 – 132.

Hendriks, B. W. H. and Andriessen, P., 2002, Pattern and timing of the post-Caledonian denudation of northern Scandinavia constrained by apatite fission-track thermochronology: *in* Doré, A. G., Cartwright, J., Stoker, M. S., Turner, J. P. and White, N., eds., Exhumation of the North Atlantic Margin: Timing, Mechanisms and Implications for Petroleum Exploration, Geological Society of London Special Publication, v. 196, p. 117–137.

Hillis, R.R., 1995, Quantification of Tertiary exhumation in the United Kingdom southern North Sea using sonic velocity data: AAPG Bulletin, v. 79, p. 130–152.

Holford, S.P., Green, P.F., and Turner, J.P., 2005, Palaeothermal and compaction studies in the Mochras borehole (NW Wales) reveal early Cretaceous and Neogene exhumation and argue against regional Paleogene uplift in the southern Irish Sea: Journal of the Geological Society, London, v. 162, p. 829-840.

Hurford, A.J., 1986, Cooling and uplift patterns in the Lepontine Alps, South Central Switzerland and an age of vertical movement on the Insubric fault line: Contributions to Mineralogy and Petrology, v. 92, p. 413-427.

Japsen, P. 2000. Investigation of multi-phase erosion using reconstructed shale trends based on sonic data. Sole Pit axis, North Sea: Global and Planetary Change, v.24, p. 189-210.

Japsen, P., Green, P.F. and Chalmers, J.A., 2005, Separation of Palaeogene and Neogene uplift on Nuussuaq, West Greenland, Journal of the Geological Society, London, v. 162, p. 299-314.

Japsen, P., Green, P.F., Nielsen, L.H., Rasmussen, E.S. and Bidstrup, T., 2007a, Mesozoic-Cenozoic exhumation in the eastern North Sea Basin: a multi-disciplinary study based on palaeo-thermal, palaeo-burial, stratigraphic and seismic data: Basin Research, v. 19, p. 451-490.

Japsen, P., Mukerji, T. and Mavko, G., 2007b, Constraints on velocity-depth trends from rock physics models: Geophysical Prospecting, v. 55, p. 135-154.

Katz, B.J., Pheifer, R.N. and Schunk, D.J., 1988, Interpretation of discontinuous vitrinite reflectance profiles: AAPG Bulletin, v. 73. p. 926-931.

Ketcham, R.A., Donelick, R.A. and Carlson, W.D., 1999, Variability of apatite fission-track annealing kinetics: III. Extrapolation to geological timescales: American Mineralogist, **v.** 84, p. 1235 – 1255.

Laslett, G.M. and Galbraith, R.F., 1996, Statistical modelling of thermal annealing of fission tracks in apatite: Geochimica et Cosmochimica Acta, v. 24, p. 5117-5131.

Laslett, G.M., Kendall, W.S., Gleadow, A.J.W. and Duddy, I.R., 1982 Bias in measurement of fission track length distributions: Nuclear Tracks, v. 6, p. 79-85.

Laslett, G.M., Green, P.F., Duddy, I.R. and Gleadow, A.J.W., 1987, Thermal annealing of fission tracks in apatite 2. A quantitative analysis: Chemical Geology (Isotope Geoscience Section), v. 65, p. 1-13.

Logan, P. and Duddy, I.R., 1998, An investigation of the thermal history of the Ahnet and Reggane Basins, Central Algeria, and the consequences for hydrocarbon generation and accumulation: *in* MacGregor, D.S., Moody, R.T. and Clark-Lowes, D.D., eds., Petroleum Geology of North Africa, Geological Society, London, Special Publications, v. 132, p 131-155.

MacKenzie, A.S. and McKenzie., D. 1983. Isomerization and aromatization of hydrocarbons in sedimentary basins formed by extension. Geological Magazine, v. 120, p. 417-528.

Marie, J.P.P., 1975, Rotliegendes stratigraphy and diagenesis: *in* Woodland, A.W., ed., Petroleum and the continental shelf of north-west Europe, Applied Science, London, p. 205–211.

Mark, D., Green, P.F., Parnell, J., Kelly, S.P., Lee, M.R. and Sherlock, S.C., 2008, Late Palaeozoic hydrocarbon migration through the Clair field, West of Shetland, UK Atlantic margin: Geochimica et Cosmochimica Acta, v. 72, p. 2510-2533.

Morais Neto, J.M., Green, P.F., Karner, G.D. and Alkmim, F.F. 2008: Age of the Serra do Martins Formation, Borborema Plateau, northeastern Brazil: Constraints from apatite and zircon fission track analysis. Boletim Geociencias Petrobras v.16, p. 23-52.

Morton, A.C. 1984. Stability of detrital heavy minerals in Tertiary sandstones from the North Sea Basin. Clay Minerals, v. 19, p. 287-308.

Naeser, C.W. and Faul, H., 1969, Fission track annealing in apatite and sphene: Journal of Geophysical Research, v. 74, p. 705-710.

Naeser C.W. and Forbes R.B., 1976, Variation of fission track ages with depth in two deep drill holes: EOS (abstract), v. 57, p. 363.

Naeser, C.W., Naeser N.D. and McCulloh T.H, 1989, The application of fission track dating to the depositional and thermal history of rocks in sedimentary basins: *in* Naeser N.D. and McCulloh T.H., eds., 1989, Thermal history of sedimentary basins – methods and case histories: Springer-Verlag, New York, p. 157-180.

O'Brien, G.W., Lisk, M., Duddy, I., Eadington, Cadman, S. and Fellows, M., 1996, Late Tertiary fluid migration in the Timor Sea: A key control on thermal and diagenetic histories? APEA Journal, v. 36, p. 399-426.

Parnell, J., Carey, P. F., Green, P. and Duncan, W., 1999, Hydrocarbon migration history, West of Shetland: integrated fluid inclusion and fission track studies: *in* Fleet, A.J. and Boldy, S.A.R., eds., Petroleum Geology of Northwest Europe, Proceedings of the 5th Conference, Geological Society, London, p. 613-625.

Parnell, J., Green, P.F., Watt, G. and Middleton, D., 2005, Thermal history and oil charge on the UK Atlantic Margin: Petroleum Geoscience, v. 11, p. 99-112.

Parnell, J., Bowden, S.A., Osinski, G.R., Lee, P., Green, P.F., Taylor, C. and Baron, M., 2007, Organic geochemistry of impactites from the Haughton impact structure, Devon Island, Nunavut,

Canada: Geochimica et Cosmochimica Acta, v. 71, p. 1800-1819.

Persano, C., Bishop, P. and Stuart, F.M., 2006, Apatite (U – Th)/He age constraints on the Mesozoic and Cenozoic evolution of the Bathurst Region, New South Wales: evidence for antiquity of the continental drainage divide along a passive margin: Australian Journal of Earth Science, v. 53, p. 1041–1050.

Rohrman, M., van der Beek, P., Andriessen, P. and Cloetingh, S., 1995, Meso-Cenozoic morphotectonic evolution of southern Norway: Neogene domal uplift inferred from apatite fission track thermochronology: Tectonics, v. 14, p. 704–718.

Spiegel, C., Kohn, B.P., Raza, A., Raiuner, T. and Gleadow, A.J.W., 2007, The effect of low-temperature exposure on apatite fission track stability: A natural annealing experiment in the deep ocean: Geochimica et Cosmochimica Acta, v. 71, p. 4512-4537.

Stephenson, J., Gallagher, K. and Holmes, C., 2006, A Bayesian approach to calibrating apatite fission track annealing models for laboratory and geological timescales: Geochimica et Cosmochimica Acta, v. 70, p. 5183-5200.

Tagami, T., Carter, A. and Hurford, A.J., 1996, Natural long term annealing of the zircon fission-track system in Vienna Basin deep borehole samples: constraints upon the partial annealing zone and closure temperature: Chemical Geology, v. 130, p. 147–157.

Tissot, B.P. and Welte, D.H., 1984, Petroleum formation and occurrence: Springer-Verlag.

Turner, J.P., Green, P.F., Holford, S.P. and Lawrence, S.R., 2008, Thermal history of the Rio-Muni (West Africa) – NE Brazil margins during continental breakup: Earth and Planetary Science Letters, v. 270, p. 354–367.

Vrolijk, P., Donelick, R., Queng, J. and Cloos, M., 1992, Testing models of fission track annealing in apatite in a simple thermal setting; Site 800, Leg129: *in* Larson, R. and Lancelot, Y., eds., Proceedings of the Ocean Drilling Program, Science Results, v. 129 p.169–178.

Wagner, G.A., 1968, Fission track dating of apatites, Earth and Planetary Science Letters, v. 4, p. 411-415.

Wagner, G.A. and Reimer, G.M., 1972. Fission track tectonics: the tectonic interpretation of fission track ages: Earth and Planetary Science Letters, v. 14, p. 263-268.

Wagner, G.A. and Van den Haute, P., 1992, Fission-track dating: Kluwer Academic Publishers, 285pp.

Wilkins, R.W.T., Wilmshurst, J.R., Russell, N.J., Hladky, G., Ellacott, M.V. and Buckingham, C. 1992. Fluorescence alteration and the suppression of vitrinite reflectance. Organic Geochemistry, v. 18, p. 629-640.

Young, D., Myers, A.T., Munson, E.L. and Conklin, N.M., 1969, Mineralogy and geochemistry of fluorapatite from Cerro de Mercado, Durango, Mexico: US Geological Survey Professional Papers, v. 650-D, p.D84-D93.

Zachos, J.C., Pagani, M., Sloan, L.C., Thomas, E. and Billups, K. (2001) Trends, rhythms, and aberrations in global climate 65 Ma to present. Science, v. 292, p. 686–693.

APPENDIX D

Vitrinite Reflectance Measurements

D.1 New vitrinite reflectance determinations

New vitrinite reflectance data were collected as part of this study, with details of determinations described in sections D.1 and D.2 below.

Samples

Samples were submitted for vitrinite reflectance determination Energy Resources Consulting Pty Ltd (ERC), Brisbane, Queensland, who now provide the organic petrography services previously provided by Keiraville Konsultants since the death of Dr Alan Cook. Results and sample details are summarised in Table D.2, while supporting data, including maceral descriptions and raw data sheets, are presented in the following pages. Any additional results provided by the client are listed in Table D.3.

Equipment

A Leica MP4500P microscope system with Hilgers DISKUS software (http://www.hilgers.com/Engl_index.html) is used in the analysis. Reflectance standards: spinel 0.42%, YAG 0.90%, GGG 1.72%. Full calibration is undertaken at the beginning of the microscope session and checked periodically during the session. With the equipment, it is possible to alternate from reflectance to fluorescence mode to check for associated fluorescing liptinite, or importantly with some samples, to check for bitumen impregnation, or the presence, intensity and source of oil-cut.

Sample preparation

Sample preparation methods may vary slightly depending upon whether samples are core or drill cuttings, and the methods described here are referred to as "Whole rock" sample preparation used for Geotrack samples.

With core samples, a flat face perpendicular to bedding is prepared by grinding. This is placed in a 30mm diameter mould along with several randomly orientated grains. The whole is mounted in epoxy resin.

With cuttings, the samples are passed through a 2mm sieve and where necessary are gently cracked in a mortar and pestle. This is then mounted in epoxy resin.

The epoxy resin mounted samples are polished using a variety of wet and dry papers, diamond polishing compounds and colloidal silica. The polished samples are dried in a desiccator for a minimum of 12 hours prior to analysis. Samples are normally mounted in cold setting polyester resin and polished using Cr_2O_3 and MgO polishing powders. Epoxy resins or araldite can be used if required. Large samples of coals and cokes can be mounted and examined.

Vitrinite Reflectance measurement

The procedure used generally follows Australian Standard (AS) 2486, but has been slightly modified for use with dispersed organic matter (DOM). A mechanical stage is used to traverse the sample in a regular pattern. Mean maximum reflectance in oil of the organic matter is determined by rotating the microscope stage. Reflectance is determined of a 2 μm^2 area at 546 nm using a total magnification of 500X. For each sample, a minimum target of 25 fields is measured (the number may be less if vitrinite is rare or if a limited number of particles of vitrinite is supplied, as may be the case with hand-picked samples). If wide dispersal of vitrinite reflectance is found, the number of readings (N) is increased until a stable mean is obtained.

Vitrinite identification is made primarily on textural grounds and supplemented with morphology, colour in reflected white light, maceral associations and fluorescence colours. This allows an independent assessment to be made of cavings and re-worked vitrinite populations. Histograms are only used for population definition when a cavings population significantly overlaps the range of the indigenous population. Where such data provides additional information, the mean maximum reflectance of inertinite and/or the mean maximum reflectance of liptinite (exinite) is reported. For each field, the maximum reflectance position is located and the reading recorded. The stage is then rotated by 180° which should give the same reading. In practice, the readings are seldom identical because of stage run-out and slight surface irregularities. If the readings are within ±5% relative, they are accepted. If not, the cause of the difference is sought and the results rejected. The usual source of differences is surface relief. The measurement of both maxima results in a total of 50 measurements being taken for the 25 fields reported. Thus, the 50 readings consist of 25 pairs of closely spaced readings which provide a check on the levelling of the surface and hence additional precision.

As the vitrinite reflectance measurements are being made, the various features of the samples are noted on a check sheet to allow a sample description to be compiled. When the reflectance measurements are complete, a thorough check is made of liptinite fluorescence characteristics. At the same time, organic matter abundance is estimated using a global estimate, a grain count method or point count method as required.

Data presentation

Individual sample results are reported in the following format:

ERC No.	Depth (m)	$R_V$max*1	Range*2	N*3
x10324	3106	0.79	0.64 - 0.91	25

*1 Mean of all the maximum reflectance readings obtained.
*2 Lowest Rmax and highest Rmax of the population considered to represent the first generation vitrinite population.
*3 Number of fields measured (Number of measurements = 2N because 2 maximum values are recorded for each field)

Methods - Organic matter abundance and type.

After completion of vitrinite reflectance readings, the microscope is switched to fluorescence-mode and an estimate made of the abundance of each liptinite maceral. Excitation source for fluorescence is a CREE LED 455 nm (royal blue) with a dichroic mirror / filter system optimized to this source. Fluorescence colours are also noted. Abundances are estimated using comparison charts. The categories used for liptinite (and other components) are:

Descriptor	%	Source potential
Absent	0	None
Rare	<0.1	Very poor
Sparse	0.1<x<0.5	Poor to fair
Common	0.5<x<2.0	Fair to good
Abundant	2.0<x<10.0	Good to very good
Major	10.0<x<40.0	Very good (excellent if algal)
Dominant	>40.0	Excellent

Dispersed Organic Matter (DOM) composition

At the same time as liptinite abundances are estimated, total DOM, vitrinite and inertinite abundances are estimated and reported in the categories listed above. Liptinite (exinite) fluorescence intensity and colour, lithology and a brief description of organic matter type and abundance are also recorded in a further column. Coal is described

separately from dispersed organic matter (DOM). These data can be used to estimate the specific yield of the DOM and form a valuable adjunct to TOC data.

Lithological composition

The lithological abundances are ranked. For cuttings, these data can be useful in conjunction with geophysical logs in assessing the abundance and nature of cavings. For cores, it provides a record of the lithology examined and of the lithological associations of the organic matter.

Coal abundance and composition

Where coals are present, their abundance is recorded and their composition is reported as microlithotypes thus:

Coal major, **V**itrinite>**I**nertinite>**E**xinite, Clarodurite>vitrite>clarite>inertite.

These data give an approximate maceral composition and information about the organic facies of the coal. Where coal is a major or dominant component, and more precise maceral composition data are required, point count analyses should be requested. However, the precision of the original sampling is commonly a limiting factor in obtaining better quality data.

Abundance factor analysis

Especially where cuttings samples are used, abundance factor analyses are used to obtain an assessment of the maceral assemblages in the various lithologies. This can be done by a combination analysis using a point counter, but a large number of categories are required, and the precision is low if DOM is less than about 10%. For an abundance factor analysis (for core, 50 microscope fields of view) we assess the abundance of DOM, coal and shaly coal in 50 grains. The data can be used to plot DOM and coal abundance profiles.

Analyst: Mr Paddy Ranasinghe, previously chief assistant to Professor A. C. Cook

Mr Ranasinghe was the principal analyst at Keiraville Konsultants, working with Alan Cook, for over 25 years, and has wide experience of the application of organic petrography to coals, cokes, source rocks and source rock maturation. He is a long standing member of the International Committee for Coal & Organic Petrology (ICCP) and is the Principal Organic Petrologist at Energy Resources Consulting Pty Ltd (ERC).

D.2 Integration of vitrinite reflectance data with AFTA

Vitrinite reflectance is a time-temperature indicator governed by a kinetic response in a similar manner to the annealing of fission tracks in apatite as described in Appendix C. In this study, vitrinite reflectance data are interpreted on the basis of the distributed activation energy model describing the evolution of VR with temperature and time described by Burnham and Sweeney (1989), as implemented in the BasinMod™ software package of Platte River Associates. In a considerable number of wells from around the world, in which AFTA has been used to constrain the thermal history, we have found that the Burnham and Sweeney (1989) model gives good agreement between predicted and observed VR data, in a variety of settings.

As in the case of fission track annealing, it is clear from the chemical kinetic description embodied in equation 2 of Burnham and Sweeney (1989) that temperature is more important than time in controlling the increase of vitrinite reflectance. If the Burham and Sweeney (1989) distributed activation energy model is expressed in the form of an Arrhenius plot (a plot of the logarithm of time versus inverse absolute temperature), then the slopes of lines defining contours of equal vitrinite reflectance in such a plot are very similar to those describing the kinetic description of annealing of fission tracks in Durango apatite developed by Laslett et al. (1987), which is used to interpret the AFTA data in this report. This feature of the two quite independent approaches to thermal history analysis means that for a particular sample, a given degree of fission track annealing in apatite of Durango composition will be associated with the same value of vitrinite reflectance regardless of the heating rate experienced by a sample. Thus paleotemperature estimates based on either AFTA or VR data sets should be equivalent, regardless of the duration of heating. As a guide, Table D.1A gives paleotemperature estimates for various values of VR for two different durations of isothermal heating.

One practical consequence of this relationship between AFTA and VR is, for example, that a VR value of 0.7% is associated with total annealing of all fission tracks in apatite of Durango composition, and that total annealing of all fission tracks in apatites of more Chlorine-rich composition is accomplished between VR values of 0.7 and ~0.9%.

Furthermore, because vitrinite reflectance continues to increase progressively with increasing temperature, VR data allow direct estimation of maximum paleotemperatures in the range where fission tracks in apatite are totally annealed (generally above ~110°C) and where therefore AFTA only provides minimum estimates. Maximum paleotemperature estimates based on vitrinite reflectance data from a well in which most AFTA samples were totally annealed will allow constraints on the paleogeothermal gradient that would not be possible from AFTA alone. In such cases the AFTA data should allow tight constraints to be placed on the time of cooling and

also the cooling history, since AFTA parameters will be dominated by the effects of tracks formed after cooling from maximum paleotemperatures. Even in situations where AFTA samples were not totally annealed, integration of AFTA and VR can allow paleotemperature control over a greater range of depth, e.g. by combining AFTA from sand-dominated units with VR from other parts of the section, thereby providing tighter constraint on the paleogeothermal gradient.

Equivalent vitrinite reflectance estimation from inertinite reflectance

Inertinite is another common organic maceral with a reflectance higher than that of vitrinite. The relationship between vitrinite and inertinite reflectance can be rather variable from province to province and with stratigraphic age and there is no universal kinetic relationship available. However, comparison of vitrinite and inertinite reflectance from the same samples has allowed Geotrack to develop a reasonable calibration to provide an equivalent vitrinite reflectance level from inertinite reflectance. The correlation table is provided in Table D.1B.

Equivalent vitrinite reflectance estimation from Rock-Eval Tmax

Rock-Eval T_{max} results but they have been treated at face value in this report after conversion to Equivalent VR values using the correlation of Tissot and Welte (1984) summarised in Table D.1.C (Appendix D). This calibration is a generally accepted relationship that can provide reasonable maturity estimates when used with care, as it is known that T_{max} varies with kerogen type at the same level of maturity. In general, we recommend the use of T_{max} as a maturity indicator only when vitrinite reflectance data cannot be obtained. For this report, any Rock-Eval T_{max} data provided by the client are listed in Table D.3.

References

Burnham, A.K. and Sweeney, J.J. (1989) A chemical kinetic model of vitrinite reflectance maturation. *Geochim. et Cosmochim. Acta*, 53, 2649-2657.

Laslett, G.M., Green, P.F., Duddy, I.R. and Gleadow, A.J.W. (1987) Thermal annealing of fission tracks in apatite 2. A quantitative analysis. *Chem. Geol. (Isot. Geosci.Sect.)*, 65, 1-13.

Tissot, B. P. and Welte, D. H., (1984). Petroleum Formation and occurrence: A new approach to oil and gas exploration; 2nd ed.*: Springer Verlag*, Berlin 150-169.

Table D.1A: Paleotemperature - vitrinite reflectance nomogram based on Equation 2 of Burnham and Sweeney (1989)

Paleotemperature (°C / °*F*)	Vitrinite Reflectance (%) 1 Ma Duration of heating	10 Ma Duration of heating
40 / *104*	0.29	0.32
50 / *122*	0.31	0.35
60 / *140*	0.35	0.40
70 / *158*	0.39	0.45
80 / *176*	0.43	0.52
90 / *194*	0.49	0.58
100 / *212*	0.55	0.64
110 / *230*	0.61	0.70
120 / *248*	0.66	0.78
130 / *266*	0.72	0.89
140 / *284*	0.81	1.04
150 / *302*	0.92	1.20
160 / *320*	1.07	1.35
170 / *338*	1.23	1.55
180 / *356*	1.42	1.80
190 / *374*	1.63	2.05
200 / *392*	1.86	2.33
210 / *410*	2.13	2.65
220 / *428*	2.40	2.94
230 / *446*	2.70	3.23

Table D.1B: Equivalent vitrinite reflectance estimated from inertinite reflectance (mean fit from Geotrack unpublished correlation).

Measured Inertinite Reflectance (%)	Calculated Vitrinite Reflectance (%)
<0.80	<0.30
0.80	0.3
1.02	0.4
1.22	0.5
1.40	0.6
1.59	0.7
1.78	0.8
1.96	0.9
2.13	1.0
2.31	1.1
2.48	1.2
2.64	1.3
2.81	1.4
2.97	1.5
3.14	1.6
3.29	1.7
3.45	1.8
3.60	1.9
3.76	2.0
5.23	3.0
6.00	>3.55

Table D.1C: Equivalent vitrinite reflectance estimated from Rock-Eval Tmax (Tissot and Welte (1987))

Ro(max) (%)	Tmax (°C)
0.30	411
0.36	417
0.40	420
0.45	423
0.49	426
0.56	430
0.61	433
0.66	436
0.70	438
0.74	440
0.84	445
0.94	450
1.04	455
1.15	460
1.25	465
1.36	470
1.56	480
1.65	485
1.74	490

Table D.2: Vitrinite reflectance sample details and results - well samples from Alaska (Geotrack Report #1191)

Sample number	Depth (TVDrKB) (m)	Sample type	Stratigraphic Subdivision	Stratigraphic age (Ma)	Present temperature *1 (°C)	VR (Range) %	N
OCS-Y-2321 Burger J 001							
GC1191-1	1536-1545 *(5040-5070')*	cuttings	Top HRZ/Base Torok	127-123	55	0.53 (0.40-0.65)	25
GC1191-3	1707-1725 *(5600-5660')*	cuttings	Kalubik Gamma Ray Marker - Top HRZ/Base Torok	134-123	61	0.56 (0.46-0.67)	25
GC1191-5	1814-1832 *(5950-6010')*	cuttings	Base A Sand Facies - Top Burger C	137-134	65	0.60 (0.48-0.72)	25

Note: Some samples may contain both vitrinite and inertinite. Only vitrinite data is shown.

*1 See Appendix A for discussion of present temperature data.

Table D.3: Vitrinite reflectance sample details and results supplied by client - Alaska (Geotrack Report #1191)

Source number	Depth TVDrKB (m)	Sample type	Stratigraphic Subdivision	Stratigraphic age (Ma)	Present temperature *1 (°C)	VR (Range) %	N
OCS-Y-2321 Burger J 001							
	494-503 *(1620-1650')*	cuttings	Nanushuk	110-99	16	0.40	31
	640-649 *(2100-2130')*	cuttings	Nanushuk	110-99	21	0.46	22
	988-997 *(3240-3270')*	cuttings	Torok	123-110	34	0.46	19
	1216-1225 *(3990-4020')*	cuttings	Torok	123-110	43	0.51	36
	1426-1436 *(4680-4710')*	cuttings	Torok	123-110	50	0.57	25
	1527-1536 *(5010-5040')*	cuttings	Kalubik Fm - Torok	127-110	54	0.61	31
	1710-1719 *(5610-5640')*	cuttings	Kalubik Gamma Ray Marker - Kalubik Fm	134-123	61	0.62	35
	1917-1926 *(6290-6320')*	cuttings	Base A Sand Facies	137-136	69	0.68	14
	2039-2048 *(6690-6720')*	cuttings	Base D Sand Facies	145-140	73	0.64	35

Table D.3: Continued

Source number	Depth TVDrKB (m)	Sample type	Stratigraphic Subdivision	Stratigraphic age (Ma)	Present temperature *1 (°C)	VR (Range) %	N
OCS-Y-1413 Burger 1							
	467-467 *(1532-1532')*		Nanushuk	110-99	14	0.52	38
	621-621 *(2036-2036')*		Nanushuk	110-99	19	0.50	51
	784-784 *(2572-2572')*		Nanushuk	110-99	25	0.53	55
	934-934 *(3063-3063')*		Torok	123-110	30	0.53	47
	1063-1063 *(3487-3487')*		Torok	123-110	34	0.58	49
	1148-1148 *(3767-3767')*		Torok	123-110	37	0.55	54
	1255-1255 *(4118-4118')*		Torok	123-110	41	0.51	42
	1393-1393 *(4570-4570')*		Torok	123-110	46	0.53	52
	1533-1533 *(5030-5030')*		Kalubik Fm	127-123	50	0.60	56
	1596-1596 *(5235-5235')*		Kalubik Fm	127-123	52	0.56	53
	1627-1627 *(5339-5339')*		Kalubik Fm	127-123	54	0.57	58
	1643-1643 *(5390-5390')*		Kalubik Gamma Ray Marker	134-127	54	0.59	56
	1654-1654 *(5428-5428')*		Kalubik Gamma Ray Marker	134-127	54	0.78	57
	1674-1674 *(5491-5491')*		Kalubik Gamma Ray Marker	134-127	55	0.86	50
	1698-1701 *(5570-5580')*		Kuparuk C Equivalent	135-134	56	0.71	15
	1826-1832 *(5990-6010')*		Burger A/LCU	137-135	60	0.63	42
	1978-1984 *(6490-6510')*		Burger D	144-137	66	0.58	41
	2131-2137 *(6990-7010')*		Jurassic	150-148	71	0.78	32
	2298-2304 *(7540-7560')*		Jurassic	150-148	76	0.83	40
	2460-2463 *(8070-8080')*		Jurassic	150-148	82	0.95	44

Table D.3: Continued

Source number	Depth TVDrKB (m)	Sample type	Stratigraphic Subdivision	Stratigraphic age (Ma)	Present temperature *1 (°C)	VR (Range) %	N

Note: Some samples may contain both vitrinite and inertinite. Only vitrinite data is shown.

*1 See Appendix A for discussion of present temperature data.

GEOTRACK
OCS-Y-2321
BURGER J 001

GC1191

ERC# Client# Type	Depth (ft)	$\overline{R}$ vmax	Range	SD	N	Sample description including liptinite fluorescence, maceral abundances, mineral fluorescence
						Top HRZ/Base Torok
E1933 -1 Ctgs	5040-5070	0.53	0.40-0.65	0.062	25	Sparse to common sporinite and rare liptodetrinite orange to dull orange, rare cutinite dull orange. (Claystone>siltstone> carbonate. Dom abundant, I>V>L. Inertinite abundant, vitrinite common, liptinite sparse to common. Mineral fluorescence weak orange. Iron oxides rare. Pyrite common.)
		$\overline{R}$ I	0.91-1.77	0.261	10	
						Kalubik Gamma Ray Marker HRZ/Base Torok
E1934 -3 Ctgs	5600-5660	0.56	0.46-0.67	0.052	25	Common lamalginite and rare liptodetrinite orange to dull orange, sparse sporinite dull orange, sparse bituminite dull orange to weak brown. (Claystone>fine claystone>siltstone> carbonate>igneous rocks. Dom abundant, I>L>V. Inertinite and liptinite common, vitrinite sparse to common. Some alginites have well ornamented bodies and could have affinities to *tasmanitids*. Mineral fluorescence weak to moderate orange. Iron oxides rare. Pyrite abundant.)
		$\overline{R}$ I	0.84-1.85	0.267	10	
						Base A Sand Facies Top Burger C
E1935 -5 Ctgs	5950-6010	0.60	0.48-0.72	0.061	25	Common lamalginite and rare liptodetrinite dull orange to weak brown. (Fine calcareous claystone>siltstone> carbonate>sandstone. Dom abundant, I>L>V. Inertinite and liptinite common, vitrinite sparse. Mineral fluorescence weak orange. Iron oxides rare. Pyrite abundant.)
		$\overline{R}$ I	0.84-1.39	0.130	10	

Plates

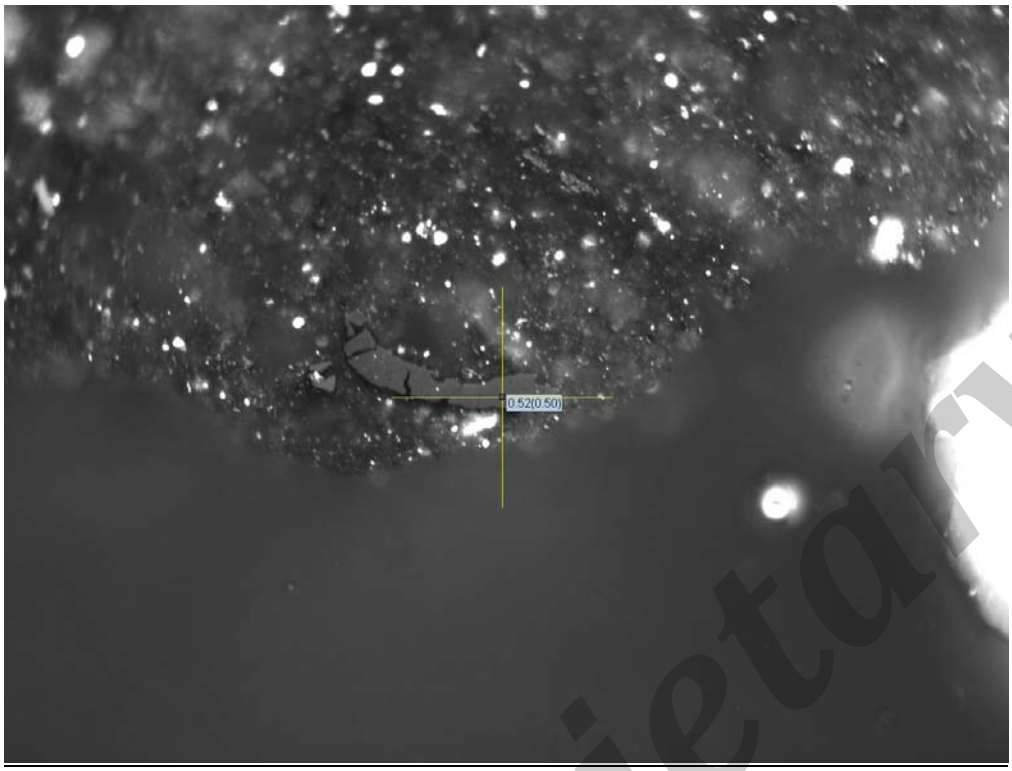

E1993A – GC1191-1 - Detrovitrinite in claystone, Rv max = 0.52%, reflected white light, X50

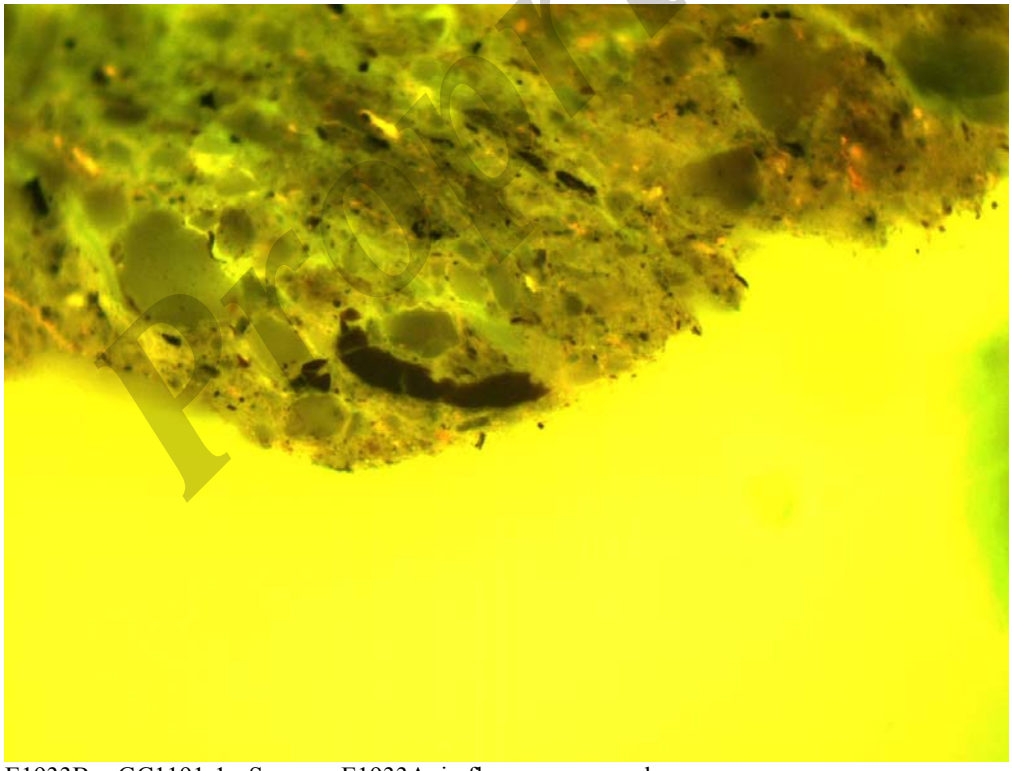

E1933B – GC1191-1 - Same as E1933A, in fluorescence mode

Plates (cont.)

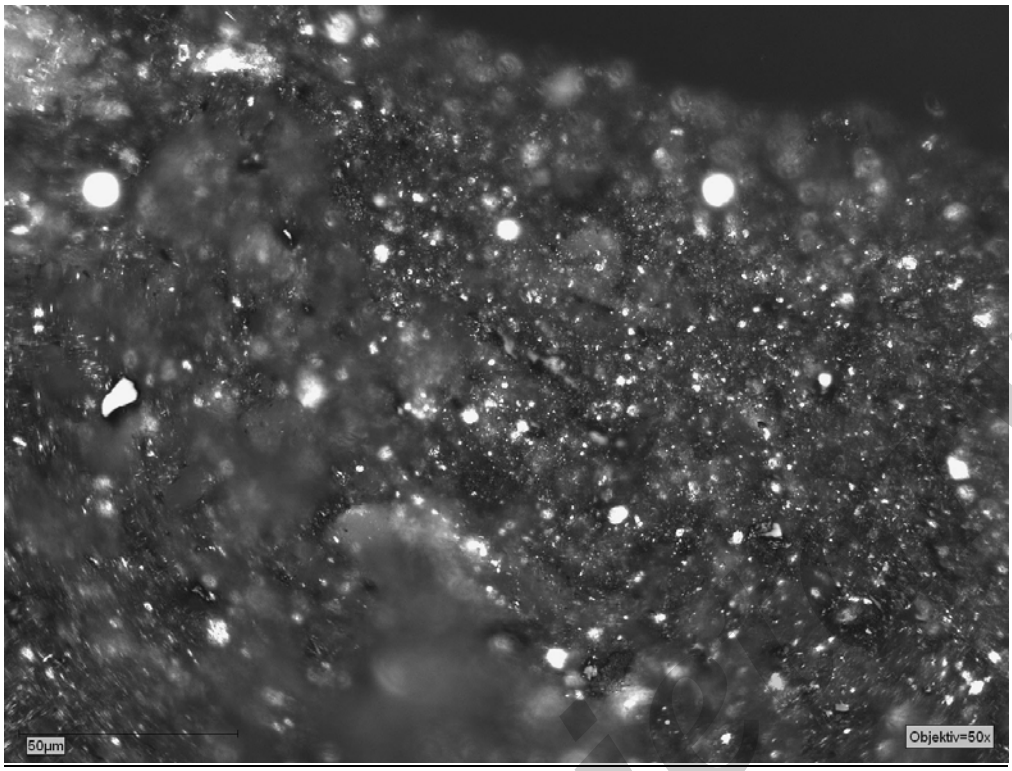

E1933C – GC1191-1 - Sporinite in claystone, reflected white light, X50

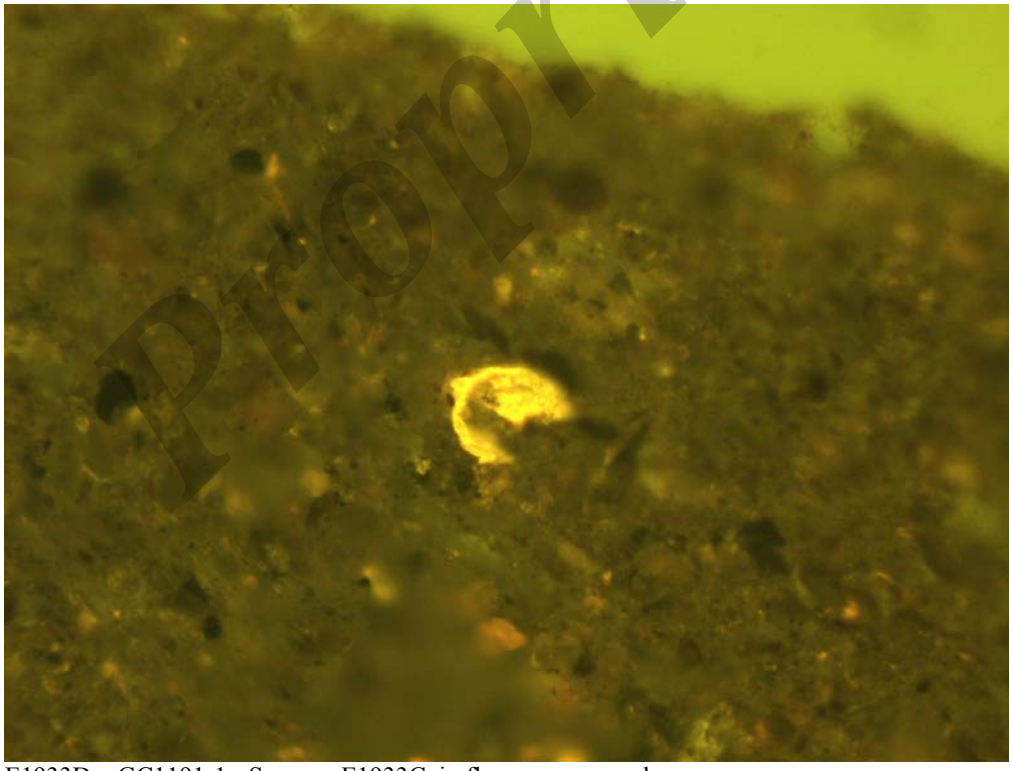

E1933D – GC1191-1 - Same as E1933C, in fluorescence mode

Plates (cont.)

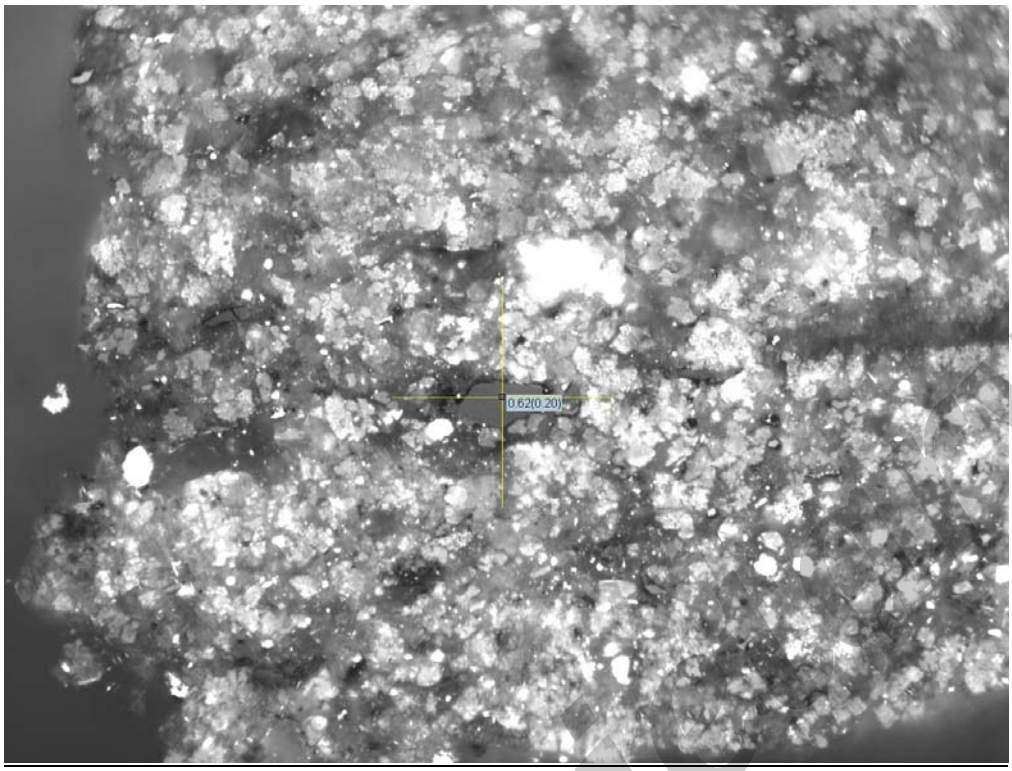

E1934A – GC1191-3 - Detrovitrinite in carbonate, Rv max = 0.62%, reflected white light, X50

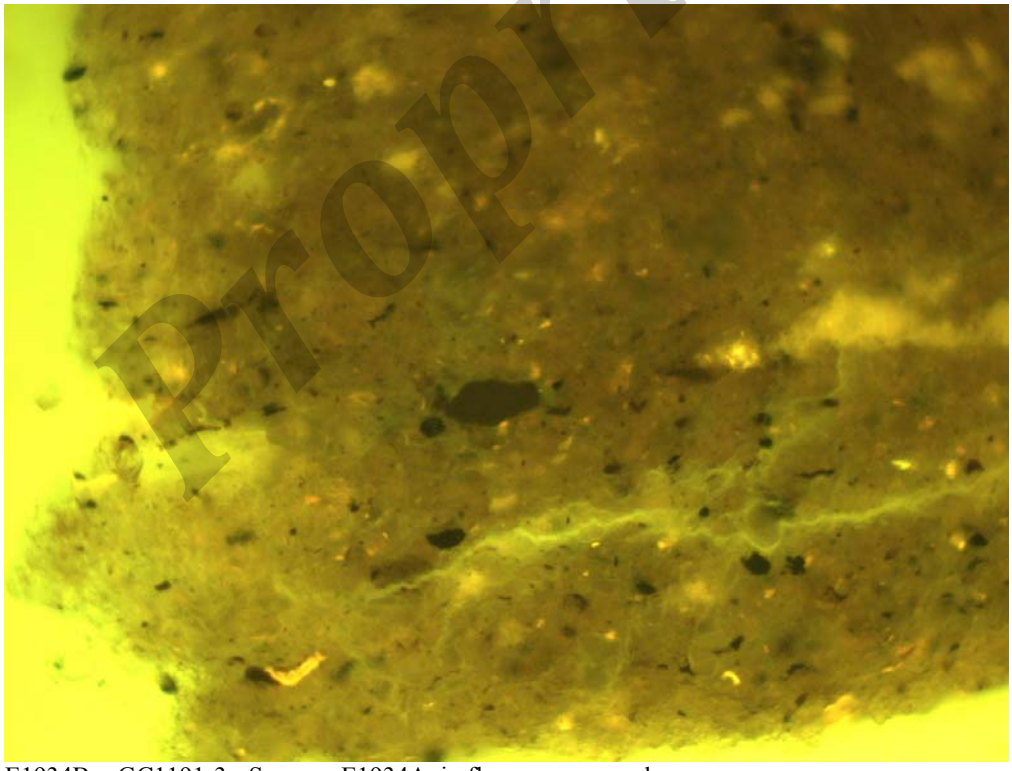

E1934B – GC1191-3 - Same as E1934A, in fluorescence mode

Plates (cont.)

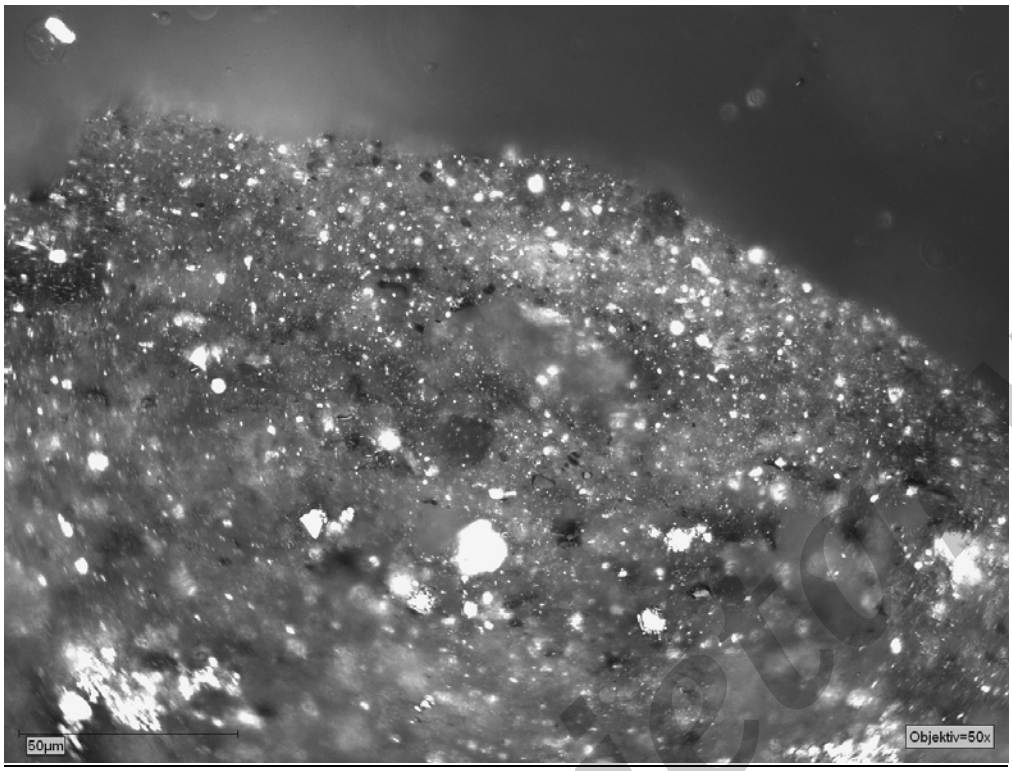

E1994C – GC1191-3 - Abundant lamalginite in claystone, reflected white light, X50

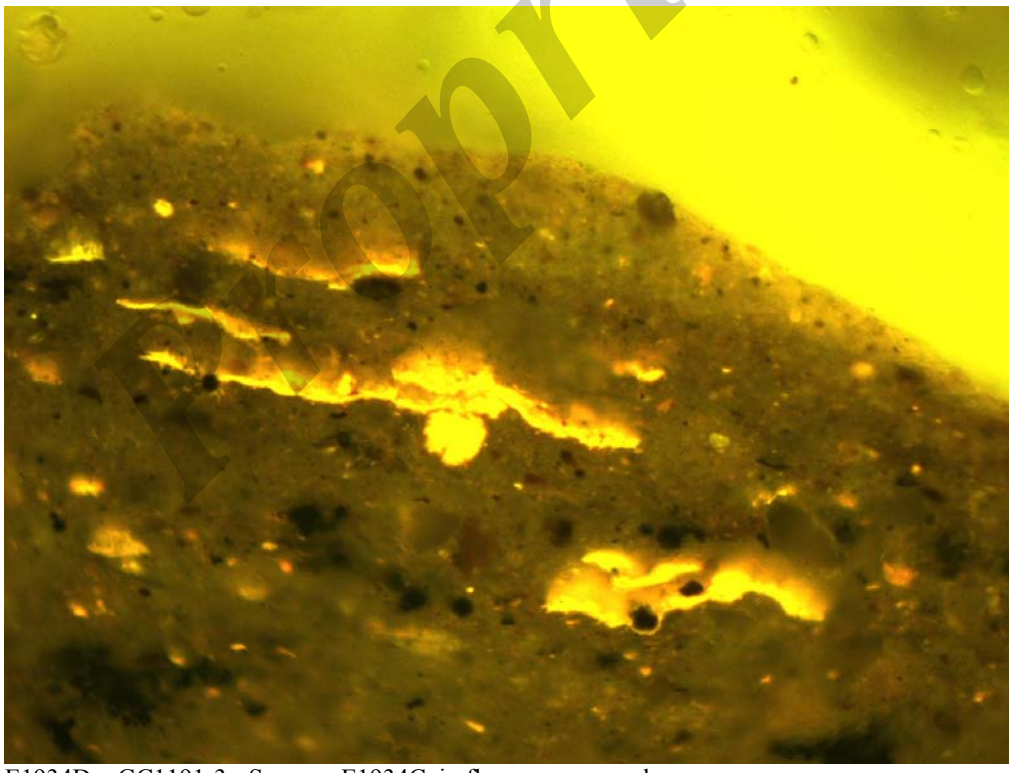

E1934D – GC1191-3 - Same as E1934C, in fluorescence mode

Plates (cont.)

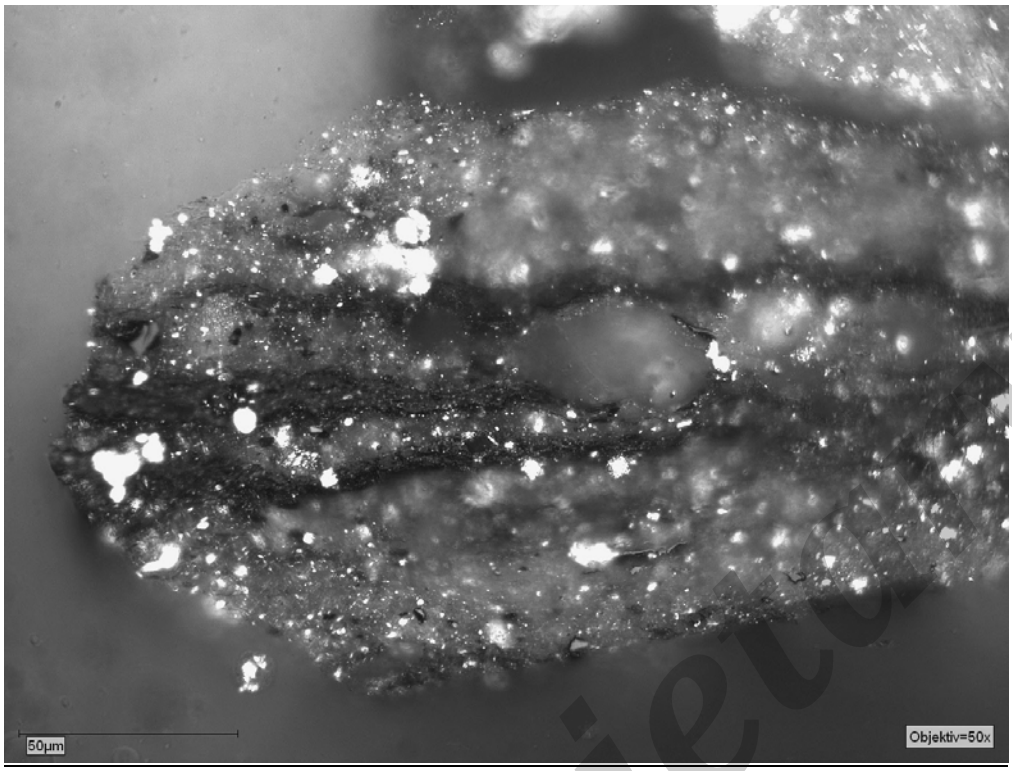

E1994E – GC1191-3 - Lamalginite and bituminite in claystone, reflected white light, X50

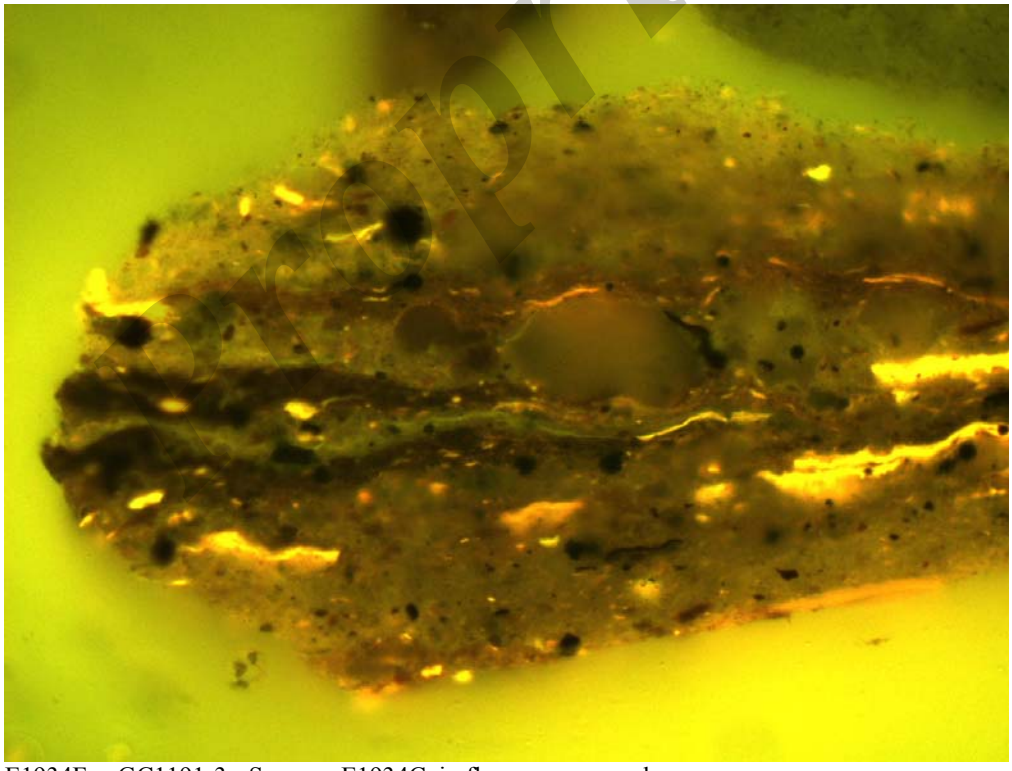

E1934F – GC1191-3 - Same as E1934C, in fluorescence mode

Plates (cont.)

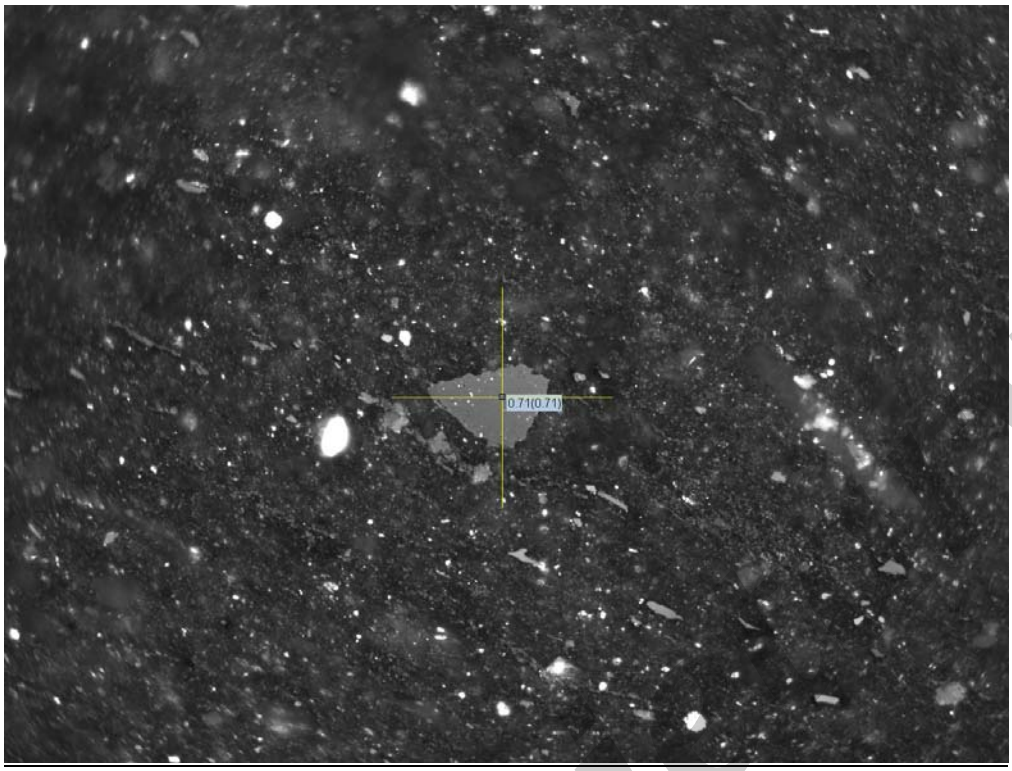

E1935A – GC1191-5 - Detrovitrinite in fine calcareous claystone, Rv max = 0.71%, reflected white light, X50

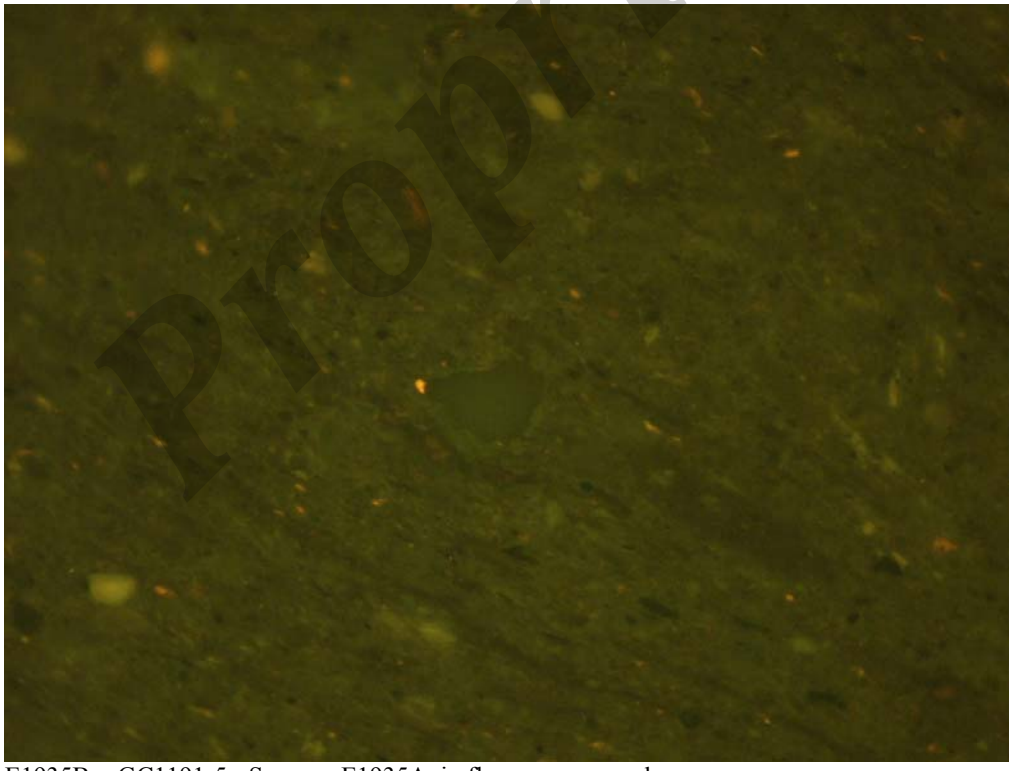

E1935B – GC1191-5 - Same as E1935A, in fluorescence mode

Plates (cont.)

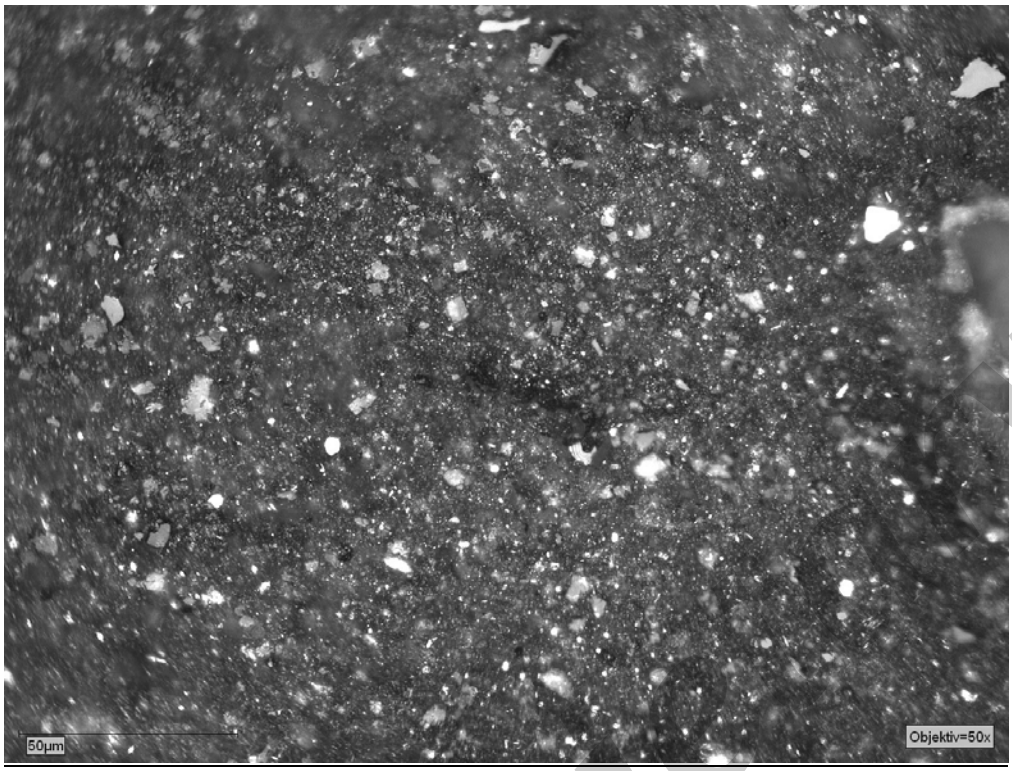

E1935C – GC1191-5 - Weak fluorescing lamalginite in fine calcareous claystone, reflected white light, X50

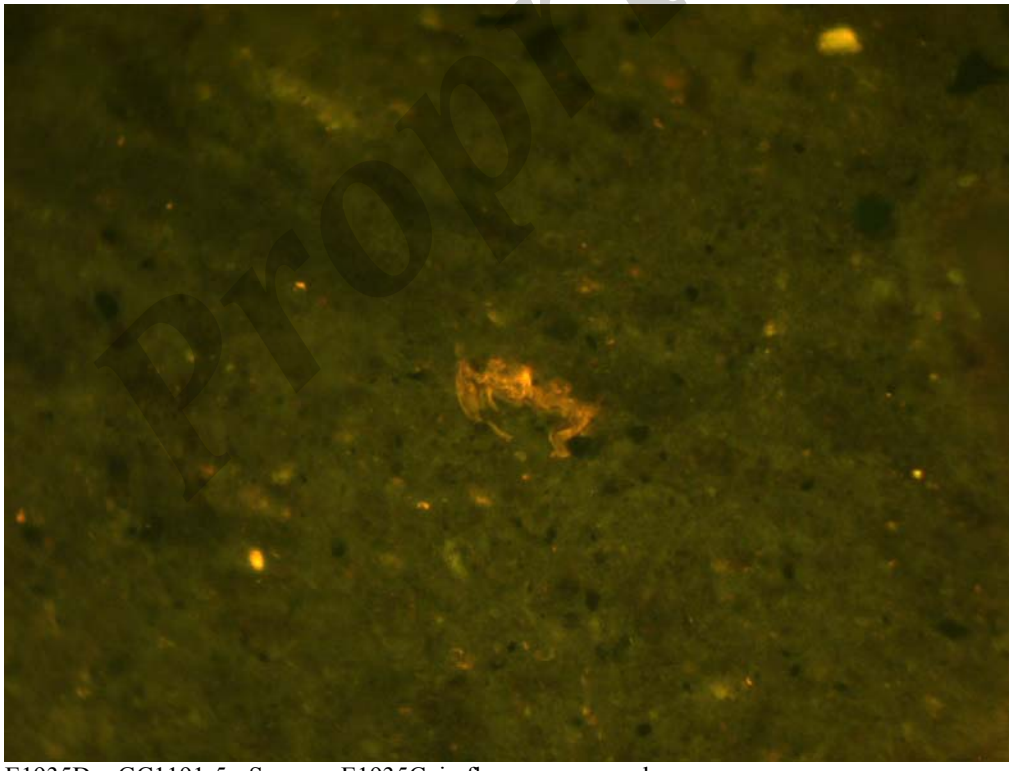

E1935D – GC1191-5 - Same as E1935C, in fluorescence mode

Energy Resources Consulting Pty Ltd
PO Box 54, Coorparoo
QLD 4151, AUSTRALIA

Telephone: +61 7 3394 3011
Fax: +61 7 3394 3088
Email: Paddy.Ranasinghe@gmail.com

GC1191-1, OCS-Y-2321, Burger J 001, 5040-5070ft, Ctgs(E1933)

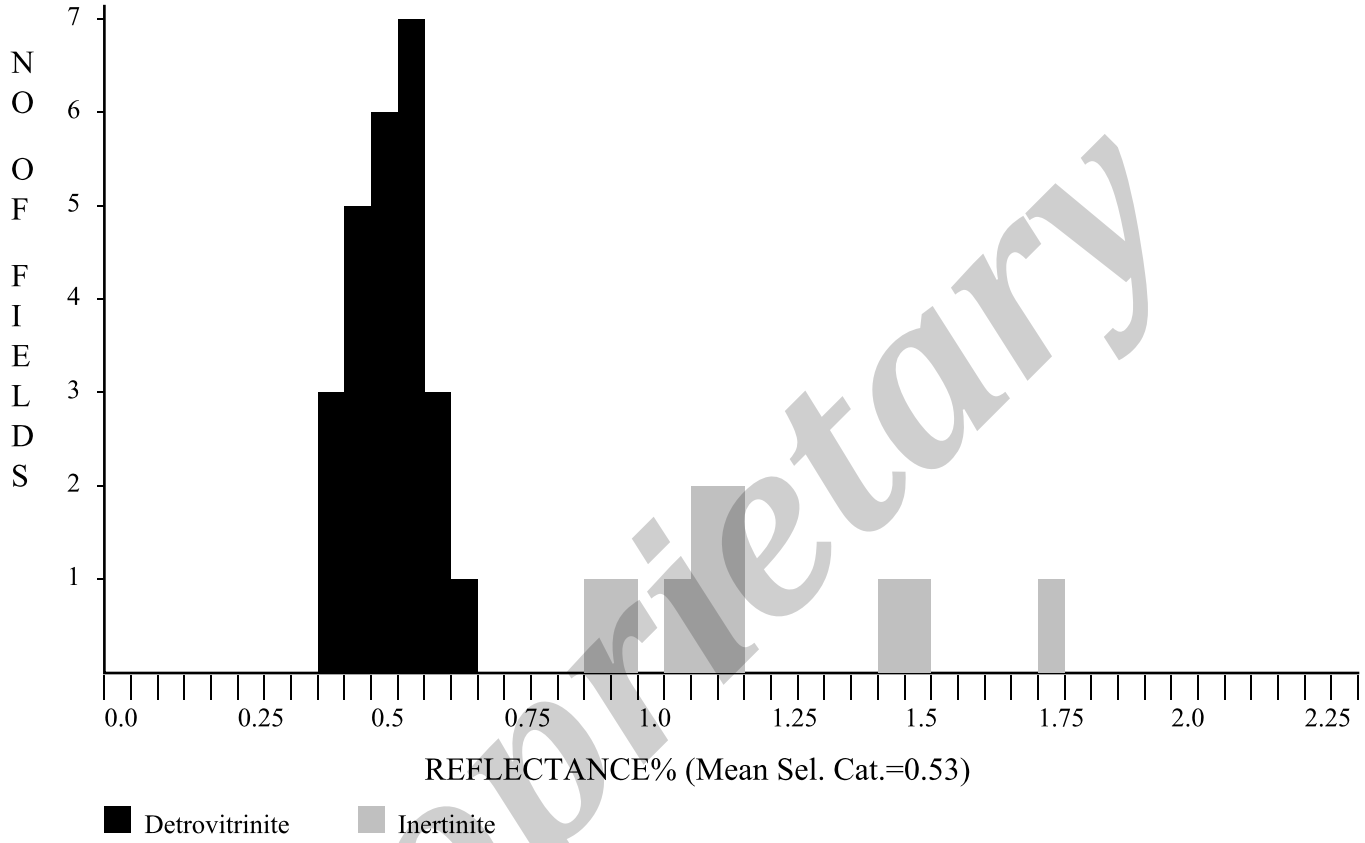

Maceral Category	N	Mean	Standard Deviation
Detrovitrinite	25	0.53	0.062
Inertinite	10	1.23	0.261
Total	35	0.73	0.353

Selected categories: Detrovitrinite:

No. of Readings:	25
Mean of Selected Categories:	0.53
Standard Deviation of Selected categories:	0.062

Energy Resources Consulting Pty Ltd
PO Box 54, Coorparoo
QLD 4151, AUSTRALIA

Telephone: +61 7 3394 3011
Fax: +61 7 3394 3088
Email: Paddy.Ranasinghe@gmail.com

GC1191-3 OCS-Y-2321, Burger J 001, 5600-5660ft, Ctgs(E1934)

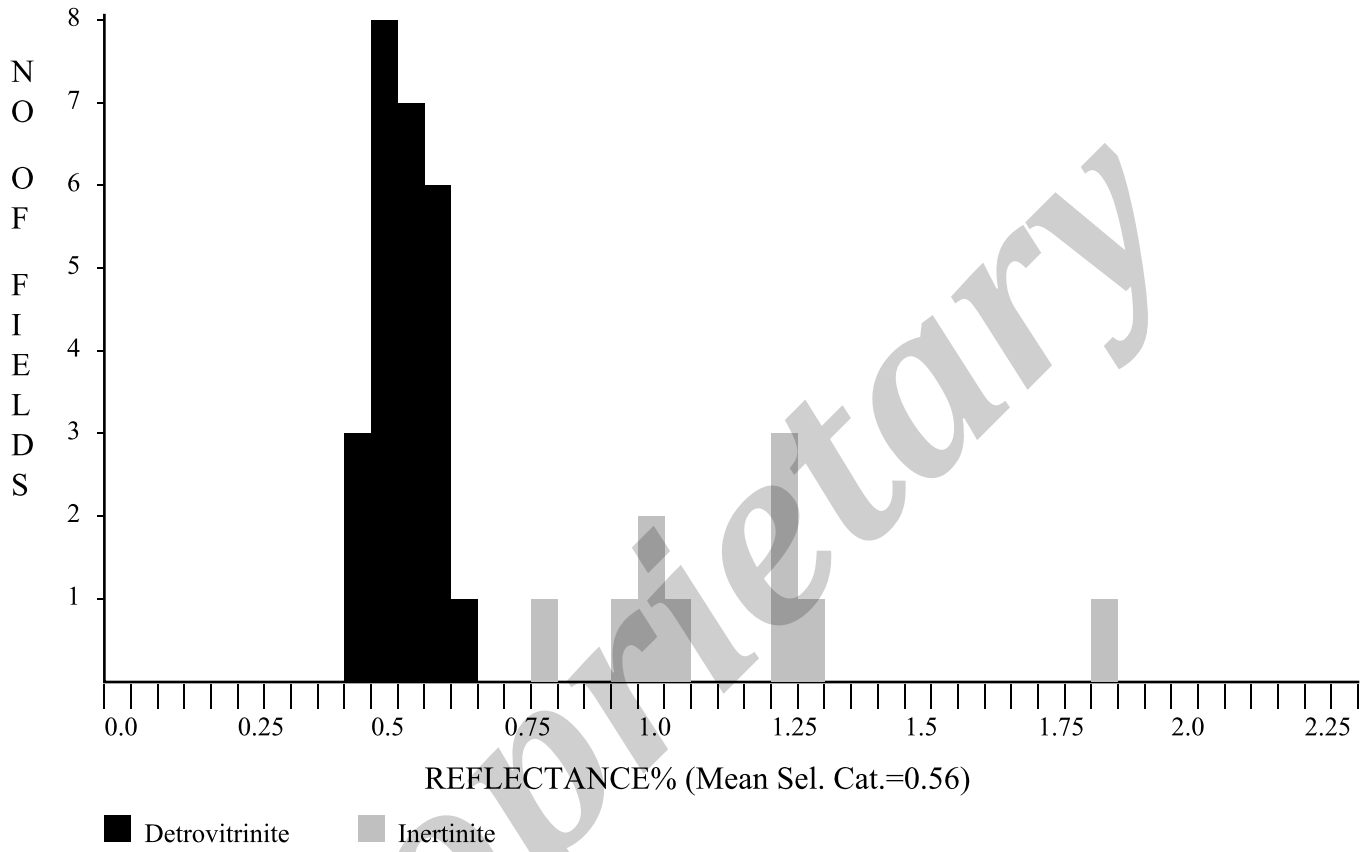

Maceral Category	N	Mean	Standard Deviation
Detrovitrinite	25	0.56	0.052
Inertinite	10	1.19	0.267
Total	35	0.74	0.323

Selected categories: Detrovitrinite:

No. of Readings:	25
Mean of Selected Categories:	0.56
Standard Deviation of Selected categories:	0.052

Energy Resources Consulting Pty Ltd
PO Box 54, Coorparoo
QLD 4151, AUSTRALIA

Telephone: +61 7 3394 3011
Fax: +61 7 3394 3088
Email: Paddy.Ranasinghe@gmail.com

GC1191-5OCS-Y-2321, Burger J 001, 5950-6010ft, Ctgs(E1935)

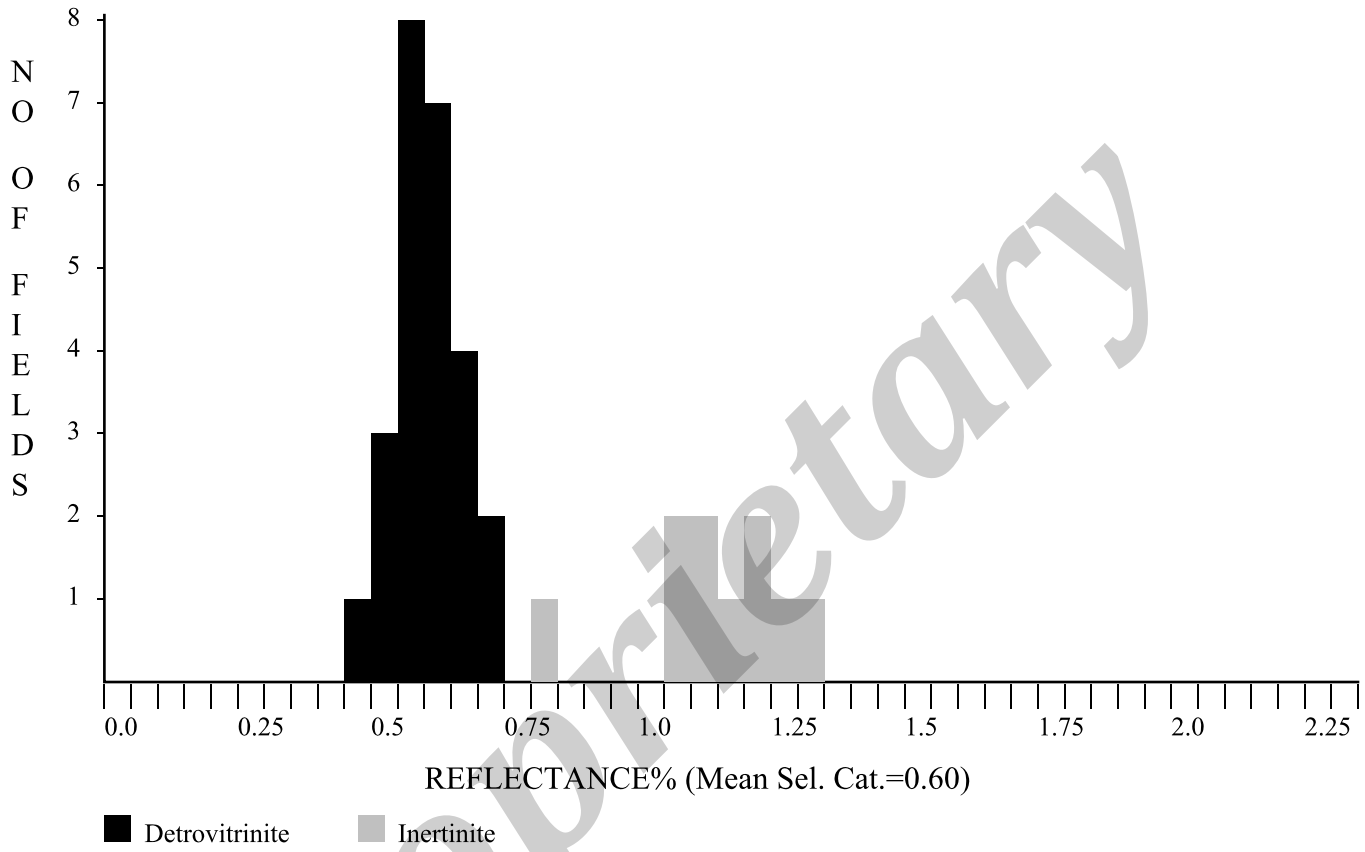

Maceral Category	N	Mean	Standard Deviation
Detrovitrinite	25	0.60	0.061
Inertinite	10	1.14	0.130
Total	35	0.76	0.260

Selected categories: Detrovitrinite:

No. of Readings:	25
Mean of Selected Categories:	0.60
Standard Deviation of Selected categories:	0.061

R	N	Range	R	N	Range	R	N	Range	R	N	Range	R	N	Range	R	N	Range	R	N	Range	R	N	Range	R	N	Range
0.4	1	Detro	0.7			1			1.3			1.6			1.9			2.2			2.5			2.8		
0.41			0.71			1.01			1.31			1.61			1.91			2.21			2.51			2.81		
0.42			0.72			1.02			1.32			1.62			1.92			2.22			2.52			2.82		
0.43	2		0.73			1.03			1.33			1.63			1.93			2.23			2.53			2.83		
0.44			0.74			1.04			1.34			1.64			1.94			2.24			2.54			2.84		
0.45			0.75			1.05			1.35			1.65			1.95			2.25			2.55			2.85		
0.46	2		0.76			1.06			1.36			1.66			1.96			2.26			2.56			2.86		
0.47			0.77			1.07	1		1.37			1.67			1.97			2.27			2.57			2.87		
0.48	2		0.78			1.08			1.38			1.68			1.98			2.28			2.58			2.88		
0.49	1		0.79			1.09			1.39			1.69			1.99			2.29			2.59			2.89		
0.5			0.8			1.1			1.4			1.7			2			2.3			2.6			2.9		
0.51	3		0.81			1.11	2		1.41			1.71			2.01			2.31			2.61			2.91		
0.52	1		0.82			1.12			1.42			1.72			2.02			2.32			2.62			2.92		
0.53	2		0.83			1.13			1.43			1.73			2.03			2.33			2.63			2.93		
0.54			0.84			1.14			1.44			1.74			2.04			2.34			2.64			2.94		
0.55			0.85			1.15			1.45			1.75			2.05			2.35			2.65			2.95		
0.56	5		0.86			1.16			1.46			1.76			2.06			2.36			2.66			2.96		
0.57	1		0.87			1.17	1		1.47			1.77	1	Inert	2.07			2.37			2.67			2.97		
0.58			0.88			1.18			1.48			1.78			2.08			2.38			2.68			2.98		
0.59	1		0.89			1.19	1		1.49	1		1.79			2.09			2.39			2.69			2.99		
0.6	2		0.9			1.2			1.5			1.8			2.1			2.4			2.7			3		
0.61	1		0.91	1	Inert	1.21			1.51			1.81			2.11			2.41			2.71			3.01		
0.62			0.92			1.22			1.52			1.82			2.12			2.42			2.72			3.02		
0.63			0.93			1.23			1.53			1.83			2.13			2.43			2.73			3.03		
0.64			0.94			1.24			1.54	1		1.84			2.14			2.44			2.74			3.04		
0.65	1	Detro	0.95			1.25			1.55			1.85			2.15			2.45			2.75			3.05		
0.66			0.96			1.26			1.56			1.86			2.16			2.46			2.76			3.06		
0.67			0.97			1.27			1.57			1.87			2.17			2.47			2.77			3.07		
0.68			0.98	1		1.28			1.58			1.88			2.18			2.48			2.78			3.08		
0.69			0.99			1.29			1.59			1.89			2.19			2.49			2.79			3.09		

VITRINITE%	INERTINITE%	LIPTINITE%	OIL DROPS	BITUMEN
0.6	2.0	0.5	0.0	0.0

TV	DV	Sfus	Scler	Fus	Macr	Id	Micr	Spor	Cut	Sub	Res	Ld	Bituminite	Telalginite	Lamalginite	Oil cut
			0.0		0.0	0.0		0.5	<0.1	0.0	0.0	<0.1	0.0	0.0	0.0	

Sample Number: E1933 Well Name: GC1191-1, Burger J 001 Depth: 5040-5070ft Sample Type: Ctgs

Date: 2016-04-15 Op: SPR FGV - First Generation Vitrinite, RV - Reworked Vitrinite, BTT - Bituminite, B - Bitumen, Inert - Inertinite, Cav - Cavings, DA - Drilling Mud Additives

R	N	Range	R	N	Range	R	N	Range	R	N	Range	R	N	Range	R	N	Range	R	N	Range	R	N	Range	R	N	Range
0.4			0.7			1			1.3			1.6			1.9			2.2			2.5			2.8		
0.41			0.71			1.01			1.31			1.61			1.91			2.21			2.51			2.81		
0.42			0.72			1.02			1.32			1.62			1.92			2.22			2.52			2.82		
0.43			0.73			1.03			1.33			1.63			1.93			2.23			2.53			2.83		
0.44			0.74			1.04	2		1.34	1		1.64			1.94			2.24			2.54			2.84		
0.45			0.75			1.05	1		1.35			1.65			1.95			2.25			2.55			2.85		
0.46	1	Detro	0.76			1.06			1.36			1.66			1.96			2.26			2.56			2.86		
0.47			0.77			1.07			1.37			1.67			1.97			2.27			2.57			2.87		
0.48	1		0.78			1.08			1.38			1.68			1.98			2.28			2.58			2.88		
0.49	1		0.79			1.09			1.39			1.69			1.99			2.29			2.59			2.89		
0.5	1		0.8			1.1			1.4			1.7			2			2.3			2.6			2.9		
0.51			0.81			1.11			1.41			1.71			2.01			2.31			2.61			2.91		
0.52	2		0.82			1.12			1.42			1.72			2.02			2.32			2.62			2.92		
0.53	2		0.83			1.13			1.43			1.73			2.03			2.33			2.63			2.93		
0.54	3		0.84	1	Inert	1.14			1.44			1.74			2.04			2.34			2.64			2.94		
0.55			0.85			1.15			1.45			1.75			2.05			2.35			2.65			2.95		
0.56	3		0.86			1.16			1.46			1.76			2.06			2.36			2.66			2.96		
0.57	2		0.87			1.17			1.47			1.77			2.07			2.37			2.67			2.97		
0.58	1		0.88			1.18			1.48			1.78			2.08			2.38			2.68			2.98		
0.59	1		0.89			1.19			1.49			1.79			2.09			2.39			2.69			2.99		
0.6	2		0.9			1.2			1.5			1.8			2.1			2.4			2.7			3		
0.61			0.91			1.21			1.51			1.81			2.11			2.41			2.71			3.01		
0.62	2		0.92			1.22			1.52			1.82			2.12			2.42			2.72			3.02		
0.63	1		0.93			1.23			1.53			1.83			2.13			2.43			2.73			3.03		
0.64	1		0.94			1.24			1.54			1.84			2.14			2.44			2.74			3.04		
0.65			0.95			1.25			1.55			1.85	1	Inert	2.15			2.45			2.75			3.05		
0.66			0.96			1.26	1		1.56			1.86			2.16			2.46			2.76			3.06		
0.67	1	Detro	0.97	1		1.27	1		1.57			1.87			2.17			2.47			2.77			3.07		
0.68			0.98			1.28			1.58			1.88			2.18			2.48			2.78			3.08		
0.69			0.99			1.29	1		1.59			1.89			2.19			2.49			2.79			3.09		

VITRINITE%	INERTINITE%	LIPTINITE%	OIL DROPS	BITUMEN
0.5	1.7	1.5	0.0	0.0

TV	DV	Sfus	Scler	Fus	Macr	Id	Micr	Spor	Cut	Sub	Res	Ld	Bituminite	Telalginite	Lamalginite	Oil cut
			0.0		0.0	0.0		0.2	0.0	0.0	0.0	<0.1	0.1	0.0	1.2	

Sample Number: E1934 Well Name: GC1191-3, Burger J 001 Depth: 5600-5660ft Sample Type: Ctgs

Date: 2016-04-15 Op: SPR FGV - First Generation Vitrinite, RV - Reworked Vitrinite, BTT - Bituminite, B - Bitumen, Inert - Inertinite, Cav - Cavings, DA - Drilling Mud Additives

R	N	Range	R	N	Range	R	N	Range	R	N	Range	R	N	Range	R	N	Range	R	N	Range	R	N	Range	R	N	Range
0.4			0.7			1			1.3			1.6			1.9			2.2			2.5			2.8		
0.41			0.71	1		1.01			1.31			1.61			1.91			2.21			2.51			2.81		
0.42			0.72	1	Detro	1.02			1.32			1.62			1.92			2.22			2.52			2.82		
0.43			0.73			1.03			1.33	1	Inert	1.63			1.93			2.23			2.53			2.83		
0.44			0.74			1.04			1.34			1.64			1.94			2.24			2.54			2.84		
0.45			0.75			1.05	1		1.35			1.65			1.95			2.25			2.55			2.85		
0.46			0.76			1.06			1.36			1.66			1.96			2.26			2.56			2.86		
0.47			0.77			1.07			1.37			1.67			1.97			2.27			2.57			2.87		
0.48	1	Detro	0.78			1.08			1.38			1.68			1.98			2.28			2.58			2.88		
0.49			0.79			1.09	1		1.39			1.69			1.99			2.29			2.59			2.89		
0.5	1		0.8			1.1			1.4			1.7			2			2.3			2.6			2.9		
0.51			0.81			1.11			1.41			1.71			2.01			2.31			2.61			2.91		
0.52			0.82			1.12			1.42			1.72			2.02			2.32			2.62			2.92		
0.53	1		0.83			1.13	1		1.43			1.73			2.03			2.33			2.63			2.93		
0.54	1		0.84	1	Inert	1.14	1		1.44			1.74			2.04			2.34			2.64			2.94		
0.55	2		0.85			1.15			1.45			1.75			2.05			2.35			2.65			2.95		
0.56	1		0.86			1.16	1		1.46			1.76			2.06			2.36			2.66			2.96		
0.57	1		0.87			1.17			1.47			1.77			2.07			2.37			2.67			2.97		
0.58	1		0.88			1.18			1.48			1.78			2.08			2.38			2.68			2.98		
0.59	3		0.89			1.19			1.49			1.79			2.09			2.39			2.69			2.99		
0.6	1		0.9			1.2	1		1.5			1.8			2.1			2.4			2.7			3		
0.61	1		0.91			1.21			1.51			1.81			2.11			2.41			2.71			3.01		
0.62	4		0.92			1.22			1.52			1.82			2.12			2.42			2.72			3.02		
0.63	1		0.93			1.23	1		1.53			1.83			2.13			2.43			2.73			3.03		
0.64			0.94			1.24			1.54			1.84			2.14			2.44			2.74			3.04		
0.65			0.95			1.25			1.55			1.85			2.15			2.45			2.75			3.05		
0.66	2		0.96			1.26			1.56			1.86			2.16			2.46			2.76			3.06		
0.67			0.97			1.27			1.57			1.87			2.17			2.47			2.77			3.07		
0.68	1		0.98			1.28	1		1.58			1.88			2.18			2.48			2.78			3.08		
0.69	1		0.99			1.29			1.59			1.89			2.19			2.49			2.79			3.09		

VITRINITE%	INERTINITE%	LIPTINITE%	OIL DROPS	BITUMEN
0.3	1.5	0.6	0.0	0.0

TV	DV	Sfus	Scler	Fus	Macr	Id	Micr	Spor	Cut	Sub	Res	Ld	Bituminite	Telalginite	Lamalginite	Oil cut
			0.0		0.0	0.0		0.0	0.0	0.0	0.0	<0.1	0.0	0.0	0.6	

Sample Number: E1935 Well Name: GC1191-5, Burger J 001 Depth: 5950-6010ft Sample Type: Ctgs

Date: 2016-04-15 Op: SPR FGV - First Generation Vitrinite, RV - Reworked Vitrinite, BTT - Bituminite, B - Bitumen, Inert - Inertinite, Cav - Cavings, DA - Drilling Mud Additives

APPENDIX E

Apatite compositions measured by electron microprobe

A.1 Results

Chemical compositions of all grains analysed in this report were analysed by electron microprobe. In contrast to measurements of wt% Cl described elsewhere in this Report, these full compositions were measured using the Cameca SX50 machine at the University of Melbourne. Results were provided as an Excel file via email. Analytical conditions and details of detection limits etc are summarised below.

A.2 Analytical conditions for apatite analysis

Hardware: Cameca SX50 Electron Microprobe with four Vertical Wavelength Dispersive Spectrometers (WDS). Roland Circle 160mm.

Analysing Crystals used:

Heavy Elements (Fe, Cr, Mn, Zn, Ni, V, La) LiF (Lithium Fluoride) 100 crystal with d-spacing of 4.026 Angstroms.
All using **k-alpha xray** lines. La **l-alpha xray** line. Spectrometers #1 and 3

Intermediate Elements (Ti, Ca, K, Cl, S) PET (Polyethylene Terrephthalate) crystal with d-spacing of 8.75 Angstroms.
All using **k-alpha xray** lines . Spectrometer #2

Heavy Elements (Y, Ce) PET (Polyethylene Terrephthalate) crystal with d-spacing of 8.75 Angstroms.
All using **l-alpha xray** lines . Spectrometer #2

Light Elements (Si, Mg, Al, Na, P, F) TAP (Thallium Acid Pthalate) crystal with d-spacing of 25.745 Angstroms.
All using **k-alpha xray** lines. Spectrometer #4

Heavy Element (Sr) TAP (Thallium Acid Pthalate) crystal with d-spacing of 25.745 Angstroms.
All using **l-alpha xray** lines. Spectrometer #4

Detectors: All gas flow counters, using P-10 (Argon-Methane 90:10) counter gas,
TAP and PET channels have thin polypropylene x-ray entry windows. Gas flow at atmospheric pressure (1 atm gauge)
LIF channels have thick mylar x-ray entry windows, Gas flow at 1.8 atm (2.8atm gauge).

Electron Beam:
Accelerating voltage: **15kV**. Beam Current **35nA**. Spot size 10 microns to minimise migration of volatile elements

Counting times: All **elements 20 seconds peak, 10 seconds on two backgrounds** on either side of the peak position.
Detection limits: All elements better than 0.05 elemental weight percent except for F 0.3, La 0.13, Y 0.07, Ce 0.08 elemental weight percent.

Software: PC Automation and Data Reduction Software by **SAMx** (JF Thiot) France. Matrix Correction Software Program **PAP** (Pouchou and Pichoir) integrated into the SAMx Software Package. All structural formula calculations based on Deer, Howie and Zussman.

All points digitized using Microbeam DigiMax hardware/software. All coordinates stored for later use for checking or trace element analysis by Laser Ablation ICP-MS.

Samples carbon-coated by carbon vacuum evaporation to 250 Angstroms. Thickness monitoring by resistance measurement.

Sample stage fully automated, using DC motors. Reproducibility 1 micron.

Standards for extended element set Silicate and Oxide Analysis (all values elemental wt%)

Si, Ca	Wollastonite Mg 0.12 Si 23.79 Ca 34.31 Fe 0.31 O 41.47
P	Durango apatite 17.61 P 3.8 F 0.41 Cl 39.27 Ca
Al	Aluminium Oxide Al 52.94 O 47.06
Mg	Magnesium Oxide Mg 60.30 O 39.7
Fe	Hematite Fe 69.94 O 30.06
Mn	Mn metal 100
Ti	Titanium Oxide Ti 59.95 O 40.05
K, Ta	Potassium tantalite K 14.59 Ta 67.51 O 17.91
Na	Jadeite Na 11.20 Mg 0.06 Al 13.24 Si 27.77 Fe 0.10 O 47.54
F	NaF Na 54.75 F 45.25
Cl	NaCl Na 39.34 Cl 60.66
Y	Edinburgh REE glass 11.00 Y 15.01 Ca 24.46 Si 6.72 Al 42.81 O
Ce	Edinburgh REE glass 16.83 Ce 11.75 Ca 25.11 Si 5.36 Al 40.95 O
La	Edinburgh REE glass 14.15 La 12.2 Ca 26.08 Si 5.57 Al 41.99 O